1996

Holocene to Late Pleistocene Stratigraphy of the Mahakam Delta, Kalimantan, Indonesia.

Johan C. Sydow
Louisiana State University and Agricultural & Mechanical College

HOLOCENE TO LATE PLEISTOCENE STRATIGRAPHY OF THE MAHAKAM DELTA, KALIMANTAN, INDONESIA

A Dissertation

Submitted to the Graduate Faculty of the
Louisiana State University and
Agricultural and Mechanical College
in partial fulfillment of the
requirements for the degree of
Doctor of Philosophy

in

The Department of Oceanography and Coastal Sciences

by
Johan C. Sydow
B.Sc.Honours, University of Cape Town, 1988
M.S., Louisiana State University, 1992
May 1996

ACKNOWLEDGMENTS

The person I'm most indebted to for completion of this work is my supervisor Dr. Harry H. Roberts. Harry put in a huge effort to get this project off the ground, a logistical nightmare that would require a volume in itself just to describe. His guidance and support throughout the study were invaluable. Floyd DeMers, Walker Winans, and Bill Gibson of the Coastal Studies Institute Field Support Group were the crucial members that prepared, built, installed and operated the extensive array of field equipment used during both field seasons. The quality, and large volume of data acquired over the relatively short field trip periods attest to the great performance of the Field Support Group. Dr. Charles Phipps constructed the underwater vibracorer, and joined us for the second field trip to operate his invention. The crews of the M/V Gagak and M/V Locater helped us overcome problems encountered when trying to operate round-the-clock with a five-member survey team. The project was sponsored by VICO, TOTAL and UNOCAL for phase 1, and VICO for phase 2. Dady Hendarmin, Rainier Latief, Tony Young, Art Astarita, and Alex Marshall, are VICO personnel that were particularly helpful and supportive throughout the project. Advice and suggestions by the committee members, Drs. James Coleman, Dag Nummedal, Stephen Murray, Chester Wilmot, and Robert Gambrell were appreciated, and contributed significantly towards a better quality manuscript. Mrs. Celia Harrod assisted with drafting of the maps.

TABLE OF CONTENTS

ABSTRACT

Late Pleistocene depositional cycles of the Mahakam shelf contain stratal geometries that indicate a progradational continuum, from falling stage in sea level through to initial rise. These findings contrast with popular sequence stratigraphic concepts which predict that large, rapid sea-level falls, typical of the Late Pleistocene, should result in sediment bypass of the entire shelf. The Mahakam shelf is a mixed siliciclastic-carbonate depositional setting. Extensive, thick carbonate buildups are produced by prolific green algal *Halimeda* bioherm accretion during transgression and highstand flooding of the shelf.

The 60 by 200 km study area lies within 2° of the equator, in the Makassar Strait on the east coast of Kalimantan, Indonesia. Stratigraphic architecture and sedimentary facies of the shelf have been mapped using over 3000 line km of single channel seismic and side-scan sonar, plus bottom sediment samples, and 44 short cores. This offshore data complements an earlier onshore study of the modern delta by TOTAL Indonesia (Allen et al. 1979).

The stratigraphic framework is subdivided into depositional cycles bounded by prominent, regional shelf-flooding surfaces. A stratigraphic model is proposed to explain the sequential development of units and surfaces within a depositional cycle. Oblique clinoforms within the last cycle transform downdip into sigmoid clinoforms. This transition reflects a relative sea level change from falling phase to initial lowstand rise. Updip horizontal extensions of sigmoid clinoforms onlap an interpreted exposure surface which truncates oblique clinoform topsets. These horizontal strata are interpreted to represent delta platform aggradation due to accommodation created landward of the prograding delta front during initial lowstand

rise. Accelerated sea level rise results in lowstand-delta abandonment and a backstepping shoreline transgression.

Eustasy is the dominant control on shelf accommodation and stratigraphic architecture. In addition, rapid basement subsidence, structural warping and faulting, and distribution of thick carbonates and abandoned siliciclastic depocenters influence accommodation and distribution of lowstand delta depocenters.

A comparison of the P1 Depositional Cycle of the Mahakam and Mississippi-Alabama shelf reveals significant differences in the stratigraphic framework. These stratigraphic variations reflect differences in the geological settings of the two study areas.

CHAPTER 1. INTRODUCTION

The primary objective the Mahakam River delta study is to establish the stratigraphic framework that results during one sea-level cycle of deposition on the Mahakam shelf and upper slope, east Kalimantan (Borneo), Indonesia (Figure 1.1, 1.2). Late Pleistocene to Holocene depositional cycles of the shallow subsurface, specifically the last glacio-eustatic cycle deposits (<125 ky BP), were the focus of this investigation. Over 3000 line km of single-channel seismic reflection, side-scan sonar, and bathymetry profiles (Figure 1.3), 137 surface sediment samples, 53 vibracores from the modern delta plain, and 44 vibracores and piston cores from the shelf and slope (Figures 1.4, 1.5) were acquired in the ~60 by 200 km study area.

Important advantages of data sets from such young strata, when compared to older, deep subsurface or outcrop data, are the following: 1) The shallow burial depths (<200 m) and modern shelf setting allows imaging by single-channel seismic reflection methods with very high resolution (1 - 3 m in the vertical), which is an order of magnitude greater resolution than multi-channel deep subsurface data. Three dimensional reconstruction of the stratigraphy from continuous seismic cross sections is limited only by the grid spacing. Outcrop studies tend to be two-dimensional, and stratigraphic reconstructions at the scale of a depositional system (10's to 100's of kilometers) is difficult due to the limited extent of even the best oucrop exposures (~10 km). 2) Geological and environmental processes, and the paleogeography, that influenced these relatively young deposits can often be related to those of the modern setting. The sea-level history for this section is relatively well known. These factors are difficult, sometimes impossible, to evaluate in older strata, which makes it difficult to establish realistic depositional models. 3) Radionuclide (C^{14}, U^{234}-Th^{230}), biostratigraphic, and stable-isotope dating methods suitable for this stratigraphic interval potentially offer the chronologic resolution (10^2 - 10^4 yrs) necessary to

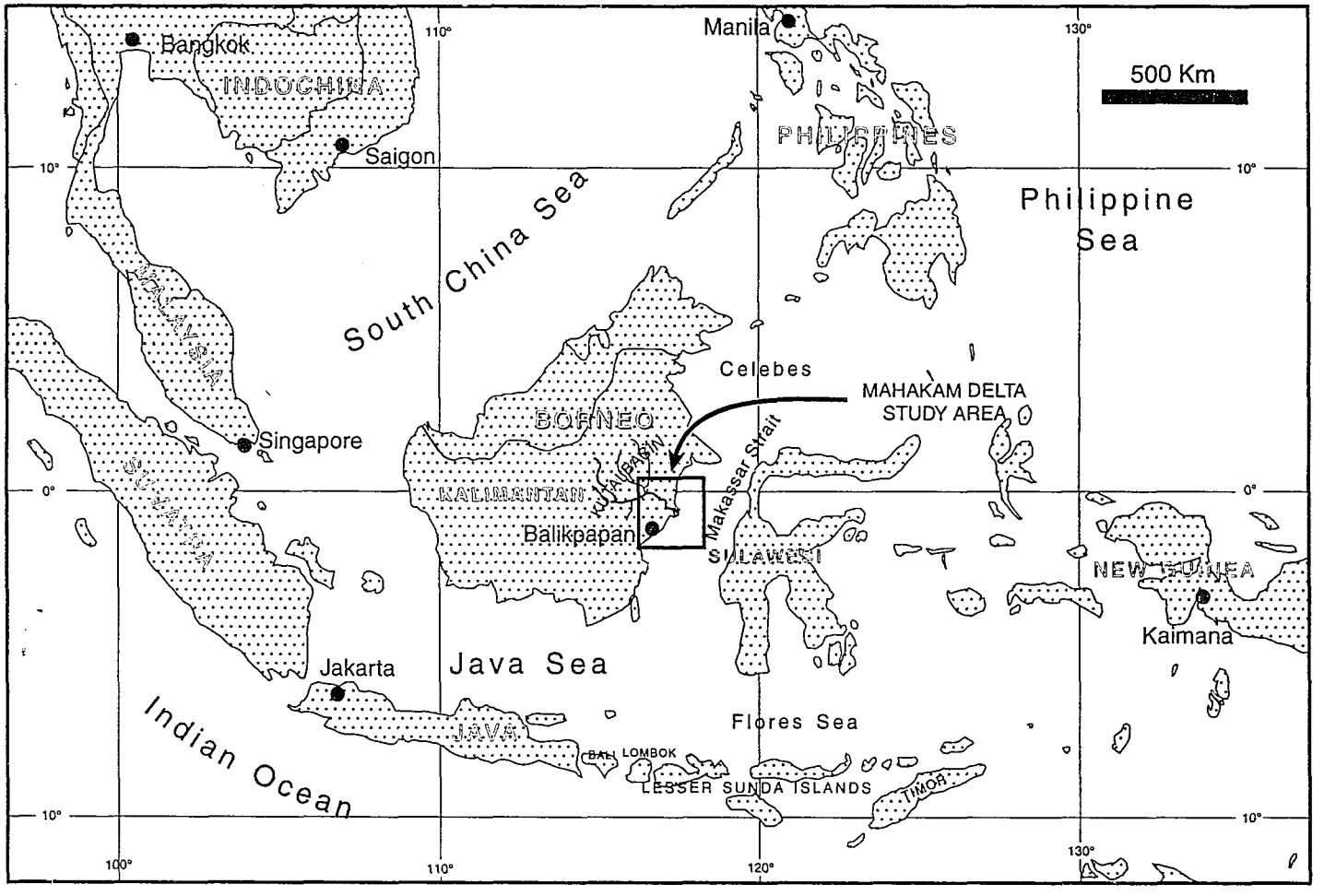

Figure 1.1 Location of the study area.

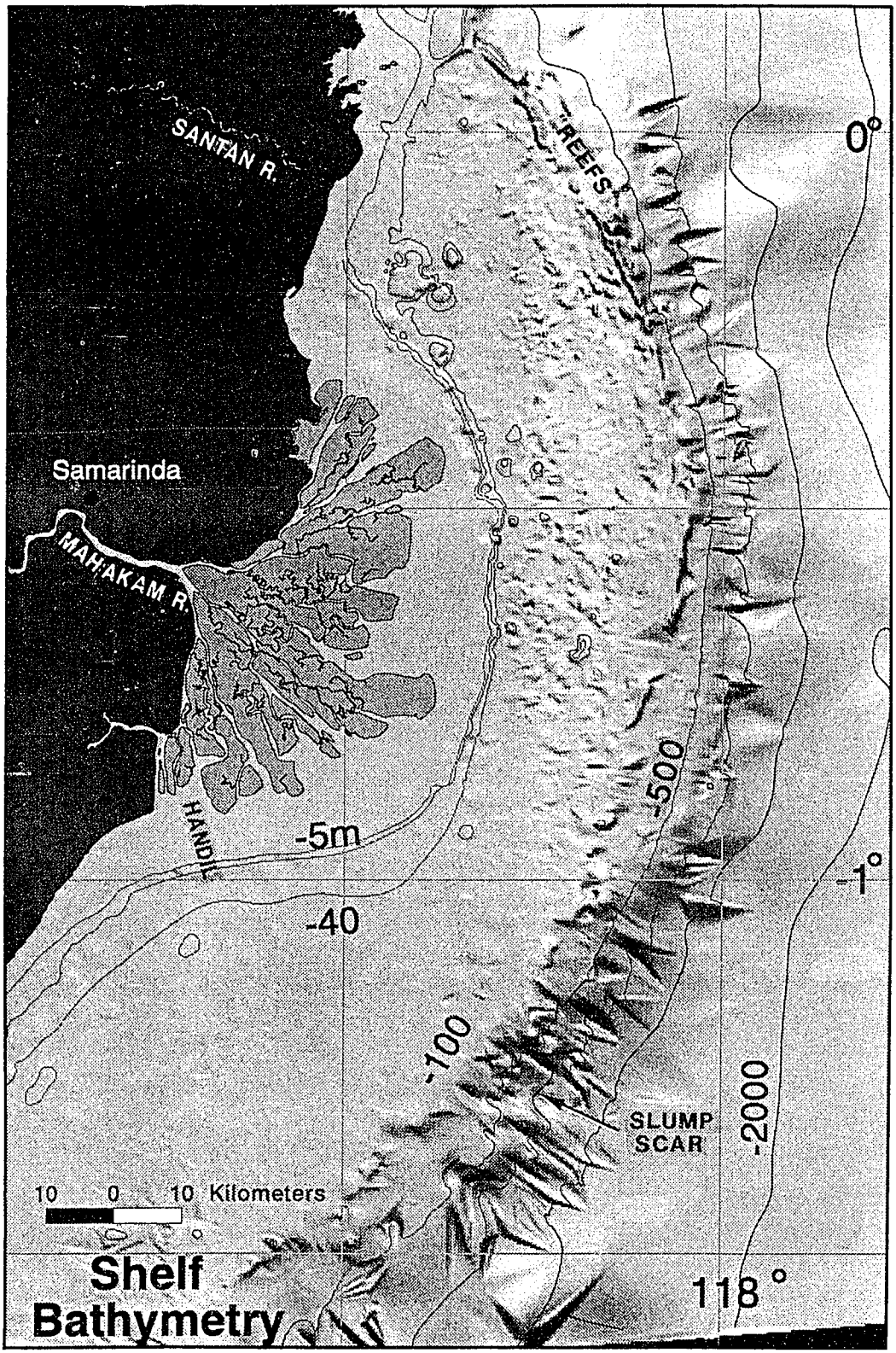

Figure 1.2 Shaded relief representation of shelf bathymetry. Contours in meters. Representation of slope bathymetry is limited by sparse data distribution.

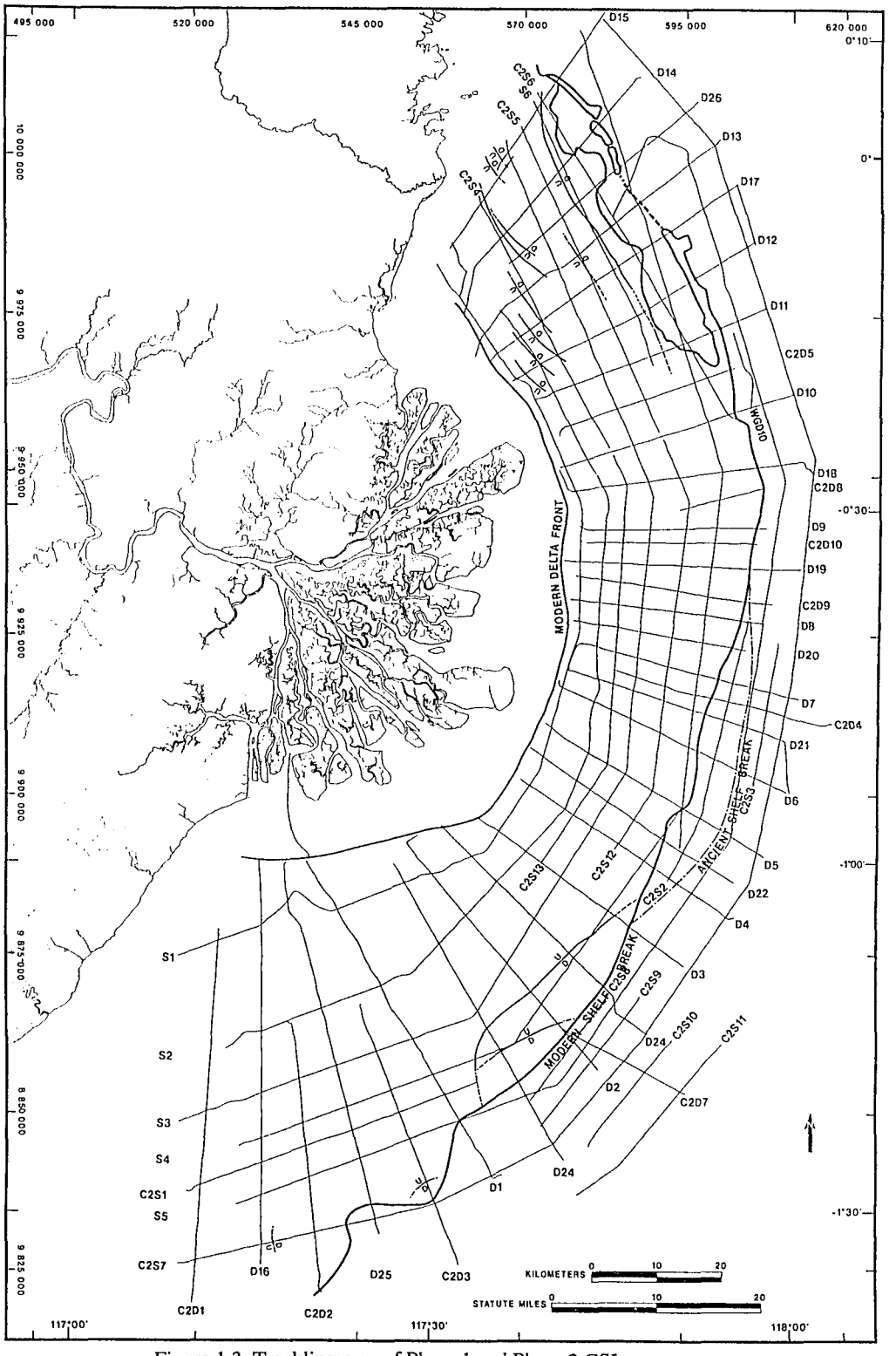

Figure 1.3 Trackline map of Phase 1 and Phase 2 CSI surveys.

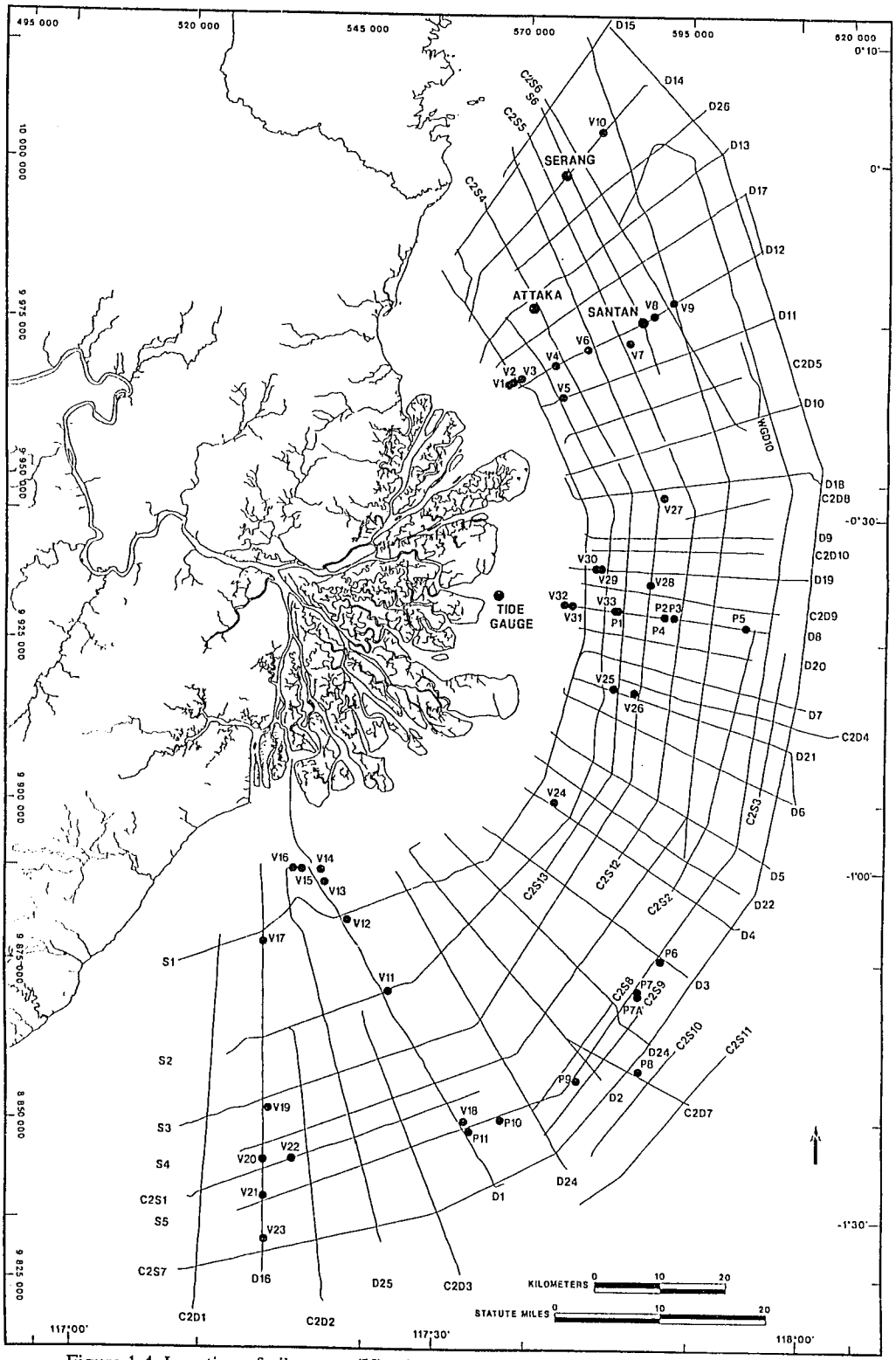

Figure 1.4 Location of vibracore (V), pistoncore (P), platform borings Attaka, Serang and Santan, and tide gauge sites.

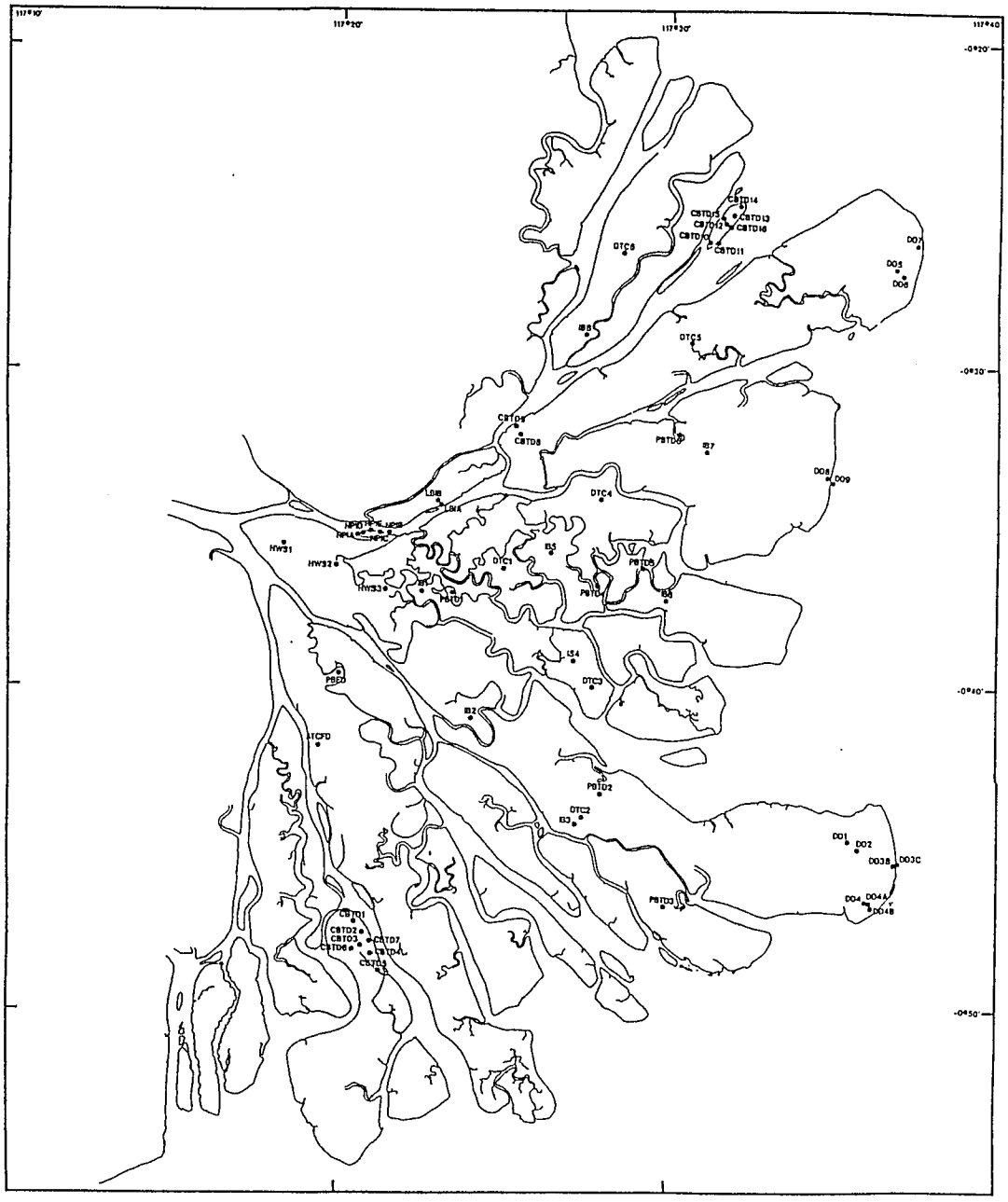

Figure 1.5 Location of onshore vibracore sites.

adequately constrain the chronostratigraphy, and link depositional units to the established sea-level curve. Chronologic resolution of pre-Pleistocene strata (> 1 my, Miall, 1992) is usually too coarse to distinguish individual depositional cycles, not to mention the chronostratigraphic units that make up these cycles.

The Mahakam shelf is the offshore extension of the Kutei Basin (Van de Weerd and Armin, 1992), a prolific hydrocarbon producing region with over 5 billion barrels of recoverable hydrocarbons in place. Concepts gained from this study will help guide exploration and production efforts of Neogene fluvio-deltaic plays beneath the shelf and the onshore. The depositional environment of the Neogene deltaic plays is thought to be similar to the Late Pleistocene setting. An understanding of reservoir and source rock distribution within the cyclic framework of the Late Pleistocene will constrain interpretations of the deeper, deformed, and poorly resolved oil bearing strata.

Of more widespread application, the resulting data-driven Mahakam case-study will help constrain and refine present sequence-stratigraphic concepts (Posamentier and Vail, 1988; Vail et al., 1991; Van Wagoner et al., 1990; Posamentier et al., 1992; Hunt and Tucker, 1992). The geological setting of the study area differs significantly from similar studies of the last glacial-lowstand shelf deposits in the Gulf of Mexico (Suter and Berryhill, 1985; Winker and Edwards, 1983; Kindinger, 1988, 1989: Sydow and Roberts, 1994; Anderson, in press) and north Mediterranean (Piper and Perissoratis, 1991; Trincardi and Field, 1991; Tesson et al., 1993; Bellotti et al. 1994; Trincardi et al., 1994). Some of the major differences are: 1) The Mahakam shelf is influenced by a strong lonshore current, intermediate tides, high fluvial discharge, low wave-energy, and a warm monsoonal-equatorial setting, as opposed to more commonly studied wave and fluvially dominated, temperate climate depositional systems. 2) The shelf is a mixed siliciclastic - carbonate environment. 3) Four converging lithospheric plates create a complex southeast Asian tectonic setting

(Figure 1.6). Neogene strata of the Kutei basin are uplifted and folded onshore, and rapid subsidence, structural warping and faulting influences the Late Pleistocene strata on the shelf.

A comparison of deposits formed during the same depositional cycle, but in different geological settings, will help constrain the relative influence on the stratigraphic architecture of some of the numerous variables .

The onshore Mahakam delta plain has been intensively studied by TOTAL under the direction of Dr. G. Allen (Allen et al., 1979). Published studies from the Late Pleistocene to Holocene offshore region do not exist.

1.1 OBJECTIVES

The first objective of the study was to extend our knowledge of the Holocene-modern delta from the well studied onshore (Allen et al., 1979) into the offshore shelf and upper-slope region. Seismic profiles, side-scan sonographs, underway samples, and short (<6m) offshore cores were used to define, characterize, and map the Holocene offshore facies. The onshore cores were collected primarily for palynological purposes, however, the additional sedimentological information was used to augment TOTAL's onshore data sets. The second objective was to define the Late Pleistocene depositional cycles beneath the shelf and upper-slope using the seismic database. Detailed seismic stratigraphic mapping and characterization was completed within this cyclic framework. Few of the short vibracores penetrated into the top of the Pleistocene. Interpretation of the Pleistocene seismic stratigraphy relied heavily on the understanding gained from the Holocene section, and concepts learned from correlative deposits cored in the Gulf of Mexico (Roberts et al., 1991; Sydow et al., 1992; and Sydow and Roberts, 1994; Anderson et al., in press). Deep (100-130m), discontinuously cored platform borings presently undergoing analysis will contribute significantly to the data base of the Pleistocene section, but these data will not be included in this manuscript.

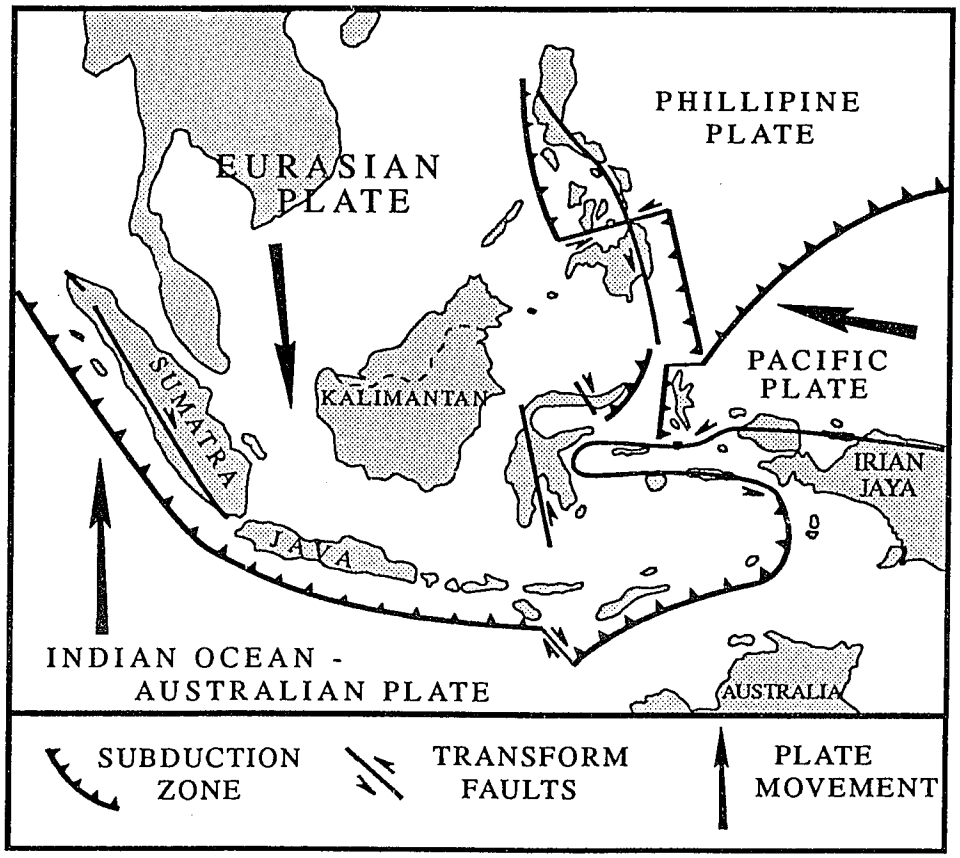

Figure 1.6 Major lithospheric plates of SE Asia. Modified from Katili (1973).

1.2 PHYSIOGRAPHIC SETTING

1.2.1 Mahakam Delta

The Mahakam delta is situated in the 250 km wide Makassar Strait, between 0°- 2° S Latitude, and 116.3°- 118° E Longitude, in the Indonesian archipelago. The delta forms a 5000 km^2 platform which protrudes 50 km onto the inner Mahakam shelf as a gently arcuate feature (Figure 1.2). A relatively steep (1.0°-2.5°) delta front defines the topographically distinct outer edge of the delta. Most of the subtidal portions of the delta platform are less than 5 m deep at mean low tide, the break in slope onto the steep delta front occurs between 5 and 10 m water depth. Tidal flats 1 to 5 km wide, merge landward with the fan-shaped, vegetated, intertidal delta plain. The supratidal portion of the 2000 km^2 delta plain is restricted to the small apex region of the delta.

1.2.2 Mahakam Shelf

Seaward of the steep delta front is the prodelta apron which pinches out on the inner shelf. The arcuate edge of the Mahakam shelf is situated 25 to 50 km seaward of the delta front (Figure 1.2). An abrupt shelf break occurs between 80 and 120 m water depth. Upper slope gradients may be more than 25°, dropping to the Makassar deep at 2500 m water depth within 30 km of the shelf-edge. Morphological differences separates the shelf into northern, central, and southern sectors. The southern sector is 50 km wide, has a gentle seaward gradient (± 1:900), and is generally smooth and featureless. Very rugged, high relief topography characterizes the 25 km wide central sector, which has an overall gentle seaward gradient (± 1:1000). The northern sector has a steep (± 1:300) seaward gradient. Aside from a few isolated patch reefs, the inner shelf of the northern sector is relatively smooth, and the outer shelf is rugged . A down-faulted terrace at 160 m depth occurs along the shelf-margin of the northern sector . The outer-edge of this terrace is delineated by a 80 to 120 m high, 1-2km wide, discontinuous reef wall (Figure 1.2).

1.2.3 **Drainage Basin**

The Mahakam River drains a 75000 km^2 basin which extends from coastal lowlands to the mountainous interior of Kalimantan. The entire region is covered by tropical rainforest and nearly all of it is underlain by Tertiary sedimentary rocks (Prokasih Report, anonymous, 1993). Structural uplift occurs along the coast, immediately landward of the delta. Thus there is no coastal plain or river floodplain associated with the incised, distal Mahakam River valley. The Mahakam River meanders some 250 km through a large, subsiding alluvial basin, situated between the coastal uplift region and the mountainous interior. Swamps and lakes characterize this alluvial basin.

1.2.4 **Rainfall, Discharge and Sediment Supply**

Annual rainfall varies between 2000 mm at the coast and 4000 mm in the mountainous interior, and is weakly seasonal. Kalimantan experiences two wet seasons, which correspond to the beginning of the northwest (NW) monsoon during November and December, and the transitional period from northwest to southeast (SE) monsoons during March to May (TAD report, 1982). Drier southeast monsoon winds blow during the northern summer, dry and wet monthly rainfall figures differ by a factor of two in the mountainous interior. Rainfall data and limited discharge measurements suggest an average fluvial discharge of 3000 m^3/s at Samarinda, some 20 km from the head-of-passes, about 1/3 of the Mississippi River discharge. The volume sediments within the Holocene delta platform suggest an average sediment load of some 8×10^6 m^3 during the last 7 ky (Allen et al., 1979), about an order of magnitude less than the Mississippi River. To place the size of the Mahakam system into perspective, Milliman and Meade (1983) estimate that the 21 largest rivers of the world deliver about 50 % of the total sediment supplied to the oceans. Only some 50 rivers in the world deliver sediments in excess of 10×10^6 t/yr (Milliman and Meade,

1983). The Mahakam River is therefore of intermediate magnitude in sediment supply and discharge.

1.3 OCEANOGRAPHIC SETTING

1.3.1 Low Wind and Wave Impact

Wind, wave, and current data in the Makassar Strait are scarce. The low-latitude setting, within 2° of the equator, ensures that typhoons and cold-front passages do not impact the study area. Wave energy generated by the dominant southeast and northwest monsoonal winds is minimal due to the restricted fetch across the Makassar Strait. Significant wave heights exceed 80 cm less than 5% of the time (TOTAL internal report, 1986).

1.3.2 Delta Plain and Nearshore Hydrography

Currents on the shallow (<5 m) delta platform have never been measured but are probably dominated by semi-diurnal on-off transport of the large tidal prism that results from the 50 to 300 cm neap-spring tidal range (Figure 1.7). Almost the entire 2000 km^2 delta-plain is flooded during the spring phase of the tide, and as a result, is dissected by a network of sinuous tidal channels with flared inlets. The tide influences river flow as far upstream as Samarinda, yet the high fluvial discharge is able to maintain a vertically stratified water-column within the major distributaries. A salt wedge extends some 30 km upstream of the distributary mouth at Handil Dua, and migrates some 5 km with the tides (Allen et al., 1979). A residual two-layered estuarine circulation is therefore expected in the distributaries. Allen et al. (1979) documented a turbidity maximum associated with the upstream limit of salt intrusion, with sediment concentrations of up to 1 g/l. River plume suspended sediment concentrations are less than 1 mg/l immediately off the Handil Dua distributary mouth (Eisma et al., 1989).

At sub-tidal frequencies, an offshore pressure gradient is set up by dispersive buoyancy forces associated with the low density river-derived fresh-water cap within

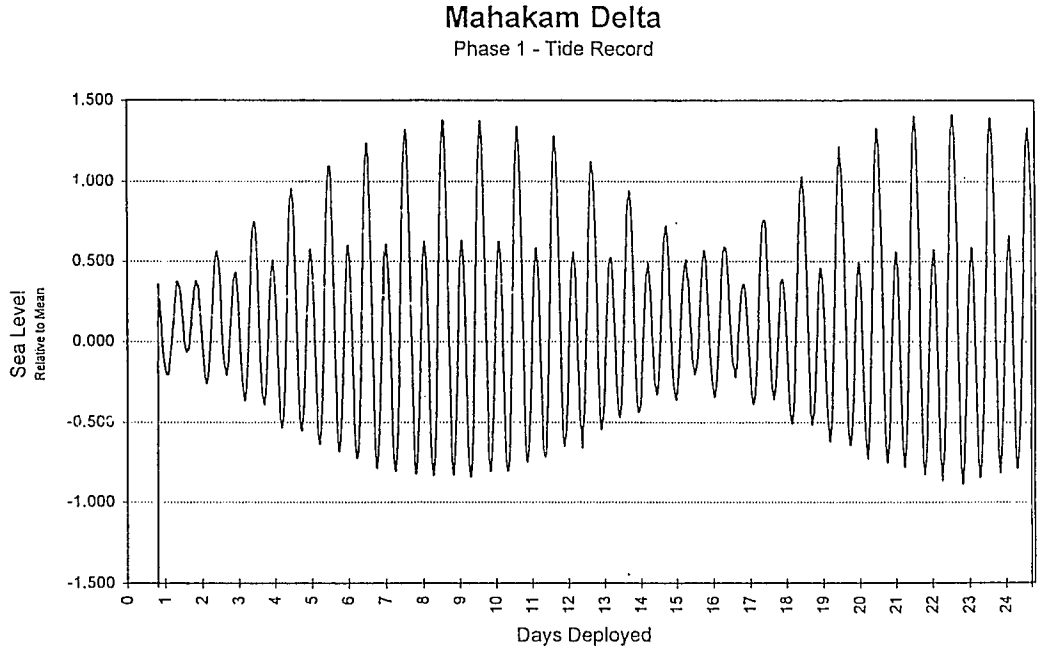

Figure 1.7 Tide gauge data from the inner subtidal delta platform showing the influence of the asymetric, semi-diurnal tide.

the upper 10 m of the water column (Figure 1.8). In the absence of significant Coriolis force the sediment laden fresh-water plume has a net offshore transport, however, the Throughflow current (described later) dilutes and deflects the plume to the south. Eisma et al. (1989) detected a weak plume of lower salinity, higher turbidity (0.5-0.3 mg/l) water that extended 400 km southeast from the river mouth . Processes related to hypopycnal buoyant plumes are well documented from other regions that experience large fresh-water influx and strong near-surface density gradients (Wright, 1989; Wiseman, 1986).

1.3.3 **Stratified Water column**

CTD (conductivity, temperature, depth) casts on the shelf and in the strait illustrate the major water masses and the highly stratified nature of the water column (Figure 1.8). A 40 to 60 m thick mixed surface layer is separated from deeper water by a steep thermocline which extends to a water depth of 350-400 m. Near the coast the mixed layer is capped by a 10 to 15 m thick coastal wedge of lower salinity water due to Mahakam River discharge (Figure 1.8).

High tropical temperatures, high regional fluvial discharge, and excess of precipitation over evaporation result in the low salinity (<34‰), high temperature (>26°) nature of the mixed layer throughout Southeast Asian waters. The low salinity surface water is transported into the Makassar Strait from the South China Sea and Vietnam Gulf via the Java Sea during the NW monsoon (November -March). General westward transport during the SE monsoon (Figure 1.9) replaces the low salinity surface water in the Makassar Strait with Pacific surface water (Wyrtki, 1961).

The thermocline layer (Discontinuity layer of Wyrtki, 1961), from 28° to 10° C, has a fine structured, stepped pattern. Sharp discontinuities occur at 50, 85, (Figure 1.8) and 175 meters. Between 1993 and 1994 the depths and intensities of the of these discontinuities varied. The fairly low thermal gradient between 40 and 85 meters may represent a shelf-bottom mixed layer (Pingree and Griffiths, 1977). The steep density

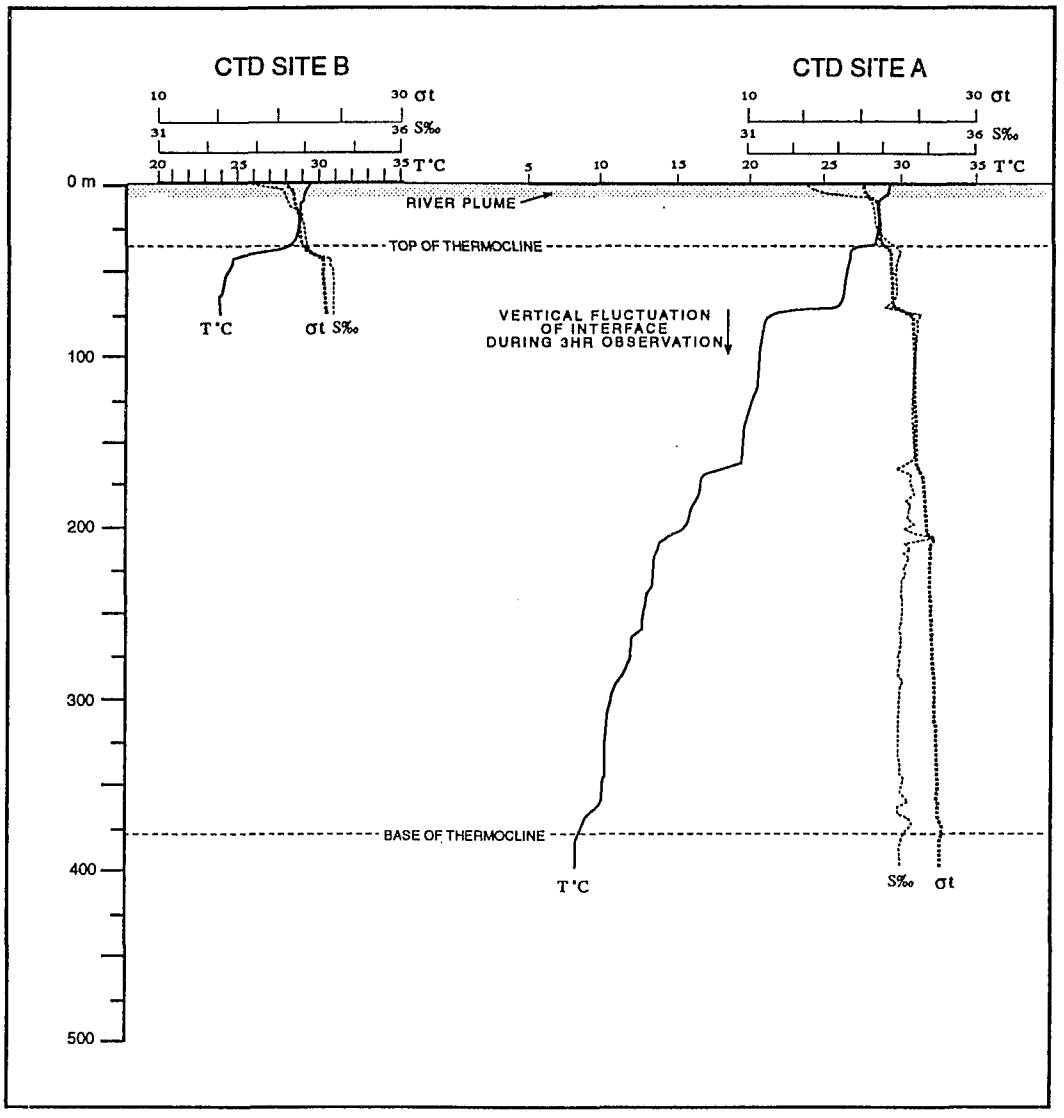

Figure 1.8 CTD profiles from the shelf and upper slope. The water column is highly stratified.

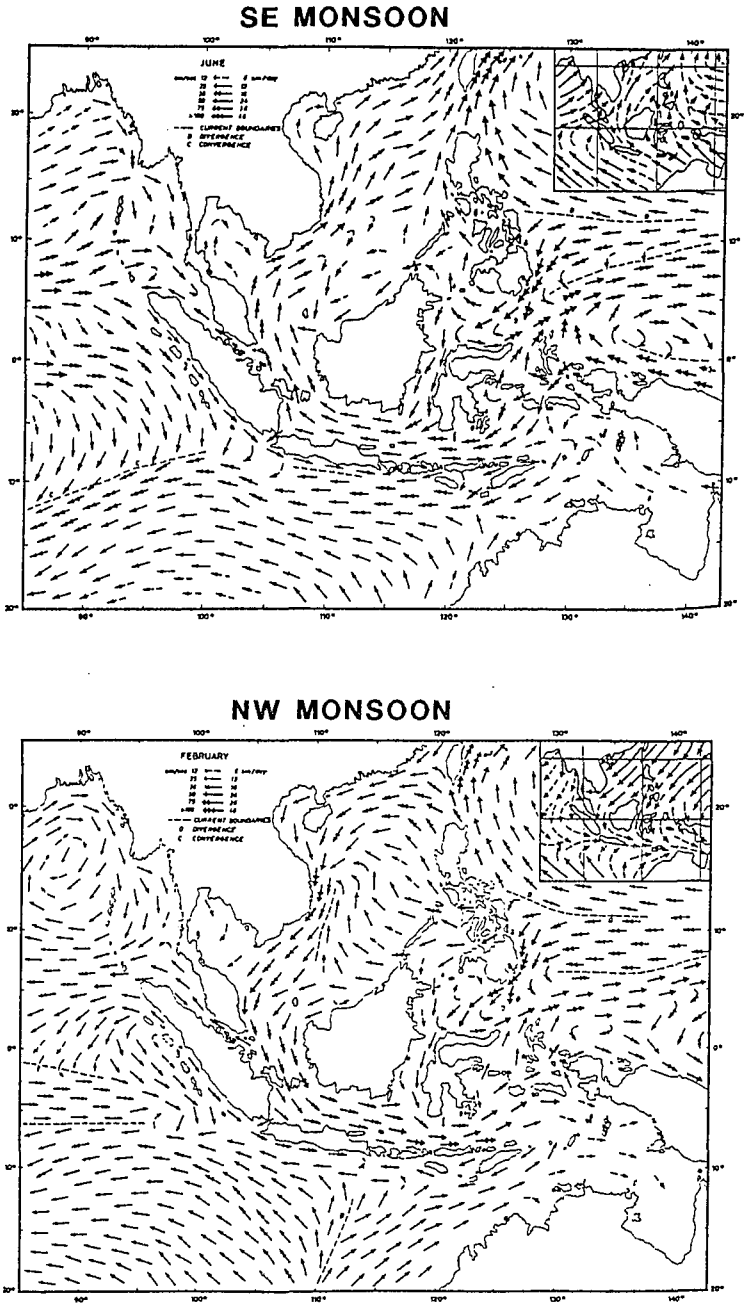

Figure 1.9 Regional surface currents during the two monsoon season. From Wyrtki (1961).

gradient across the entire thermocline (5kg/m^3 density difference across 300 m water depth) results in a Brunt-Vaisala buoyancy frequency (N) of 0.013 rad.s^{-1}, an order of magnitude higher than N values for the open ocean The sharp discontinuities at 40 and 85 m (2kg/m^3 density difference across 5 m water depth) have very large N values of about 0.05 rad.s^{-1}. The waters of the thermocline originate from the north Pacific (Gordon, 1994).

Pacific intermediate waters fill the Makassar Strait below 400 m, and Pacific deep waters below 1000 m. An 550 m deep sill in the South Makassar Strait restricts southward transport at depth.

1.3.4 **Indonesian Throughflow Current**

Formation of North Atlantic Deep Water (NADW) in the North Atlantic and subsequent upwelling in the worlds oceans is balanced mainly by a conveyor belt-like return flow in the warm thermocline layer (Gordon, 1986). Most of the return flow from NADW upwelled in the Pacific is via the Indonesian Archipelago Throughflow current (hereafter termed the Throughflow current), with minor amounts via the Bering Strait and Drake Passage (Gordon, 1986). In addition, the trade winds cause a sea level set-up in the West Pacific, and set-down in the East Indian Oceans. An average dynamic height difference of 16 cm exists between the West Pacific and Indian Oceans across the Indonesian archipelago (Wyrtki, 1987). Consequently, a large water transport of up to 18 Sv (10^6 m^3/s) flows from the Pacific to the Indian Oceans (Wyrtki, 1961, 1987; Gordon, 1994; Fieux et al., 1994). Most of this Throughflow passes through the Makassar Strait into the Flores and south Banda seas, exiting via the Timor trough. (Gordon, 1994; Ffield and Gordon, 1992). A smaller volume exits through the Lombok Strait (Murray and Arief, 1988). Dynamic height difference is restricted to the top 200m of the water column, and is strongly modulated by the monsoonal winds (Wyrtki, 1987; Murray and Arief, 1988; Arief and Murray, in press). Sea-level setup in the West Pacific, and set-down in the east Indian Ocean by

the SE monsoon wind , produces up to 30 cm dynamic height difference from May to October (Wyrtki, 1987). Monsoon related seasonal transports through Lombok Strait vary by a factor of four (Murray and Arief, 1988).

Direct current measurements in the Makassar Strait are restricted to one 61 hr observation station in 2000 m water depth off the Mahakam shelf during the Snellius 1 expedition in August 1933 (Figure 1.10). Strong net transport to the south was observed in the top 200 m, with maximum flow of 84 cm/s at 50 m water depth (Lek, 1938). Calculations based on a 20 dyn cm difference between the southern and northern end of Makassar Strait indicate a mean southerly transport of 40 cm/s in the top 200 m across the entire strait (Wyrtki, 1961). In the Makassar Strait the Throughflow current is present year-round, but is more intense during the SE monsoon (Wyrtki, 1961). This strong Throughflow current sweeps across the shelf in the study area. Surface current moorings in support of hydrocarbon-production platform placements at the base of the delta front indicate that the Throughflow impinges on the delta front. Surface flow is dominantly to the south with currents in excess of 80 cm/s immediately seaward of the delta platform (TOTAL internal Report, 1986)(Figure 1.10). During the NW monsoon the Throughflow current decreases and may reverse.

1.3.5 **Internal Tides and Waves**

Well developed water-column stratification, substantial tidal influence, and abrupt seafloor topography (steep shelf edge, shelf edge ridges and pinnacles) are ideal conditions for generation of large internal waves at tidal frequencies (Wunsch, 1975; Huthnance, 1981). Internal waves are common features in the highly stratified waters of Southeast Asia (Apel et al., 1985). Interaction of internal waves with the outer shelf may have a significant impact on cross-shelf sediment transport and deposition, water transport and mixing, and supply of inorganic nutrients to the outer shelf from

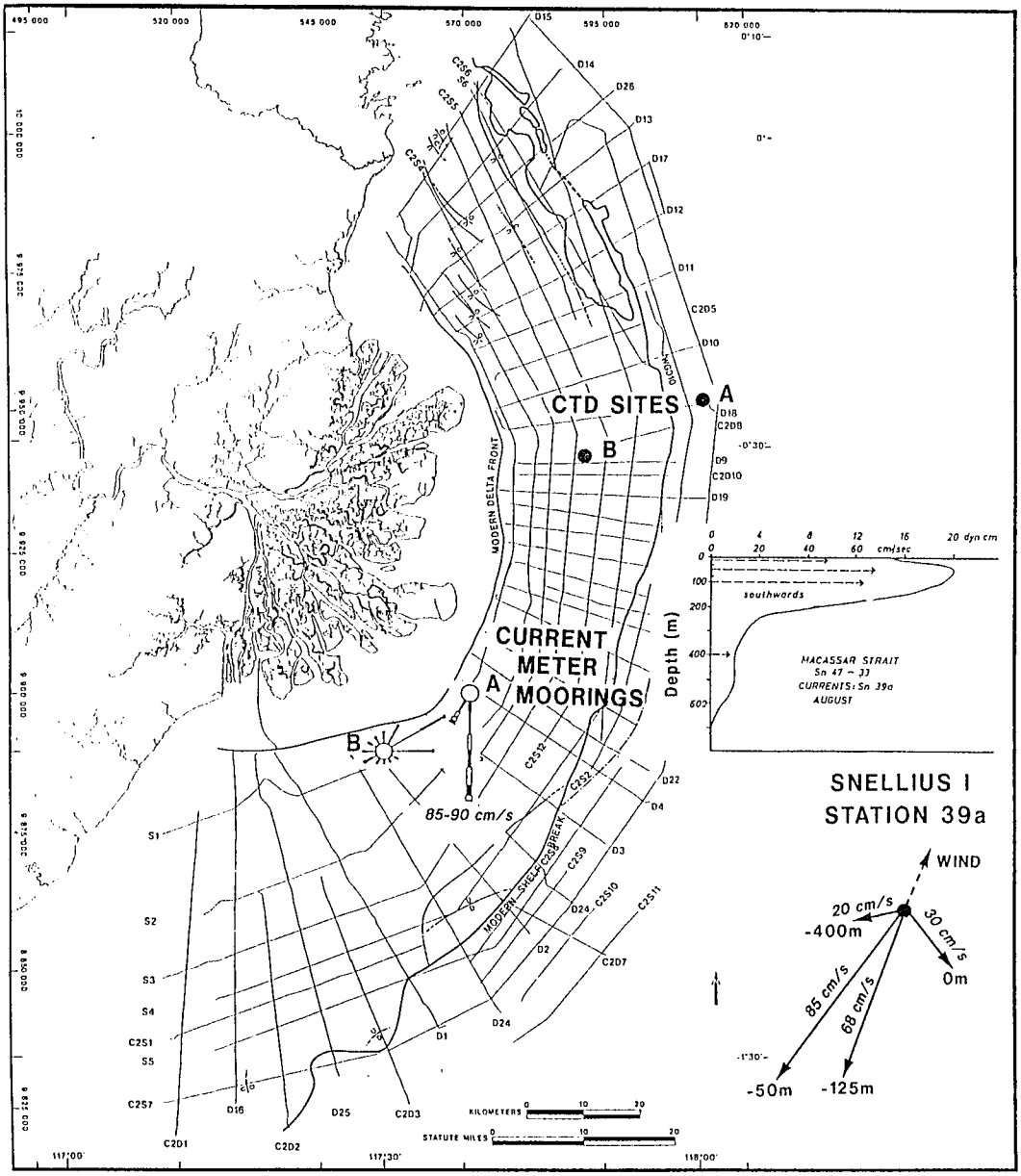

Figure 1.10 Current data from the Makassar Strait (Lek, 1938), and inner shelf (TOTAL internal report, 1986). The southerly throughflow current sweeps across the shelf, and impinges on the delta front. Shelf current meters were deployed for over one year, the Makassar Strait mooring was occupied for only 61 hrs. Shelf current roses are representative of most of the year, except for December and January (NW monsoon) when current directions may reverse. Mooring B illustrates the lee effect south of the delta platform. CTD sites A and B are also plotted.

deeper waters (Brickman and Loder, 1993; Heathershaw et al., 1987; Pingree and Mardell, 1981; Butman et al., 1979).

Progressive along-current changes in salinity, oxygen, and temperature profiles within the thermocline in the Makassar Strait imply vertical diffusivity values (vertical mixing rates) of 3×10^{-4} m^2/s, an order of magnitude greater than the interior oceanic thermocline (Ffield and Gordon, 1992). A strong nutrientcline exists across the 15° to 20°C layer (150-220 m) in the Pacific North Equatorial Current, the ultimate source of the Indonesian Throughflow. Deep to shallow water nutrient concentration ratios across this nutrientcline changes from 5:1 to only 2:1 between the Pacific ocean and the Banda Sea (Gordon, 1986). Increasing nutrient levels along the Throughflow path of the Indonesian archipelago again support high vertical mixing rates thought to be caused largely by internal waves. Localized wind-induced upwelling is another contributing factor to mixing of the water-column (Wyrtki, 1961; Ilahude, 1978).

Large amplitude vertical isotherm displacements of 25 m and 65 m occurred at 50 m and 400 m water depths, respectively, at a semi-diurnal frequency, 60 km off the Mahakam Shelf during the Snellius I expedition (Lek, 1938). During this project's 1994 cruise, repeated CTD casts over a 3hr period, within 5 km of the shelf edge (CTD site A, Figure 1.10), similarly reveal a 22 m depression of a distinct density interface from 78 m to 100 m (Figure 1.8). Large amplitude internal tides are therefore present in the Makassar Strait, and probably impact the outer Mahakam Shelf.

Amplitude, phase speed and energy of an internal wave, and hence, its impact on the shelf, are proportional, in part, to the density gradient across the thermocline (Rosenfeld, 1990; Holloway, 1984; Munk, 1981). Internal waves migrating onto a shelf generally dissipate within 1-2 wavelengths (20-40 km), and may collapse to form internal bores (Baines, 1982). Bottom currents generated by internal waves may intensify when the wave encounters steep topography, such as the shelf edge/upper

slope (Rosenfeld, 1990; Holloway, 1985). Although the wavelengths, velocities and directions of propagation of internal tides in the Makassar Strait are not documented, the observed large vertical density contrast and wave amplitudes suggest that the internal tide may be an important physical process in the outer-shelf depositional environment.

An indication of the magnitude of shelf currents that can be expected from the internal tide is illustrated by documented examples from nearby regions of similar internal stratification and tidal range: NW Australian Shelf, Andaman Sea, and Sulu Sea. Internal tides with a wavelength of 16 km, amplitude of 10-25 m, and phase velocity of 0.4 m/s on the NW Australian shelf produced baroclinic currents of up to 8 cm/s, about half the magnitude of the barotropic (surface tide) currents (Holloway, 1984). Larger amplitude internal waves in the Andaman and Sulu Seas (50-90 m, similar to Makassar Strait) had wavelengths of 20-75 km, and phase speeds of 2.2-2.5 m/s, and produced semidiurnal horizontal baroclinic currents of up to 30 to 50 cm/s. In the latter example, superimposed on the long wavelength internal tide were 30-90 m high solitary waves, or solitons, with 5-8 km wavelengths, which generated an additional 50 to 100 cm/s currents (Apel et al., 1984; Osborne and Burch, 1980). Whether or not such solitons occur in the Makassar Strait is not known.

1.3.6 **Southern Oscillation**

The Indonesian archipelago is situated in the West Pacific warm pool, a region defined by surface water temperatures greater than 28°C. The warm pool is the result of westward transport of surface waters by the trade winds, and accumulation against the Indonesian archipelago: a semi-permeable western boundary. Vertical convection associated with this thermal anomaly results in high rainfall within the warm-pool region. The warm pool is not stationary, but oscillates back and forth along the Pacific equator, a result of complex feedback effects between ocean and atmospheric processes (Philander, 1992). These 3 - 9 yr oscillations are associated with a

complementary high and low pressure see-saw effect between the Indian and West Pacific oceans, a phenomenon known as the Southern Oscillation (Philander, 1992). During extreme eastward migrations of the warm pool the trade winds fail along the Chilean coast, cold-water upwelling stops and heavy rains ensue, a scenario known as an El Nino event (Philander, 1992). El Nino - Southern Oscillation (ENSO) events also have important implications for climate over the Indonesian Archipelago. Eastward migration of the warm pool convection region is often associated with droughts during the June to November (SE monsoon) months for regions south of the equator (Flohn, 1986; Ropelewski and Halpert, 1987). Southern Indonesia experienced up to 90% loss of rainfall during the 1982 ENSO event. Over Borneo the drought was not as extreme, but extended dry periods in the normally humid rainforest of the Mahakam drainage basin resulted in one of the all time largest forest fires in recorded history (Flohn, 1986). Such variations in rainfall would probably have important effects on Mahakam River discharge and sediment supply. Surprisingly, Wyrtki's (1987) analysis of sea-level and dynamic height differences between the West Pacific and Indian Ocean suggests no influence on the Throughflow current at ENSO frequencies.

1.4 PHYSIOGRAPHY DURING GLACIAL PERIODS

During the Late Pleistocene glacial periods, the paleogeography and the rates of physical processes differed from that of the present, and must be considered when interpreting the stratigraphy resulting from an entire glacio-eustatic sea-level cycle.

1.4.1 Late Quaternary Sea level History

In a review of research on Quaternary sea level change, Matthews (1990) concluded that estimates of interglacial and interstadial sea level maxima during the past 125 ky are fairly well constrained by data from raised coral terraces, and that chronologic constraints are well established by orbitally tuned composites of equatorial, deep sea, planktonic oxygen isotope curves, and radiometric dates from

raised coral terraces (Figure 1.11). However, very little reliable data are available to determine the amplitudes of the glacial and stadial sea level minima. Most estimates based on morphosedimentary features for the last glacial maximum sea-level lowstand range between 90 and 130 m below present (eg: Curray, 1960; Bloom, 1983; Suter and Berryhill, 1985; Fairbanks, 1989; Sydow et al., 1992). Glacial sea-level minimum estimates based on ice-volume calculations vary between -77 m and -163 m (Bloom, 1983). Due to the effects of hydroisostasy and glacioisostasy a globally applicable eustatic curve is probably not realistic (Peltier, 1990, Kidson, 1982). Figure 1.12 shows the shoreline location during the last glacial maximum (Biswas, 1973, and Batchelor, 1979, in Gupta et al., 1987). Over 3×10^6 km^2 of present shallow seas was exposed as dry land, which represents at least half of the present Indonesian archipelago sea-surface area (Verstappen, 1980).

1.4.2 **Glacial Rainfall and Circulation Patterns**

Subaerial exposure of large surface areas during glacials has important implications on regional atmospheric and oceanic circulation patterns and on rainfall. Verstappen (1980) and Thorpe et al. (1990) speculate that loss of warm, convective sea-surface area means drier monsoonal winds during glacials. More widespread drier-climate vegetation (although not prevalent), and Pleistocene red latosols and latterites, are some of the sparse data that suggest longer dry seasons (Verstappen, 1980). Widespread sandy and gravelly alluvium deposits and coarse humid alluvial fans (Verstappen, 1980; Gupta et al., 1987; Thorpe et al., 1990) indicate higher bedload transport by rivers, which would be expected during a drier climate when vegetation cover differed and chemical weathering decreased.

Palynologic evidence from deep sea cores (lower fern-pollen content) also indicate drier glacial climate for the Australasian and east Indonesian regions (Van der Kaars, 1991; Barmawidjaja et al., 1993). Extensive montane forests which occurred

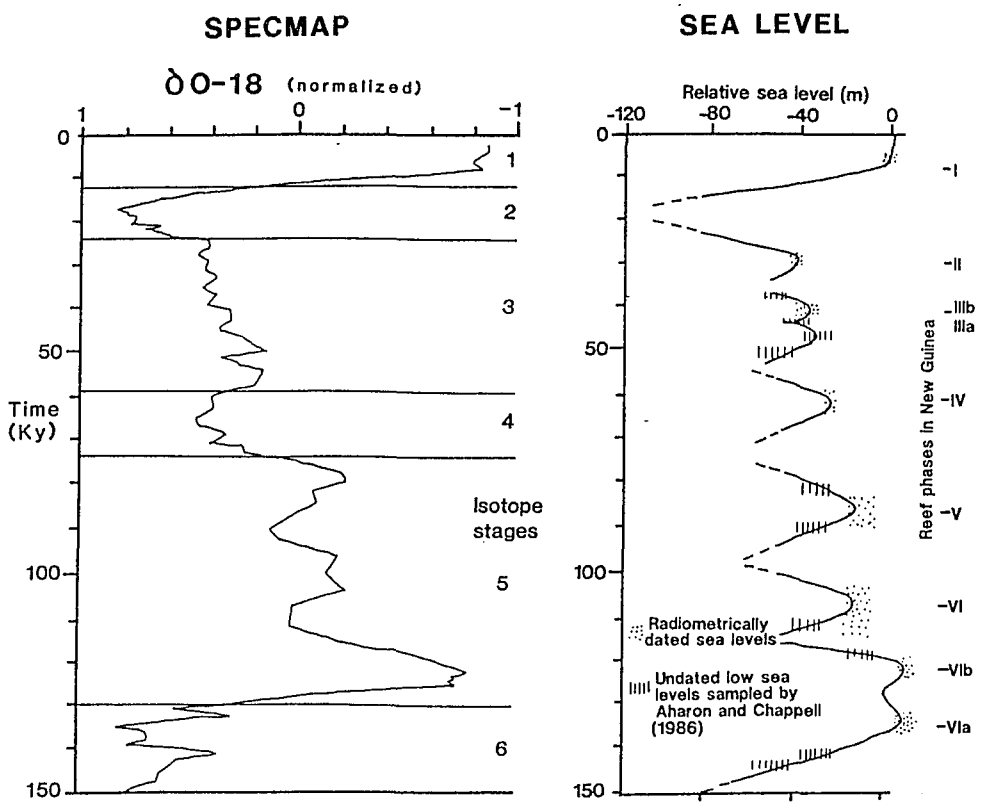

Figure 1.11 Sea level curve from raised coral terraces of the Huon Peninsula, Papua New Guinea (Aharon and Chappel, 1986), and the SPECMAP composite oxygen-isotope curve for the last 150 ky (Martinson et al., 1987)).

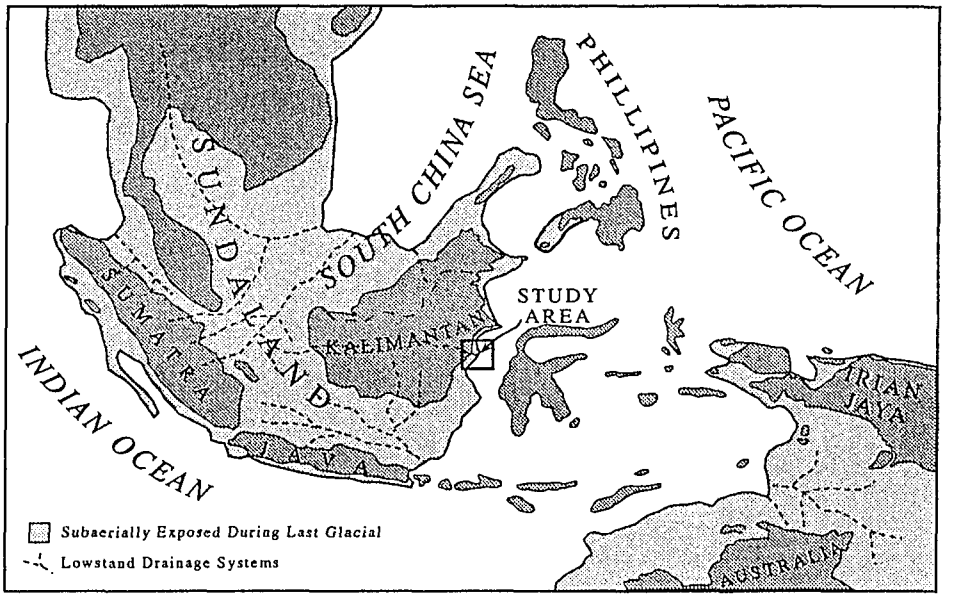

Figure 1.12 Location of the lowstand shoreline during the last glacial maximum based on sea-level minimum estimates of -100 m. The entire Sundaland peninsula and north Australian shelf were exposed, reduced the regional sea-surface area by 3 million sq.km. Modified from Gupta et al. (1987).

at lower elevations than today is evidence for steeper lapse rates and therefore cooler high altitude conditions (numerous examples in Barmawidjaja et al., 1993).

Deep sea core planktonic foraminifera assemblages indicate steeper latitudinal sea surface temperature (SST) gradients, and equatorial SST that were similar or possibly slightly cooler (<2°C) than today (Moore et al., 1981). Similar evidence from cores in the Indonesian archipelago also shows glacial SST similar to the modern. Depleted ∂O18 values (in addition to ice-volume effect) of the glacial planktonic forams in the Indonesian deep sea cores reflect higher sea surface salinities (Barmawidjaja et al., 1993; Ahmad et al., 1995). Higher salinities indicate higher rates of evaporation to precipitation, i.e., drier climate, and possibly the fact that low sea-levels and subaerial exposure of the Java Sea cut off the eastward transport of low salinity surface waters .

1.4.3 **Weaker Indonesian Throughflow ?**

Grain size variations of loess deposits in central China suggest stronger winter monsoonal winds (NW monsoon) during glacials, caused by steeper latitudinal thermal gradients between the warm tropical ocean and cooler continental interior (Xiao et al., 1993). Lower glacial summer temperatures over the continental interior would cause a weaker thermal gradient and weaker winds during the SE Monsoon, an interpretation supported by poorly developed pedogenic zones in glacial loess deposits (Xiao, 1993). Weakened winter monsoons (smaller grain size) and stronger summer monsoons (better developed pedogenesis) occur during isotope stages 1, 3 and 5 (Figure 1.11). The SE monsoon accelerates the Indonesian Throughflow current, while the NW monsoon raises the Indian Ocean water surface and retards throughflow (Wyrtki, 1987; Murray and Arief, 1988). The grain size data would therefore imply weaker throughflow currents during the Glacial isotope stadials 4 and 2. In addition, NADW production diminished by a factor of 2 during glacials (Boyle and Keigwin, 1985; Duplessy et al., 1988), which consequently diminished the global "conveyor

belt" circulation (Gordon, 1986), and could possibly further retard the Throughflow current.

1.5 GEOLOGICAL SETTING

Information in this section draws heavily from a regional SE Asian synthesis by Hutchison (1989), and a review of Kalimantan stratigraphy by Van de Weerd and Armin (1992).

1.5.1 Regional Geology of SE Asia

The Indonesian Archipelago is a result of the collisional impact of three major lithospheric plates (Figure 1.6): the Eurasian plate, moving southeast, the Pacific plate, moving west; and the Indian Ocean-Australian plate, moving north (Ritsema et al., 1989). A complex jumble of subduction zones, accreted terranes, magmatic arcs, back-arc spreading basins, microplates and marginal seas is the result. Southwestern Borneo is part of the Sundaland peninsula: a core region of pre-Mesozoic basement consisting of accreted island arcs and continental crust (incorporates the SE Asian peninsula, Sumatra, Java, SW Borneo, and associated shallow water shelf regions, Figure 1.12).

Major plate-tectonic restructuring occurred during the early Tertiary, when the Indian-Australasian continental plate collided with the Eurasian continental and Pacific oceanic plates (McCabe and Cole, 1989; Hutchison, 1989; Van de Weerd and Armin, 1992). This period was accompanied by rifting of the South China Sea, counter-clockwise rotation of the tip of the Sundaland Peninsula (SW Borneo), start of subduction along NW Borneo, and opening of the Makassar Strait as the southern arm of Sulawesi detached from Borneo (Hutchison, 1989; McCabe and Cole, 1989). The Mahakam shelf is the modern offshore extension of the Kutei Basin, an E-W oriented trough which was initiated during the above Eocene/Oligocene plate restructuring.

The last important tectonic episode occurred during the Early and Middle Miocene, when South China Sea rifting and associated subduction along NW Borneo

ended, the Sulu and Celebes back-arc spreading basins opened, and subduction along northern Sulawesi was initiated (McCabe and Cole, 1989).

1.5.2 **Kutei Basin**

The originally 10 km thick Paleogene fill of the upper Kutei basin (western half of basin, Figure 1.13) experienced structural inversion and deep erosion following the early to middle Miocene tectonic episode (Van de Weerd and Armin, 1992). The Neogene to Modern depocenter of the lower Kutei basin shifted east to its present position beneath the modern coast and Mahakam shelf (Figure 1.13). Upper Miocene to Pliocene sediments onshore have experienced uplift and deformation (Figure 1.14).

The upper Kutei basin is filled with sediments ranging from non-marine clastics, to deep marine shales and platform carbonates. Initial eastward progradation of the thick deltaic wedge commenced during the latest Oligocene, and reached its present location by the Middle Miocene. A 5 to 7 km thick sequence of fluviodeltaic deposits, with some interbedded carbonates, are vertically stacked beneath the modern delta and shelf.

1.5.3 **Structural Setting of the Mahakam Shelf**

A total of 5 to 7 km of deltaic sediment fill in 25 my yields a rough estimate of 200 to 350 m/my average basement subsidence, an order of magnitude higher than maximum globally averaged rates of 18 m/my (Guidish et al., 1984), and more similar to the extreme rates encountered in the northern Gulf Of Mexico salt withdrawal basins (up to 1500 m/my, Van Hinte, 1978). The rapid subsidence region is separated from the onshore uplift and deformation region (Figure 1.14) by a hinge-line that parallels the modern shoreline (not including the delta shoreline), and passes more or less through the apex of the modern delta (Van de Weerd and Armin, 1992). Multi-channel seismic indicates normal faulting and gentle folding is actively deforming the young Neogene strata subsiding beneath the present shelf (Magnier et al., 1975). A NNW oriented zone of en-echelon, down-to-the-basin normal faults impacts the NE

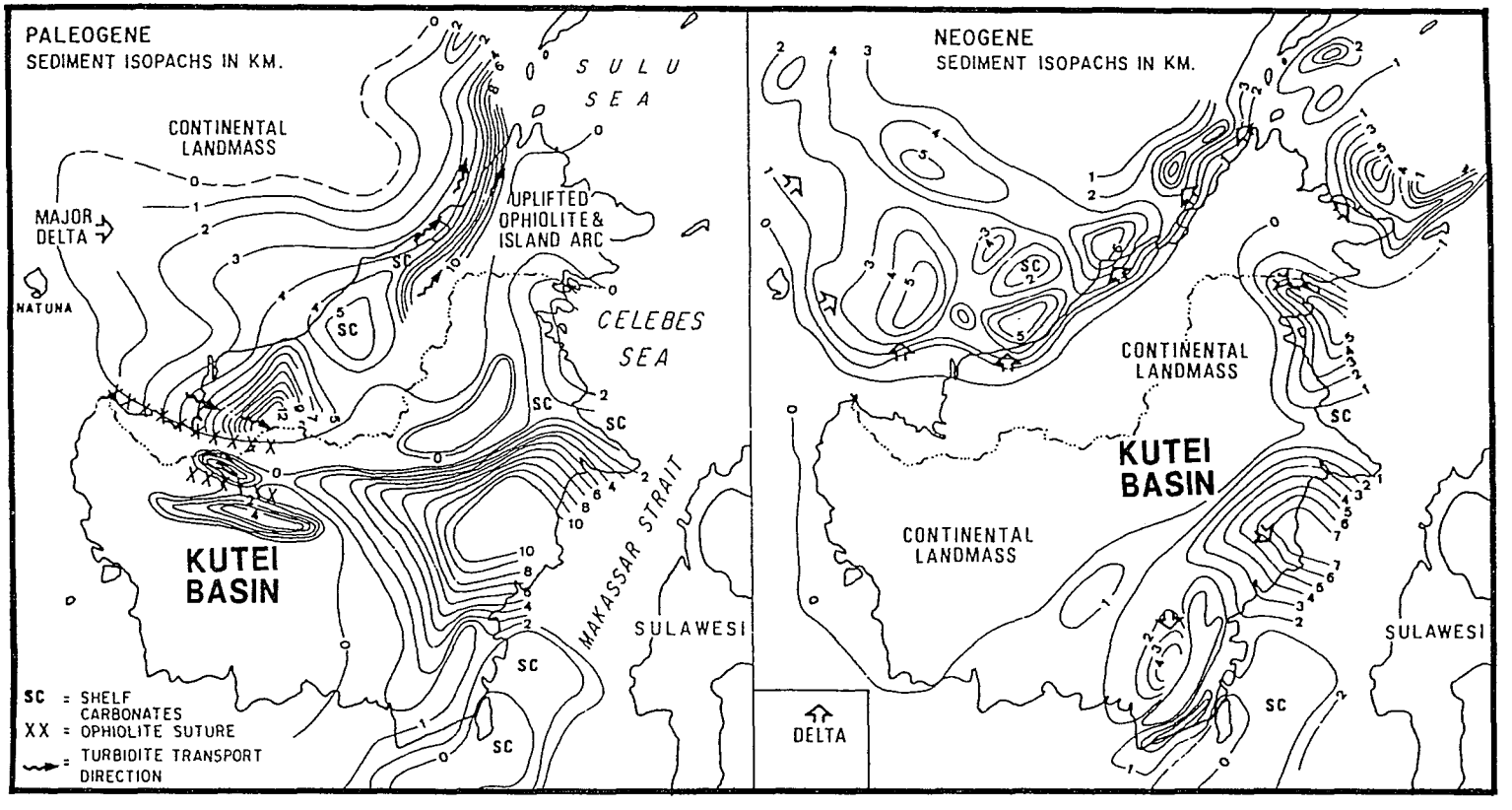

Figure 1.13 Isopach maps of upper (Oligocene-Early Miocene) and lower (Middle-Miocene to present) Kutei Basin sediment fill. Modified from Hutchison (1989).

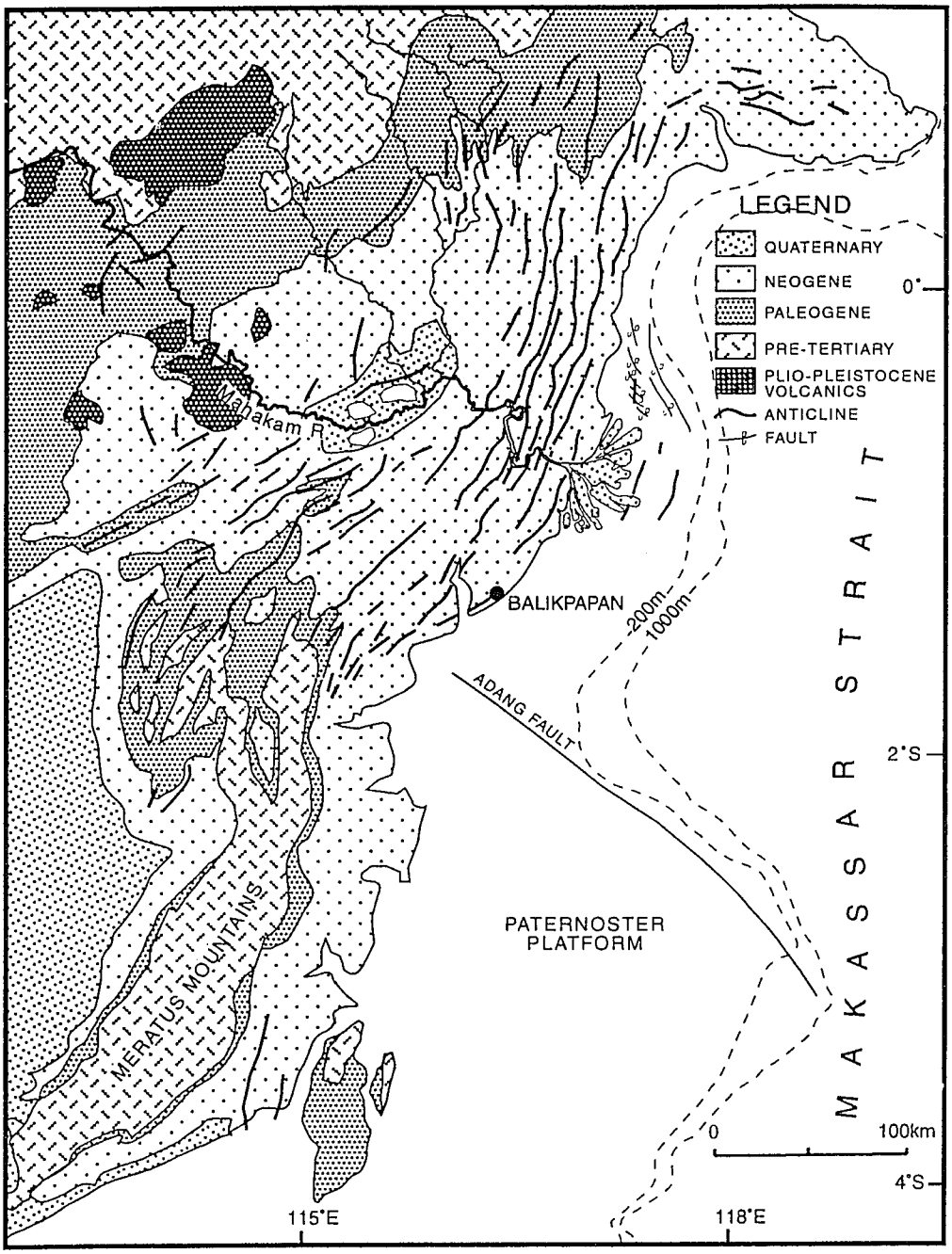

Figure 1.14 Lower Kutei basin geology. Note the structural trends immediately landward of the modern Mahakam River delta. Modified from Van de Weerd and Armin (1992).

Mahakam shelf. The southern edge of the Kutei basin is separated from the Paternoster carbonate platform by a fault zone (Figure 1.14). Structural uplift occurs along the northern margin. Although there is abundant seismic activity associated with extensive subduction and faulting at a regional scale, Ritsema et al.'s (1989) epicenter map indicates that eastern Borneo is a seismically inactive area, but may be affected by shocks from epicenters along eastern Sulawesi.

CHAPTER 2. DATA AND METHODS

The combined 1993 Phase-1, and 1994 Phase-2 field seasons aboard the MV Gagak and MV Locater, respectively, totaled over 40 24 hr workdays of data collection. More than 3000 line km high-resolution single-channel seismic reflection, side-scan sonar, and bathymetry data, 137 surface-sediment samples, 53 vibracores from the modern delta plain, 44 vibracores and piston cores from the offshore, and numerous CTD casts were acquired. The seismic data grid covers a 200 km by 60 km area, with 5 to 10 km grid spacing (Figure 1.3). No previous offshore survey data have been published, although UNOCAL and TOTAL acquired a few minisparker lines across the shelf. Due to minimal previous data coverage in the offshore, Phase-1 was designed to collect a coarse grid of seismic and bottom samples in order to gain a first-cut understanding of the stratigraphy and modern sediment distribution. Based on Phase-1 results infill seismic data and cores were collected during Phase-2 (Figure 1.4). Details on instrument configurations and specifications, core and sample processing procedures, data quality, and approach to data analysis are covered in this chapter.

2.1 EQUIPMENT

2.1.1 Navigation

Ship location and steering was achieved with a Magnavox MX4200d global positioning system (GPS) used in conjunction with an in-house designed navigation program running on a 486 Dell personal computer. The GPS system was operated without a differential remote transceiver, and position accuracy is generally within a 50 m radius of true location. Position fixes were updated at one-second intervals and recorded every two minutes. Fix marks and fix-mark data (fix no., Lat.- Long., bearing, speed over ground, date and time) were stored as ASCII text in a disk file, and also relayed to the other data acquisition systems.

2.1.2 **Seismic Systems**

2.1.2.1 ORE Geopulse Boomer

This excellent, very-high-resolution, single channel seismic acquisition system provided the main data base for detailed stratigraphic mapping. The sound source consisted of two 1 ft diameter metal plates suspended in a rubber diaphragm, which are forced together by a short, powerful electrical pulse to produce a wide-band 400-14 000 Hz signal with minimal reverberation. The return signal was high and low-pass filtered between 400 and 2000 Hz. Vertical resolution was less than 1m, but penetration was restricted to a maximum of 250 milliseconds two-way-time (ms) under ideal conditions. A 1 second firing rate resulted in 2 to 3 meter shot spacing. Signal attenuation and fresnel-zone expansion in deeper water restricted operating water depth to less than 250 m. The sound source was towed about 25 m behind the stern on the port side of the acoustically noisy prop wash. A solid plastic 10 m hydrophone streamer was towed adjacent to the boomer. This high frequency seismic system is very sensitive to acoustical interference caused by breaking waves, but only one day of poor surveying conditions were encountered during both cruises.

2.1.2.2 Water Gun

Seismic Systems model S-15 water gun is a pneumatic seismic source which uses compressed air and a piston to explosively expulse a 15 cu.in. water chamber, which in-turn creates a vacuum bubble that generates a low reverberation sound pulse on implosion. The energy of the 200 to 800 Hz wide-band signal is centered around 400 Hz. A vertical resolution of about 2 m, and a penetration of 500 ms, was commonly achieved on the Mahakam shelf. The main sound signal was preceded by a weak, lower frequency pulse generated when the water chamber was emptied. This precursor signal was often seen as a weak "ghost" reflector above the seafloor and seafloor multiple, but generally did not interfere with the subsurface data. A two second firing rate resulted in 4 - 6 m shot spacing. The sound source was towed about 30 m behind the stern on the

starboard side of the prop wash, and the sound was picked up on the same hydrophone streamer used for the boomer. The water gun system produced deeper penetration, yet lower resolution data used to map deeper strata that were not adequately imaged by the Geopulse boomer. A weak triggering pulse from the firing controller caused misfiring problems during the phase 1 cruise, and the system was abandoned halfway through the survey. Almost zero downtime during phase 2 resulted in over 1000 line km of excellent quality data.

2.1.2.3 Digital Data Acquisition System (Delph 2)

Sound-source triggering, signal acquisition, real-time and post-survey processing, and digital data storage was controlled by the Delph 2 digital acquisition system operating on a modified 486 Dell personal computer. Both sound sources were operated synchronously using staggered firing and listening times, and data storage in separate files. There was no signal interference between the two sound sources, but a trial run with a more powerful Seismic Systems GI Gun resulted in remnant sound energy from the GI Gun interfering with the Geopulse return signal.

The Delph 2 system allowed real time monitoring, optimization, and basic processing of the return signals. Processing of single-channel data was limited to gain optimization, high and low pass filtering, swell filtering, stacking of adjacent shots and predictive deconvolution. Sampling frequency for the Geopulse signal was 8000 Hz for a 250 ms sweep, and the water-gun was 4000 Hz at 500 to 1000 ms sweeps. Incoming data were stored on a 500 megabyte hard drive and downloaded onto 8 mm Exabyte magnetic tape at the end of each survey line. Navigation fixes were incorporated into the stored data.

As backup, data was also recorded in analog format on EPC recorders. Over 1000 line km's of digital data were lost during Phase 1 due to a faulty pre-amplifier on the Delph motherboard. The ORE Geopulse amplifier was successfully modified to

replace this pre-amp with minimal signal loss. The problem recurred during Phase 2, but was immediately discovered and circumvented.

2.1.2.4 Side-Scan Sonar

An EG&G Model 260 digital side-scan sonar system, in conjunction with the Model 380 digital recorder, was used to image sea floor morphology and surface texture. The system operates at the 100 kHz frequency to image a 200 m wide swath along each track line. Due to the potential threat of equipment damage posed by the highly variable shelf topography the side scan fish was towed at a shallow depth, about 50 m off the sea floor.

2.1.2.5 Precision Depth Recorder

The sparse data distribution of published bathymetry charts was augmented with depth profiles from a Raytheon Model DSF-6000 precision depth recorder mounted along the side of the ship.

2.1.3 Conductivity, Temperature, Depth (CTD) Profiler

A Seabird Model SBE-19 self contained CTD system was deployed during both cruises to establish stratification properties of the water column, and to calibrate the precision depth recorder for speed of sound through the water column. Depth, salinity, and temperature are measured by a quartz pressure transducer, a seawater conductivity sensor, and a YSI linear thermistor, respectively. The self contained CTD was fitted with a 200 m pressure transducer for Phase 1, and a 1000 m transducer during Phase 2. The underway sampler or side-scan winches were used for deployment.

2.1.4 Tide/Wave Recorder

Tide and surface wave sea level fluctuations during Phase 1 and 2 were monitored on the inner sub-tidal delta platform by a self-contained Sea Bird Model SBE-26 pressure transducer tide/wave recorder. The instrument was strapped to an oil-platform support leg in 3 m water depth. Pressure and temperature were recorded at 15 minute intervals for estimates of tidal variation, and wave heights and energy were

recorded every six hours with a sampling "burst" rate of 2 samples/second for a duration of 250 seconds.

2.1.5 Underway Bottom Sampler

Based on the design of Dr. Charles Phipps at the University of Sydney, Australia, an in-house built underway bottom sediment sampler was used to obtain samples on sediment type and microfaunal distributions while collecting seismic. The torpedo-shaped coring device has a core-catcher at the front end and a cloth bag on the rear end to retain sediments. The sampler was rapidly lowered by free-wheeling the winch. A change in cable tension indicated when the sampler reached the sea floor , the clutch was then engaged and the forward motion of the ship immediately retrieved the sampler, which was quickly pulled on-board with the hydraulic winch. A 3 to 5 minutes deployment time was possible in 100 m water depth. Using this sampler, 137 bottom sediment samples were collected, to a maximum water depth of 130 m. The sampler saved much time and money, however, the resulting sediment sample was thoroughly mixed and homogenized. Sample mixing destroyed information on sediment structures and living-faunal concentrations in the top few centimeters of the sediment column. Samples were stained and preserved with an ethanol - Rose Bengal solution, and stored in plastic sample jars.

2.1.6 Sediment Cores

Both land based and underwater vibracorers, and a piston corer were deployed to collect a total of 97 undisturbed sediment cores of up to 6 m long. VICO personnel collected 53 cores on the subaerial delta plain, augmenting the numerous cores collected by TOTAL (Allen et al., 1979). 32 vibracores were collected from the offshore shelf, and a further 11 piston cores were retrieved from the shelf and slope, down to 900 m water depth. These cores provided information on sediment lithology, texture, and structure, microfaunal and palynological distributions, and material for radiometric dating. The purpose of collecting these relatively short cores was to obtain undisturbed

sediment samples in order to document Holocene sediment characteristics and distribution. However, there was also some limited stratigraphic use as a few cores penetrated through present highstand deposits into underlying transgressive units, and in a few cases, pierced the top-of-Pleistocene surface.

Recently, three 100 - 120 m deep, discontinuously cored (20 -25 % recovery) UNOCAL platform borings have become available to the study, however, the results will not be ready for inclusion into this manuscript. These long borings will yield very useful lithologic, paleontologic, and chronologic information on the Latest Pleistocene depositional cycles.

2.1.6.1 Portable Vibracorer

The land based vibracorer uses a simple collapsible tripod to support the 7.5 cm diameter, 6 m long, aluminum coring tube. A concrete-vibrator head is clamped to the core tube, powered by a portable gasoline motor. A ratchet winch system attached to the tripod pulls the core out of the ground, and the core tube is cut into meter lengths and clearly labeled on-site.

2.1.6.2 Submersible Vibracorer

The underwater vibracorer was designed and built by Dr. Charles Phipps, and uses electrically powered motors in a water-proof stainless-steel housing attached to the top of the coring tube to create the vibrations that drives the core into the sediments. A 7 m high aluminum frame with fold-out support legs encased the core tube, and was lowered and retrieved using the ship's loading-crane and winch. Electrical power from the ship was supplied via cable to the vibracorer. Once the corer had been lowered to the sea floor the motor was operated for 10 to 20 seconds, which was usually sufficient for 5 to 6 m penetration. Cores were immediately cut into meter lengths, sealed, and clearly labeled. Use of the vibracorer was discontinued after 32 samples because of a leak in the electric-motor housing.

2.1.6.3 Piston Corer

A Model 2175 Benthos piston corer weighted with 450 kg of lead obtained up to 6 m long cores. Cores were contained within a 67 mm plastic core liner. This device replaced the broken vibracorer for the last 6 shelf-coring sites, and was used to retrieve 5 cores on the slope. Again, the ship loading crane and cable winch were used for deployment and retrieval. The only setback with this device was the potential for core disturbance of poorly consolidated muds due to rapid core penetration. The plastic liners were cut into meter long sections, sealed, and labeled immediately after retrieval.

2.1.6.4 Core Processing

Cores were split longitudinally, one half being archived. The remaining half was photographed in color and black-and-white, visually logged, and subsampled. Critical or representative cores were further subdivided into 30 cm lengths and slabbed for X-ray radiography. X-Ray radiographs are sensitive to density differences between sediment particles, and are particularly useful in analyzing apparently featureless muddy lithologies as they accentuate detailed stratification, sedimentary structures, fossils, and diagenetic alteration zones. Cores were subsampled every 50 cm for micropaleo/palynology, X-ray diffraction, and silica/carbonate content analyses. Organic geochemistry samples were taken at 1 m intervals. C^{14} radio-isotope dating samples were taken where suitable shell or plant-organic material was encountered.

Most of the geochemical sample analyses are not available for incorporation at this stage of the project. Micropaleontology and palynology analyses of bottom and core samples were performed by Drs. Sen Gupta and Wrenn, respectively, and is also an ongoing process. Details on sediment sample processing procedures and results will be published elsewhere by the aforementioned researchers and their students.

2.2 MAPPING AND INTERPRETATION STRATEGY

The seismic stratigraphy was mapped using the basic methodology of Mitchum et al. (1977). Procedures consisted of identifying significant mappable units and

surfaces according to reflection terminations, nature of bounding reflections and surfaces, internal reflection configurations, three-dimensional geometry, lateral extent and scale. The same approach was successfully used to map Late Pleistocene shelf stratigraphy in the Gulf of Mexico (Sydow and Roberts, 1994; Sydow, 1992), where the seismic interpretation was calibrated against data from continuous borings.

Vibracores, bathymetry, underway samples, seismic, and previous work (Allen et al., 1979; Gayet and Legigan, 1987; Carbonel et al., 1987; Carbonel and Moyes, 1987; Gastaldo and Huc, 1992) were incorporated into an understanding of Holocene highstand stratigraphy and depositional processes on the delta platform, shelf and upper slope. Interpretation of the Pleistocene seismic stratigraphy was based on this understanding of the Holocene section, as well as concepts gained from the Gulf of Mexico study.

It should be kept in mind that this manuscript represents ongoing research, and is really a first cut interpretation of a region that has not been previously studied (the offshore). Future incorporation of sample analyses from vibracores and data from Unocal platform borings will significantly strengthen the ultimate results of the study.

CHAPTER 3. HOLOCENE DEPOSITIONAL ENVIRONMENTS AND STRATIGRAPHY

The subaerial portion of the delta platform has been extensively studied by workers of the TOTAL oil company (Allen et al., 1979). In addition, a 637 m boring (25% recovery) was drilled through the modern delta plain during the MISEDOR project (Numerous articles in Combaz, 1987; Carbonel and Moyes, 1987; Gayet and Legigan, 1987). Gastaldo and Huc (1992) collected 40 vibracores from the delta plain and shallow near-shore regions. Data collected for the above onshore studies were augmented by a further 53 vibracores acquired for this project. The main focus of the present study was to extend the Mahakam delta database into the offshore region, and to document the nature of Pleistocene depositional cycles buried beneath the shelf. Interpretation of the Pleistocene stratigraphy was based on the understanding gained from the study of the modern highstand Holocene depositional system.

Holocene sediment characteristics, facies distributions, and stratigraphy were mapped from bottom samples, vibracores, piston cores, and seismic profiles. Seismic coverage started at the edge of the shallow delta platform, restricted landward by shallow water and poor seismic data caused by biogenic gas in the modern sediments of the delta. Depositional environments of the delta and shelf were divided into seven main categories: delta plain, subtidal delta platform, delta front, prodelta, carbonate bioherms, carbonate reefs, and starved marine (Figure 3.1).

Subenvironments and sedimentary facies assemblages of each environment are described in the first section of this chapter. The second part focuses on distribution and stratigraphy of the Holocene, followed by a discussion of the depositional processes that appear to influence the modern delta platform and shelf.

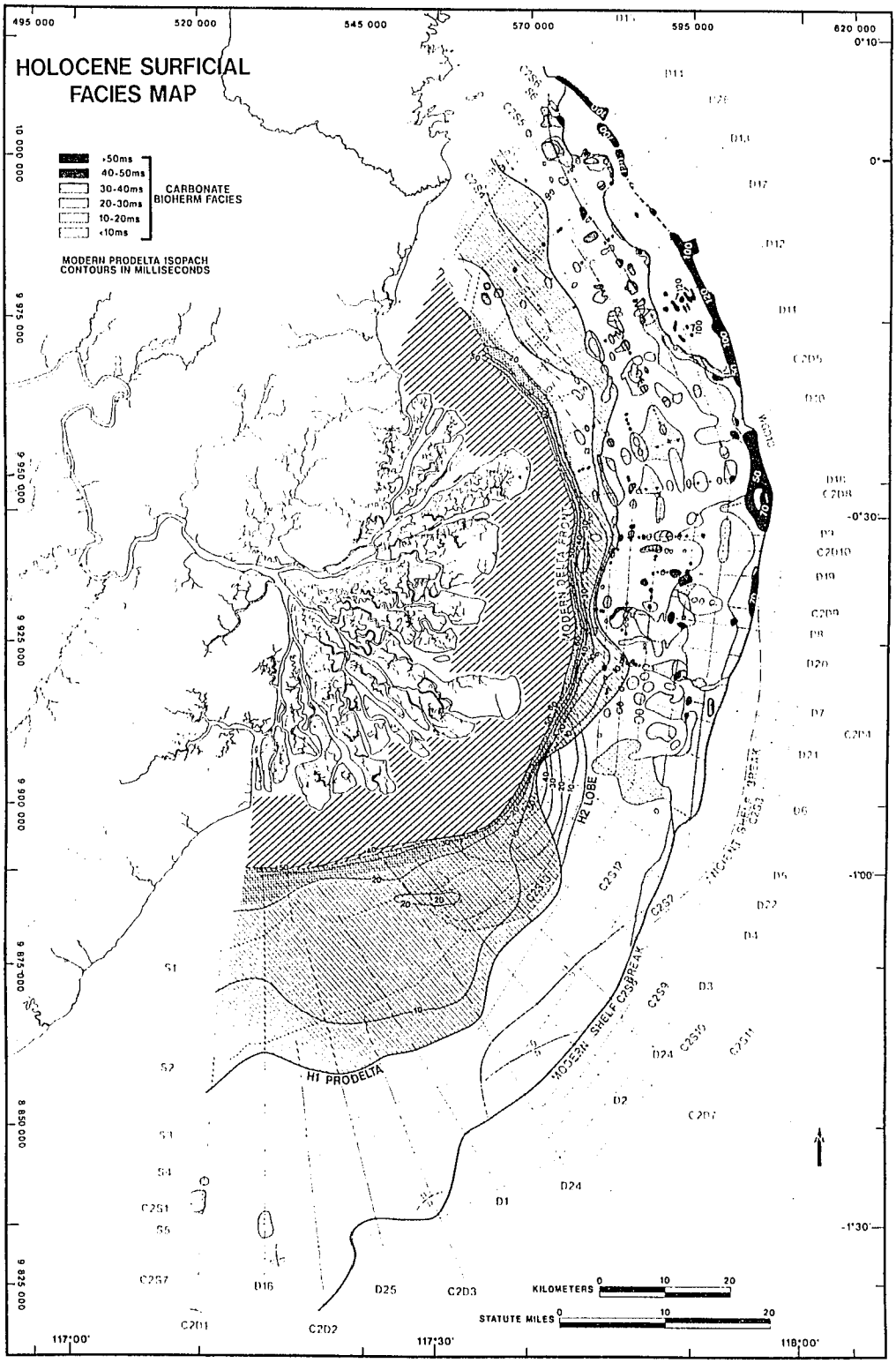

Figure 3.1 Map of Holocene sediment distributions and thicknesses on the Mahakam shelf. Regions not covered by deltaic or carbonate facies represent areas of sediment starvation or scour.

3.1 DEPOSITIONAL ENVIRONMENTS

3.1.1 Delta Plain

Allen et al. (1979) subdivided the delta plain into a supratidal region, near the apex of the delta, and a tidal delta plain that incorporates most of the vegetated delta platform. Elevation of the tidal delta plain is that of mean high tide, and therefore floods during the spring phase of the tidal cycle. Swamps dominate the delta plain: 1) hardwood forest to mixed hardwood/nipa palm swamps in the supratidal region; 2) nipa palm swamps on the tidal delta plain; and 3) mangrove swamps along the outer edge of delta-plain headlands, the top of newly accreted bars, and along channel banks. A network of fluvial distributary and tidal channels dissect the delta plain. Fluvial channels occur in the supratidal region, and both fluvial and tidal channels in the tidal delta plain.

3.1.1.1 Swamp Facies

Sediments of all three swamp facies consists of organic rich, dark to light gray mottled, stiff mud (Figure 3.2). Organic content varies. The top meter contains mostly roots, and is locally peat to muddy peat. Layered plant particulates are more common deeper in cores, and finely disseminated plant particulates occur throughout. Root burrows distort the faint evidence of bedding, and produces the mottled appearance. Weak oxide aureoles may be evident around roots. Faunal remains are absent or rare in the delta plain. The different swamp sediments can be differentiated by their phytological composition (Gastaldo and Huc, 1992).

3.1.1.2 Fluvial Distributaries

The Mahakam river bifurcates three to four times as it crosses the broad delta plain, the major distributaries are located along the northern and southern sectors of the delta. Channels are straight to anastomosing, and numerous tidal channels intersect these distributaries. Distributaries of the southern sector, near Handil Dua (Figure 1.2) are the most active, and have subaqueous extensions beyond the delta plain onto the

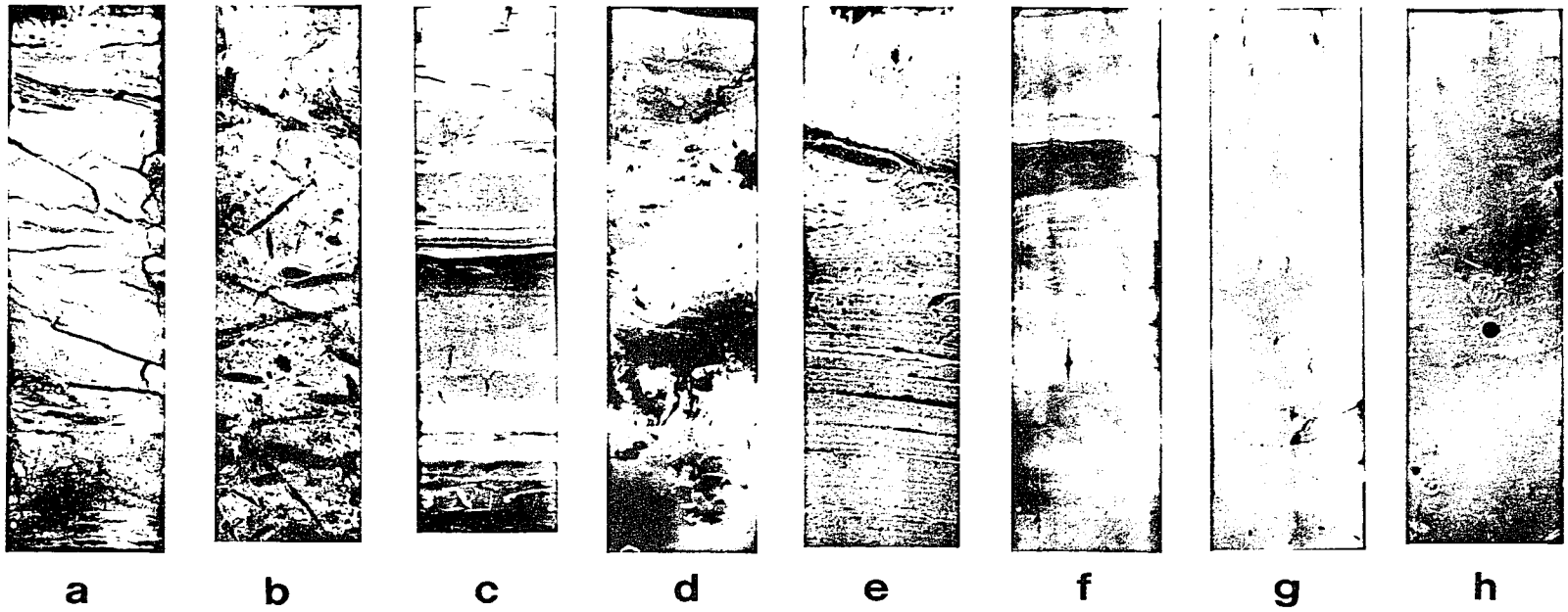

Figure 3.2 Representative X-ray radiographs of depositional facies sampled in cores. Lighter tones indicate denser material. Core diameter is 7.5 cm. a) Vibracore NP1A, cross-bedded sands of a fluvial distributary channel bar. b) Vibracore IB7 , organic rich swamp deposits. c) Vibracore DD1, tidal mud flats, dark layers are organic drapes. d) Vibracore DD8, shell-rich subtidal delta platform muds buried beneath the distal delta plain. e) Vibracore V14, organic rich, bedded muds of the sub-tidal platform/delta-front transition. f) Vibracore V , delta front mud. g) Vibracore V3, Massive mud with incipient diagenetic nudules from the lower delta front. h) Fossilliferous prodelta mud. Continued on next page.

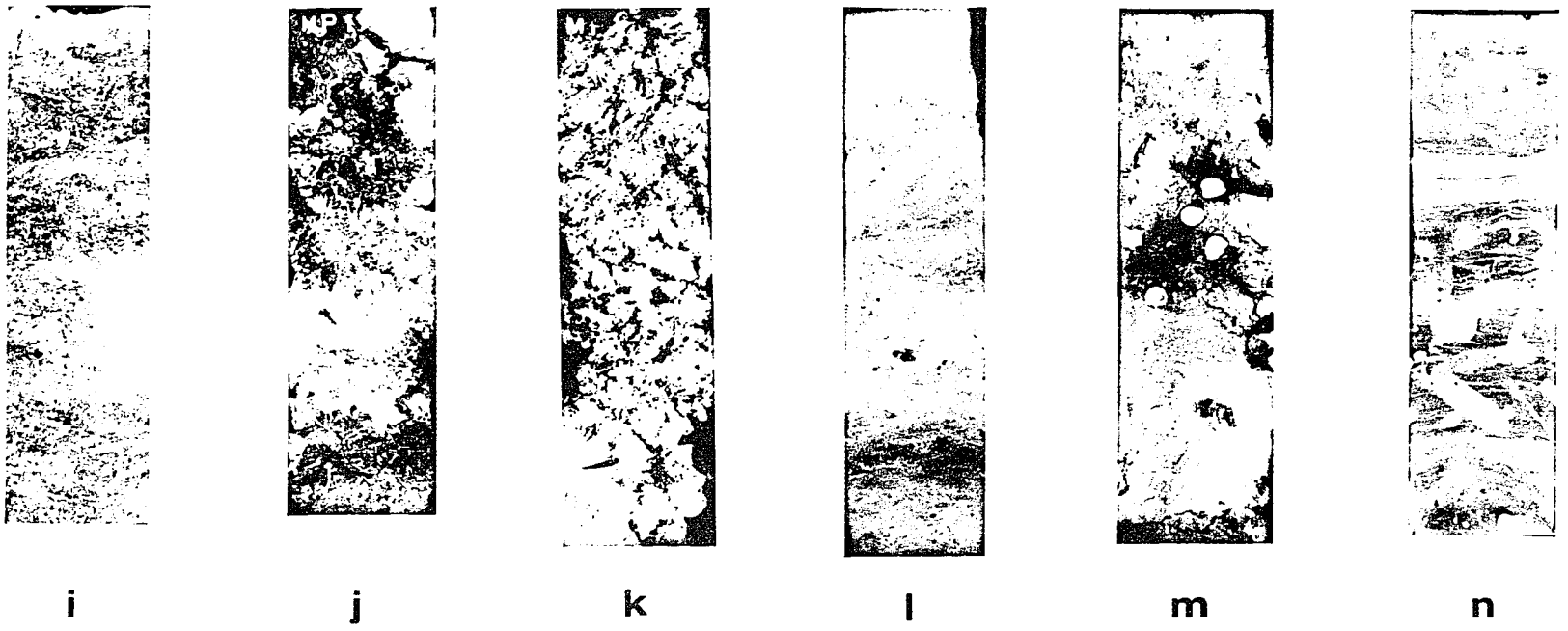

Figure 3.2 continued i) Vibracore V20, shelly shelf mud. j) Piston core P1, *Halimeda* wackestone/siliciclastic shelf mud transition at the top of a bioherm. k) Piston core P1, *Halimeda* wackestone from interior of a bioherm. l) Piston core P6, bioturbated, muddy bioclastic sand from the upper slope. m) Vibracore V5, fossilliferous sand above the transgressive ravinement surface. Coiled "shells" are the tests of the giant foraminifera *Operculina* ammonoides. n) Vibracore V18 at the shelf edge, burrowed Pleistocene delta platform to delta front muds. Burrows are filled with shelly shelf mud and originate at the modern sea floor.

shallow sub-tidal platform, almost to the delta front. There are no levees associated with the distributaries. Allen et al. (1979) subdivided each distributary into a proximal, fluvially dominated section, and a distal, tidally influenced section.

Proximal channels are relatively straight and narrow, 7 to 10 m deep (locally 15m) and 1 - 1.5 km wide. The thalweg meanders within this straight channel and is covered with sand waves and dunes. The meanders define alternating lateral accretion bars which constitute the thickest, and coarsest depositional units of the Mahakam delta. Lateral accretion bars have an erosional base, contain clean, trough crossbedded to massive, medium to coarse sand with drapes of plant particulates. CSI vibracores penetrated the upper, fining portions of exposed bars (cores ATCFDP, LBI-A, LBI-B, NPIA to NPIE, Figure 1.5), starting in cross-bedded medium sands (Figure 3.2), then flaser bedding to alternating mud-sand couplets, lenticular bedding, and finally, organic-rich mud typical of swamp deposits at the top.

Distal distributaries are tidally influenced and experience two-layered residual circulation where net flow is upstream along the channel bed (Allen et al. 1979). Mid-channel bars are the common channel fill element. These bars have gradational bases from mud dominated subtidal platform sediments, to interbedded sands and muds, and overall, are muddier and finer grained than lateral accretion bars. Alternating mud-sand couplets at the base grade into lenticular bedding, and finally, organic mud. Animal burrows and shells are encountered in this distal setting.

3.1.1.3 Tidal Channels

The delta plain is dissected by a network of meandering tidal channels which serve to drain the large tidal prism. These channels are narrow but may be up to 20 m deep (Wrenn, pers. comm., 1994). Sediments transported in tidal channels are dominantly mud and organic matter. Vibracores PBTDP-1 to PBTDP-7, located on tidal channel point bars (Figure 1.5), contain weakly bedded to laminated organic mud, with thin lignite and silt layers. Sediments are similar to swamp deposits. Bedding is

distorted by root burrows from Nipa palm and mangroves established on top of the point bars.

3.1.2 **Intertidal Mudflats and Organic Beach Ridges**

Extensive mudflats form a transitional region between vegetated delta plain headlands and the subtidal platform. Mudflat sediments comprise parallel bedded muddy peat to organic rich mud (Figure 3.2). The inner portions of mudflats have numerous shore-parallel ridges of finely commutated plant organic matter formed by wave action (Allen et al. 1979). Mangrove swamps colonize the emergent mud flats. Vibracores DD-1 to DD-8 (Figure 1.5) through the distal headlands each contain one or two 20-50 cm thick layers of detrital peat. Bivalve shell material and some animal burrows are evident.

3.1.3 **Subtidal Delta Platform**

This environment has been termed delta front in all previous literature on the Mahakam delta. Delta front is really a morphological term that better describes the steep edge of the delta platform, and so is renamed here to subtidal platform environment. The proximal prodelta of Allen et al. (1979) is now the delta front, which is more in line with nomenclature from studies of other deltas.

Water depths of less than 5 m make this region difficult to access from land or sea, and no vibracores were collected during the present study. Allen et al. (1979) and Gastaldo and Huc (1992) collected numerous cores, focusing on the major distributary inlet areas. Additional samples were collected during the MISEDOR drilling program (Carbonel and Moyes, 1987). The greatest variety of sedimentary facies occurred on the subtidal platform: organic rich muds, interbedded mud and sand at various sand:mud ratios, and bioclastic and massive sand. These facies were identifiable from delta plain deposits by the presence of animal burrows and shells (mainly bivalves, Figure 3.2d). Foraminiferal and ostracode assemblages differentiated the inner from the

outer subtidal platform, and also distsributary from interdistributary regions (Carbonel and Moyes, 1987).

Overall the 5-10 km wide subtidal platform is mud dominated and rich in organics (4-7% total organic content (TOC), VICO data). Tidally formed shore perpendicular bars occur near active and abandoned distributary inlets. Sandy distributary mouth bars along the outer edge of the delta platform are rare, but may develop off the largest distributaries. Most offshore extensions of distributary channels terminate at a middle ground or bifurcating bar on the middle platform, and have associated sandy subaquaeous levees. A 7 m thick distributary-mouth bar occurs at the outer platform off the Handil Distributary in the south. All sand bars have gradational bases, coarsen upward, and consist of alternating mud-sand beds and bioclastic sand. The top of abandoned sand bars may contain abundant iron-oxide coated grains, formed by a combination of remobilized iron in reducing interstitial water migrating to the surface and precipitating onto grains within the oxic zone, and reworking (rolling) by tidal currents (Allen et al., 1979).

3.1.4 **Delta Front**

The steep outer edge of the delta platform is composed almost exclusively of organic-rich mud. These muds may be bedded, with thin plant-particulate and silt laminae common in shallower water. Zones of intense microburrowing are evident in X-ray radiographs (Figure 3.2), but delta front sediments are the least burrowed of all facies. Faunal remains are sparse, and barren zones were encountered in some cores and surface samples. The sediments contain a marginal marine benthic foram assemblage (Sen Gupta, 1995), and are differentiable from platform deposits based on the ostracode assemblage (Carbonel and Moyes, 1987). The barren zones probably reflect carbonate test dissolution due to low pH interstitial waters produced by the 2-5% total organic carbon content (Sen Gupta, 1995). Presence of free elemental sulfur is indicative of anoxic conditions. Tan colored nodules and incipient nodules of siderite

and magnesium-calcite are common. Bubble-phase biogenic gas generated by anaerobic decomposition of organics attenuates seismic sound signals, which causes an acoustic wipeout zone beneath the delta front (Figures 3.3, 3.4). Seven of the vibracore sites are from the delta front facies.

3.1.5 **Prodelta**

The break-in-slope at the base of the delta front, between 30 and 40 m water depth, defines the landward edge of the prodelta apron. This break-in-slope coincides with a transition from organic rich black muds of the delta front to olive green, fossilliferous massive muds of the prodelta (Figure 3.2e-h). The outer edge of the acoustic wipeout zone on seismic profiles also corresponds to this delta front to prodelta transition (Figure 3.4). Abundant foram tests cause a gritty texture to the prodelta muds. Benthic forams are a mixture of marginal-marine and marine assemblages, becoming more marine further seaward (Sen Gupta, 1995). Other fauna include gastropods, bivalves, large benthic forams and echinoid fragments. A similar trend of seaward increasing marine influence is seen in palynology analyses (Satchell and Wrenn, 1995). The high fossil content, extent of bioturbation, and low organic preservation (TOC 0.5-1.0 %) attest to much slower depositional rates and more biogenic reworking than on the delta front. Sediments of the thin, outer edge of the prodelta apron have a higher shell content and are perhaps more accurately termed shelly shelf muds (Figure 3.2). On seismic profiles the prodelta facies forms a seaward thinning apron with feint, conformable internal reflectors, and smooth topography (Figure 3.4).

3.1.6 **Bioherms and Biohermal Platforms**

Extensive bioherm mounds and platforms on the shelf are easily distinguished by their characteristic seismic facies (Figures 3.4, 3.5, 3.6, 3.7). Side scan sonar records show the mounded shape of the bioherms, and seismic data reveal internal reflections that are also mounded (Figure 3.6), or acoustically opaque (Figure 3.5). The base is

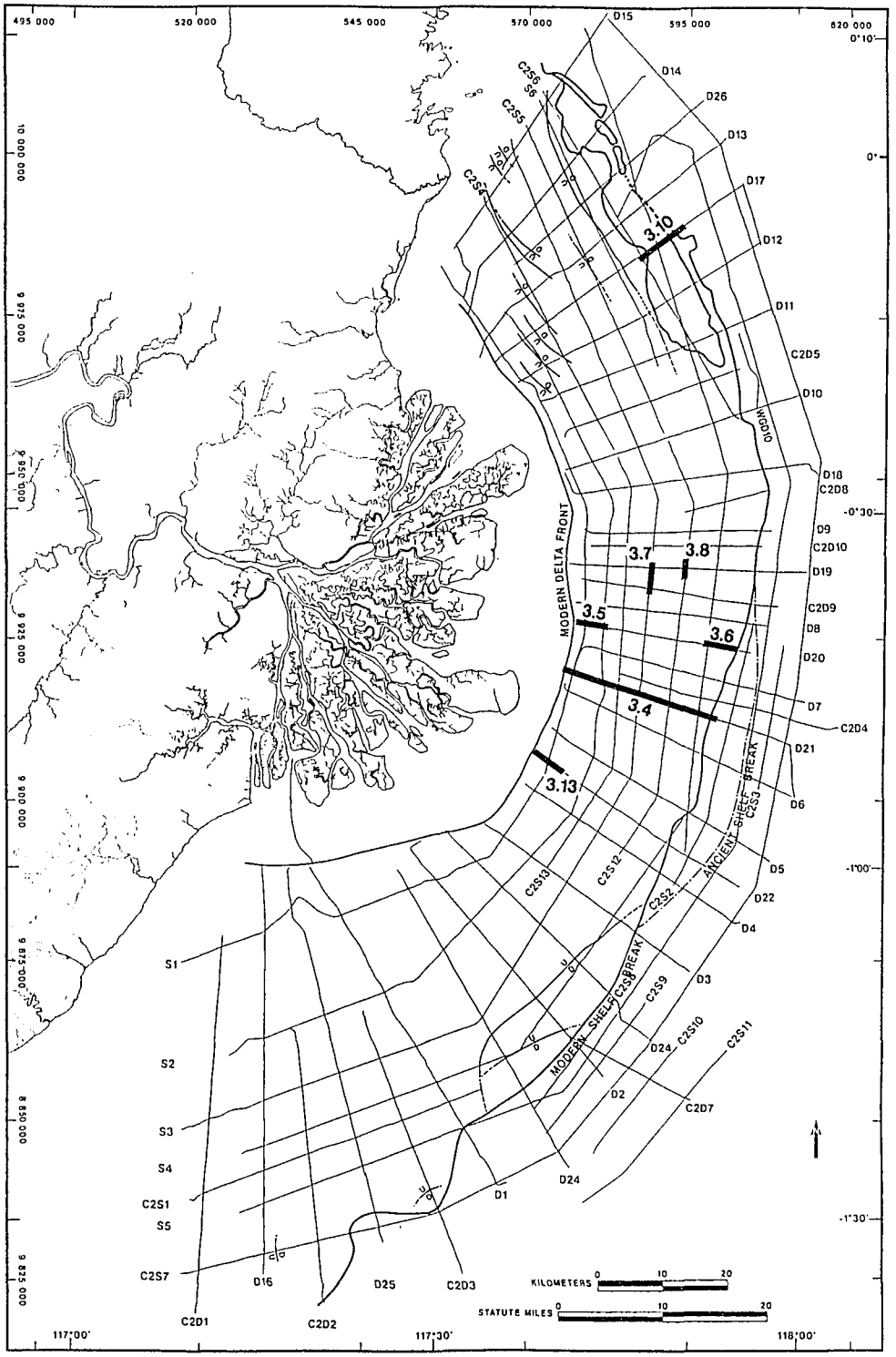

Figure 3.3 Location map of seismic profiles in Figures 3.4 to 3.10. Profiles illustrate pertinent stratigraphic features from the Holocene section.

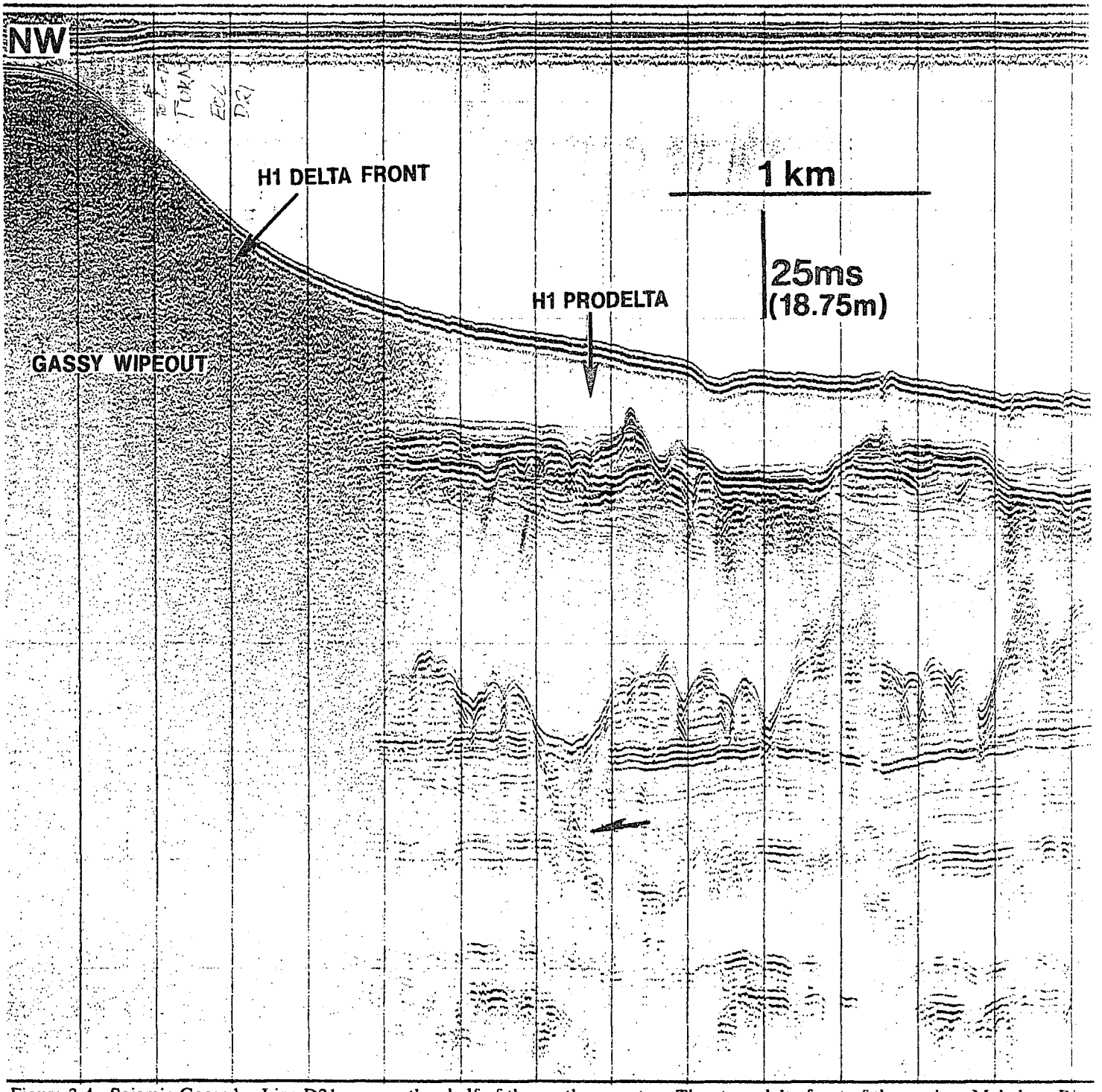

Figure 3.4 Seismic Geopulse Line D21 accross the shelf of the southern sector. The steep delta front of the modern Mahakam Rive
Surface defines the base of the Carbonates. Downlap surface DLP1 has characteristics very similar to the modern sea f
Cycle. Note gentle folding of underlying P2 deposits. Originally onlapping horizontal strata have apparent landward c

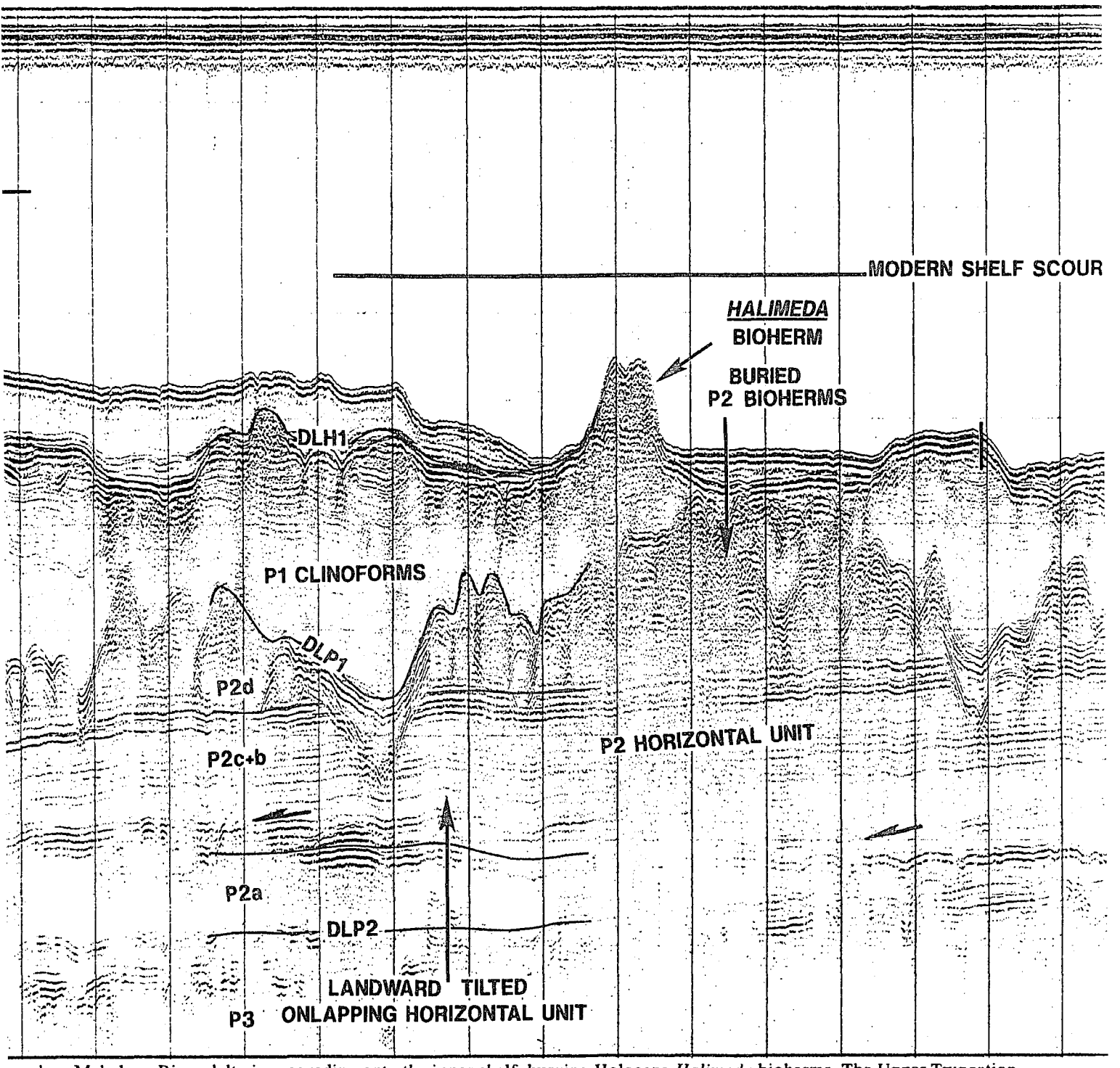

modern Mahakam River delta is prograding onto the inner shelf, burying Holocene *Halimeda* bioherms. The Upper Truncation
ilar to the modern sea floor (Surface DLH1). DLP1 to DLH1 define the lower and upper bounding surfaces of the P1 Depositional
ıve apparent landward downlap due to deformation.

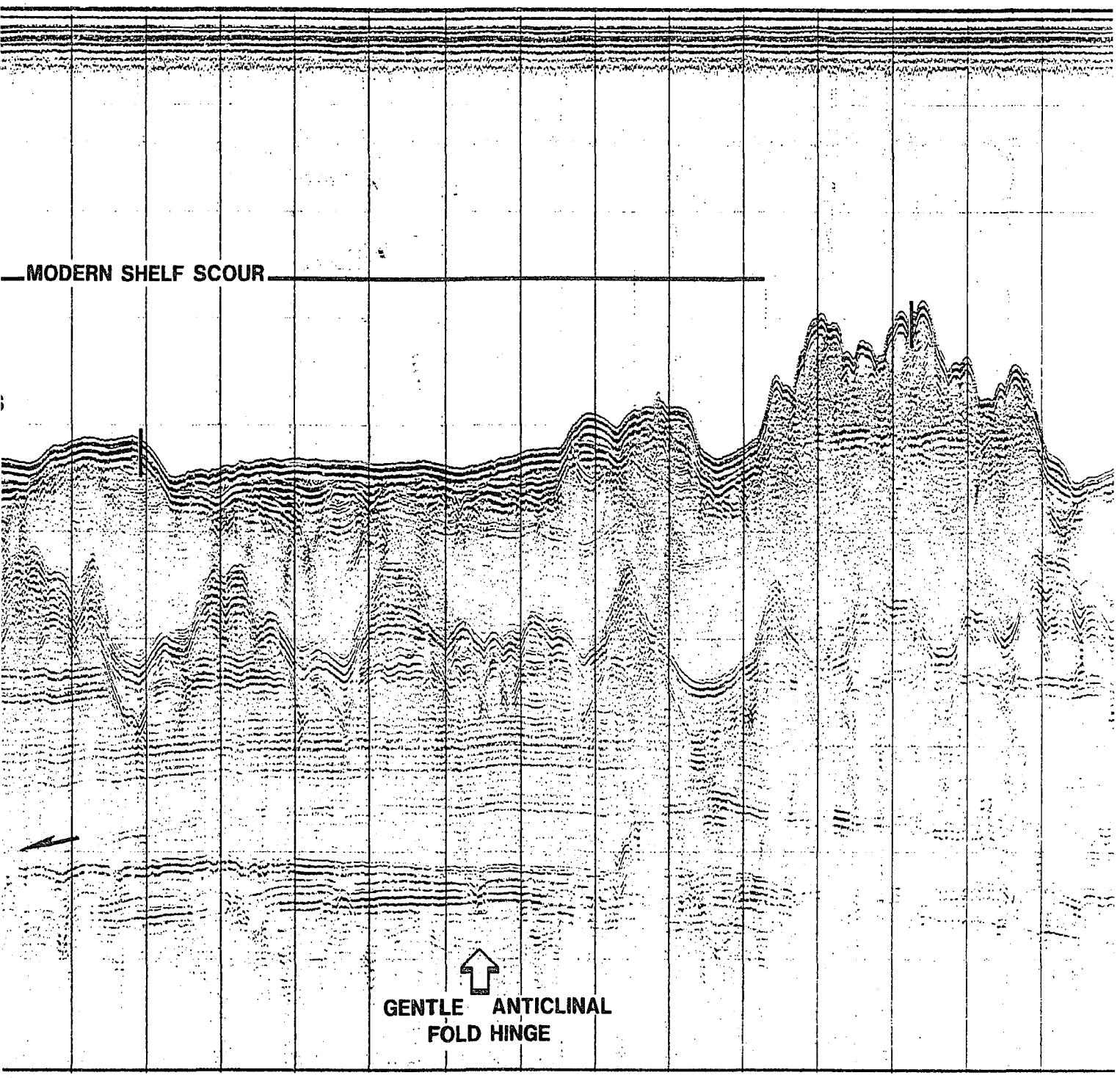

The Upper Truncation
ces of the P1 Depositional

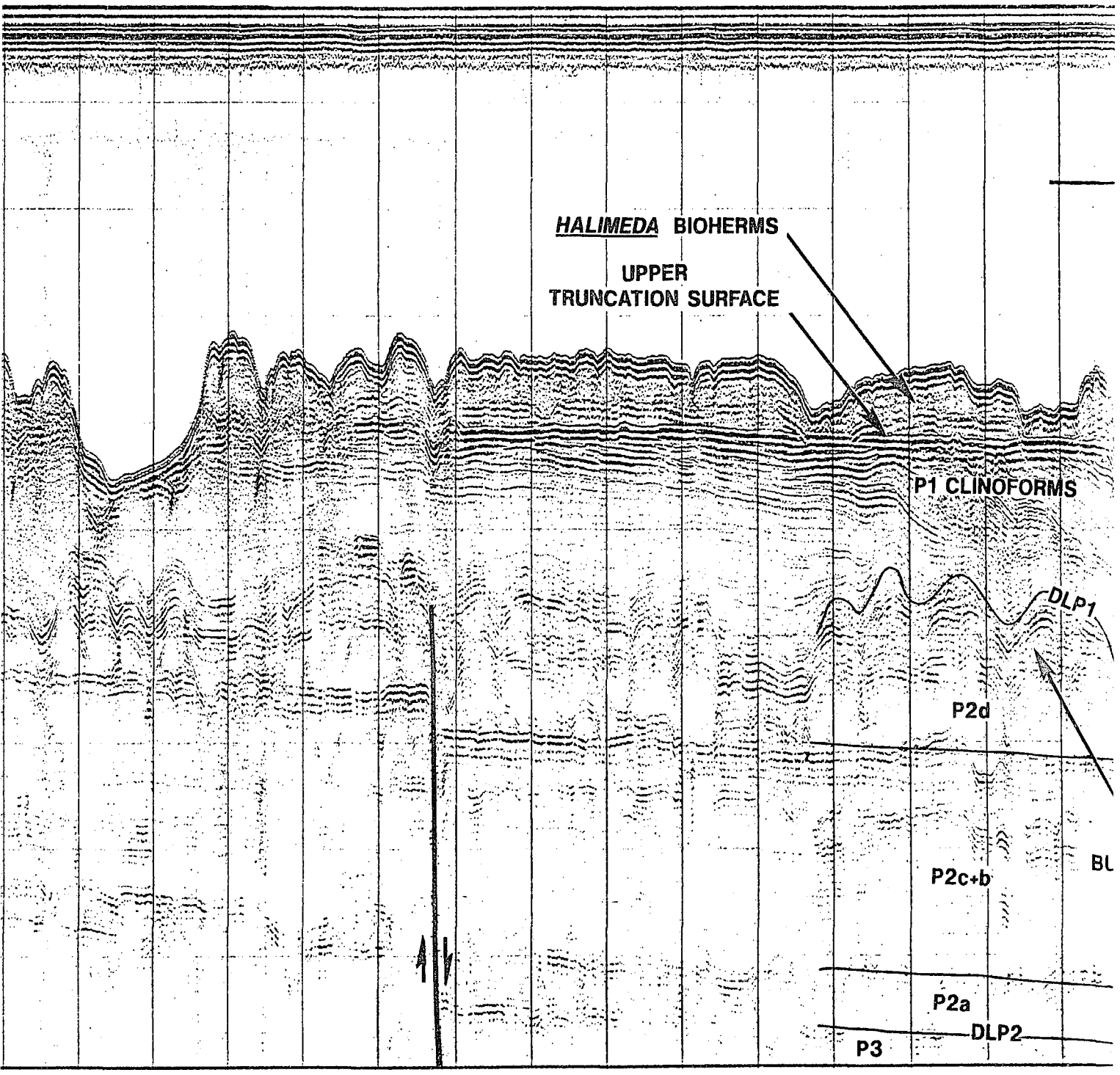
HALIMEDA BIOHERMS
UPPER
TRUNCATION SURFACE
P1 CLINOFORMS
DLP1
P2d
P2c+b
BL
P2a
DLP2
P3

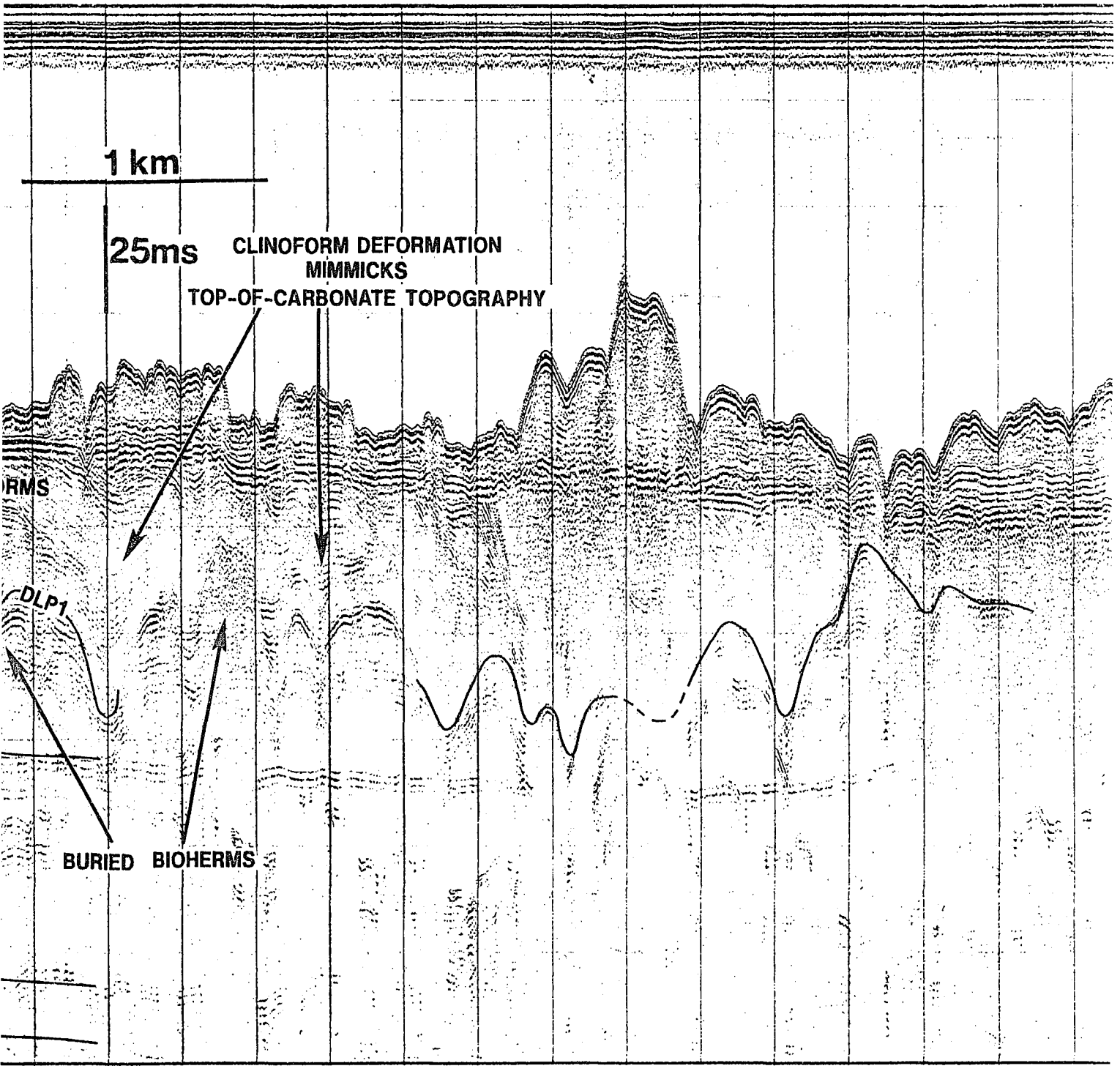
1 km
25ms
CLINOFORM DEFORMATION
MIMMICKS
TOP-OF-CARBONATE TOPOGRAPHY
RMS
DLP1
BURIED BIOHERMS

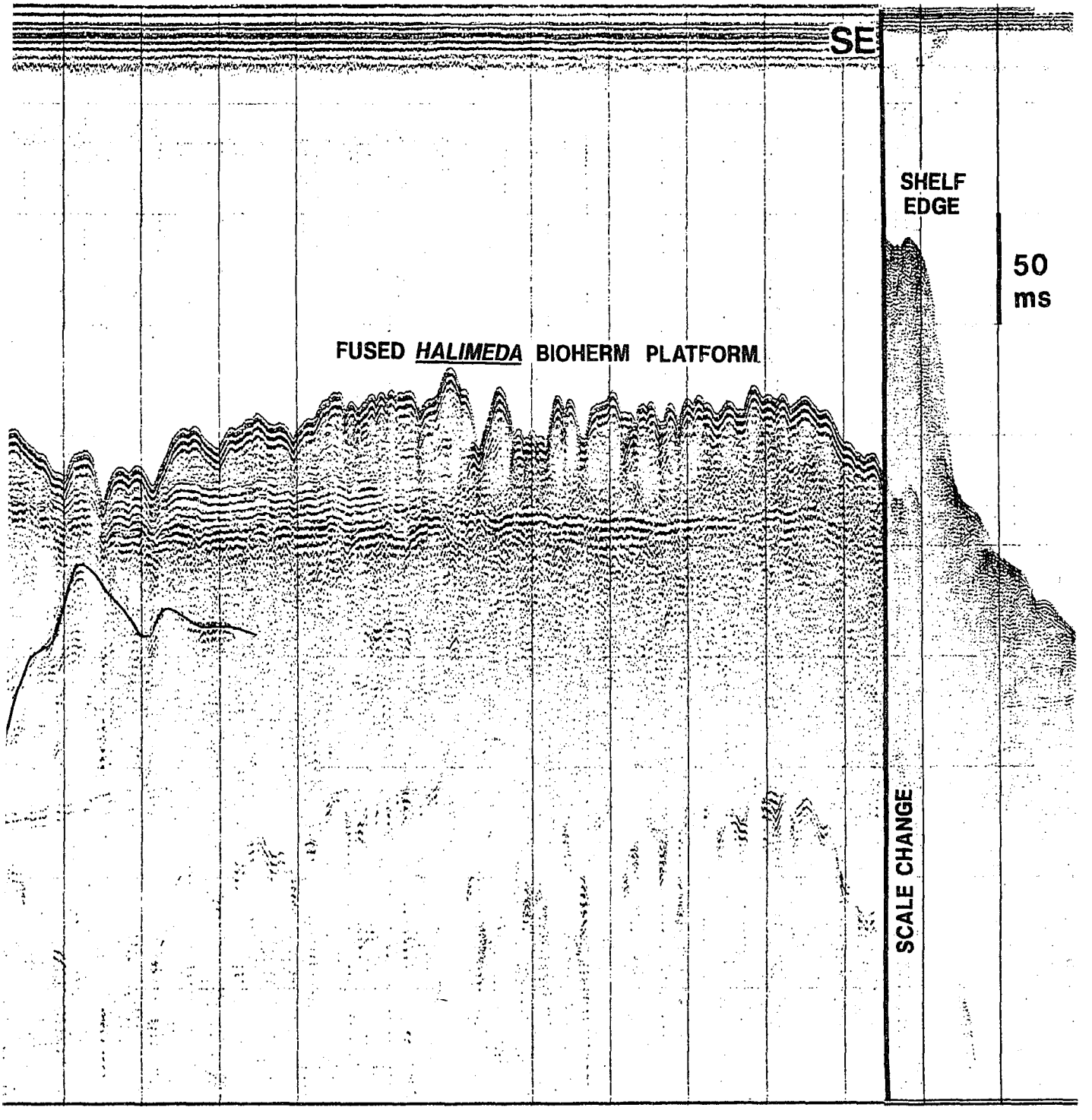
SE
SHELF
EDGE
50
ms
FUSED *HALIMEDA* BIOHERM PLATFORM
SCALE CHANGE

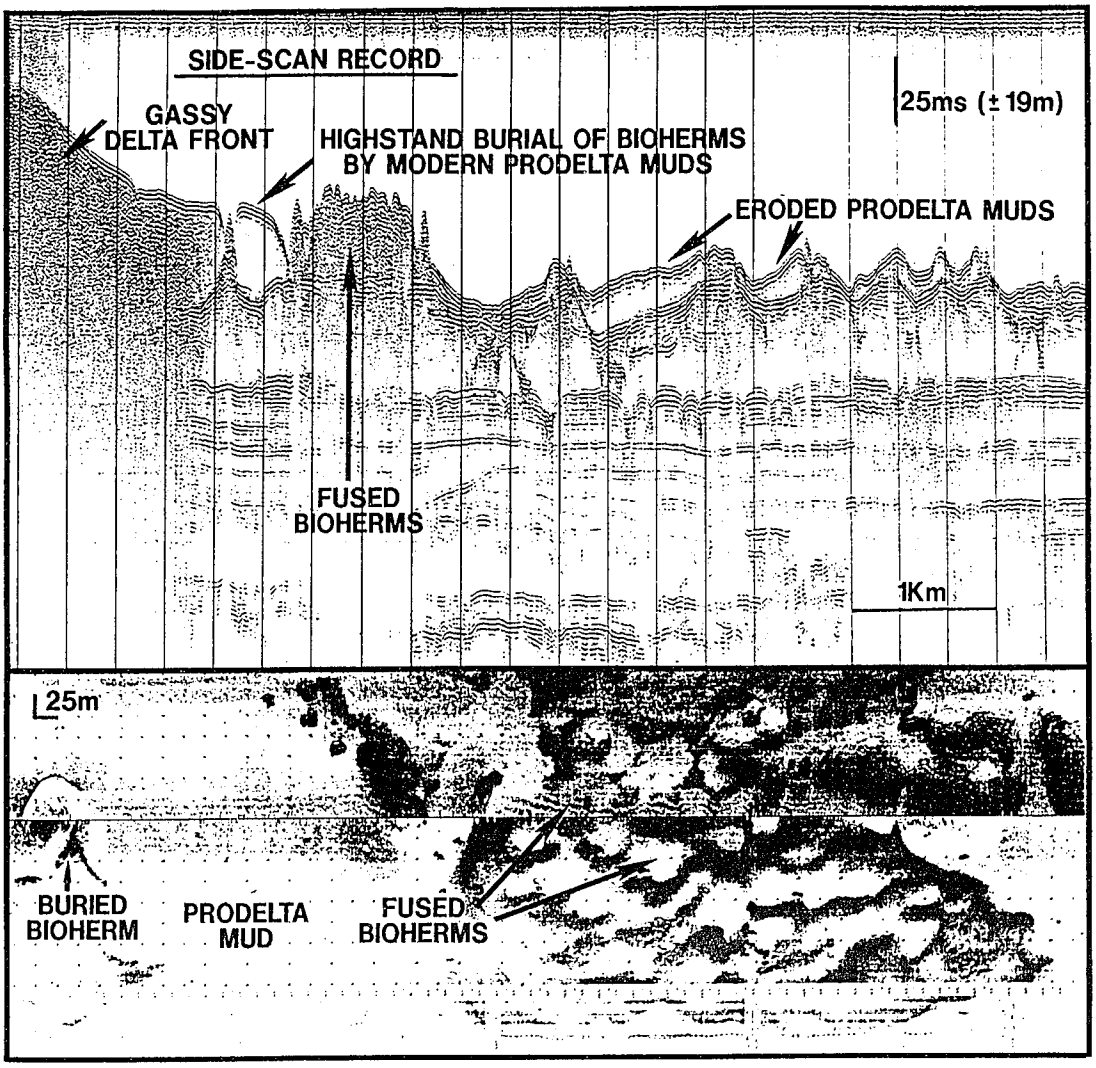

Figure 3.5 Seismic Geopulse and side-scan-sonar image Line D20, inner shelf. The modern delta is burying shelf bioherms. Fused bioherms form distinctive mounded topography clearly visible on side-scan images. The prodelta apron is poorly developed in the central sector of the shelf due to scour by the southflowing Indonesian Throughflow current.

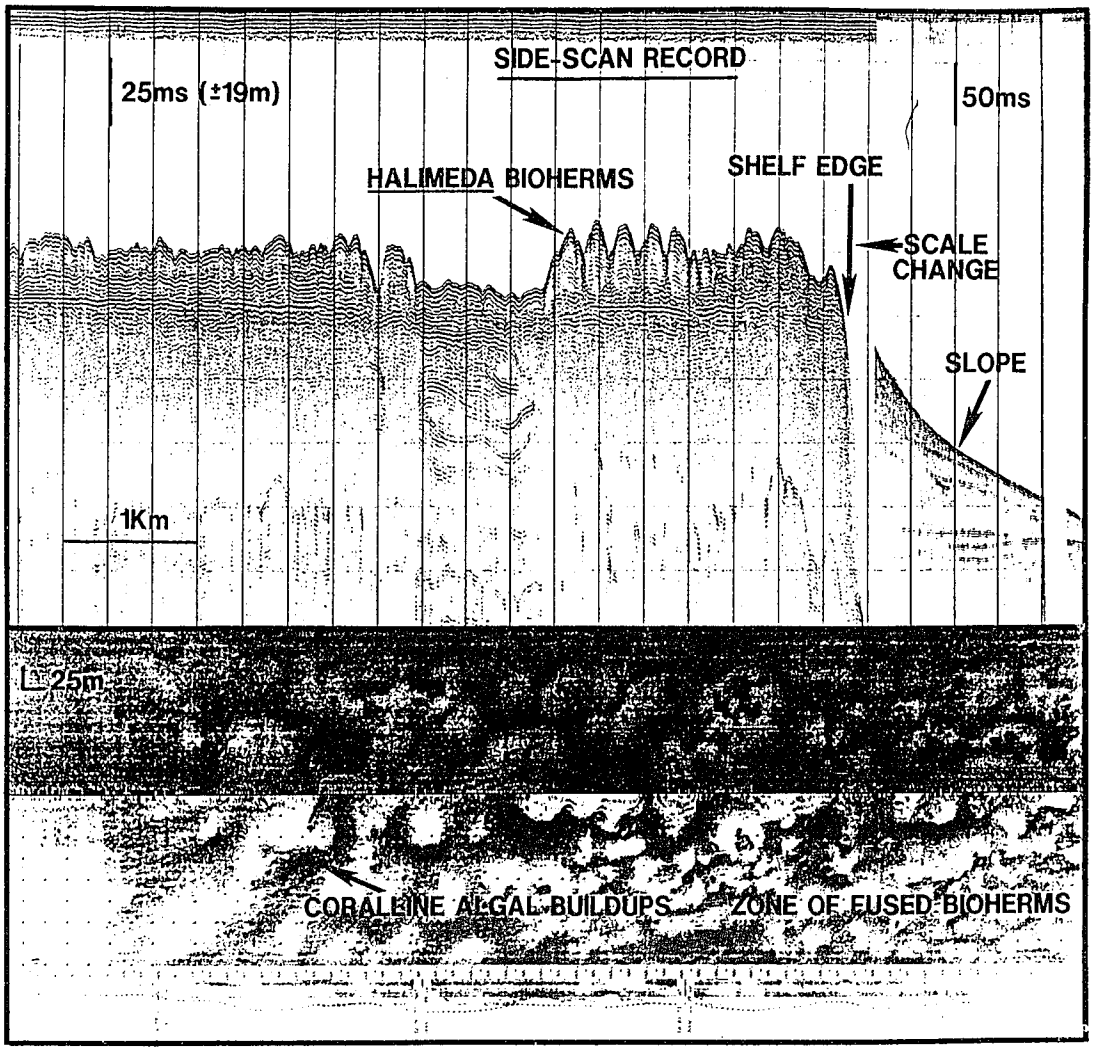

Figure 3.6 Seismic Geopulse and side-scan-sonar image Line D20, outer shelf. Extensive platforms of fused *Halimeda* bioherms cover large portions of the outer shelf, central and northern sectors. Note partial to complete acoustic attenuation beneath the bioherms. Local "hard" returns are probably coralline-algal buildups.

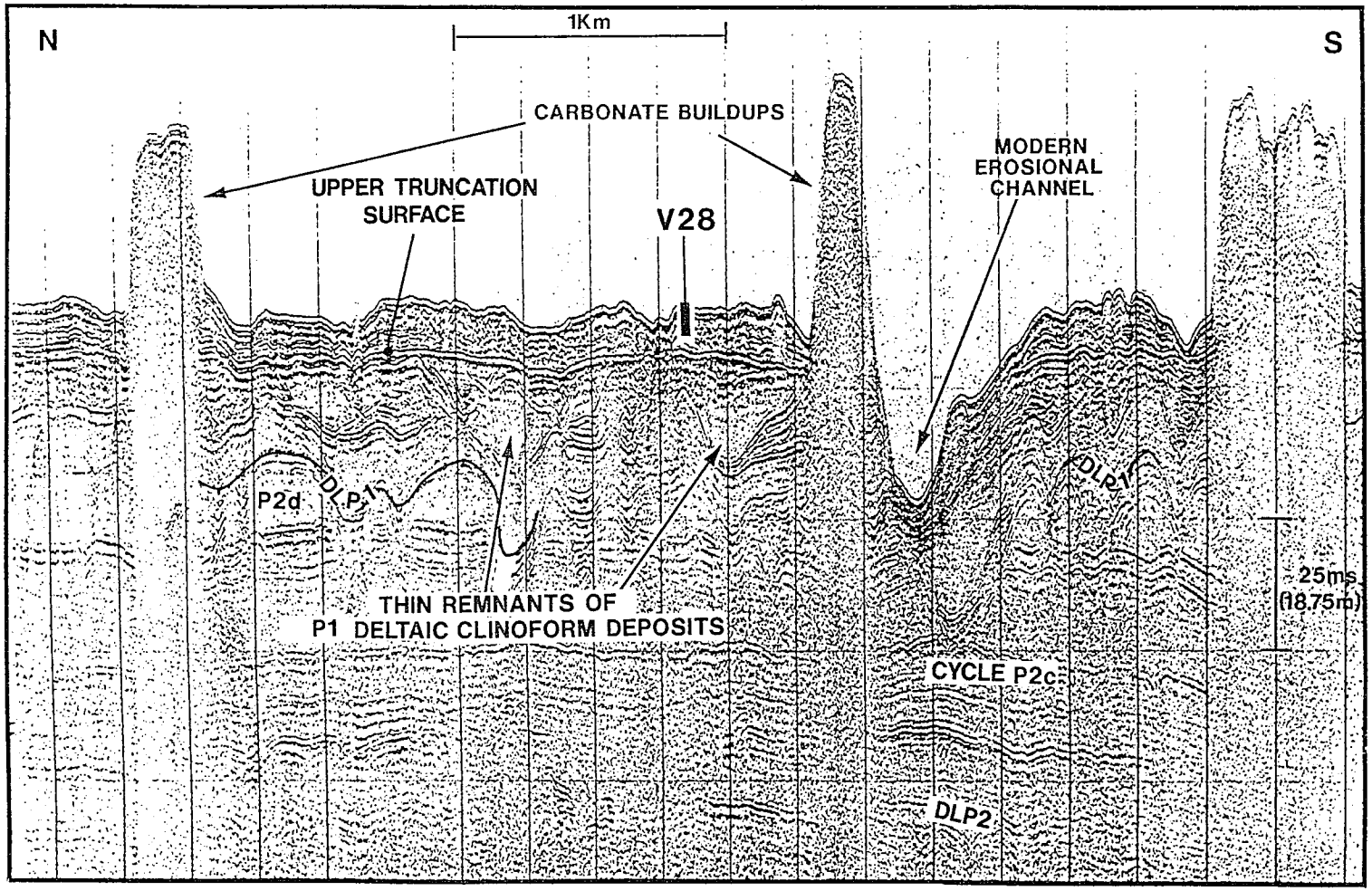

Figure 3.7 Seismic Geopulse Line S3, inner shelf of central sector. Bioherm coverage on the inner shelf is not as extensive, regions of sediment starvation or scour are interspersed by Halimeda pinnacles more than 30 m tall. Note shelf scour channel which has reoccupied the location of an older, filled shelf scour channel associated with Surface DLP1

commonly a planar surface (Upper Truncation Surface). Bioherms occur as solitary mounds, pinnacles (Figure 3.4 inner shelf, 3.7), or have fused laterally to form bioherm platforms (Figure 3.4 outer shelf, 3.6). Heights (thicknesses) vary from undramatic sea floor undulations, less than 10 ms (7.5 m), to giant mounds and pinnacles in excess of 50 ms (38 m) and 200 m to several kilometers in width (Figure 3.8).

Vibracores V6, V8, V26, V27, V28, and piston cores P1 to P5 penetrate the top of these mounds (Figure 1.4). The interior of the mounds consists of *Halimeda* wackestone (Figure 3.9). Whole to fragmented *Halimeda* flakes are the dominant constituent, large benthic foraminifera, *Amphistegina* sp, *Tinoporous* spengleri, and *Operculina* ammonoides (Sen Gupta, 1995), are also common, and coralline algal nodules are present (Figure 3.2). The Holocene mounds are loosely packed, white mud and muddy water fill the interstices. Dewatering of sediments during transportation of cores resulted in significant settling and compaction of the sediment column. Bioturbation, although probably present, is difficult to identify in these sediments.

3.1.7 **Shelf-Edge Carbonate Buildups - "Reefs"**

Large reef-like buildups (in excess of 50 ms, commonly 100 ms) occur along the shelf edge of the northern and central shelf (Figures 3.10). Pinnacles 80 to 100 m high are also growing on a 180 m deep terrace, landward of the northernmost reef walls (Figure 3.11). These buildups have "hard" returns on side-scan and are difficult to penetrate with vibracores. In the 3 to 4 m interval sampled by Vibracores V8 to V10 there was no evidence of a cemented framework typical of coral reefs. Encrusting coralline algae occur as nodules, and solitary corals were present. The foram assemblage is typical of Makassar Strait reef communities: *Amphistegina-Tinoporus - Operculina*, similar to the *Halimeda* bioherm assemblage (Sen Gupta, 1995).

3.2 STRATIGRAPHY

The transgressive boundary formed during the Pleistocene to Holocene sea level rise and flooding of the shelf, is represented by a sub-horizontal truncation surface - the

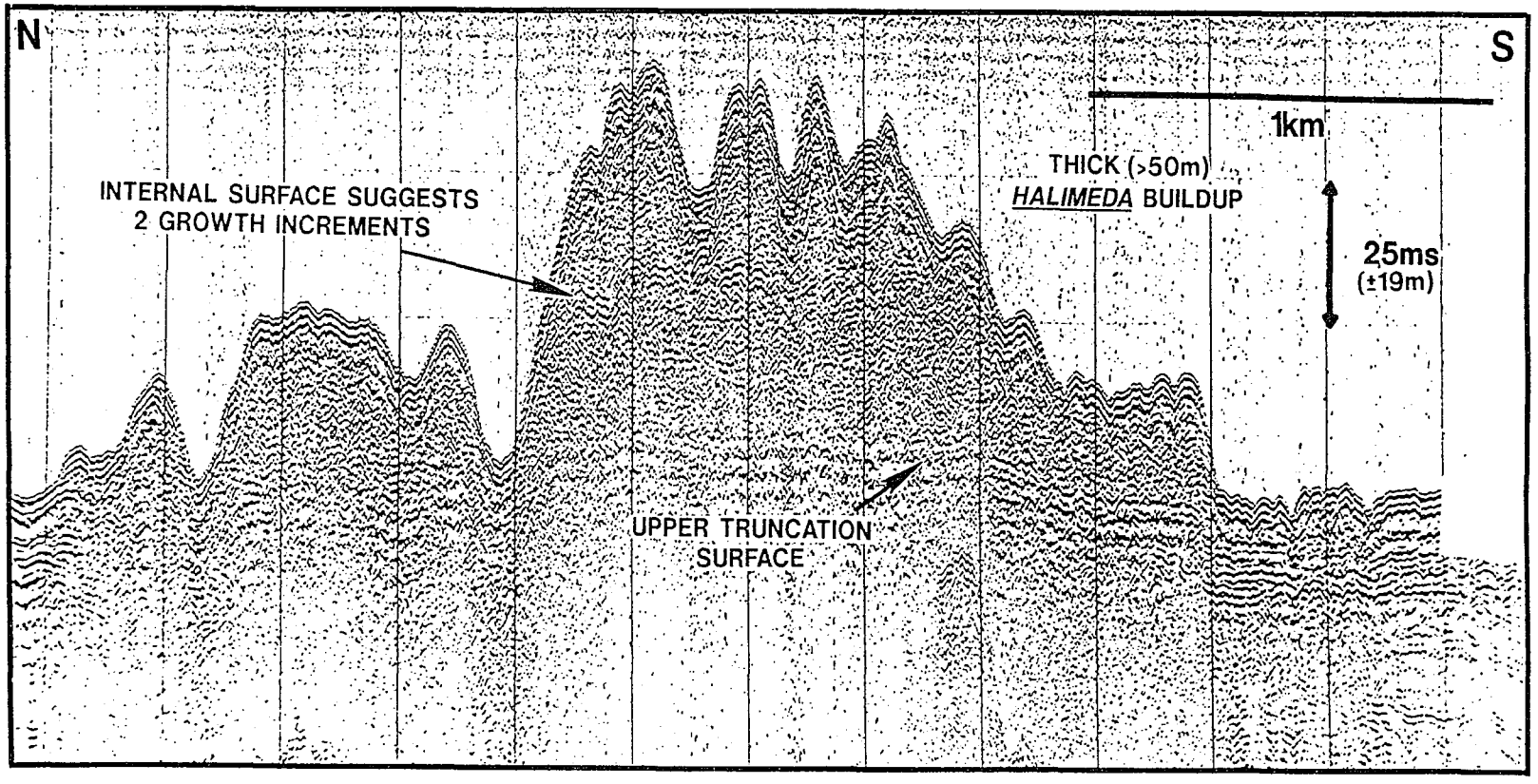

Figure 3.8 Giant Halimeda buildup on the middle shelf of the central sector.

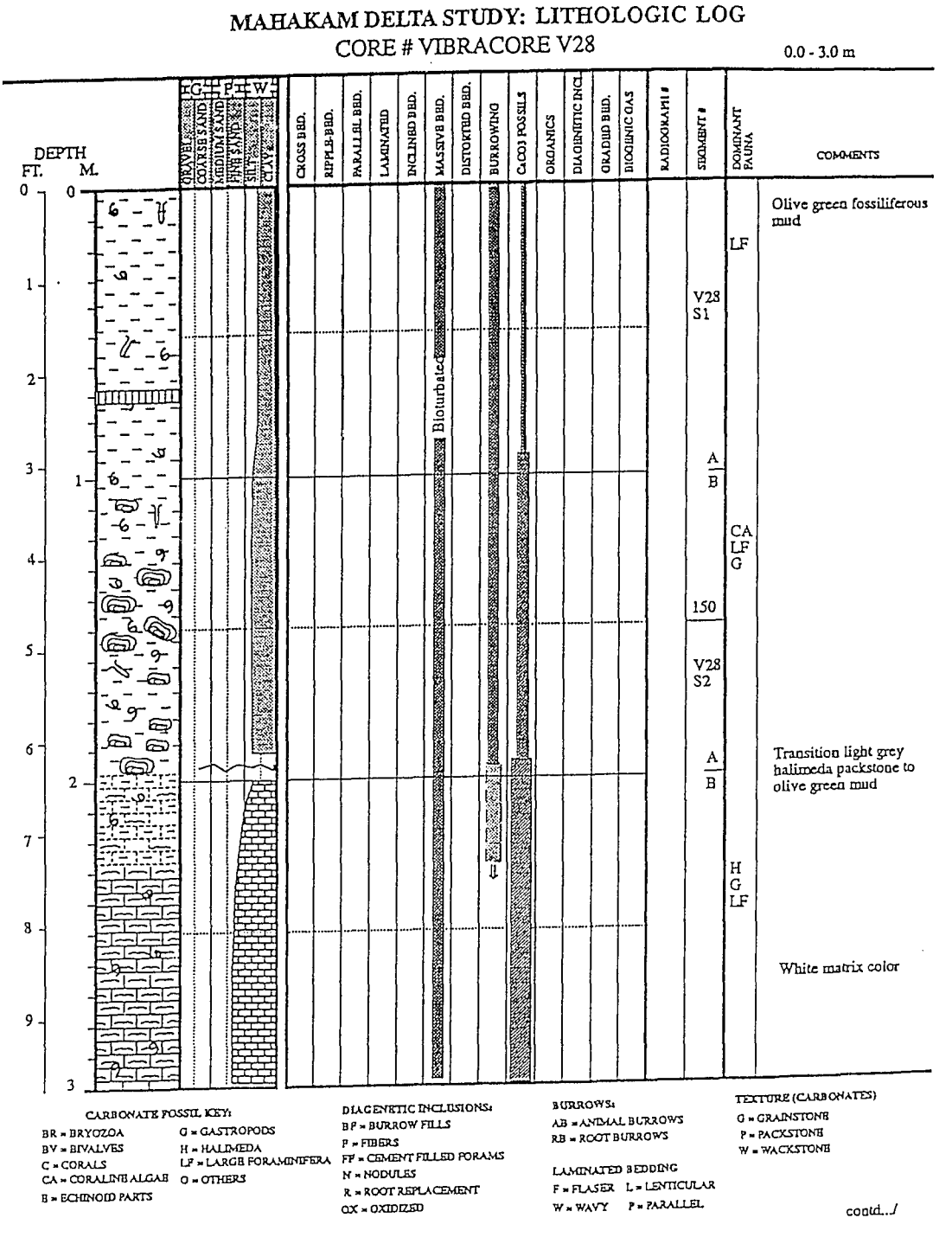

Figure 3.9 Representative lithologic log of the upper *Halimeda* bioherm stratigraphy which illustrates the transition from *Halimeda* wackestone to fossilliferous shelf mud in the top meter. Key to lithologic symbols in the Appendix. Figure continued on next page.

MAHAKAM DELTA STUDY: LITHOLOGIC LOG

CORE # VIBRACORE V28

3.0 - 4.83 m

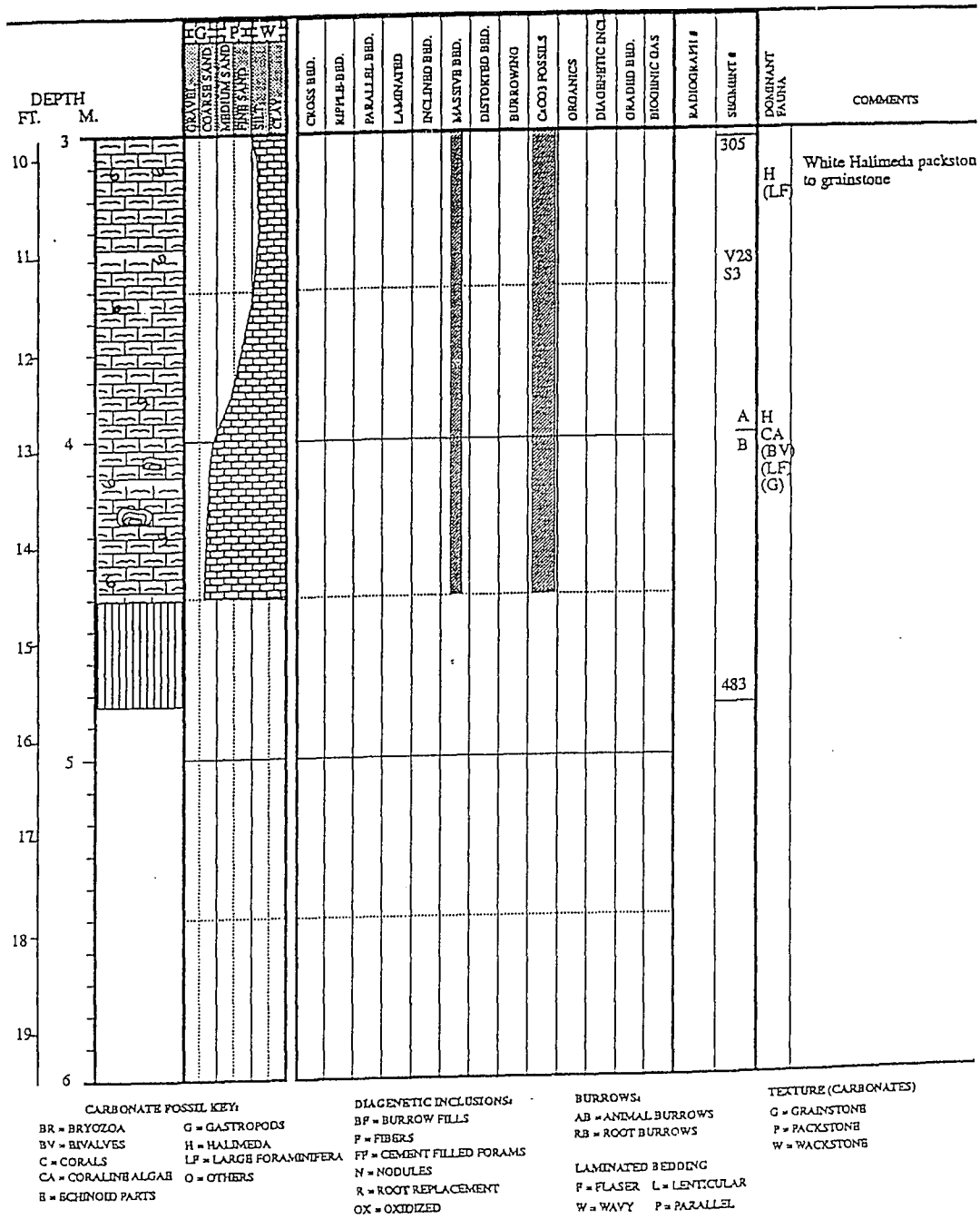

CARBONATE FOSSIL KEY:
BR = BRYOZOA
BV = BIVALVES
C = CORALS
CA = CORALINE ALGAE
E = ECHINOID PARTS
G = GASTROPODS
H = HALIMEDA
LF = LARGE FORAMINIFERA
O = OTHERS

DIAGENETIC INCLUSIONS:
BF = BURROW FILLS
F = FIBERS
FF = CEMENT FILLED FORAMS
N = NODULES
R = ROOT REPLACEMENT
OX = OXIDIZED

BURROWS:
AB = ANIMAL BURROWS
RB = ROOT BURROWS

LAMINATED BEDDING
F = FLASER L = LENTICULAR
W = WAVY P = PARALLEL

TEXTURE (CARBONATES)
G = GRAINSTONE
P = PACKSTONE
W = WACKSTONE

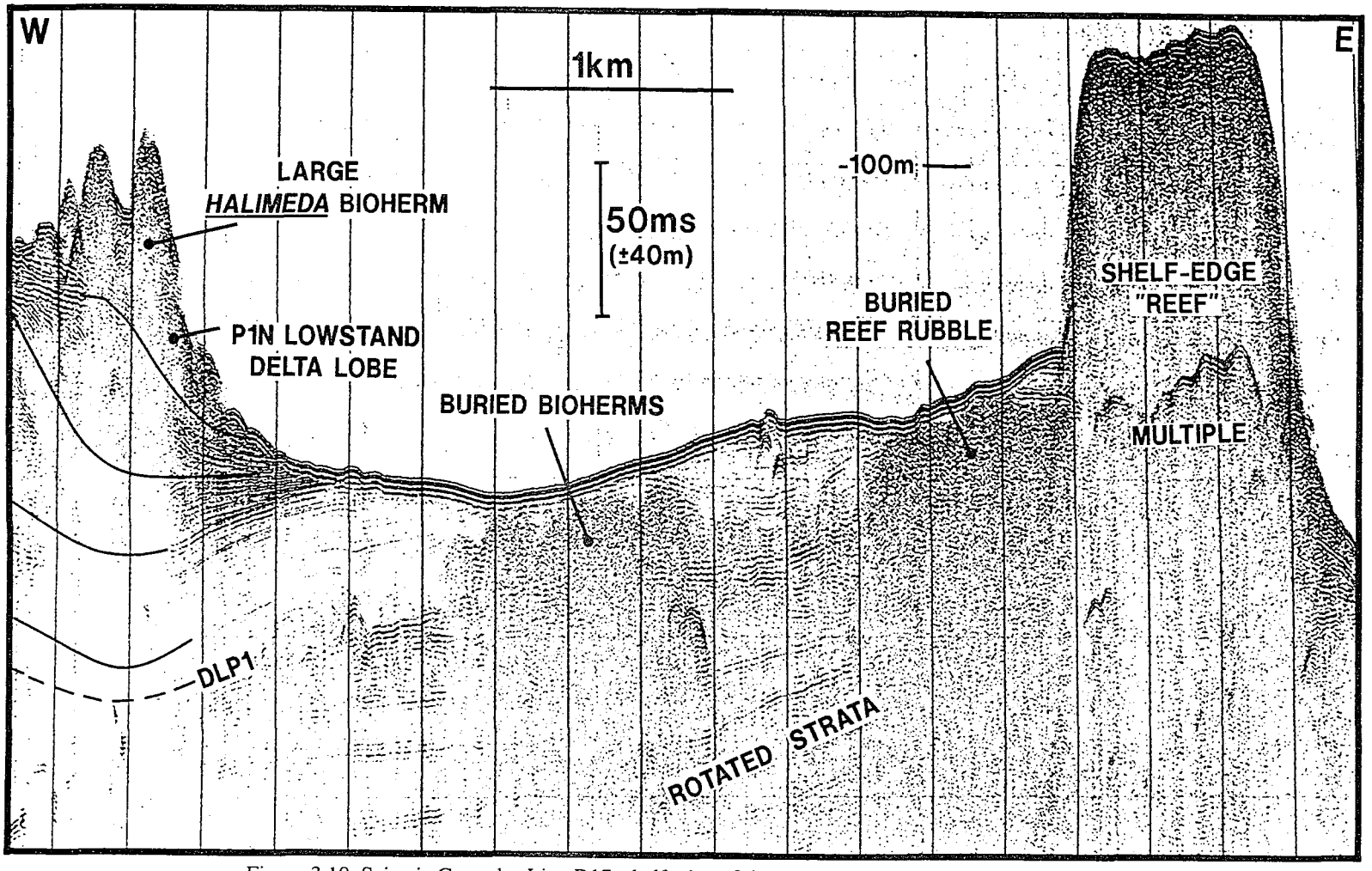

Figure 3.10 Seismic Geopulse Line D17, shelf edge of the northern sector. Cross section through a reef-like wall along the outer edge of a downfaulted, rotated fault block.

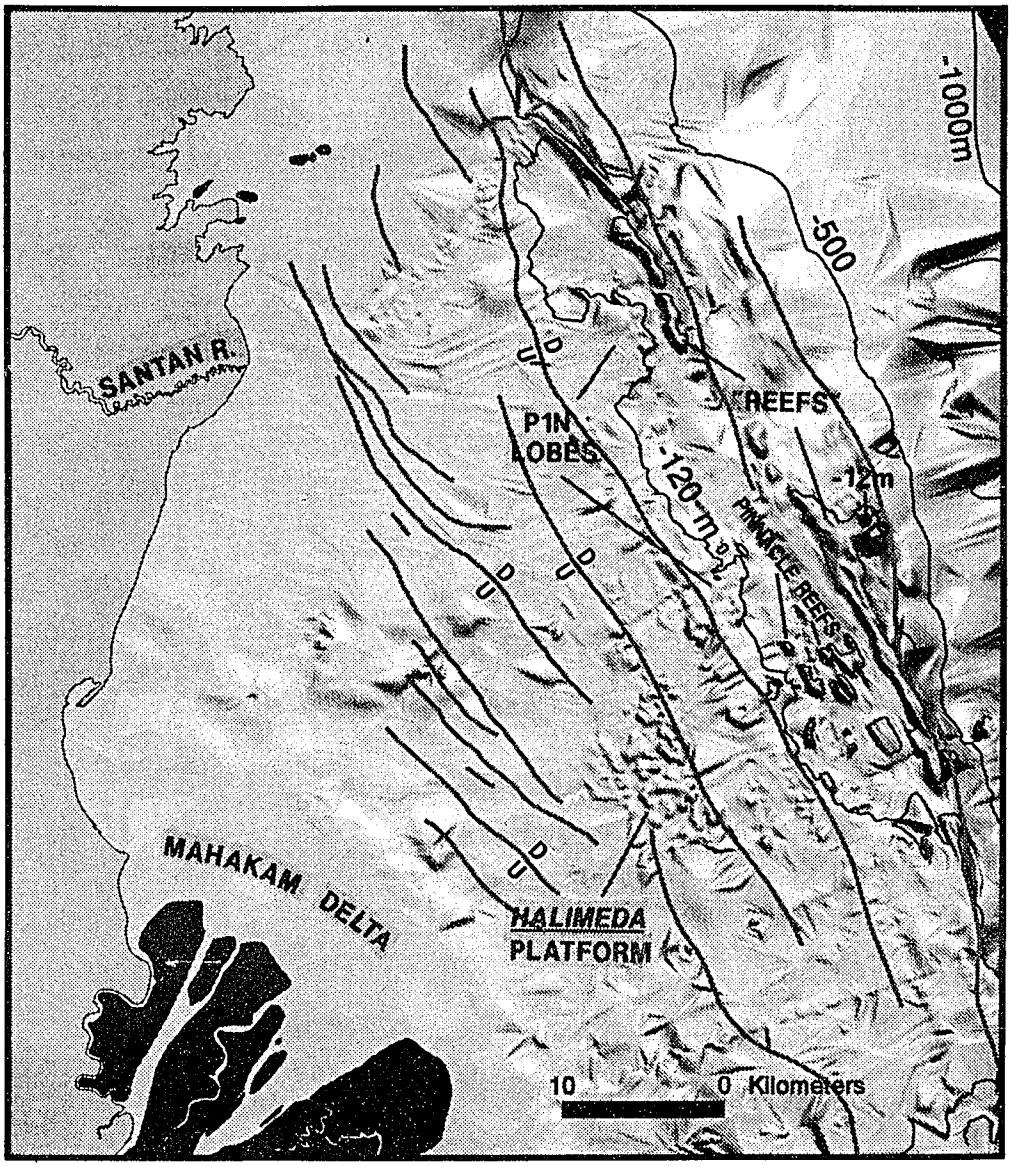

Figure 3.11 Shaded relief representation of the northern sector shelf illustrating the reef-like trends. Reef trends occur along the seaward edge of a large, downfaulted and rotated shelf block. Abundant faulting of the northern shelf influences distribution of northern lowstand depocenters.

"Upper Truncation Surface" (Figure 3.4), that bevels off the top of the youngest shelf-edge clinoform depocenter (discussed later). Vibracores through this surface (V5, V7, V17-19, V23 and V25) reveal non-marine deposits below (delta plain), and marine above (Figures 3.2m-n). The age of this surface, between ± 15 and 5 ka, is inferred from similar surfaces on shelves in other parts of the world which have been radiometrically dated (eg. Matthew's, 1990). A shell lag above, and plant organics below this surface will provide material for future dating.

The two major stratigraphic components above the transgressive surface are: 1) the Holocene Mahakam Delta platform on the inner to middle shelf; and 2) Carbonate buildups on the middle to outer shelf (Figure 3.1). The remainder of the shelf and upper slope are regions of sediment starvation or scour. Figure 3.12 is a schematic cross section from the modern delta apex to shelf edge, showing the basic Holocene stratigraphic framework. Onshore stratigraphy is based mainly on the work of Allen et al. (1979), with additional input from the MISEDOR drilling project (Carbonel and Moyes, 1987; Gayet and Legigan, 1987) and vibracores from this study. Stratigraphy of the delta front and offshore is from seismic profiles and cores acquired during the present study.

3.2.1 **Modern delta stratigraphy- H1 lobe**

The modern delta is up to 50 m thick beneath the outermost platform. Prodelta deposits at the base are 10 to 20 m thick, and thin landward. Delta front deposits are volumetrically the most important, up to 40 m thick beneath the outer platform, and also thin landward. A 10 m thick subtidal platform unit overlies the delta front. The delta succession is capped by 3 to 4 m of delta plain swamp deposits (Figure 3.12). Most of the landward thinning is accounted for by the prodelta and delta front deposits. There are no cores that penetrate the entire Holocene section of the proximal delta plain.

The seaward thinning prodelta apron attains maximum offshore extent in the southern sector, and to a lesser extent, on the northern shelf, but pinches out within 10

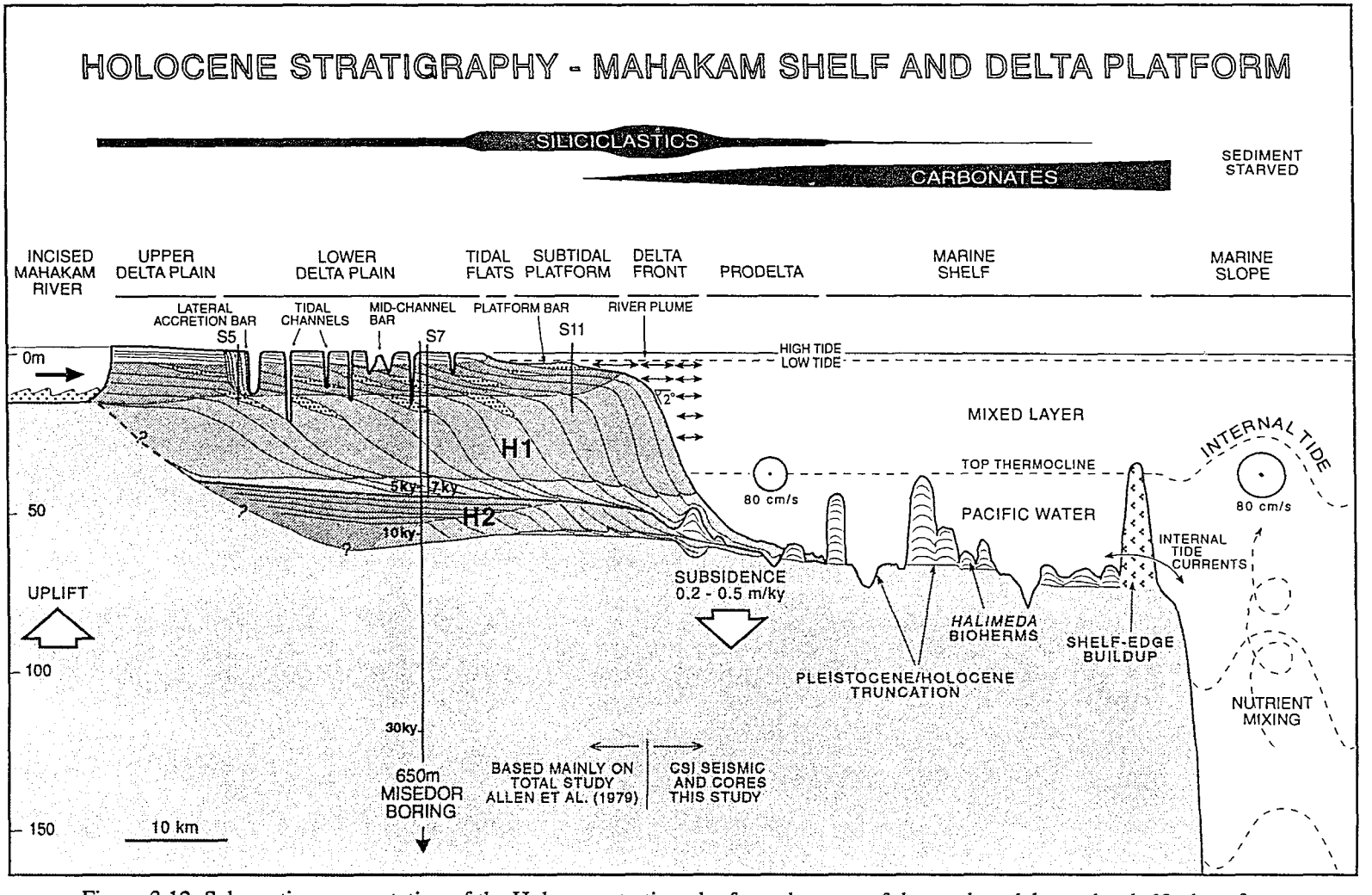

Figure 3.12 Schematic representation of the Holocene stratigraphy from the apex of the modern delta to the shelf edge of the central sector, scale is approximate. S5, S7 and S11 are TOTAL borings (Allen et al, 1979).

km of the delta platform edge in the central sector (Figure 3.1). The delta front has a gentle arcuate shape in plan view, with no obvious multi-lobed structure related to location of active distributaries (Figure 1.2).

Almost the entire delta platform consists of mud. Sands are restricted to fluvially dominated distributary channels and as bars on the subtidal platform in the vicinity of active distributaries. Sand bars were also found off the tidally dominated central sector of the delta plain. Allen et al. (1979) proposed that these latter bars are relict features of an abandoned fluvial distributary.

3.2.2 **Early Holocene delta - H2 lobe**

An earlier Holocene progradational delta cycle is partially exposed beneath the modern delta front (Figure 3.13). Clinoforms of the H2 lobe downlap the Upper Truncation Surface, and are in turn truncated by a planar surface interpreted as the product of seafloor ravinement processes. Clinoforms of the modern H1 lobe downlap onto the truncated H2 lobe. Vibracore V24 through the top of the H2 lobe contains medium gray laminated mud similar to the modern outer delta platform/upper delta front. The only evidence of fauna occurs in large burrows originating at the modern sea floor.

The truncation surface separating the H1 and H2 lobes occurs at 40 m depth. Clinoform topsets of the H2 lobe were quite close to sea level at time of deposition. The present sea level highstand was attained about 5 ky ago (Aharon and Chapell, 1986; Matthews, 1990). Prodelta sediments dated at 5-7 ka (when sea level was at or near the present level) at 50 m depth in the MISEDOR core are probably correlative with the H1 prodelta deposits on top of the H2 lobe. Even though subsidence rates are fairly high (0.2-0.35 m/ky) the elevation of the H2 lobe suggests deposition during a period of substantially lower-than-present sea level. Delta plain deposits dated at 10 ka in the MISEDOR core may correlate to the H2 deposits, an age that corresponds to the Younger Dryas climatic reversal. The Younger Dryas event interrupted the Pleistocene

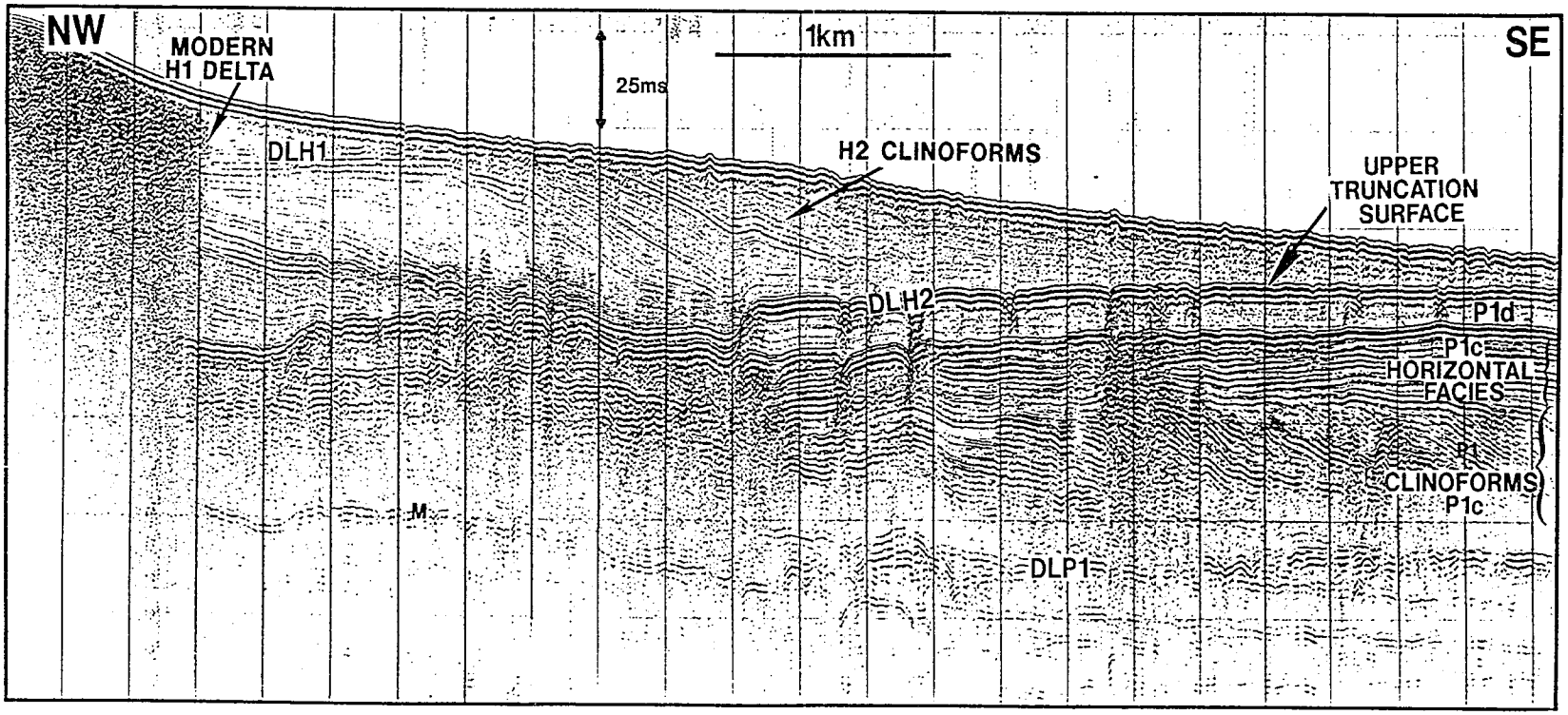

Figure 3.13 Seismic Geopulse Line D22 illustrating truncated clinoforms of the early Holocene H2 lobe downlapped by the prograding front of the modern H1 delta.

to Holocene deglacial trend, and potentially reversed, or at least slowed down the rate of eustatic rise at about the 10-12 ka time frame.

3.2.3 **Carbonate stratigraphy**

The dominant carbonate facies are the *Halimeda* bioherms. *Halimeda* bioherms occur on the outer to middle shelf of the central sector, and mainly the outer shelf of the northern sector (Figure 3.1). Bioherms fuse to form extensive platforms, commonly more than 20 m thick. The upper portions of almost all the *Halimeda* bioherm core sites have a steady matrix-color change from white/light gray to dark-gray/olive-green, that signifies an increasing terrigenous content. Within the top meter there is a dramatic decrease in *Halimeda* particles, and an increase in coralline algal nodules, bivalve and gastropod shells, and terrigenous mud (Figures 3.2j, 3.9). The foram assemblage in this upper section changes from carbonate to a muddy marine association and are abraded and discolored (Sen Gupta, 1995). Bioherms near the delta front may have some marginal marine species in the upper muddy section. The prograding delta front is burying carbonate buildups on the middle shelf (Figure 3.5).

The thick, reef-like ridges are restricted to the shelf edge in the north and north-central sectors. The northern ridge system is located along the outer edge of a downthrown, rotated fault block. Tops of tall pinnacles on the shelf may show "hard" returns on side-scan images, which suggests a possible cemented carbonate substrate.

3.3 DEPOSITIONAL PROCESSES INFLUENCING THE HOLOCENE STRATIGRAPHY

Allen et al. (1979) have published detailed accounts of the depositional processes that influences delta platform stratigraphy, especially those processes that are related to sand deposition and distribution within distributaries and on the sub-tidal platform. The first part of this section will briefly outline the processes of the delta platform that differ from more commonly studied fluvial and wave dominated deltas, and which have bearing on interpretation of the ancestral Pleistocene deltas. A

discussion on depositional processes that influence the shelf regions seaward of the delta front follows.

3.3.1 **Depositional Processes on the Delta Platform**

3.3.1.1 Tidal influence on sediment distribution

Although seasonal flooding cycles may influence sediment transport to the coast, sediment redistribution onto the delta plain is not controlled by river flood cycles. The fluvial distributaries do not have levees, and river floods in the delta are not severe. Elevation of the delta plain is controlled by mean high tide, and is about 2 m above mean sea level. The delta plain therefore floods once a day during the spring-tide phase. Suspended-load sediments are transported within the tidal prism and effectively redistributed across the entire delta plain.

Fluvial distributaries switch location through time. The southern distributaries are the most active. The northern distributaries are in a waning phase and have slightly flared inlets. A major distributary apparently traversed the central sector of the delta plain, depositing sand bars on the subtidal platform, its location now obscured by numerous tidal channels (Allen et al., 1979). The delta plain has receded somewhat in this central sector, and tidal channels have very broad, flared inlets. Such distributary switching affects the location of sand facies on the delta platform. However, the large scale abandonment and imbricate stacking of lobes that is associated with lobe switching in river dominated deltas (Coleman and Gagliano, 1964) probably does not occur in the Mahakam delta. There is no obvious multi-lobate structure to the delta front that can be related to higher depositional rates in the vicinity of active distributaries.

3.3.1.2 Limited Sand Distribution

Sand deposition is confined to the distributary channels and to the subtidal platform in the vicinity of the distributary inlets. Very little, if any, sand is transported to the delta front. Multiple bifurcations across the broad, flat delta plain reduces the

hydrological efficiency of channel flow. The salt wedge and associated residual two-layered circulation therefore penetrate far upstream and limits bedload transport in the lower channel sections. As the delta plain grew through the Holocene highstand period, so too did the volume of the tidal prism, the lengths of distributary channels, and number of channel bifurcations. The impact of tides on sediment dispersal therefore probably increased throughout the Holocene.

3.3.1.3 Sediment Distribution on the Subtidal Platform and Delta Front

Location of distributary channel inlets does not have a major influence on local delta front progradation rates. The overall smooth arcuate shape of the delta front suggests that the delta is prograding along the entire length of the front. Clay-rich sediments which flocculate at the fresh/salt water interface in the distributaries, together with organics produced in the delta plain, are redistributed across the entire sub-tidal platform and delta front by tidal currents and dispersive buoyancy forces acting on the low density river plume. Tidal currents probably diminish significantly on the delta front due to the deeper water column.

3.3.1.4 Controls on delta-facies thickness

Thickness of Holocene depositional units is controlled by water depth and additional accommodation created by syndepositional substrate compaction and subsidence. The delta plain is only 3-4 m thick, and implies an average accretion of only 1 to 1.5 mm/yr during the last 5 to 7 ky (Figure 3.12). Tidal channels are highly sinuous and it is not known if these represent migrating meanders. If meandering occurs then it is plausible that the dense network of tidal channels continuously rework and renew the thin delta plain cover. The supply of fluvial fines and locally produced organics (nipa and mangrove) that exceed accommodation volumes created by subsidence are exported to the subtidal platform and delta front by tidal processes.

Depositional water depths on the subtidal delta platform are less than 5 m. However, the thickness of subtidal platform deposits in TOTAL's borings is about 10 m,

which indicates substantial increase in accommodation due to compaction of the underlying delta front wedge (Allen et al., 1979)(Figure 3.12).

The large accommodation space, and reduced tidal currents due to the deeper water column on the delta front, results in high depositional rates on this steep outer edge of the delta platform. The high organic content and anoxic conditions suggest rapid sedimentation rates. Allen et al. (1979) estimates an average Holocene progradation rate of 5 m/yr. There is no evidence of slope failure and mass wasting on the steep delta front, a common feature of mud dominated delta systems (e.g. Roberts, 1980; Prior et al. 1986).

3.2.2 **Modern Shelf Processes**

3.2.2.1 Prodelta

Distribution of both prodelta sediments and carbonates is apparently influenced by the strong southerly Indonesian Throughflow current which sweeps across the shelf. Modern delta deposits extend less than 10 km seaward of the delta platform edge in the central sector. Seismic profiles show evidence of active scour of the delta-platform toesets in the central sector (Figure 3.5) . Protrusion of the delta platform obstructs the south flowing Throughflow current, and creates a lower energy lee environment to the north and south. Prodelta deposits accumulate in these lower energy regions (Figure 3.1). Platform current meter moorings indicate that the Throughflow current impinge on the N-S trending central sector of the delta front (mooring A, Figure 1.10), whereas weaker, variable direction flows occur in the lee of the platform further south (mooring B, Figure 1.10). Maximum thickness of prodelta sediments is about 15 m on the southern shelf sector.

3.2.2.2 Carbonate Accretion

Halimeda bioherms and erosional topography are closely associated. Bioherms tend to grow on topographic highs of the underlying Upper Truncation Surface, protecting the surface from further scour, and amplifying the erosional relief (Figures

3.5, 3.7). Once *Halimeda* algal meadows are established they baffle the erosional currents (tidal currents and Throughflow current) which results in localized sediment traps within an overall region of scour. Most of the sediments within the mounds, from gravel size to mud, is probably generated in-situ from *Halimeda* plant fragments and associated epifauna. Individual mounds eventually fuse to form carbonate platforms (Figure 3.6).

Algal carbonates are photosynthetic, and thrive in clear, nutrient rich, warm, saline water at photic-zone depths. The Throughflow current is probably important in keeping the water column clear during the period of *Halimeda* growth, diluting and sweeping south the turbid river plume and algal blooms feeding on river derived nutrients. Vertical mixing of nutrients by internal tides and upwelling enriches the usually low nutrient waters of the upper thermocline in the Makassar Strait (Ilahude, 1978; Gordon, 1986; Ffield and Gordon, 1992). Potentially, the Throughflow current would bathe the bioherms in relatively nutrient rich higher-salinity water beneficial to algal carbonate growth. High nutrient concentrations are detrimental to framework reef-building organisms and favor green algal communities (Hallock and Schlager, 1986).

The thin drape of terrigenous mud and low *Halimeda* content across the top of the bioherms indicates that bioherm accretion is not as prolific as it once was. Sometime after the modern delta started prograding onto the shelf, the higher influx of terrigenous sediments and more extensive river plume probably decreased the depth of the photic zone and impacted the *Halimeda* communities. At present the mounds are barely accreting, primarily by incremental deposition of terrigenous mud. Burrowing and currents are reworking the top of the mounds, as evidenced by the abraded nature of faunal remains (Sen Gupta, 1995). It is possible that some of the reef trends on the outer shelf are still active, locally these have accreted to within 20 m of the sea surface.

The Throughflow current is still flowing across the shelf, diluting the river plume, keeping terrigenous muds in suspension, and sweeping these fines off the shelf.

Future dating of *Halimeda* particles will establish their growth rates on the Mahakam shelf, and the timing for terrigenous input which impacted the bioherms. The earliest date of Holocene delta progradation beneath the modern delta plain established by Allen et al. (1979) is 7 ky BP.

CHAPTER 4. PLEISTOCENE STRATIGRAPHY

4.1 PLEISTOCENE STRATIGRAPHIC COMPONENTS AND THEIR SEISMIC CHARACTERISTICS

Characteristics of the Pleistocene stratigraphic components identified in seismic are discussed in the first portion of this chapter. These components are described more or less in the sequential order which they occur within a Depositional Cycle (defined below). Distributions and basic interpretation of depositional environments of identified stratigraphic elements follows. A model synthesising the sequential development of one depositional cycle is covered in the next chapter (Chapter 5). Figure 4.1 schematically illustrates the nature and stratigraphic position of components within a Depositional Cycle, to be used as a guide for this chapter. In defining the stratigraphic components and their seismic characteristics, a considerable number of seismic illustrations are required. These illustrations have been subdivided into sections containing seismic sections from the southern (Figures 4.2 to 4.13), northern (Figures 4.14 to 4.20), and central shelf sectors (Figures 4.21 to 4.23) and the slope (Figure 4.24 to 4.27), each section is preceded by a Figure location map.

4.1.1 Depositional Cycles Bounded By Downlap Surfaces

The most distinct, easily correlated and mappable regional surfaces on the shelf are the Downlap Surfaces (DL), which subdivide the stratigraphy into Depositional Cycles H1, H2, P1, P2, P3 ...etc. (H and P signify Holocene and Pleistocene, respectively). A Downlap Surface is defined by aerially extensive clinoform downlap, commonly onto a regional, high-amplitude reflection event (Figure 4.15). These surfaces are the ancient equivalent of the modern sea floor, which is presently being buried, and downlapped, by the Holocene Mahakam delta lobe (Figure 3.4). Downlap Surfaces may show evidence of erosion at a variety of scales, from less than 5 ms to more than 50 ms (<4 m, >40 m) deep cuts, especially where they are associated with carbonate buildups (Figures 3.7, 4.22). Where

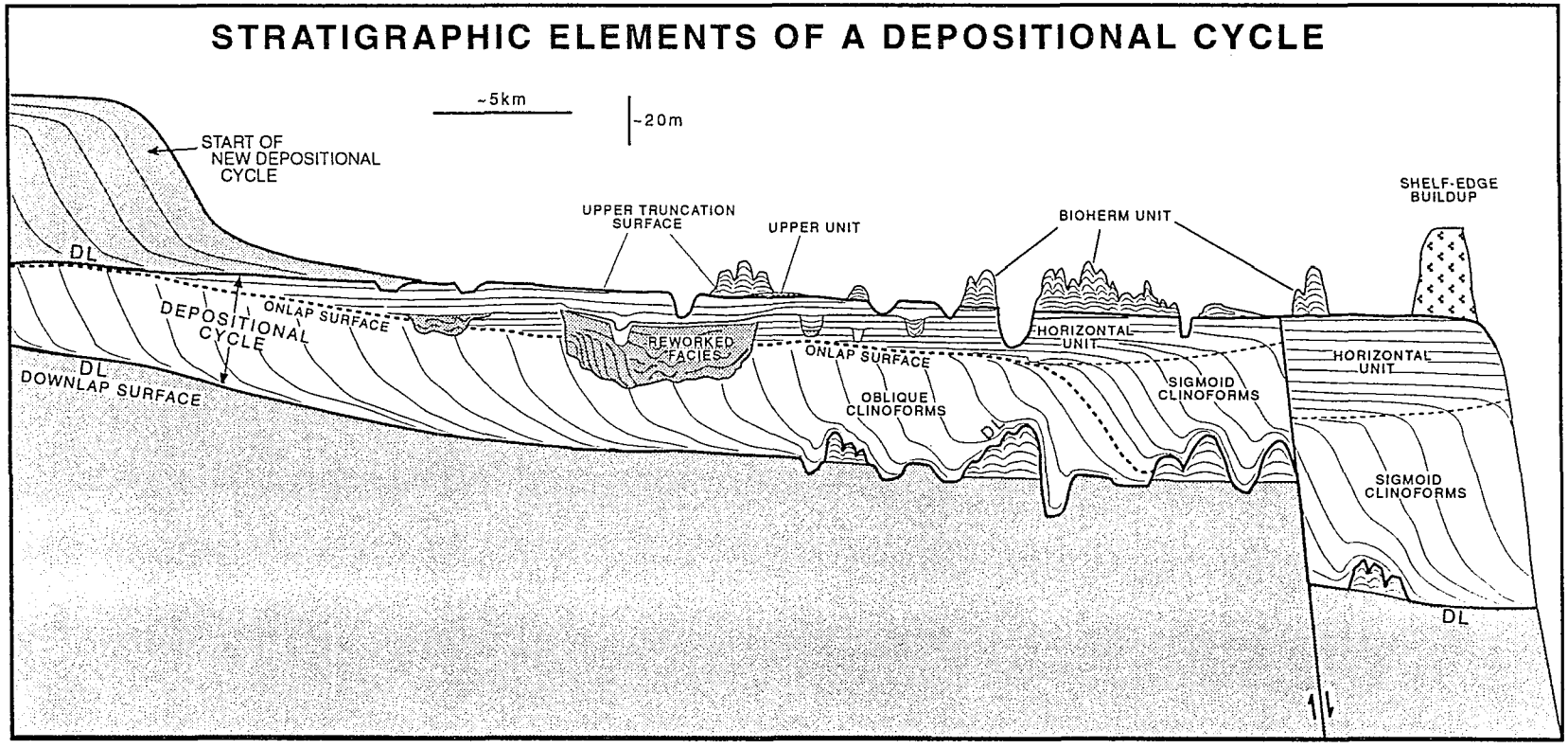

Figure 4.1 Schematic representation of units and surfaces from one Depositional Cycle discussed in this chapter.

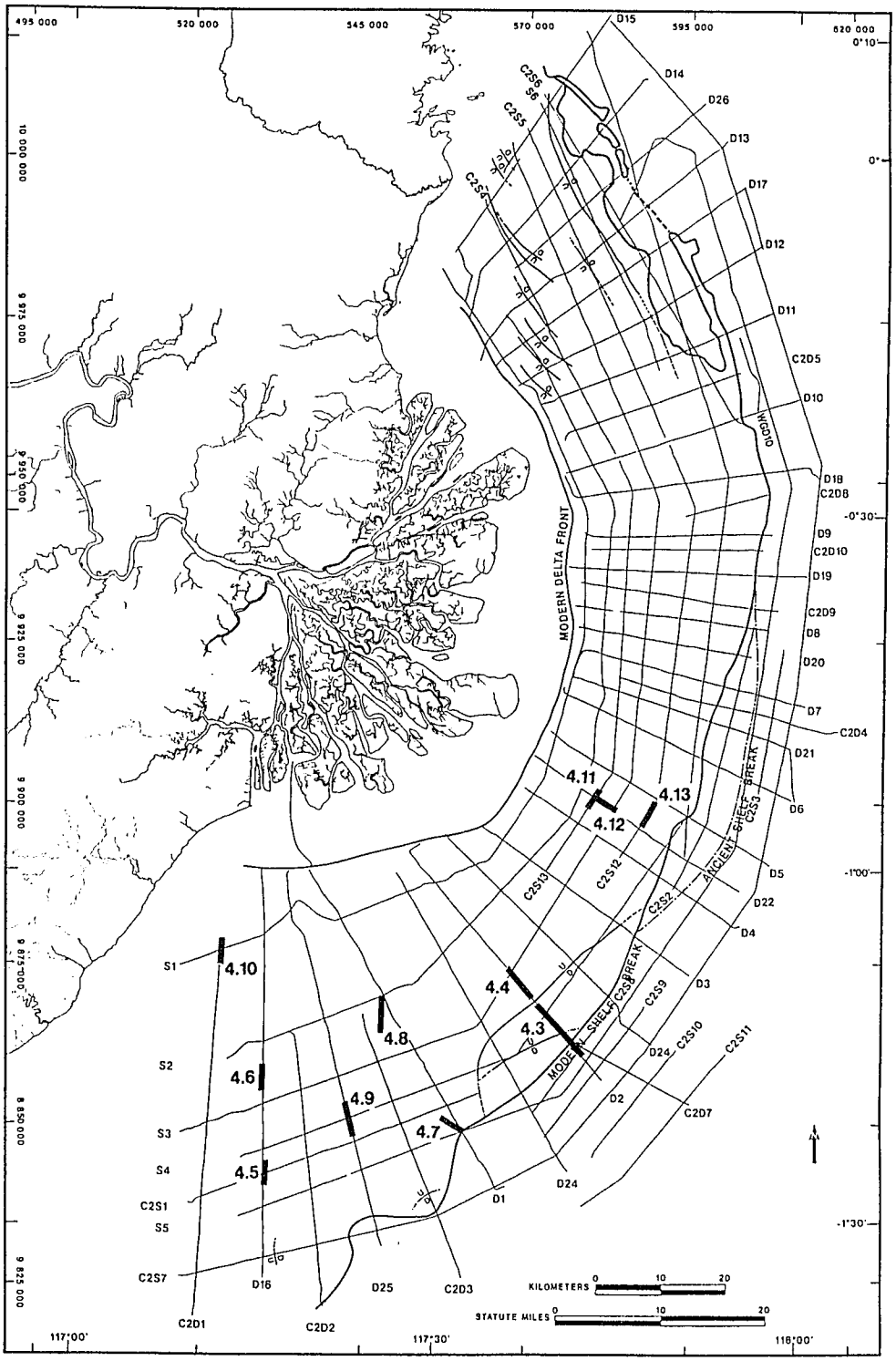

Figure 4.2 Location map of seismic profiles in Figures 4.3 to 4.13, from the southern shelf sector.

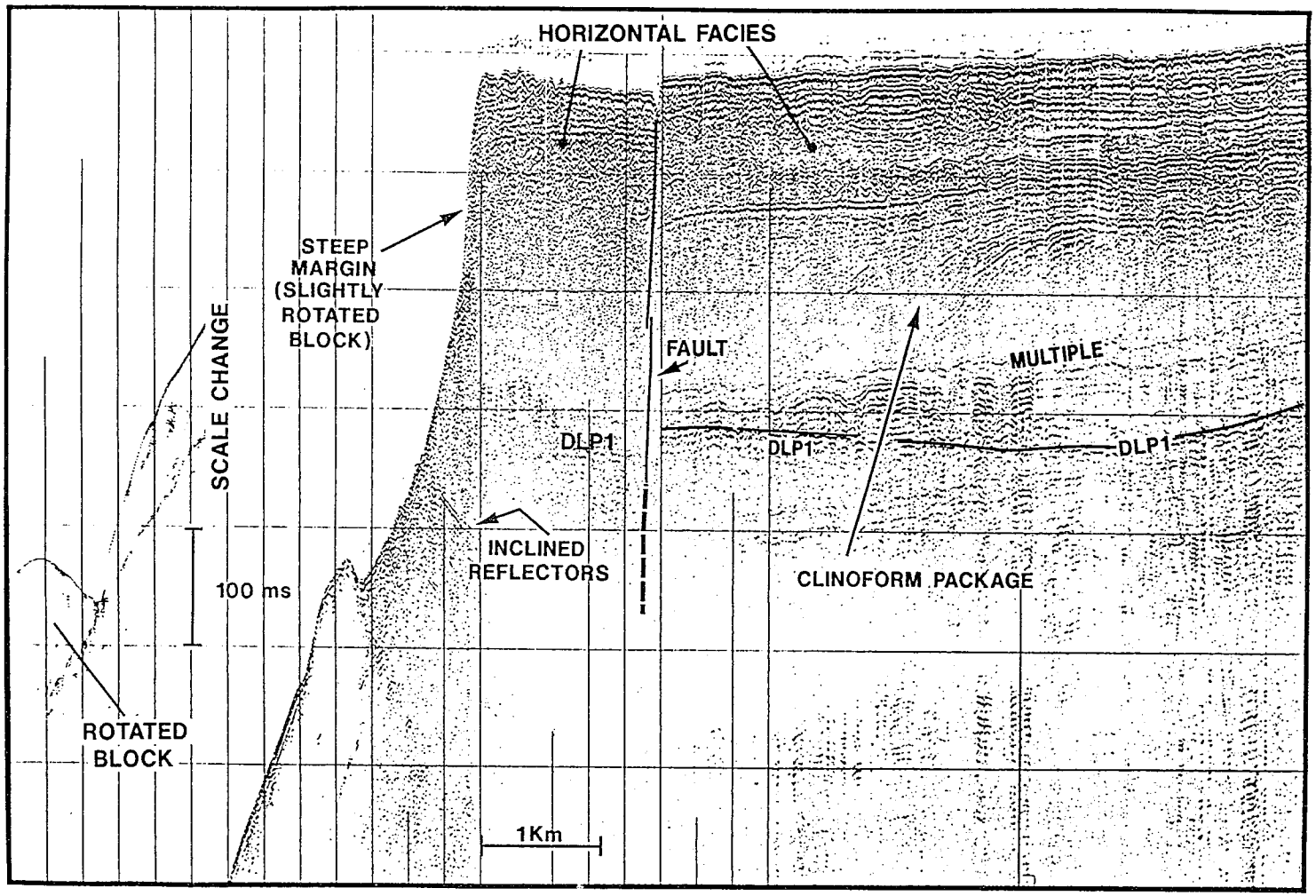

Figure 4.3 Seismic Water Gun Line D2 accross the shelf edge, illustrating thick Clinoform and Horizontal Units of the southern P1 depocenter (P1S) which underlie the shelf edge. The segment is situated on the downthrown block of a growthfault.

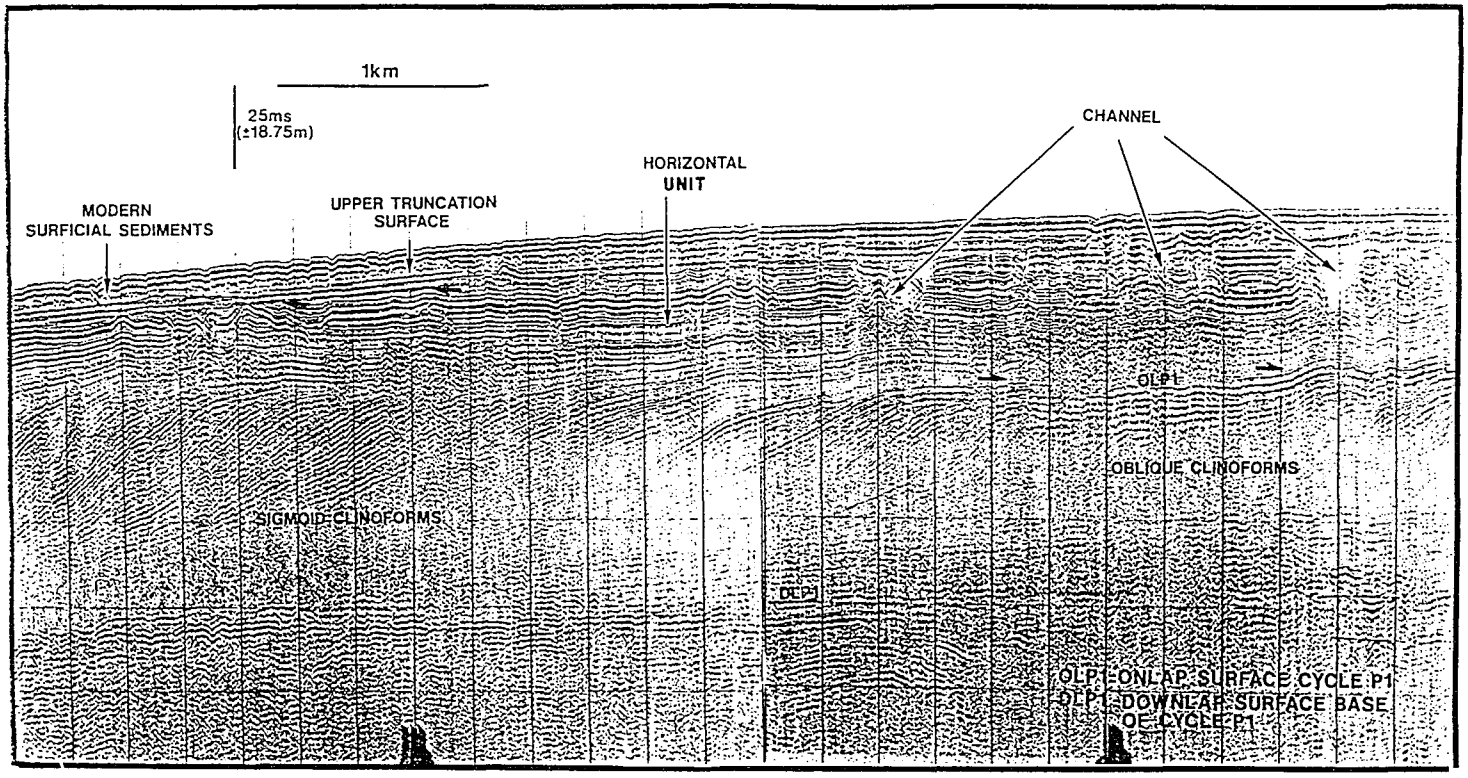

Figure 4.4 Seismic Geopulse Line D2 illustrating the transition from oblique to sigmoid clinoforms. Onlapping strata of the Horizontal Unit are updip extensions of sigmoid clinoforms.

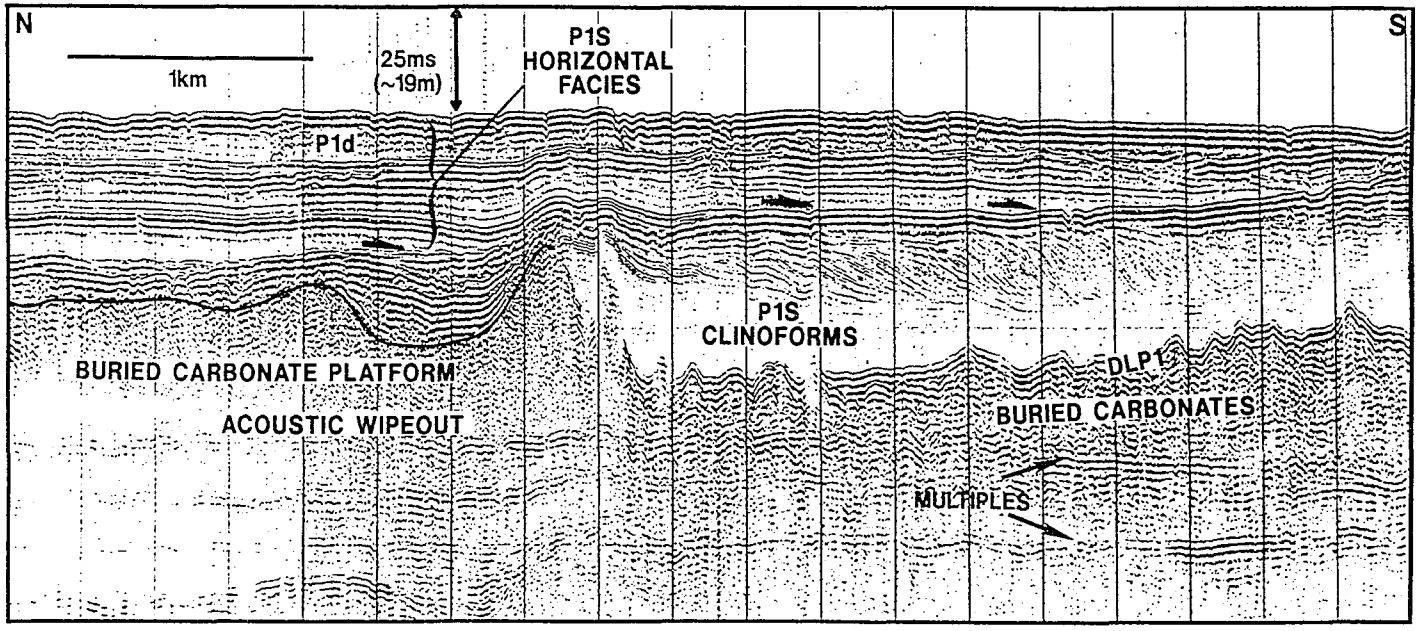

Figure 4.5 Seismic Geopulse Line D16 showing onlap terminations of horizontal strata.

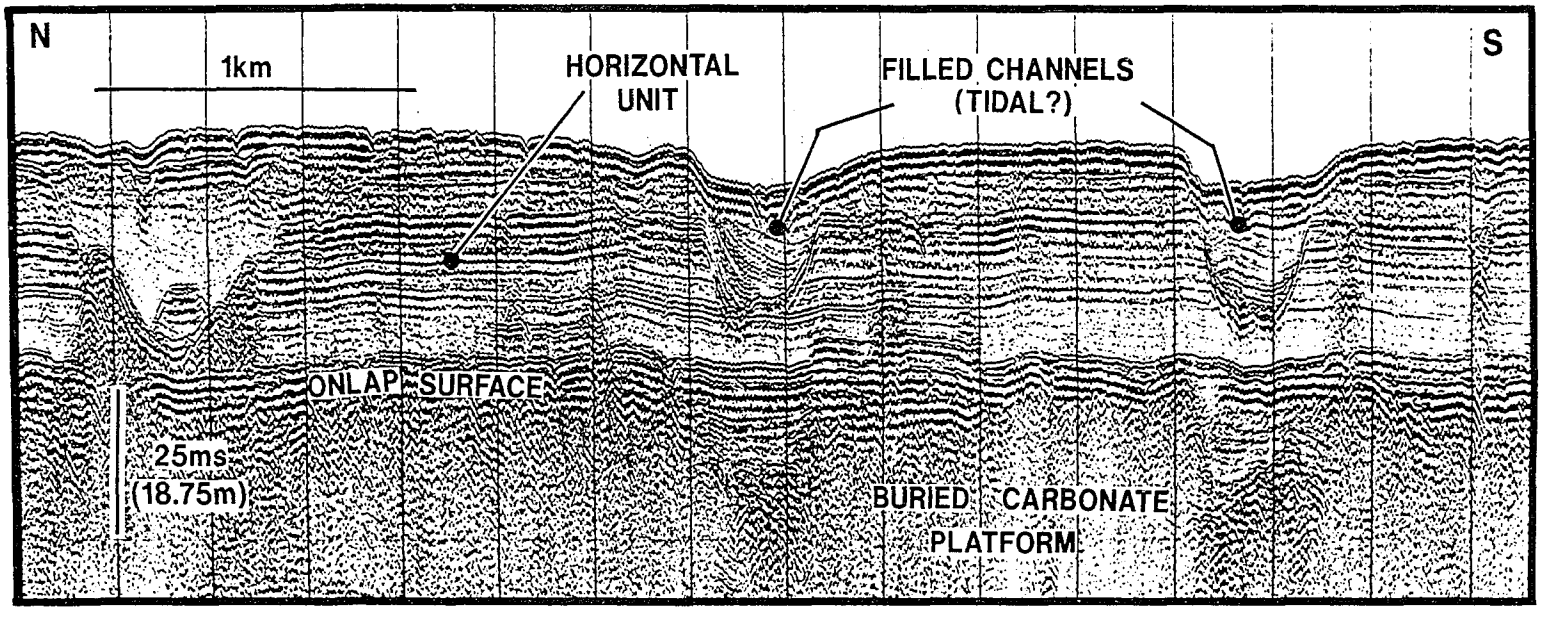

Figure 4.6 Seismic Geopulse Line D16 showing narrow, steep sided channels in the Horizontal Unit. Channels originate at a prominent, subdividing reflection event within the Horizontal Unit (most obvious for channel on the left).

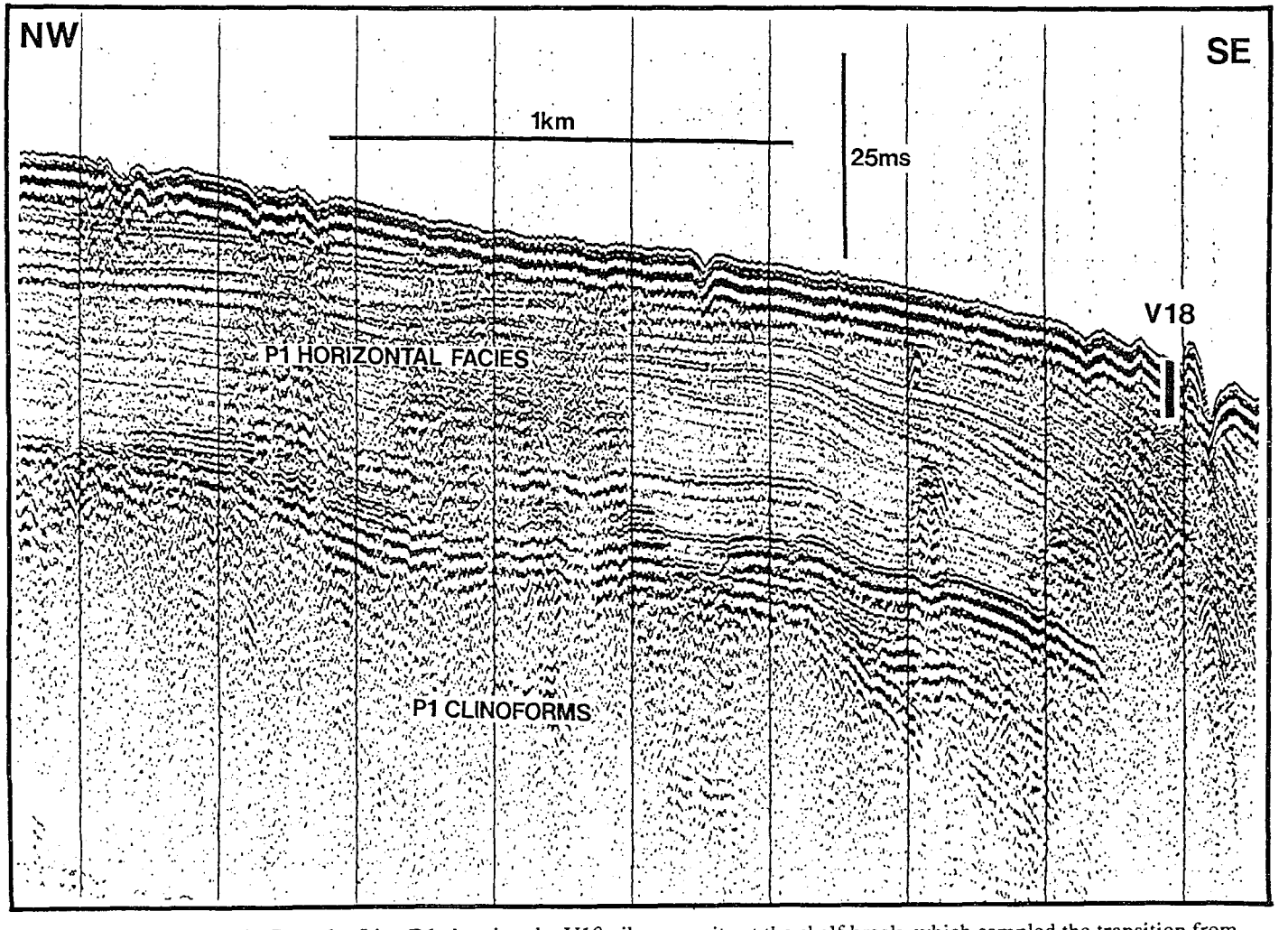

Figure 4.7 Seismic Geopulse Line D1 showing the V18 vibracore site at the shelf break, which sampled the transition from horizontal to sigmoid clinoforms of the P1N depocenter. Deltaic sediments are exposed on the sea floor at this site.

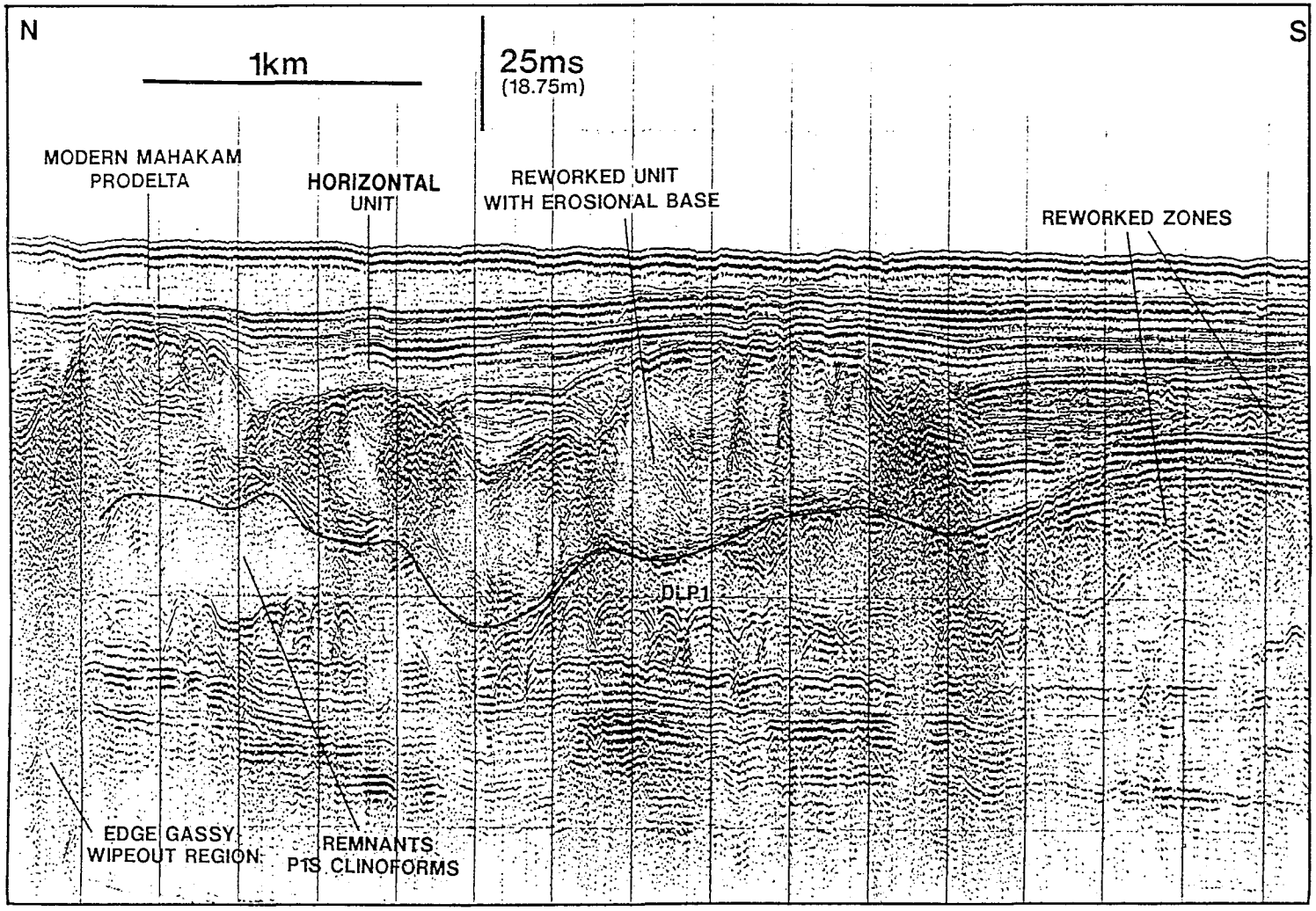

Figure 4.8 Seismic Geopulse Line D1, illustrating the complex fill of the broad, shore-normal Reworked Unit trend in P1S. Proximal region of Reworked trend is obscured by acoustic attenuation, probably due to biogenic gas.

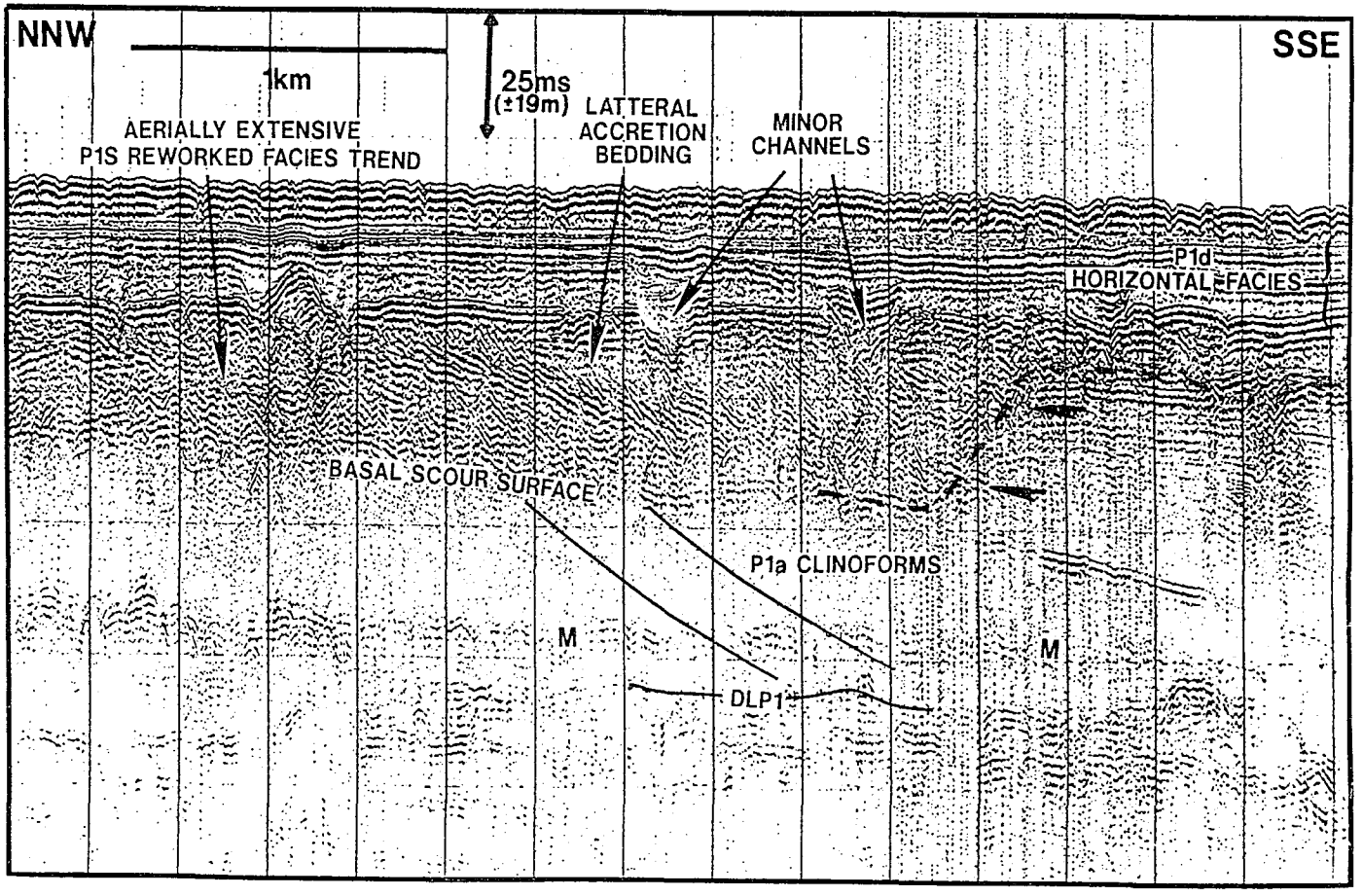

Figure 4.9 Seismic Geopulse Line D25 showing latteral accretion facies within the Reworked Unit on the outer shelf, Pleistocene P1S depocenter. M = sea floor multiple.

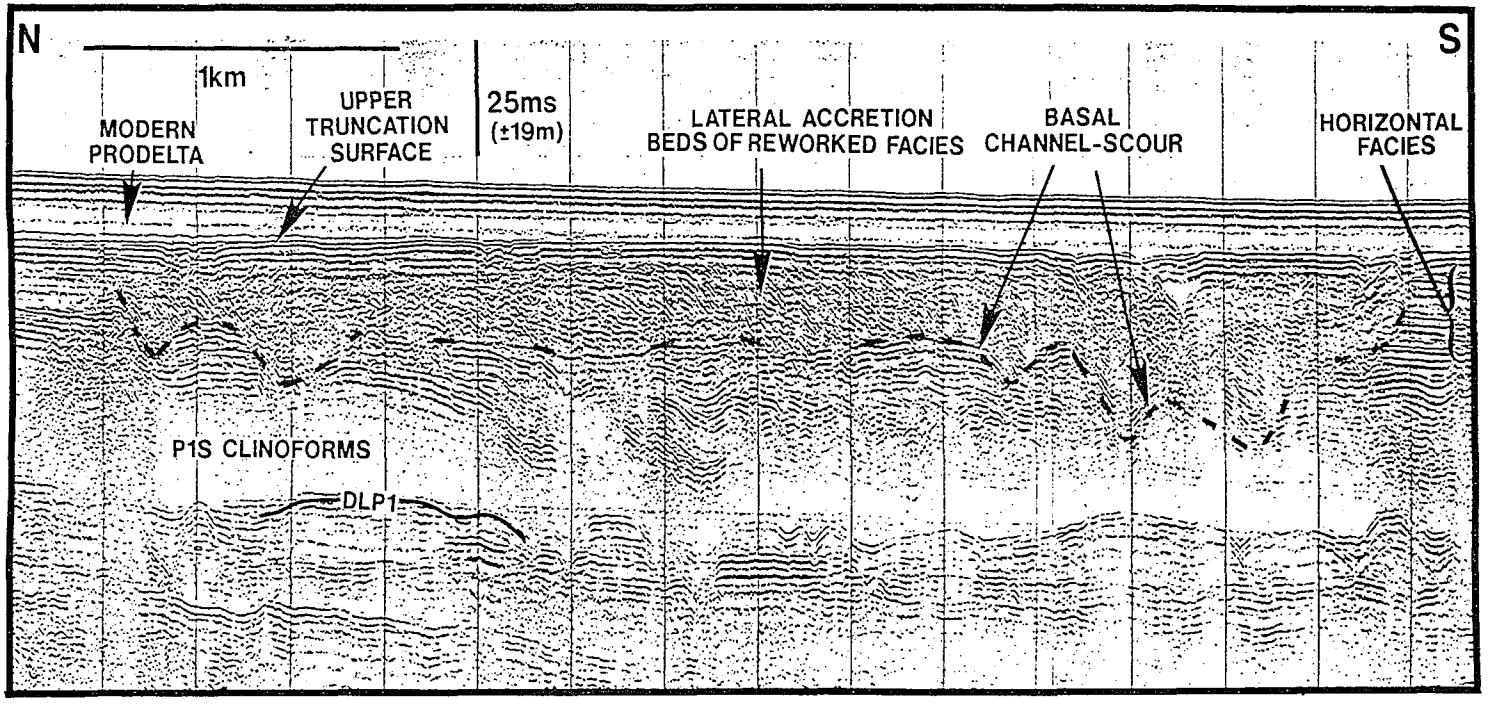

Figure 4.10 Seismic Geopulse Line C2D1 illustrating widespread lateral accretion beds of the Reworked Unit on the inner shelf, Pleistocene P1S depocenter. M = sea floor multiple.

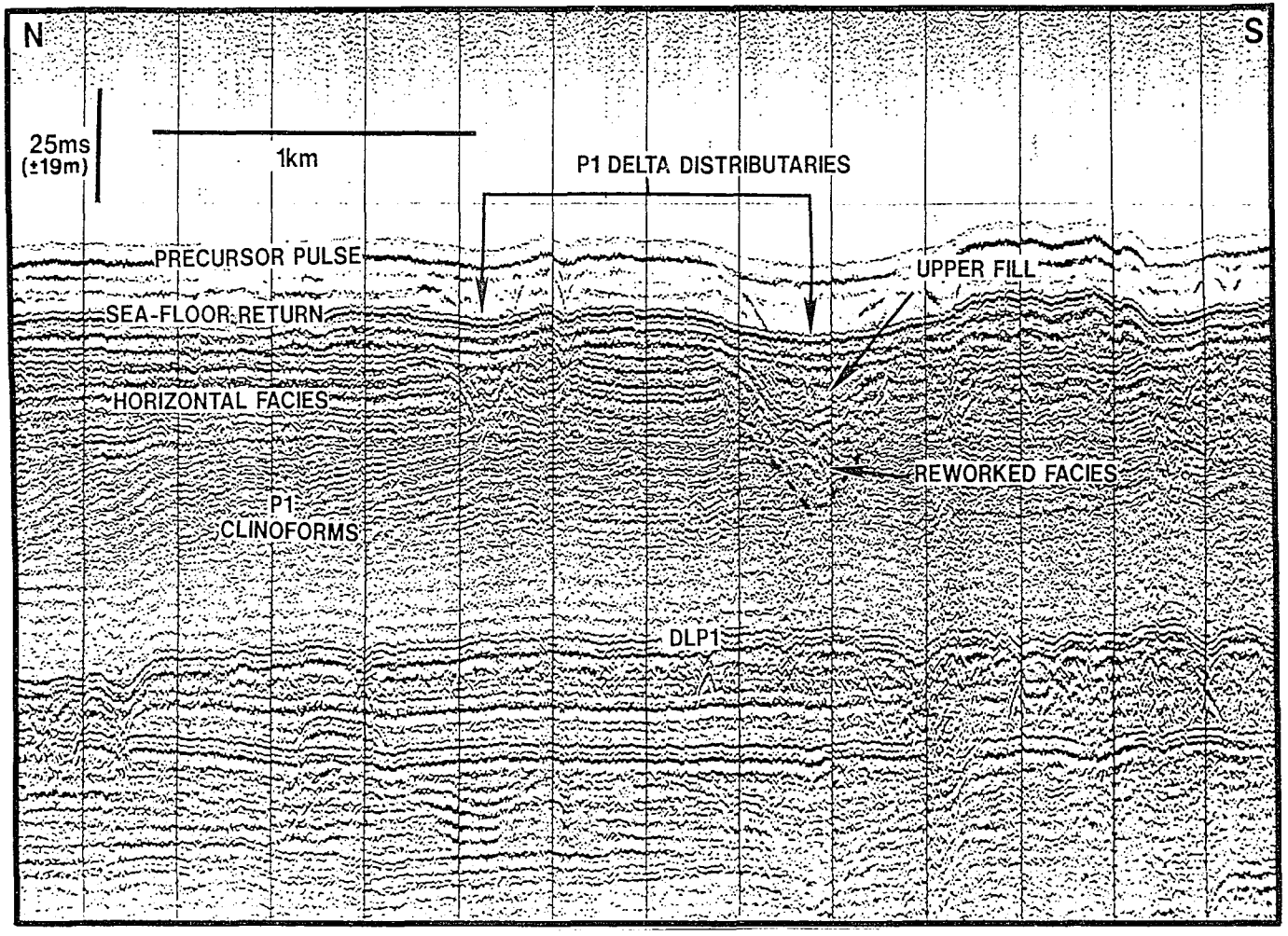

Figure 4.11 Water Gun Line C2S13, a transverse view through a narrow feeder trend in the southern P1 depocenter. Reworked seismic facies fill the lower portion of the channel.

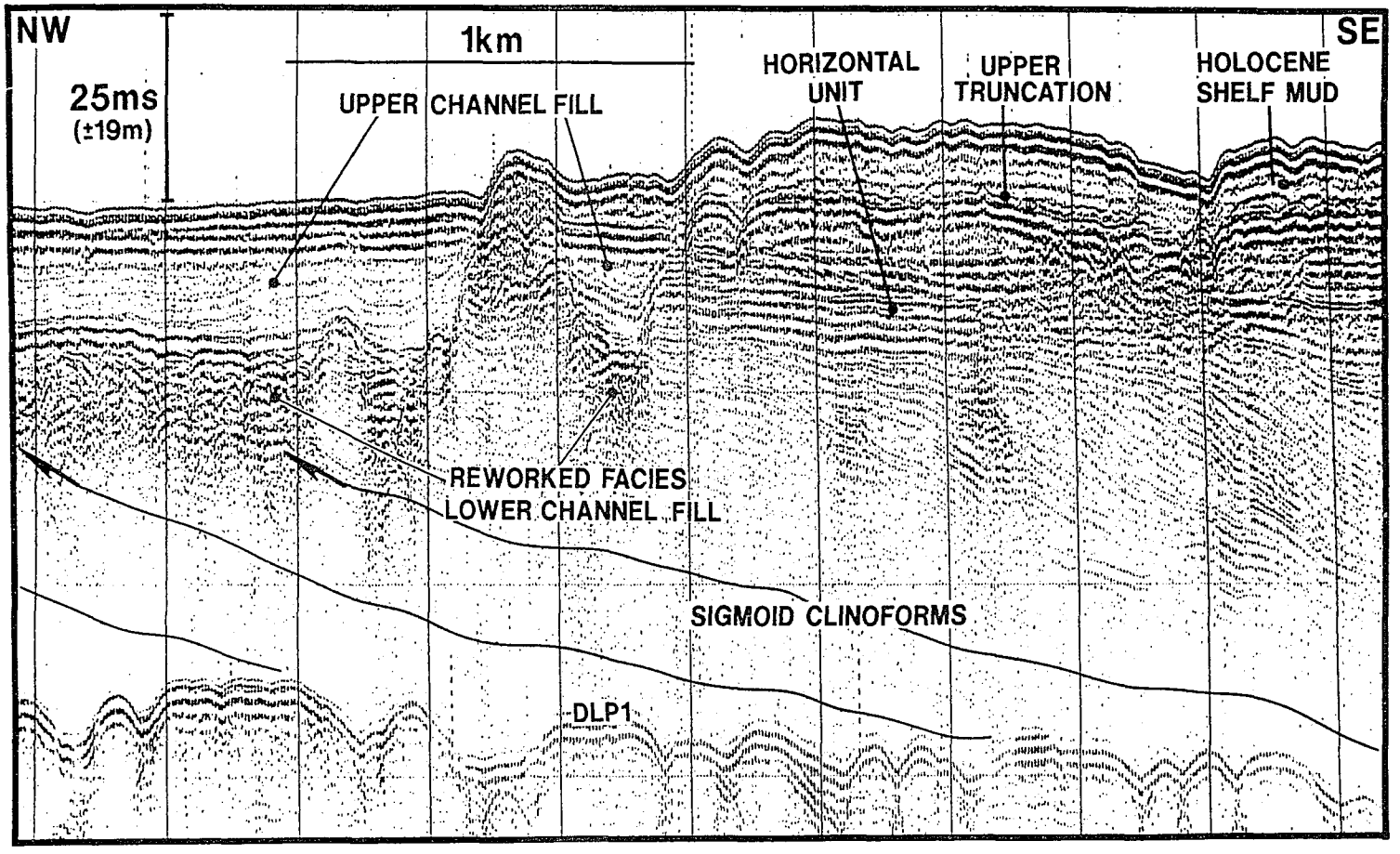

Figure 4.12 Geopulse Line D22 representing an axial-oblique view of the narrow feeder channel in preceding Figure 4.11. The channel has a lower Reworked Unit fill and an upper conformable, onlapping fill. Note the effect of the higher resolution seismic tool in this figure compared to the Water Gun profile of the transverse view of the previous figure.

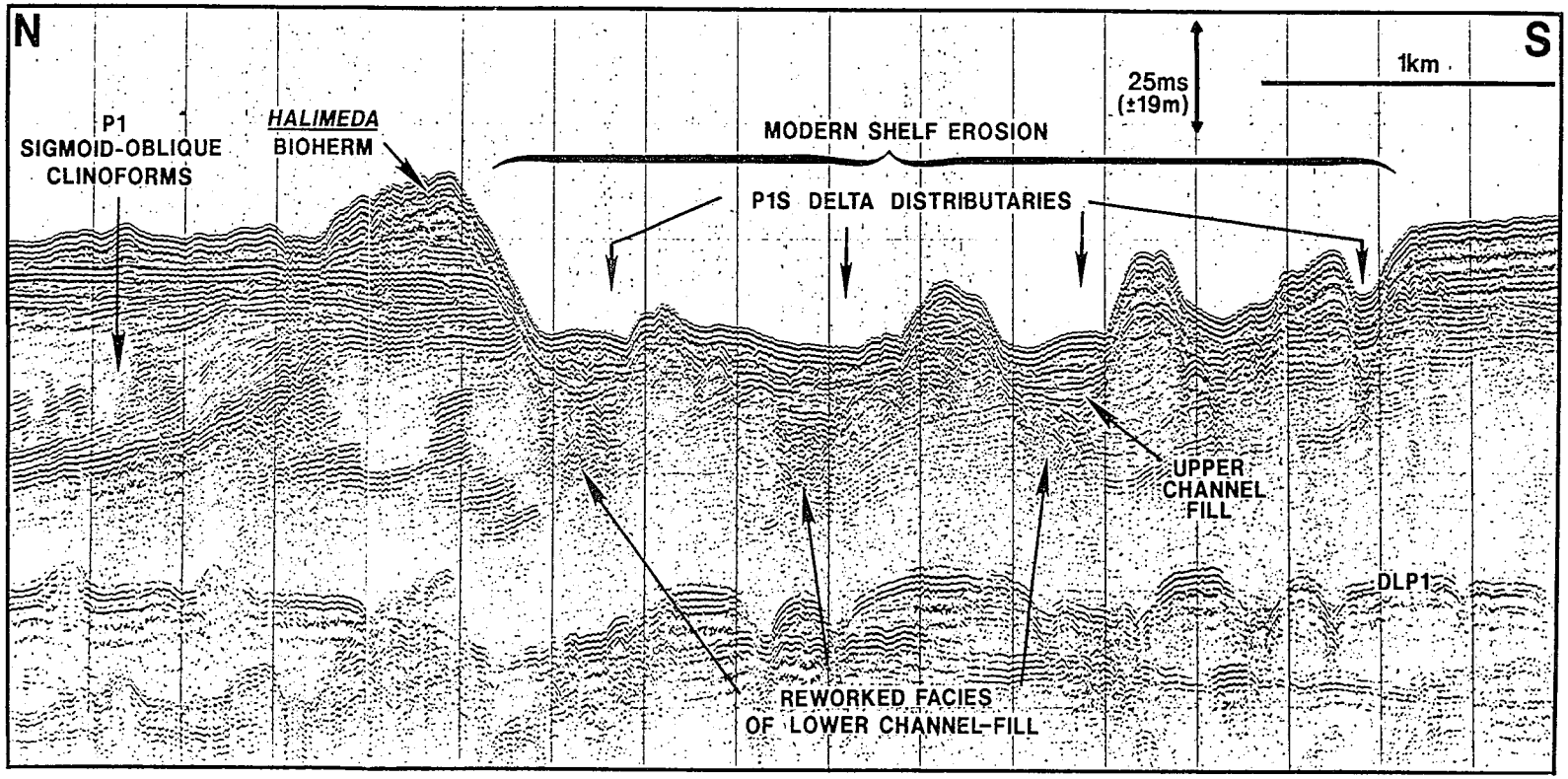

Figure 4.13 Geopule Line C2S12, downdip of the previous two figures, showing three or four channel trends incising the P1S Horizontal and Clinoform Units. Shelf scour is apparently amplified by abandoned channel trends during subsequent transgression of the lowstand delta

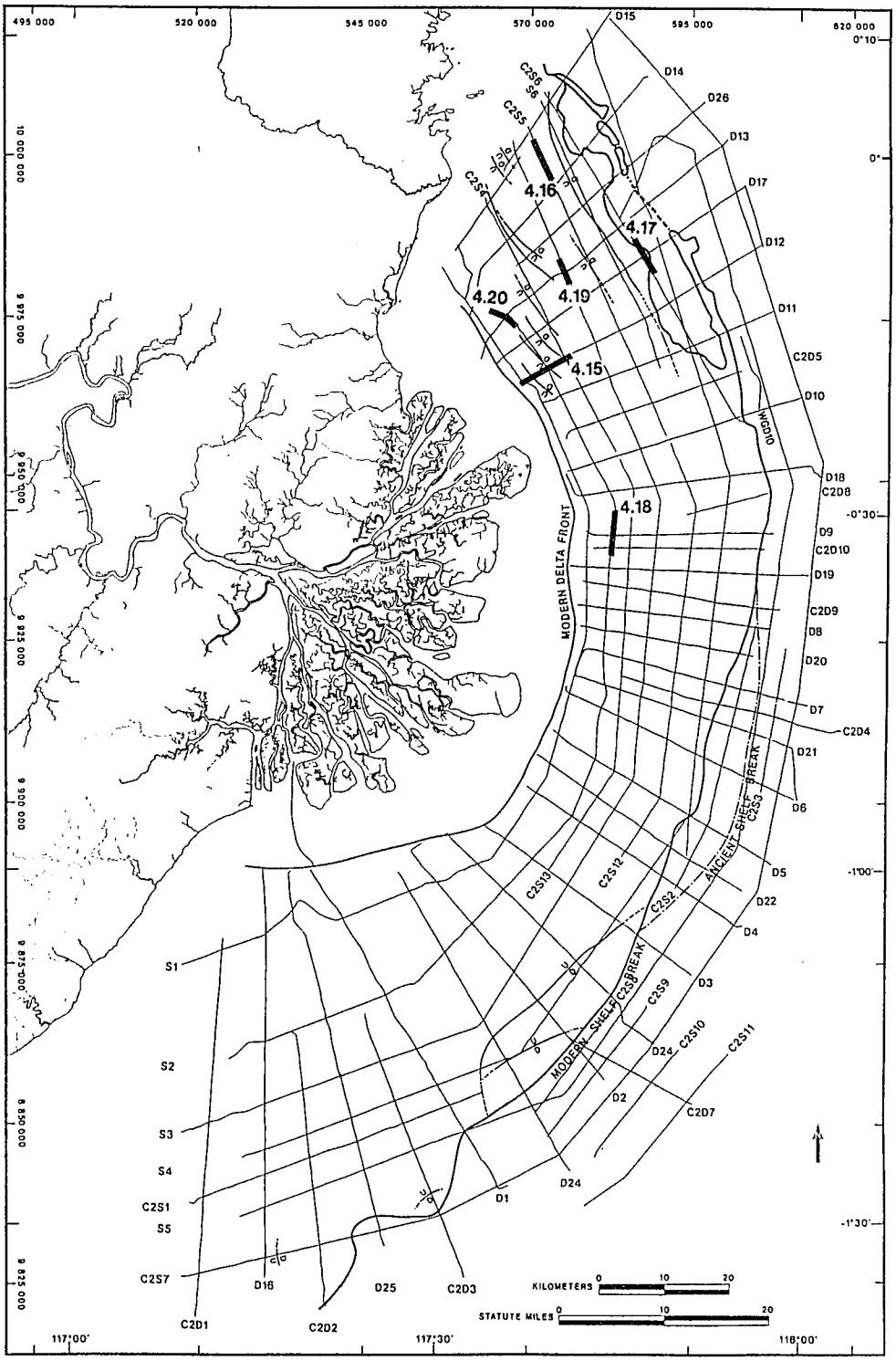

Figure 4.14 Location map of seismic profiles in Figures 4.15 to 4.20. Seismic profiles illustrate pertinent stratigraphic features from the northern shelf sector.

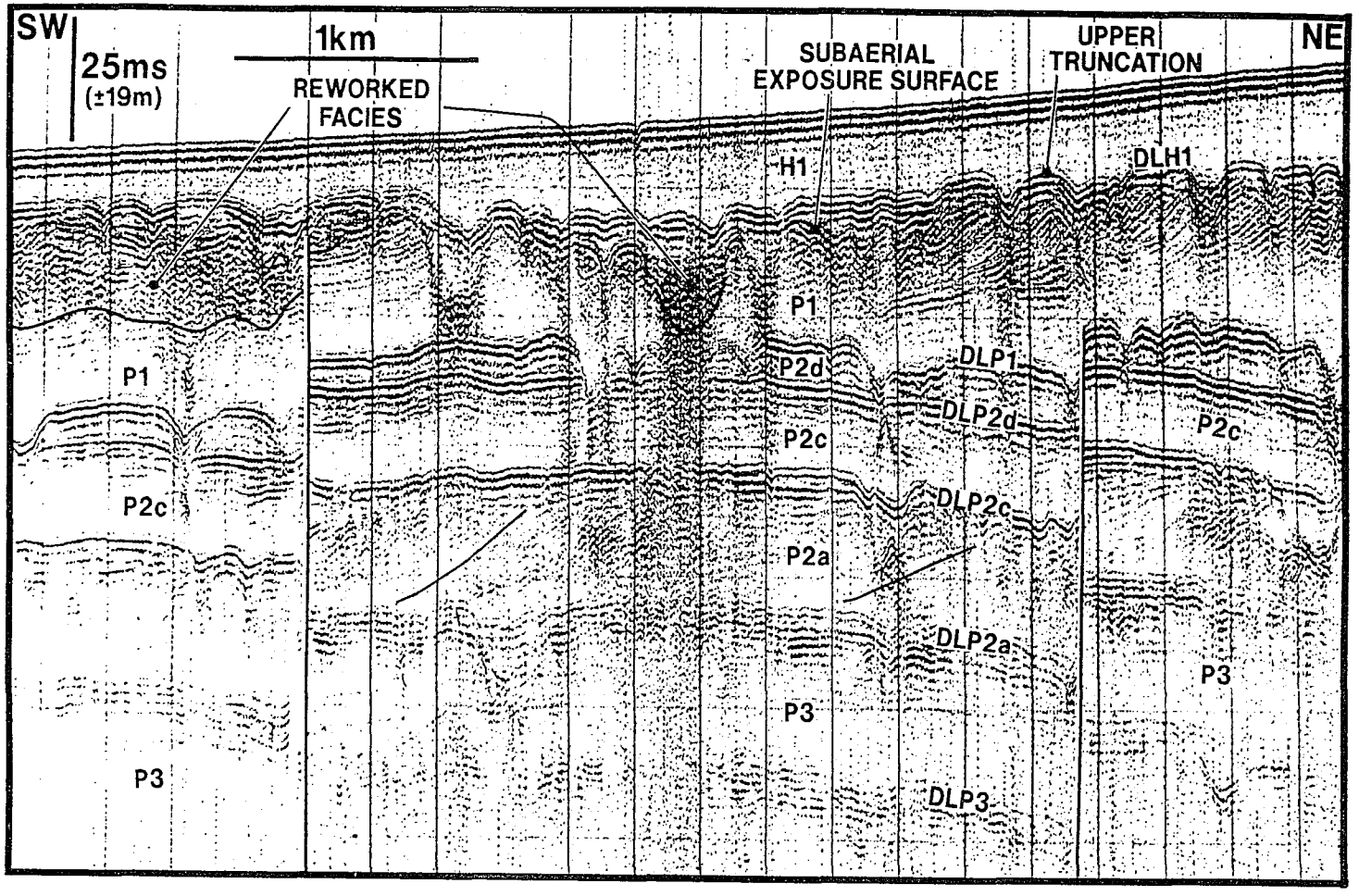

Figure 4.15 Seismic Geopulse Line D12, inner shelf northern sector. Depositional Cycles H1 to P3 are separated by high amplitude downlap surfaces DLH1 to DLP3. Note clinoforms visible in cycles H1, P1, and P2a. Strata are folded and faulted.

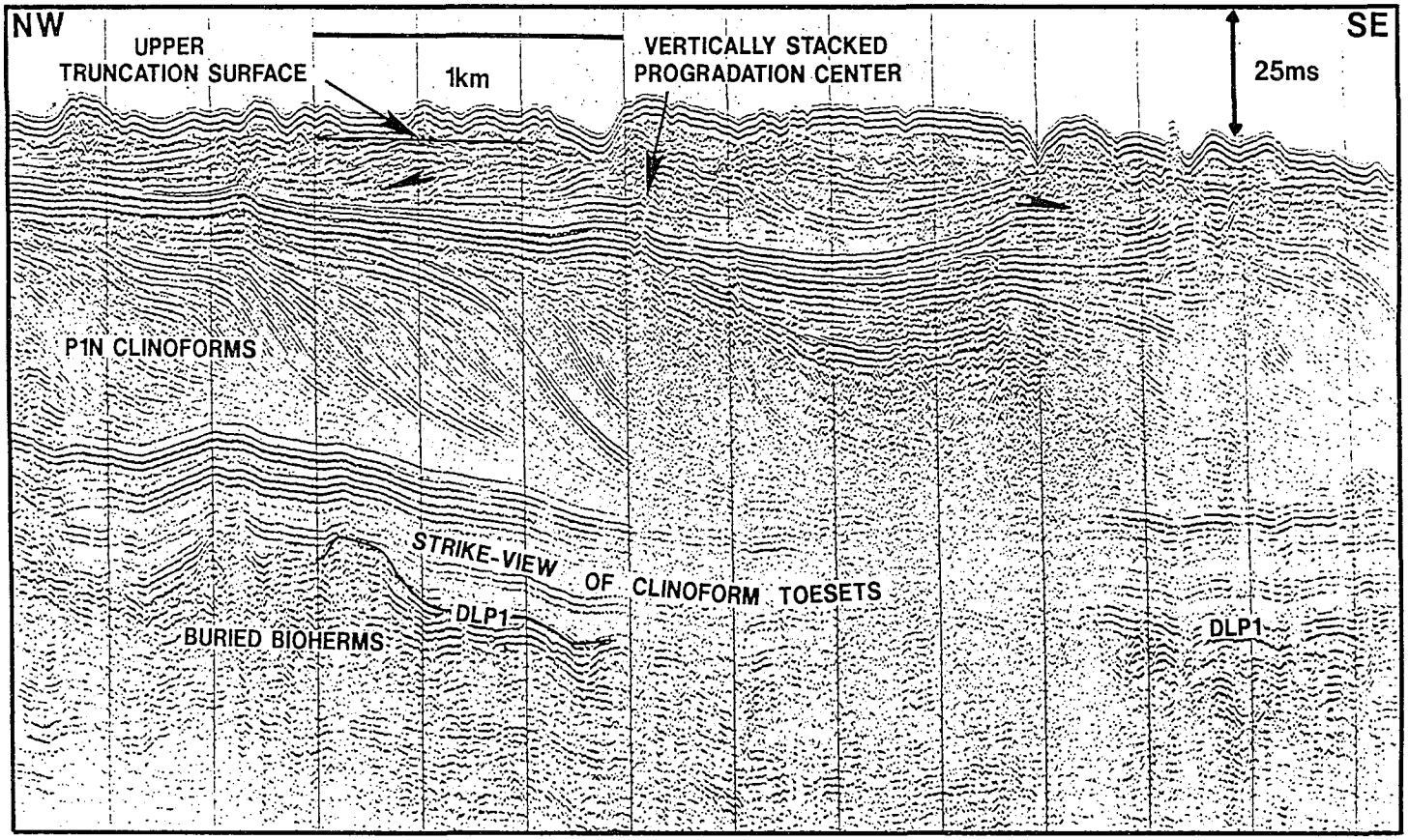

Figure 4.16 Seismic Geopulse Line C2S5 illustrating prominent clinoforms of the P1N cycle that are sourced by the small Santan River drainage system north of the Mahakam River (progradation direction is to the south). The small progradation center (diverging clinoform dips) perched on top of the main P1N depocenter is related to final transgression of the P1N depocenter.

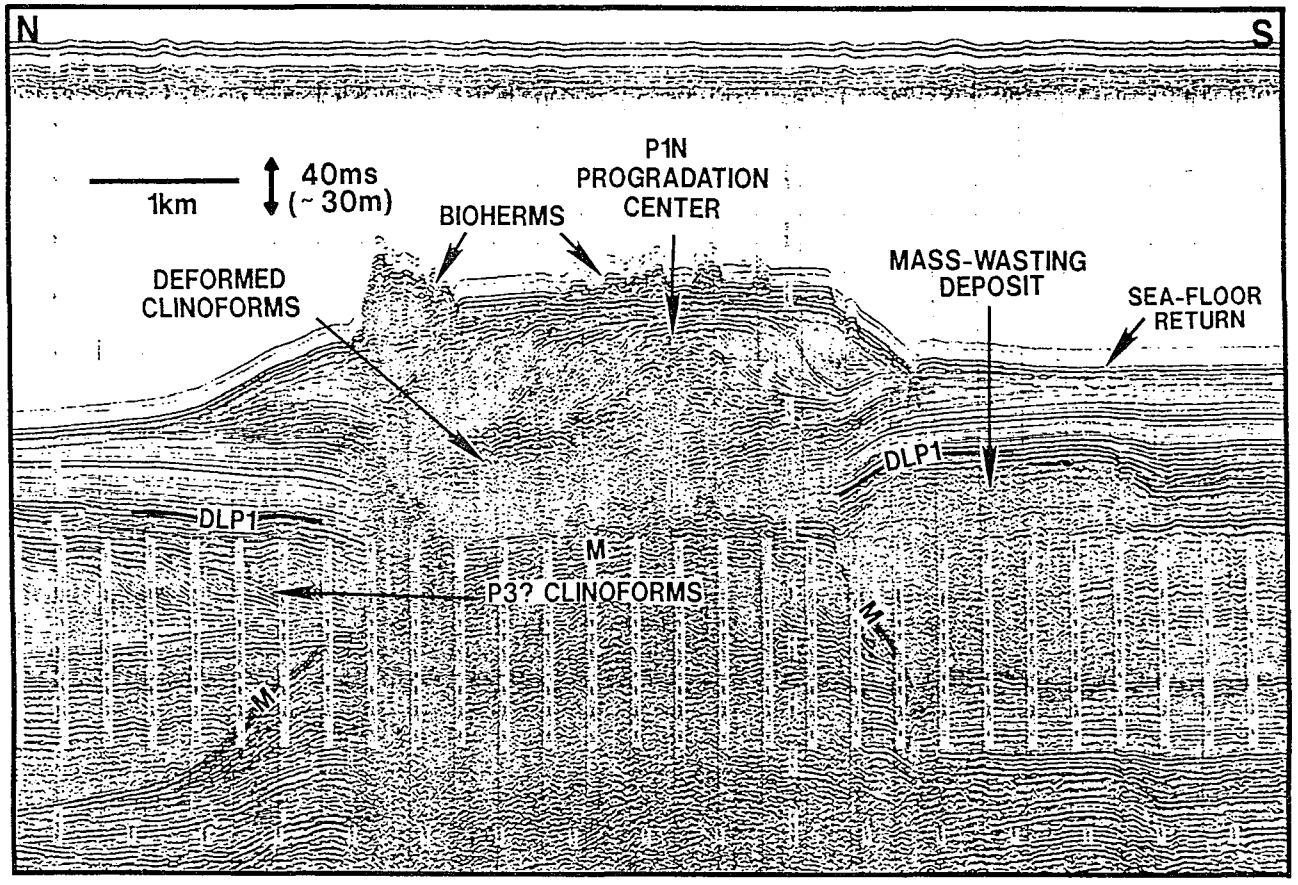

Figure 4.17 Seismic Water Gun C2S6 shows a thick, drowned P1N delta lobe. Diverging clinoform dips of the progradation center are clearly visible. This unussually thick P1N lobe is situated on the downthrown side of a large fault scarp. Note the thick bioherm growth on the topographic high created by the abandoned lobe. M = sea floor multiple.

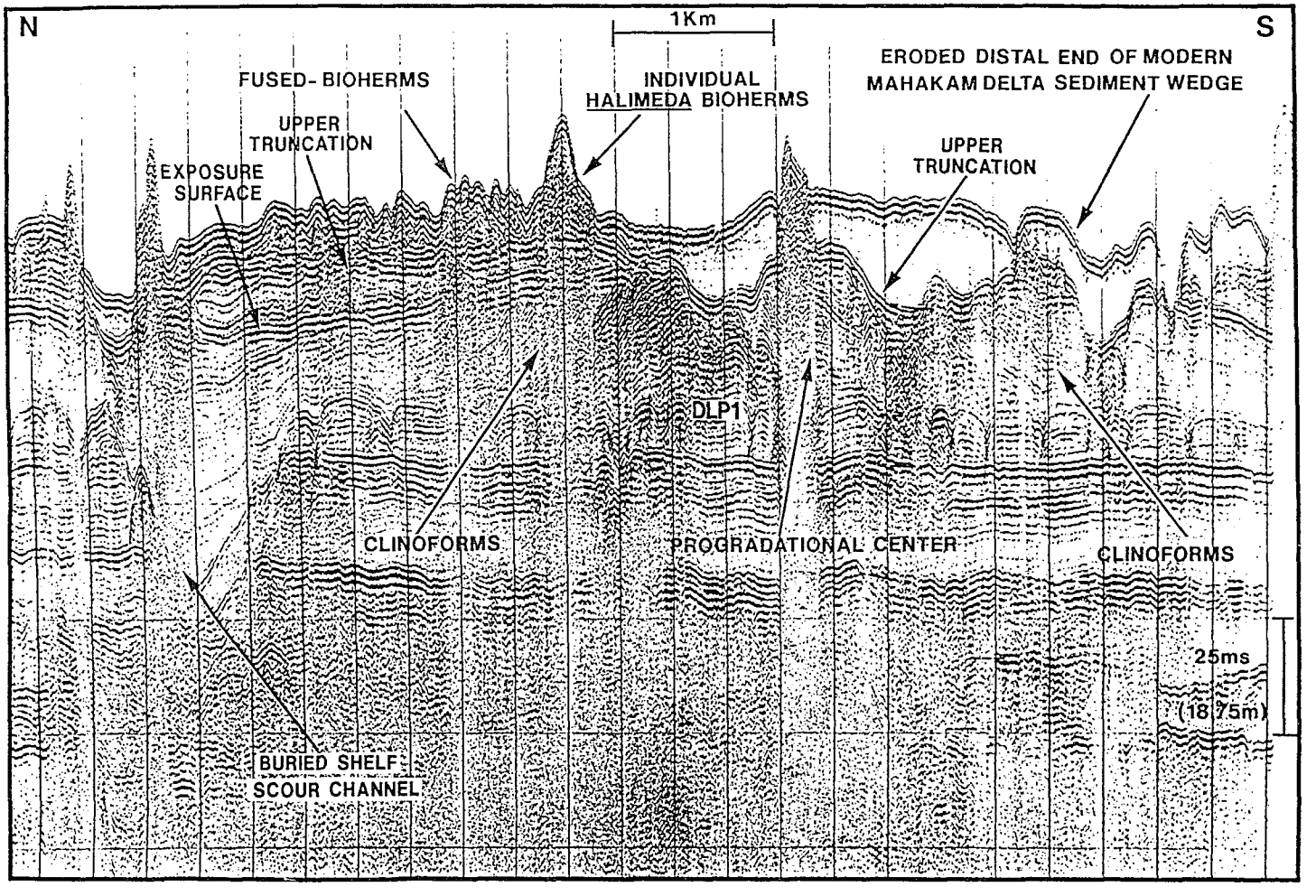

Figure 4.18 Seismic geopulse Line S2 showing a strike view through a Mahakam Delta Pleistocene cycle P1N progradation center on the inner shelf. Note diverging clinoform dips. Two erosional surfaces are visible above the Clinoform Unit on the left. The erosional Onlap and Upper Truncation Surfaces are ussually amalgamated above the P1N depocenter (right side). Bioherms are established on erosional highs of the Upper Truncation Surface.

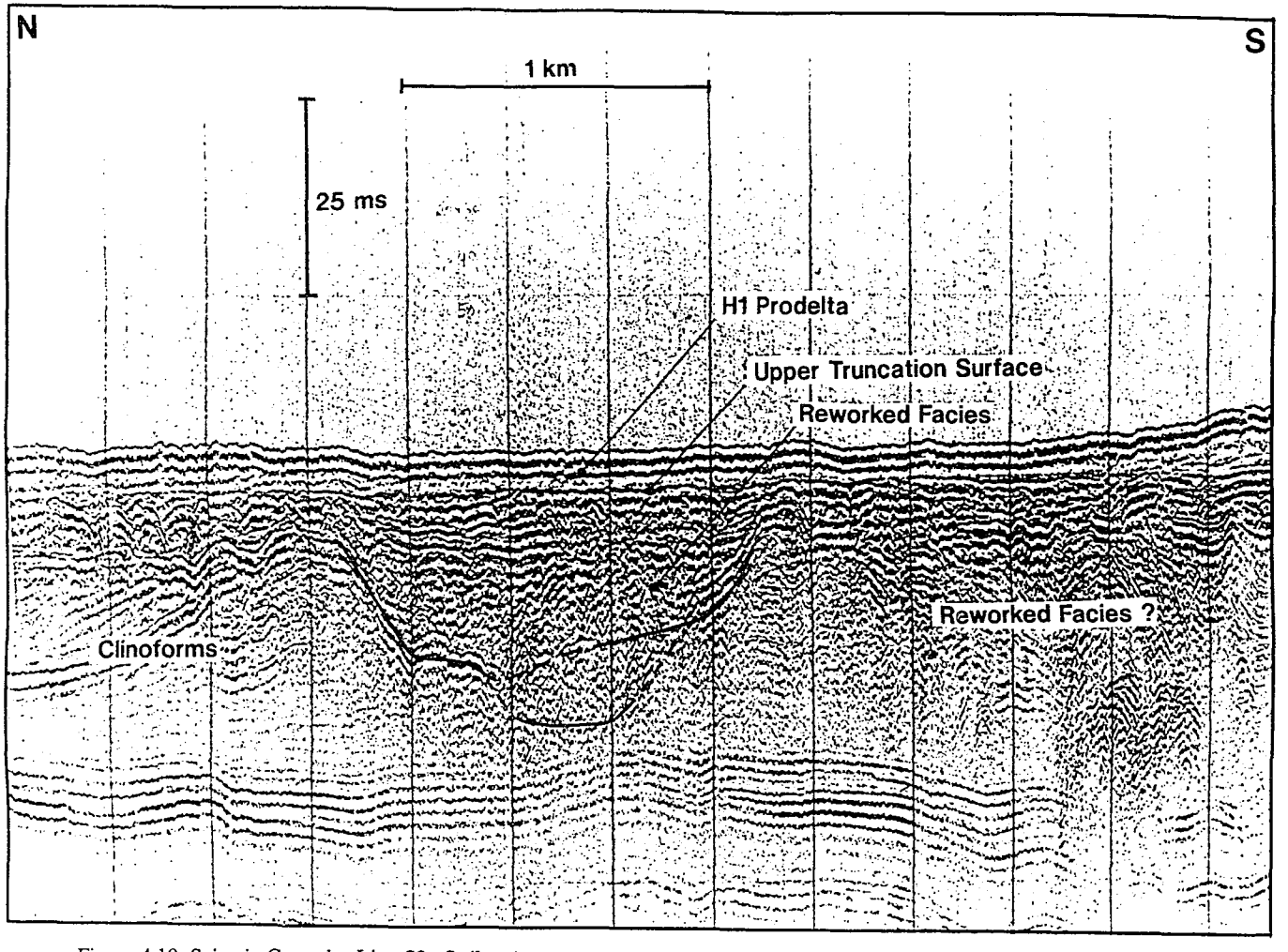

Figure 4.19 Seismic Geopulse Line S3. Strike view through a Reworked Unit trend of the P1N depocenter. Reworked facies are not as extensive as in P1S, and are best developed along axes of progradation related to the ancestral Mahakam River, less so for the smaller Santan River progradation centers. Fills on the downthrown side of growth faults are thicker than upthrown side.

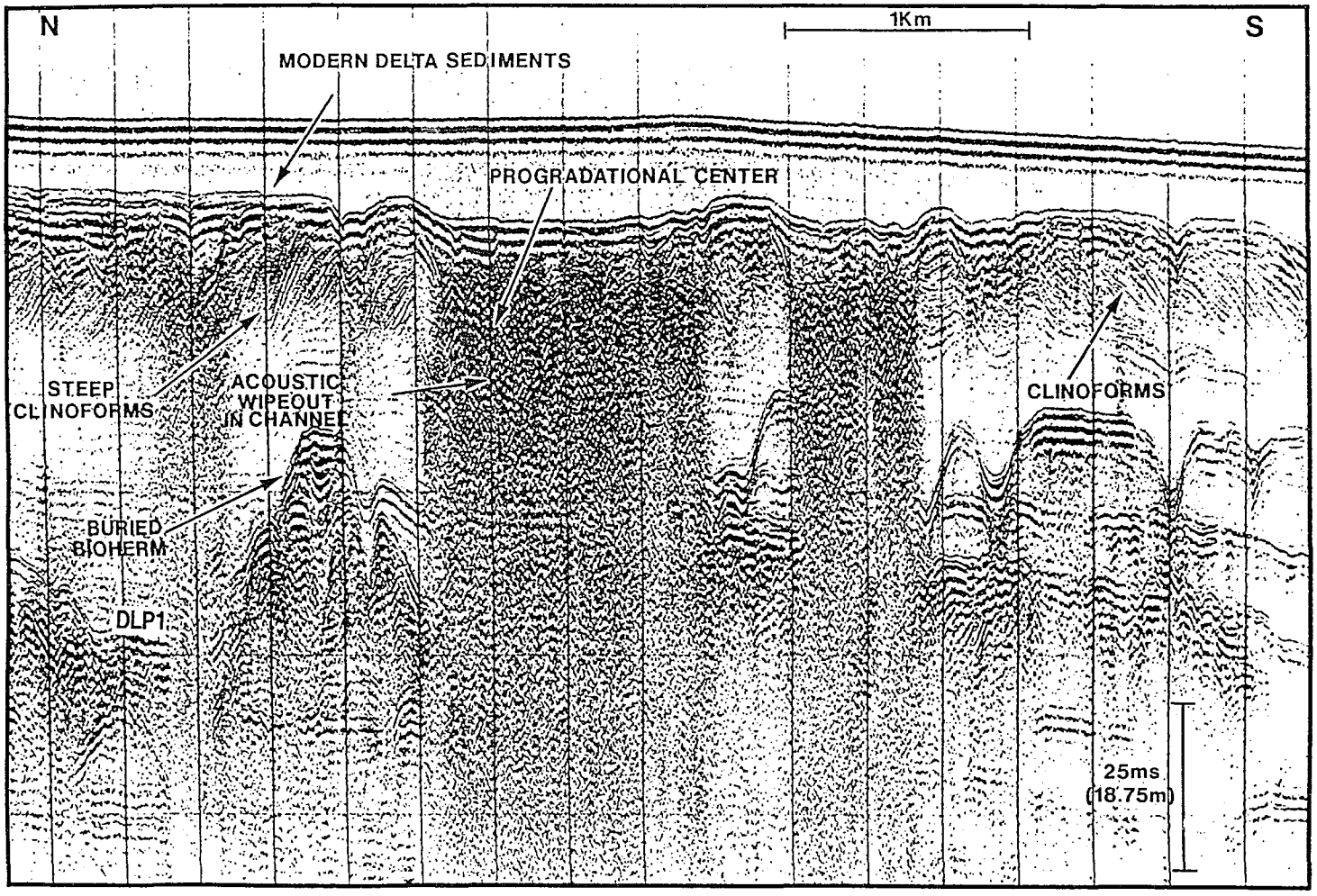

Figure 4.20 Seismic Geopulse Line S2, inner shelf. Strike view shows gassy channel fill deposits along the axis of a P1N progradation center. Clinoforms have steep dips along axes of progradation of the ancestral P1N Mahakam Delta. Note erosional relief of underlying DLP1 downlap surface.

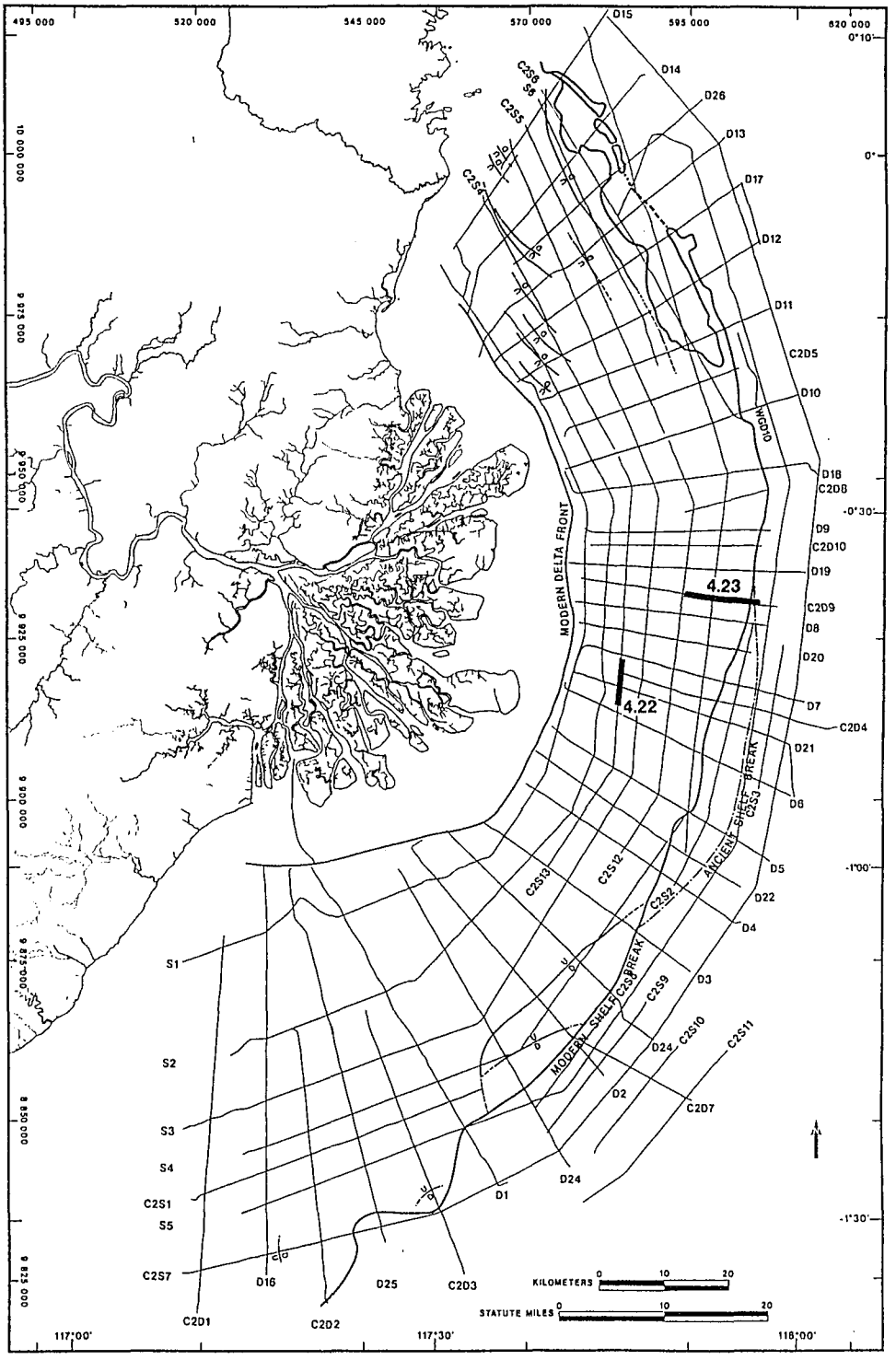

Figure 4.21 Location map of seismic profile Figures 4.22 and 4.23 from the central sector of the shelf.

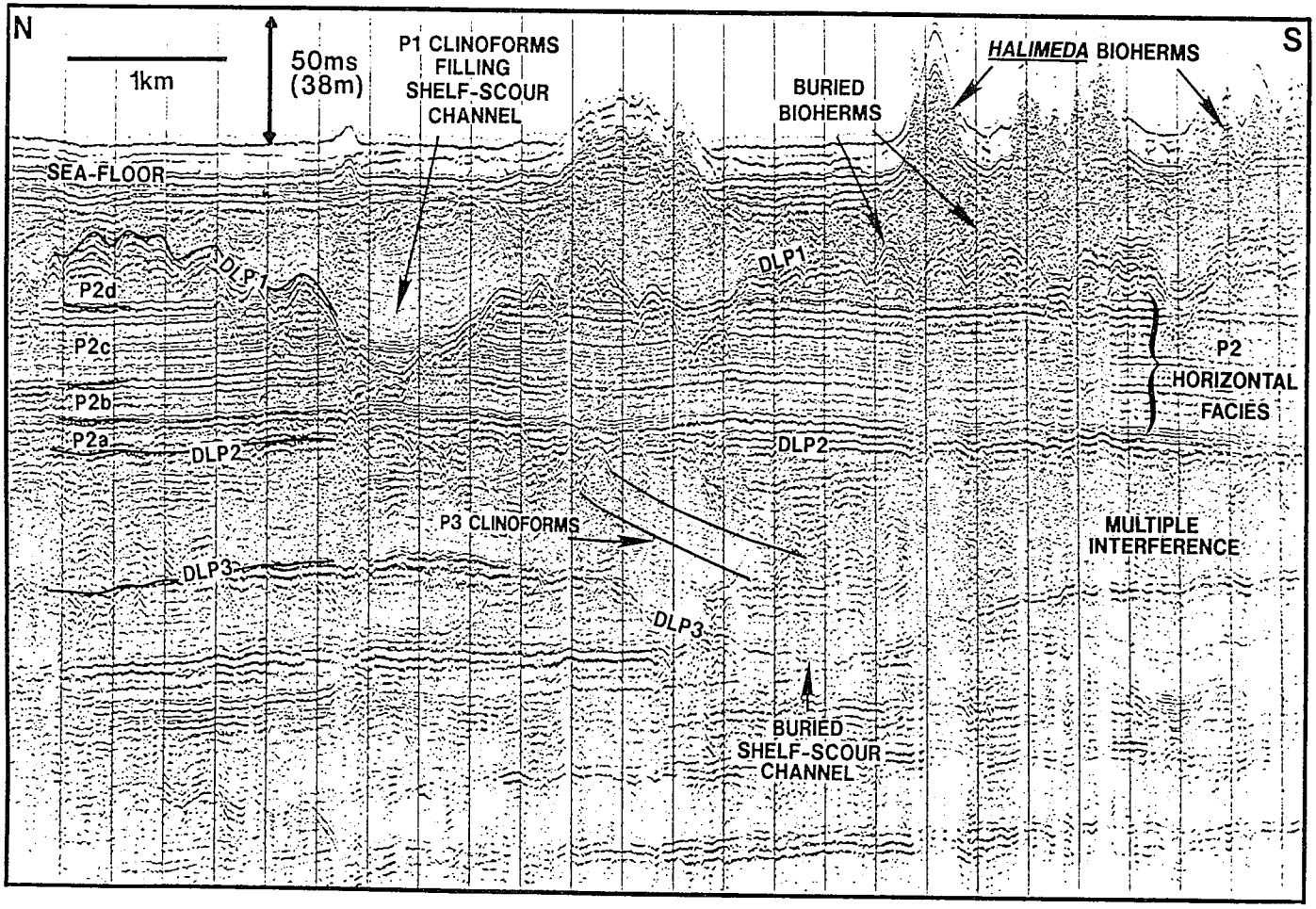

Figure 4.22 Seismic Water Gun Line C2S13. Strike view of central sector stratigraphy on the inner shelf. The P2 and P3 depocenters are located in this central sector. P3 clinoforms are obscured by multiple interference. P2c and P2b consist of stacked Horizontal Units on the inner shelf.

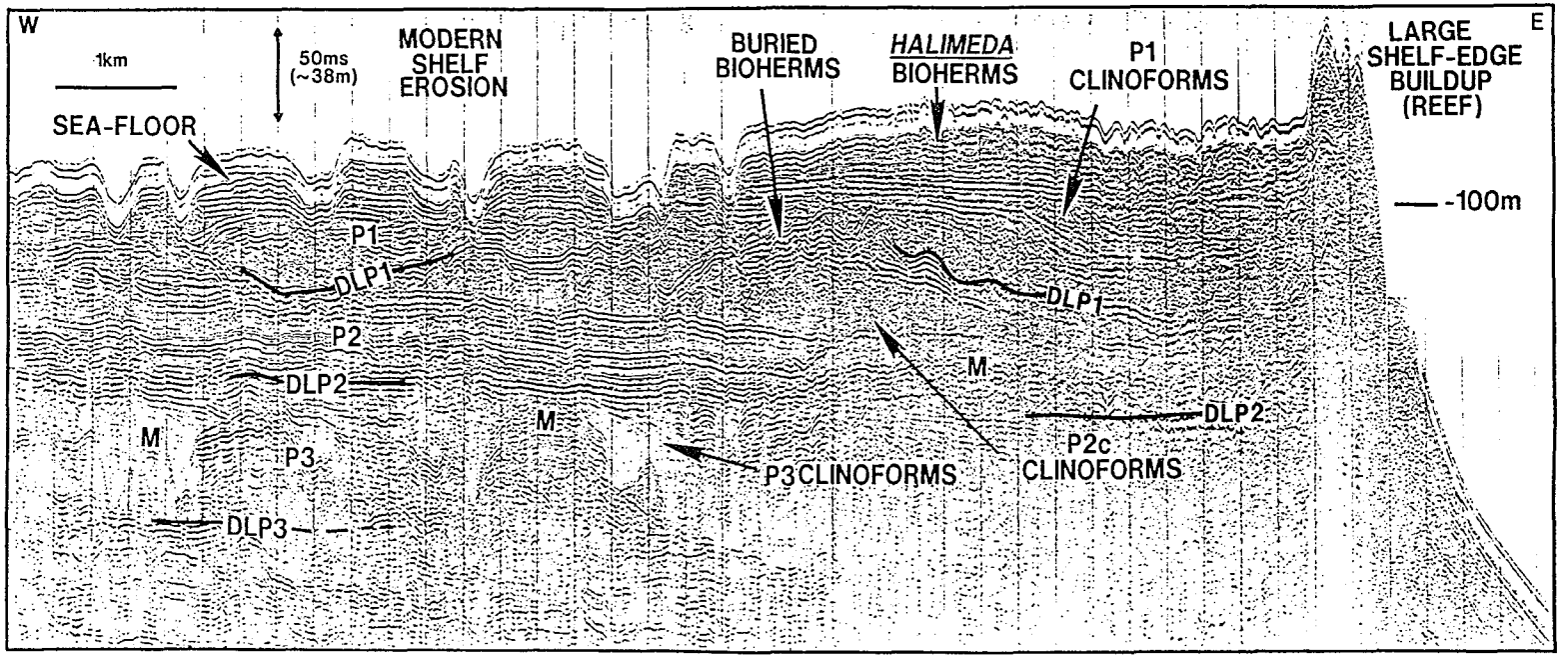

Figure 4.23 Seismic Water Gun Line C2D9. Dip profile showing outer shelf stratigraphy of the central sector. Note the poorly developed P1 cycle. P3 clinoforms are largely obscured by multiple interference. M = sea floor multiple.

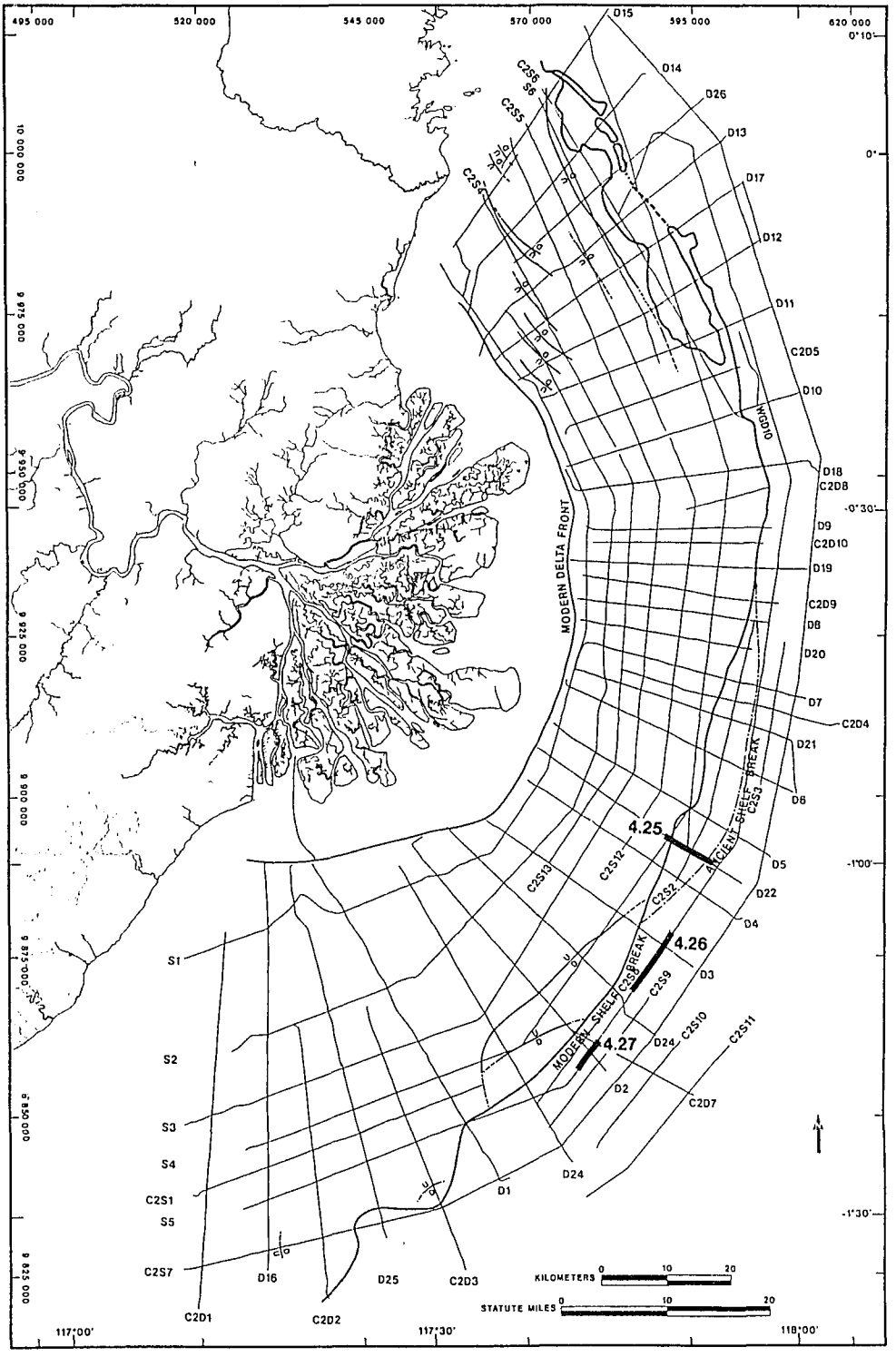

Figure 4.24 Location map of seismic profiles in Figures 4.25 to 4.27, on the slope.

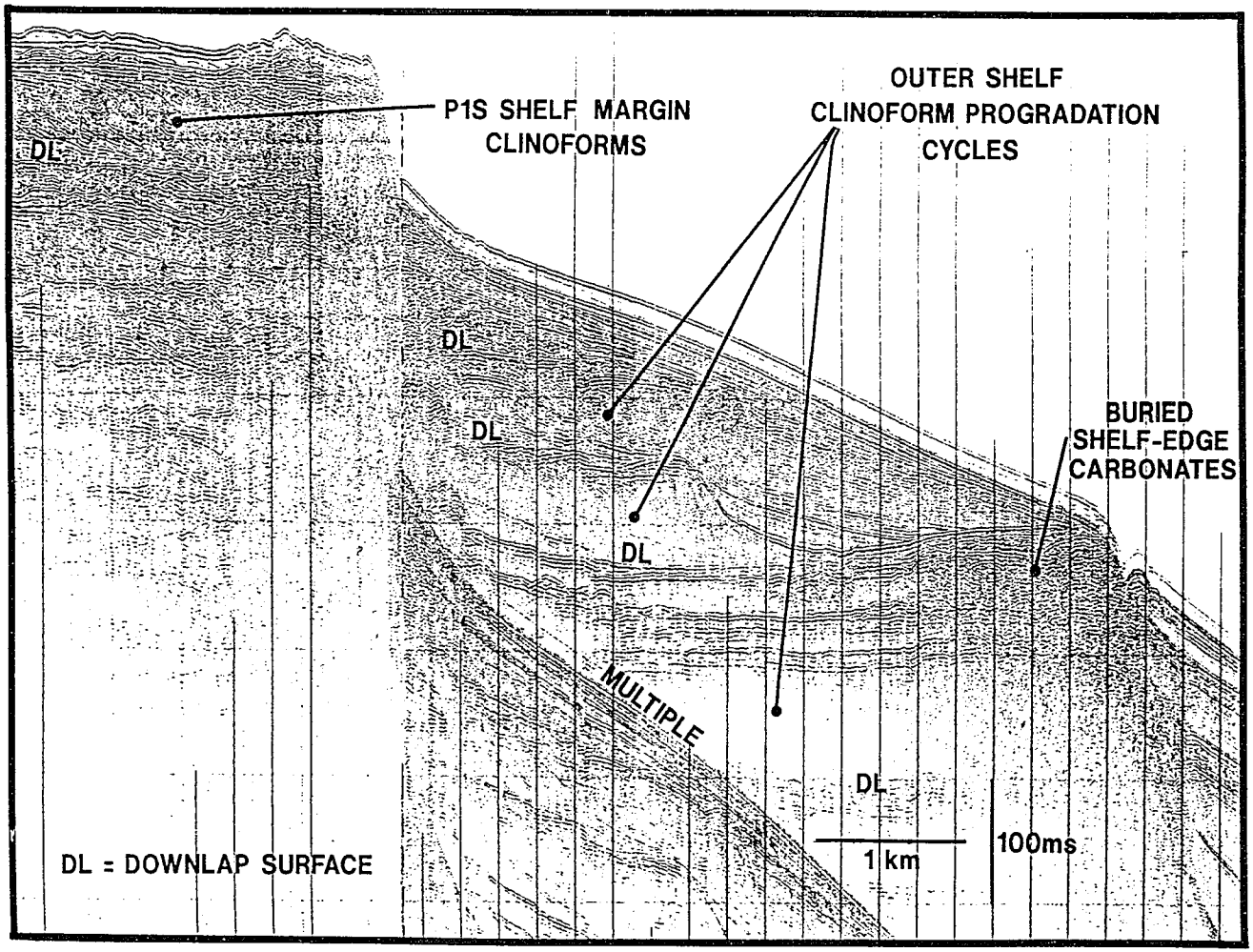

Figure 4.25 Seismic Water Gun Line D22. Depositional Cycles are stacked beneath the shelf break. Each cycle contains a Clinoform Unit and is bounded above and below by Downlap Surfaces. Due to latterally offset "shingled" stacking of successive lowstand depocenters not all Depositional Cycles are represented by a thick Clinoform Package in this single profile.

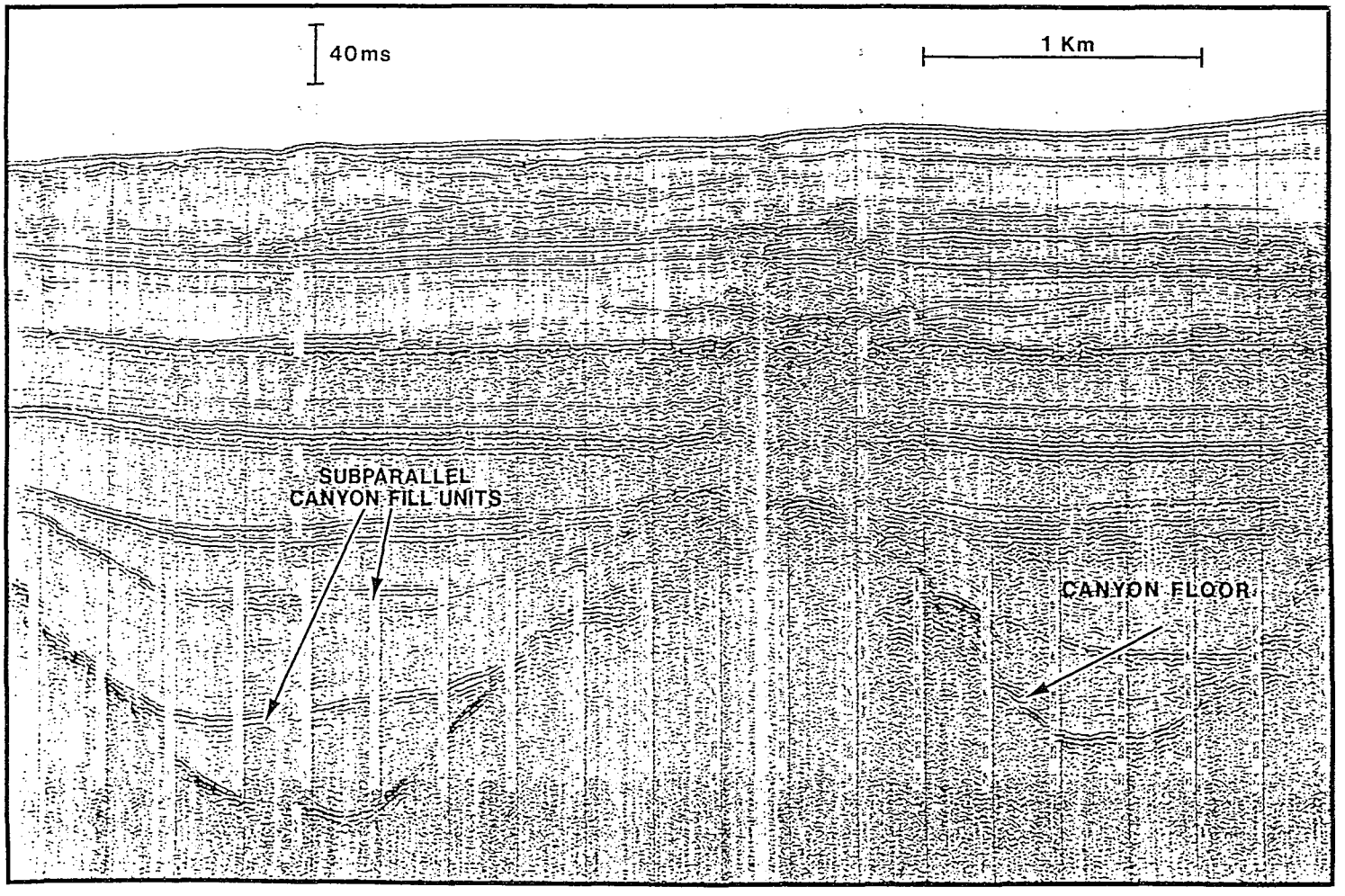

Figure 4.26 Seismic Water Gun Line S5, strike section. Thin , high amplitude zones subdivide the slope stratigraphy into Depositional Cycles, and probably represent condensed, sediment starved intervals which correlate to Downlap Surfaces on the shelf. Two small canyons are filled with conformable, cyclic slope deposits.

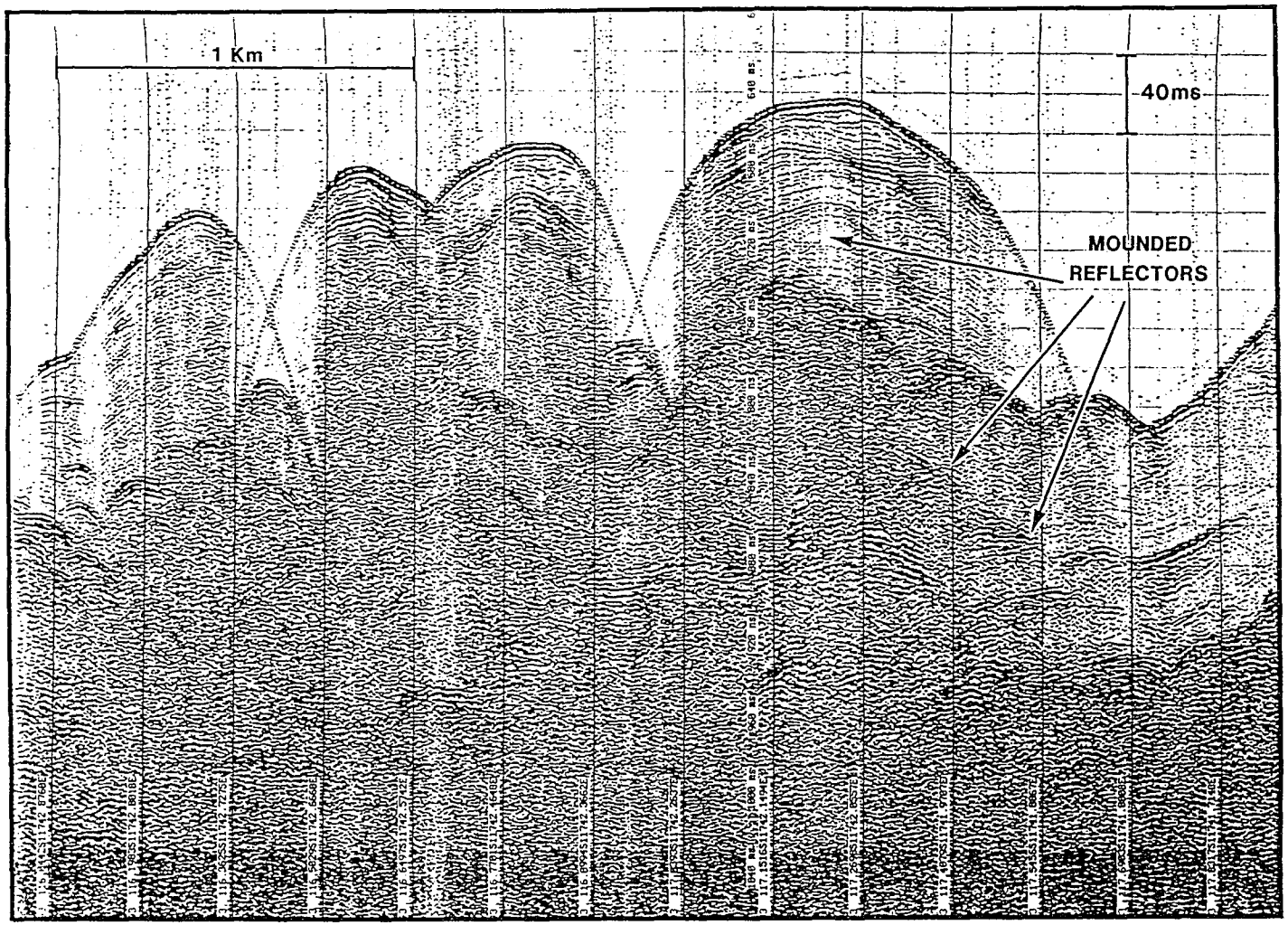

Figure 4.27 Seismic Water Gun Line S5. Strike view showing large "mounds" which are rotated slide blocks within a large slump scar downdip of the P1S depocenter (see Figure 4.3). Slump scars and chaotic to mounded deposits are comon on the steep slope.

carbonate bioherms are buried by clinoforms the surface is defined as the uneven tops of the carbonates (Figure 3.4). The equivalent of the Downlap Surface may be difficult to define on the outer shelf if overlying clinoforms are not present, or are very thin and have low dip gradients, or where it passes through the middle of amalgamated carbonate bioherms (Figure 3.7). Internal downlap may occur within the overlying Clinoform Package (Figure 4.16), and is often more obvious than the subtle, low-angle downlap terminations against the basal, regional downlap surface.

Numerous Depositional Cycles containing clinoforms, and separated by Downlap Surfaces, are stacked beneath the shelfbreak (Figure 4.25). Similar to other parts of the world, the equivalent surfaces on the slope are probably high amplitude reflections which subdivide the slope stratigraphy (Figure 4.26). Piston cores P6 to P8 through the top of stratified slope deposits on the present sea floor - the modern equivalent of buried high-amplitude zones, contain over 6 m of bioturbated, muddy bioclastic sand, composed largely of foraminifera tests (Figure 3.2).

4.1.2 **Clinoform Packages**

Progradational Clinoform Packages are volumetrically the most significant units on the shelf. Clinoform facies are easy to recognize in high-resolution seismic data from the Mahakam Shelf. Both tangential-oblique and sigmoid clinoforms occur (Figure 4.4). Maximum clinoform dips may vary from near horizontal to approximately 5°. Draping of clinoforms where they overlie carbonate mounds, together with syndepositional differential compaction, has resulted in "deformation" of clinoforms which mimics the top-of-carbonate topography (Figure 3.4). Steeply-dipping clinoforms may locally downlap onto the distal low-angle toes of preceding clinoforms resulting in internal downlap surfaces (Figure 4.16). Axes of diverging clinoform dips (seen in strike-oriented profiles), termed progradation centers, are associated with some Clinoform Packages (Figures 4.17 to 4.18). Chaotic units

interbedded with the clinoforms are rare, but may occur near the base of the package where progradation centers produce thick clinoform sets (Figure 4.17).

Vibracore V18 and piston core P11 penetrate sigmoid-clinoform topsets at the shelf edge in water depths of 93 m and 123 m, respectively (Figure 4.7). These cores contain alternating sand and dark gray organic rich mud beds, and prevalent lignite drapes, very similar to the modern subtidal delta platform and delta front (Figure 4.28). Large burrows from the modern sea floor have penetrated down to 4 m in V18, and are filled with fossiliferous shelf mud (Figure 3.2n). Shelf mud is not present at the sea floor in core V18. Vibracore site V21, situated within a modern shelf-scour channel, penetrates P1 clinoform bottomsets and contains dark to medium gray muds with finely disseminated plant organics, incipient diagenetic nodules, and very little fauna, similar to modern delta front muds.

4.1.3 **Onlap Surface**

The Onlap Surface has a gentle seaward gradient, truncates underlying oblique clinoforms, and overlain by a unit of onlapping horizontal to sub-horizontal strata (Figures 4.1, 4.4). Onlap of overlying strata onto this surface is subtle, and is most obvious where the surface has steeper relief (Figure 4.5). The Onlap Surface is generally planar, but may show erosional topography. At its seaward limit the surface turns into a sigmoid clinoform (Figure 4.4) and defines the transition from tangential-oblique (progradational) to sigmoidal (progradational/aggradational) clinoforms.

4.1.4 **Horizontal Unit**

A distinct unit of horizontal to sub-horizontal, moderate to high amplitude continuous reflections may overlie the clinoforms, and onlap the Onlap Surface (Figures 4.1, 4.3, 4.4). These reflection events are the updip extensions of progradational/aggradational sigmoid clinoforms. Higher-than-average amplitude reflections subdivide the Horizontal Unit. Steep-sided erosional channels, from less than 50 m to more than 1 km wide, and up to 25 ms deep (~ 19m), are nested within

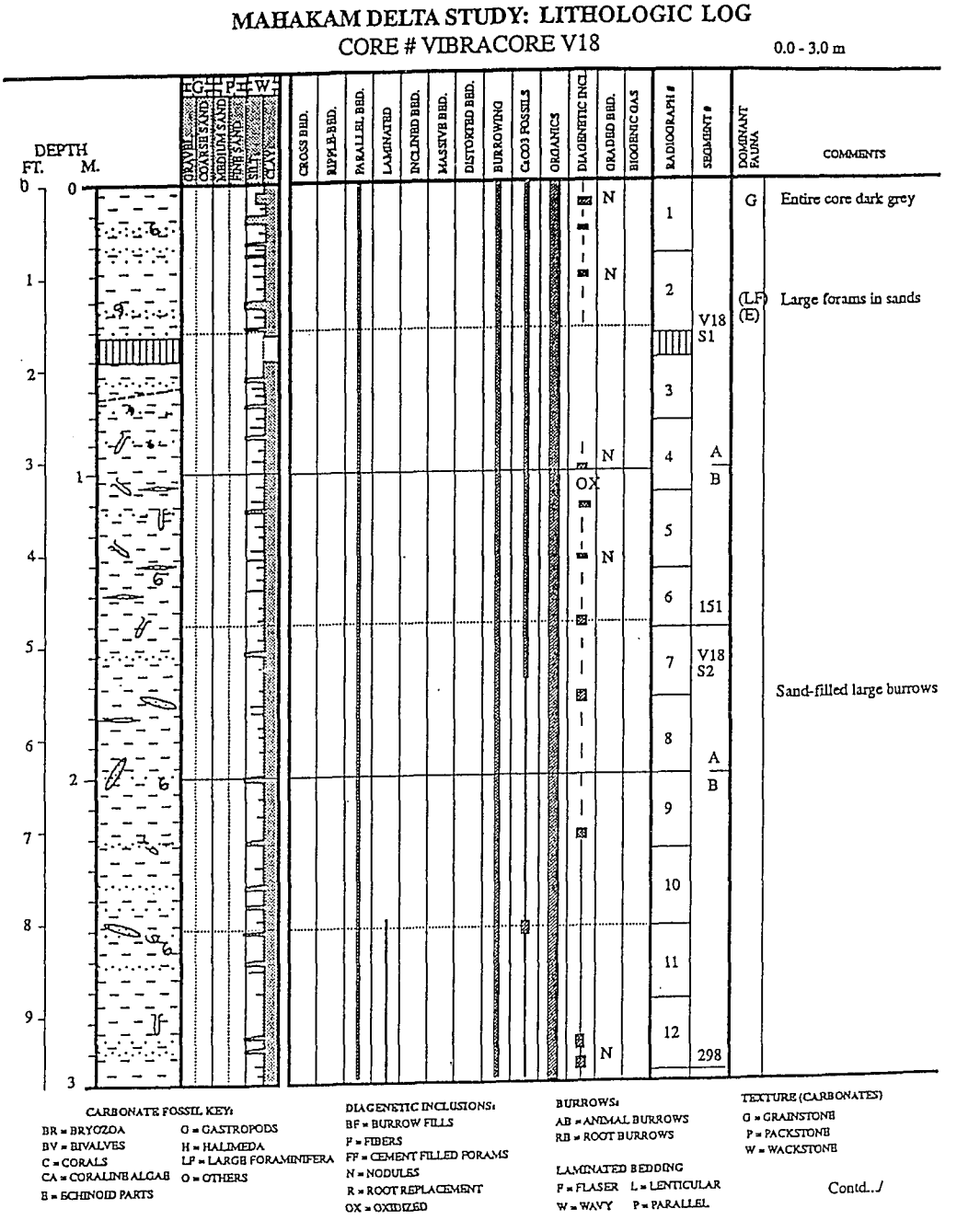

Figure 4.28 Lihologic log of vibracore V18, from the shelfbreak at 93m water depth. The core penetrates the sigmoid-clinoform-topset/horizontal-strata transition of the P1S depocenter (see Figure 4.7). Sediments are very similar to subtidal platform/delta front material of the modern delta. Burrows at the sea floor penetrate more than 3 m into the delta substrate. Key to lithologic symbols in the Appendix. Figure continued on the next page.

MAHAKAM DELTA STUDY: LITHOLOGIC LOG

CORE # VIBRACORE V18 3.0 - 5.73 m

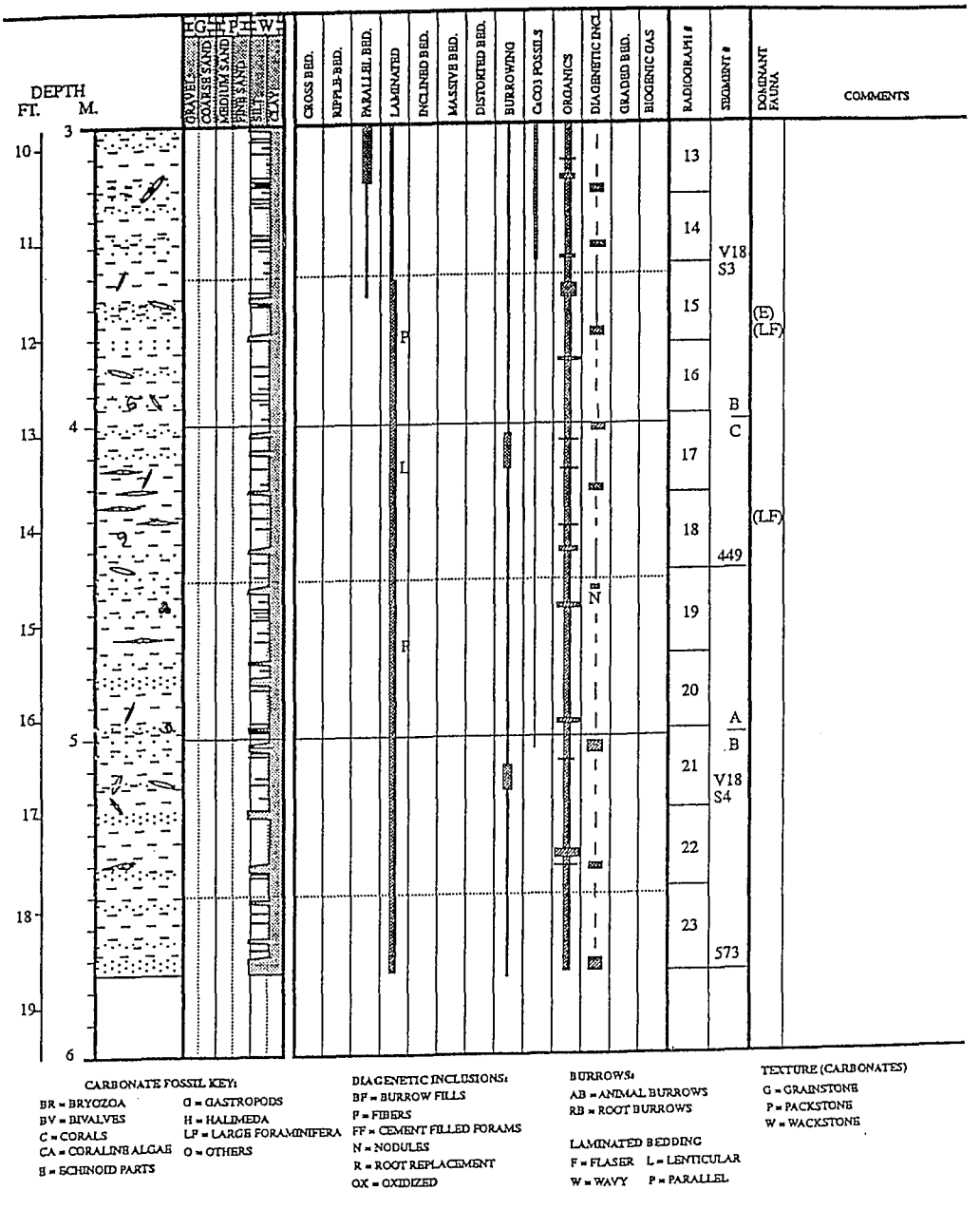

the horizontal strata (Figure 4.6). There is no evidence for extensive, if any, lateral migration of these narrow channels. Channels are filled with onlapping or inclined strata, or seismically transparent fill. In some cases the lower 10-15 ms of fill in the channel is of slightly higher amplitude and chaotic-looking Reworked Facies (explained below). Multiple levels of channels occur, the channels appear to originate at the aforementioned high-amplitude sub-dividing reflections (Figure 4.6).

Vibracores V17, V20, V20a, and V22 targeted the Horizontal Unit (Figure 1.4), but due to the stiff nature of the clay at the top of this facies penetration was poor. The clays recovered from the top were light gray, mottled clay, with roots, lignite particles, and abundant red oxidation zones. Faunal remains were absent. The sediments appeared to be a more oxidized version of the mottled organic rich clays of the modern delta plain swamps (Vibracores IB-1 to IB-8, Figure 1.5).

4.1.5 **Reworked Unit**

Zones of complex reflection configurations, including chaotic (Figure 4.19), channeled, and steep lateral accretion reflections (Figures 4.8, 4.9, 4.10), occur near the top of Clinoform Packages and within the overlying Horizontal Units. The erosional base and edge of this unit is defined by a distinct change from orderly reflections of the Clinoform and Horizontal Units to the disorderly appearance of the Reworked Unit (Figure 4.9). This erosional surface is sometimes represented by a higher-amplitude reflection event. Many steep sided channels within the Horizontal Unit have chaotic looking, high amplitude reworked facies in the lower 10-15 ms of fill (7-10 m) and an onlapping horizontal upper fill (Figures 4.11 - transverse channel section, and 4.12 - section oblique to channel axis).

4.1.6 **Upper Truncation Surface**

Erosional truncation of horizontal and clinoform reflections occurs near or at the present sea floor. Truncation may be planar (Figures 3.4, 4.4), or irregular (Figure 4.18). When the upper truncation surface is associated with carbonate bioherms it is

commonly planar where it is buried beneath the bioherms, and forms incised erosional cuts in between the bioherm (Figure 3.4). The erosional cuts into the top of the P1 cycle are still active today as interpreted from the lack of sedimentary fill (Figures 3.5, 3.7). Vibracores V5, V7, V17 to V23, and V25 all penetrate this surface (Figure 1.4). In each core the surface marks an abrupt change from marginal to non-marine below to fossiliferous, olive green prodelta/shelf muds and muddy sands above this surface (Figures 3.2m-n, 4.28 to 4.30). Large, marine sediment filled burrows penetrate into the lower non-marine unit.

4.1.7 **Bioherm Unit**

The Pleistocene equivalents of the Holocene *Halimeda* bioherms and shelf-edge buildups are found at the base of the P1 and earlier cycles (Figures 3.4, 4.5, 4.23, 4.25) . Description and interpretation of these facies has been covered in Chapter 3 under Holocene Stratigraphy.

4.1.8 **Surface Unit**

Above the Upper Truncation surface there is sometimes a thin (commonly 5 ms, up to 10 ms thick) unit that is not bioherm or prodelta facies. The Surface Unit possibly reflects reworked material associated with erosion at the Upper Truncation surface, prior to bioherm development. The coarser material encountered above the Pleistocene/Holocene boundary in cores V5, V7, V20 to V23, and V25 probably represent the Surface Unit (Figures 3.2m, 4.29), but at these locations the unit is too thin to characterize seismically. Where the Surface and Bioherm Units are absent the Upper Truncation and Downlap Surfaces coincide (Figure 4.1).

4.1.9 **Acoustic Wipeout Zones**

Acoustic penetration is limited or non-existent landward of where the modern Delta Front attains a thickness greater than about 40 ms (30 m). As explained in Chapter 3, this response is probably due to biogenic gas. Penetration is also hampered beneath thick carbonate buildups (Figure 3.4), and in regions associated with

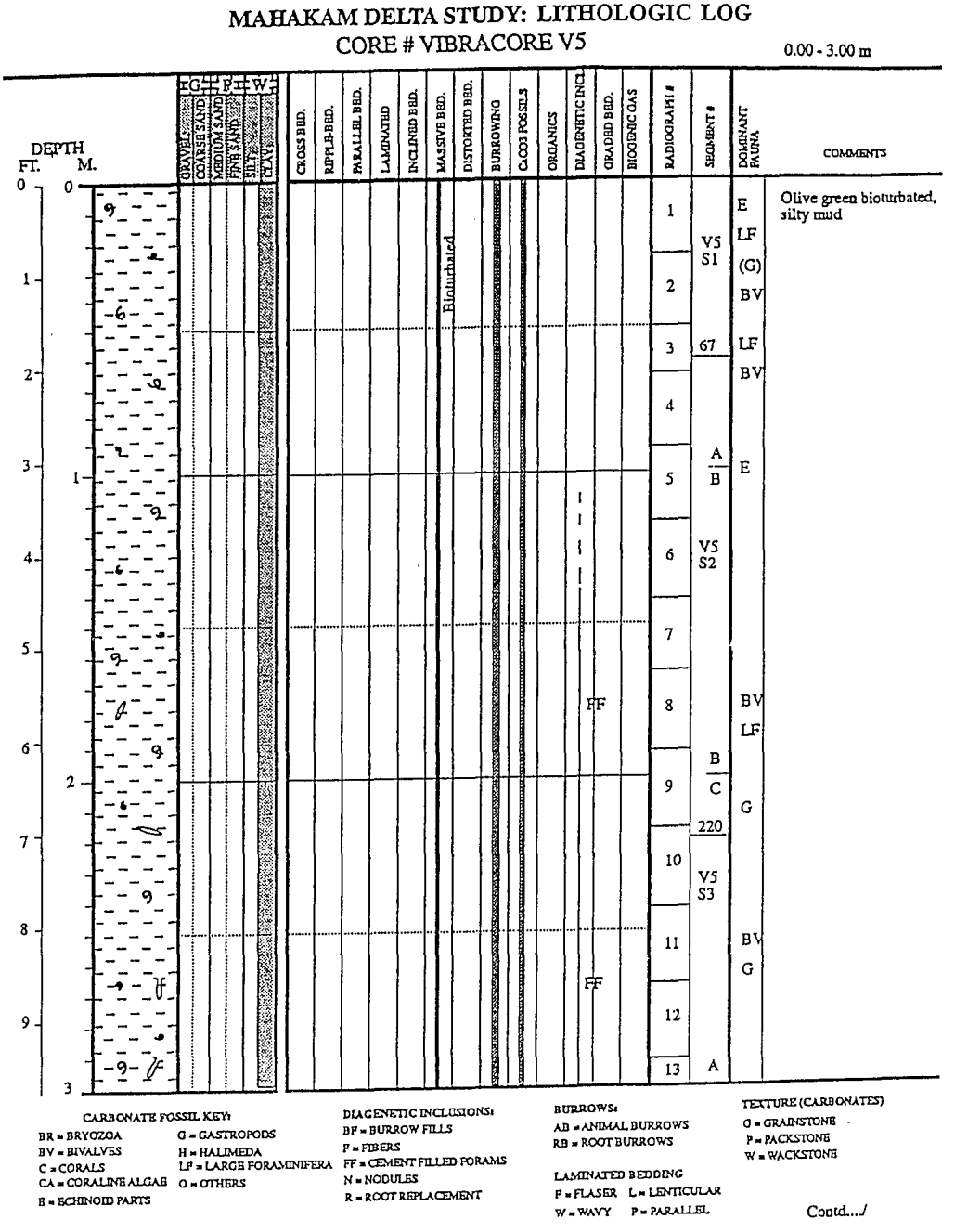

Figure 4.29 Lithologic log of vibracore V5, acquired on the inner shelf of the northern sector. The base of the core penetrates through the Upper Truncation Surface into oxidized non-marine sands at the top of steep P1N clinoforms. Key to lithologic symbols in the Appendix. Figure continued on the next page.

MAHAKAM DELTA STUDY: LITHOLOGIC LOG

CORE # VIBRACORE V5

3.00 - 5.17 m

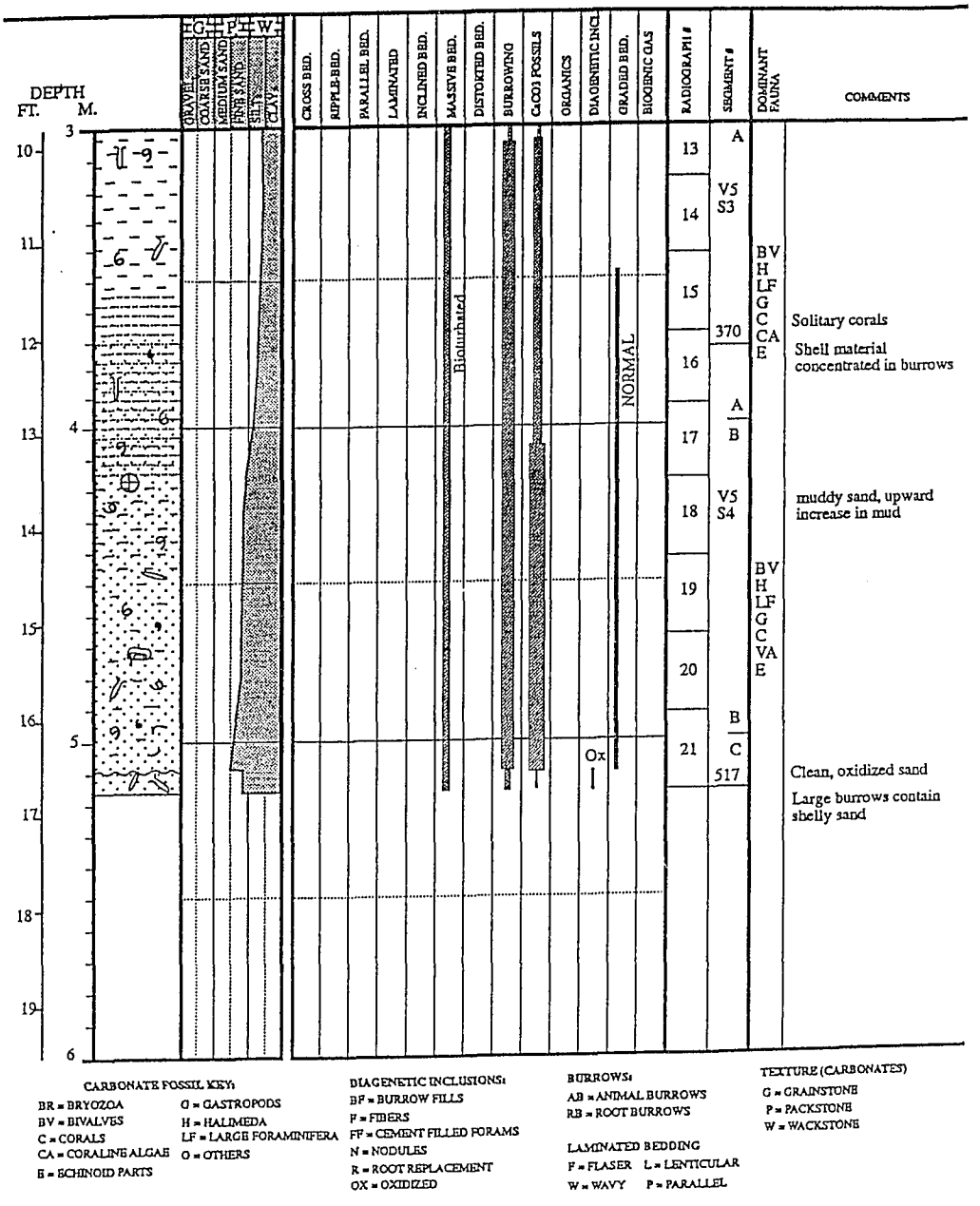

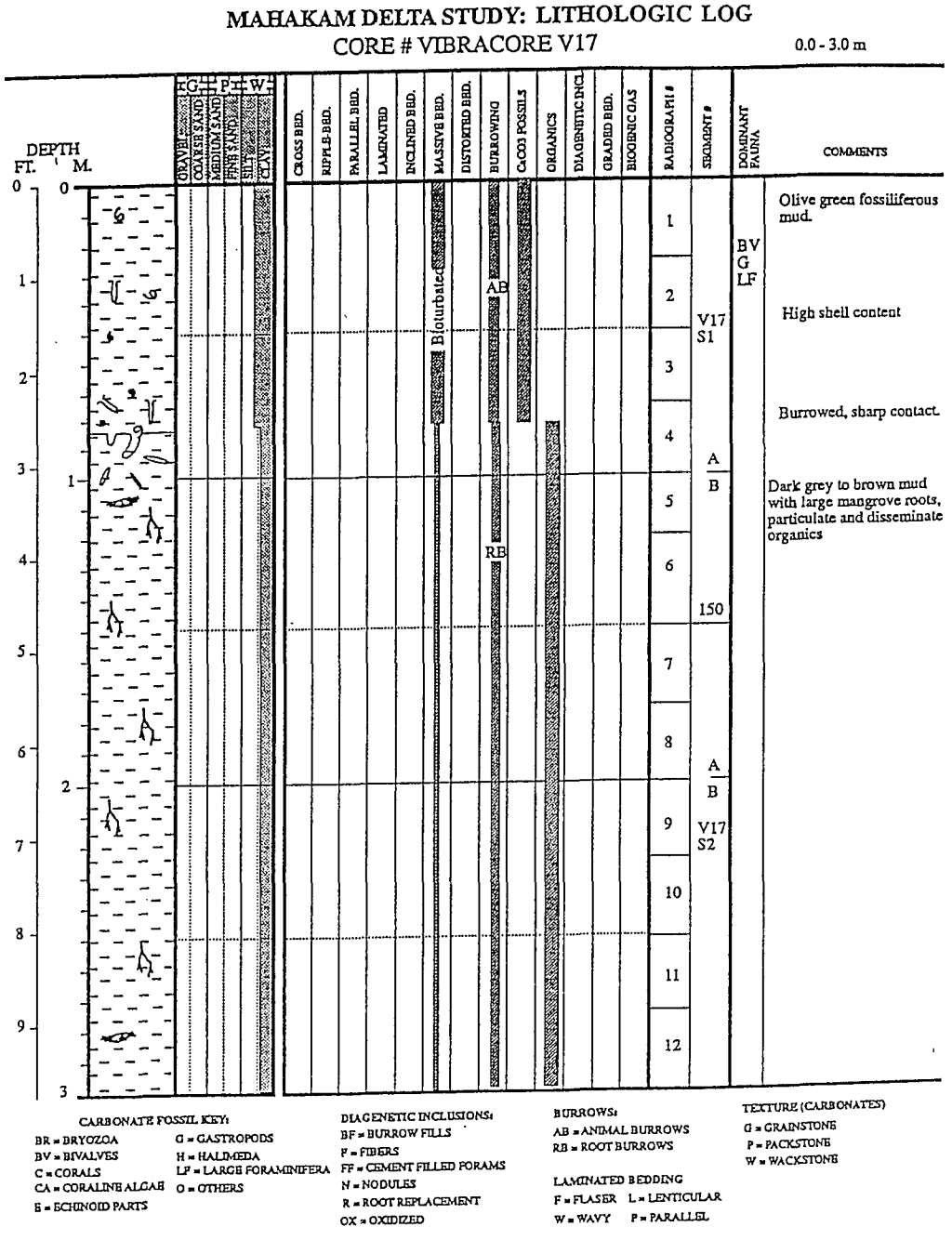

Figure 4.30 Lithologic log of vibracore V17. The core penetrates the transgressive ravinement surface (Upper Truncation) at the top of Increment P1C, southern depocenter (P1S). Key to lithologic symbols in the Appendix. Figure continued on the next page.

MAHAKAM DELTA STUDY: LITHOLOGIC LOG

CORE # VIBRACORE V17

3.0 - 5.18 m

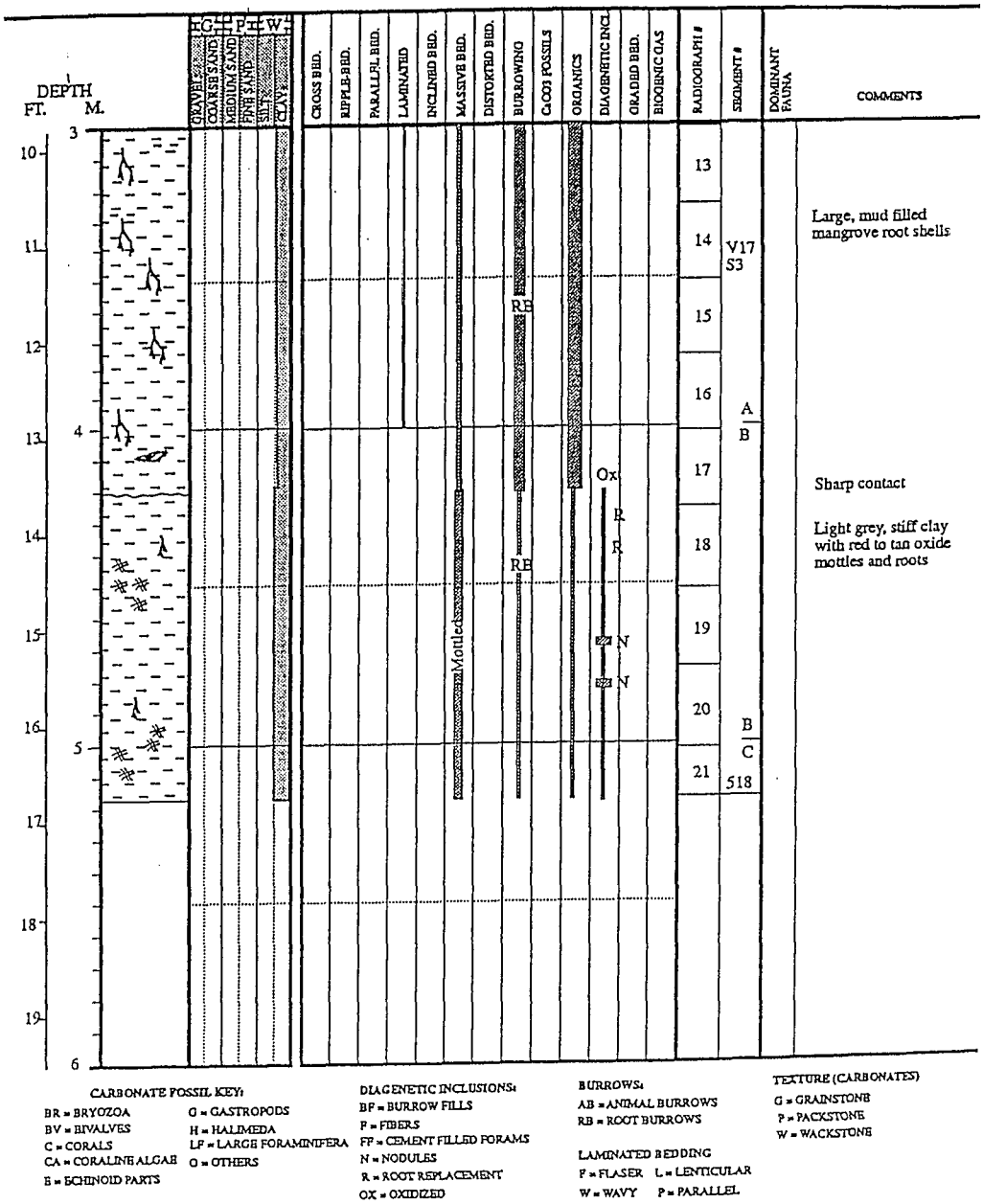

CARBONATE FOSSIL KEY:
BR = BRYOZOA
BV = BIVALVES
C = CORALS
CA = CORALINE ALGAE
E = ECHINOID PARTS
G = GASTROPODS
H = HALIMEDA
LF = LARGE FORAMINIFERA
O = OTHERS

DIAGENETIC INCLUSIONS:
BF = BURROW FILLS
F = FIBERS
FF = CEMENT FILLED FORAMS
N = NODULES
R = ROOT REPLACEMENT
OX = OXIDIZED

BURROWS:
AB = ANIMAL BURROWS
RB = ROOT BURROWS

LAMINATED BEDDING
F = FLASER L = LENTICULAR
W = WAVY P = PARALLEL

TEXTURE (CARBONATES)
G = GRAINSTONE
P = PACKSTONE
W = WACKSTONE

extensive, thick Reworked Facies (Figure 4.8). In these cases the highly reflective nature of the facies or the basal bounding surface is responsible for the limited acoustic penetration.

4.1.10 **Slope Facies**

Seismic facies on the slope include: onlapping, parallel to sub-parallel and divergent, filled canyons/slump scars, chaotic mounded facies, rotated blocks, and slump scars (Figures 4.26, 4.27). Both Phase 1 and 2 datasets are insufficient to map the units on the steep slope. Available data suggest extensive slope failures below 500 m, some of the larger slump scars are evident in the bathymetry (Figure 1.2)

4.2 **PLEISTOCENE STRATIGRAPHIC SUMMARY**

Stratigraphic relationships of the Mahakam shelf are illustrated by a series of cross sections, drawn to scale, based on the seismic data (Figure 4.31).

4.2.1 **Interpreted Depositional Environments of Seismic Stratigraphic Units**

Bounding Downlap Surfaces are interpreted to represent major marine flooding events on the shelf. The similarities of buried Downlap Surfaces and the modern sea floor support this interpretation. Similar surfaces in the Gulf of Mexico, which have been sampled from borings, represent major highstand flooding periods (1988; Coleman and Roberts, 1988; Sydow and Roberts, 1994).

In descending order of importance the Clinoform, Horizontal, and Bioherm Units make up most of the sediment volume in Cycles P1 to P3. Interpretation of the Bioherm Units is fairly straightforward based on the modern carbonate equivalents present on the shelf. The shape described by a clinoform reflection from the Pleistocene section is similar to the morphology of the modern delta platform. The Clinoform Package is thus interpreted as prograding delta front to prodelta deposits. A clinoform is taken to represent the position and shape of the steep outer edge of the delta platform at time of deposition. Limited core data (vibracores V18, V21, V24, V25, and piston core P11) confirm the deltaic origin of this unit. The updip transition

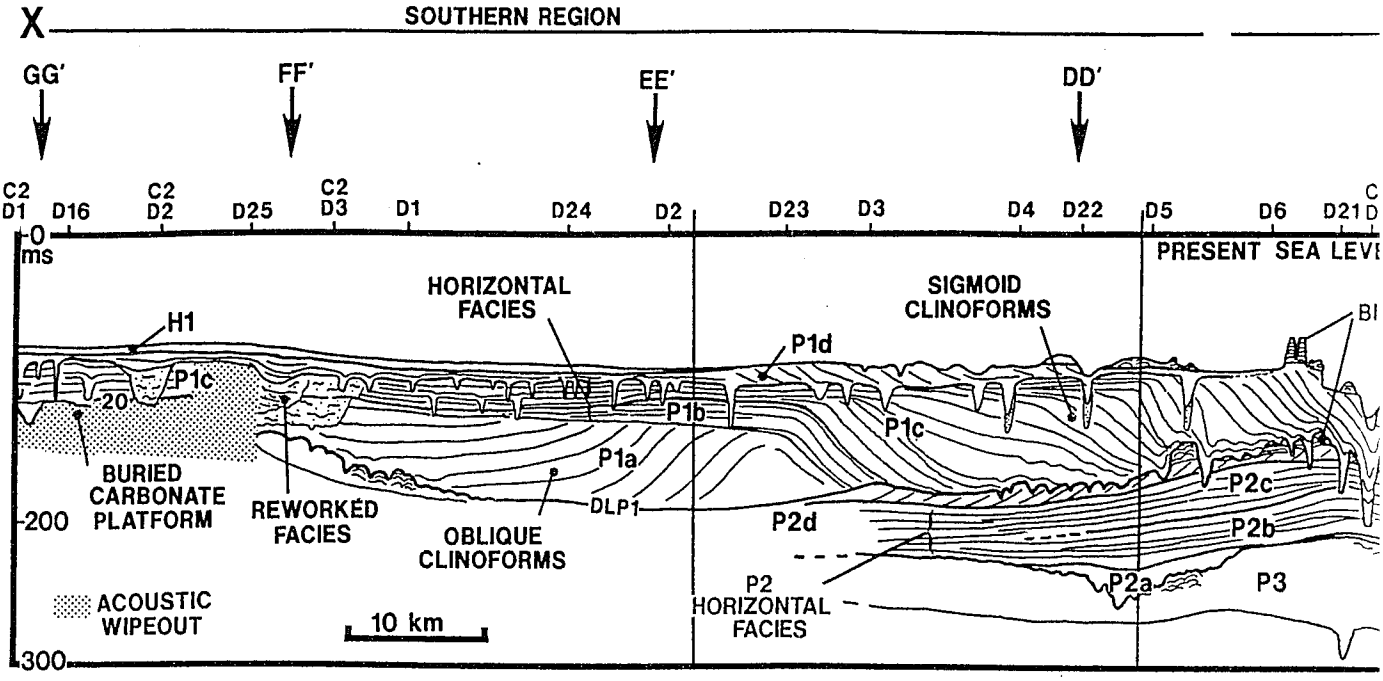

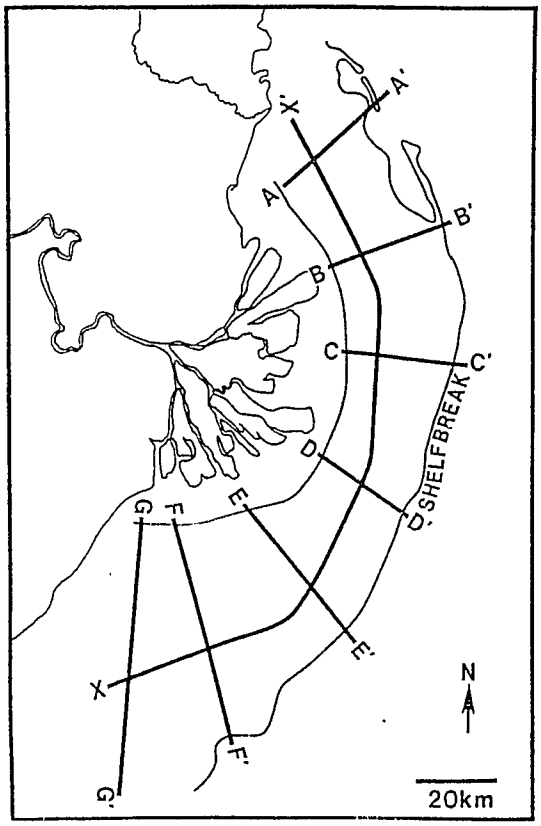

Figure 4.31 Repr
strati
H1 t

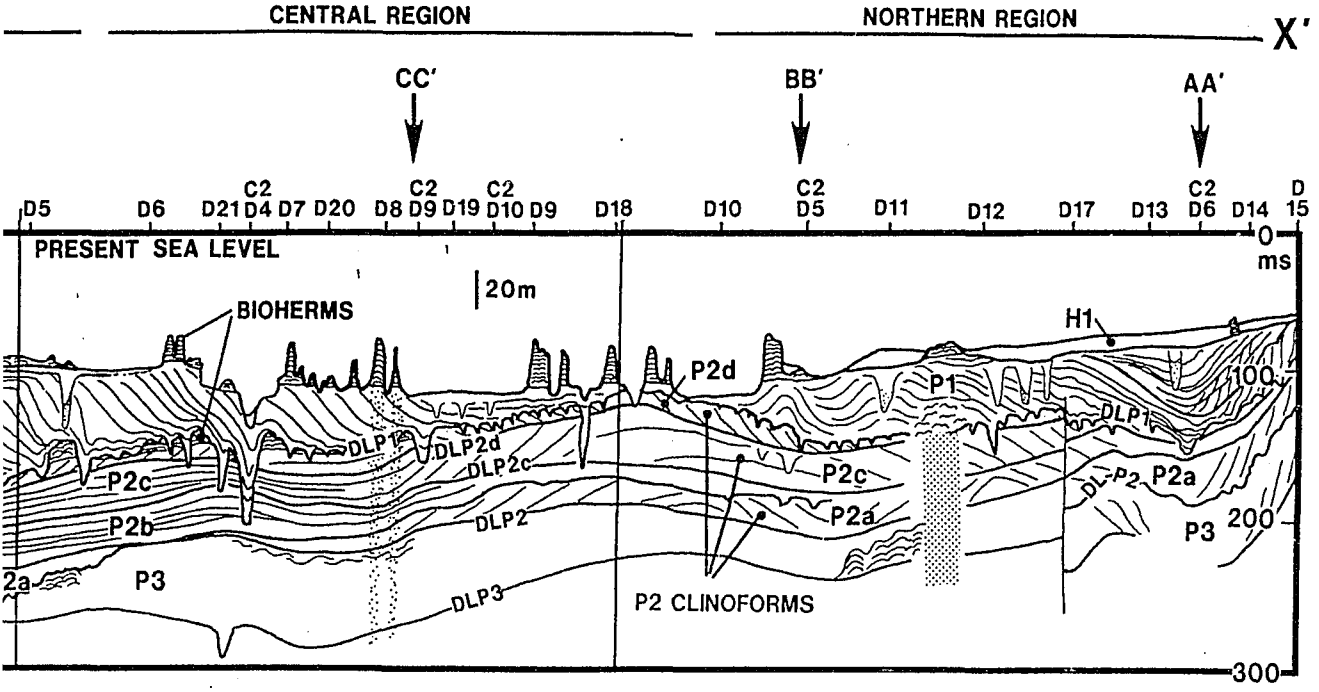

Figure 4.31 Representative cross-sections, drawn to scale, which illustrate stratigraphic relationships and distribution of major units within Cycles H1 to P3 on the shelf. Figure continued on following three pages.

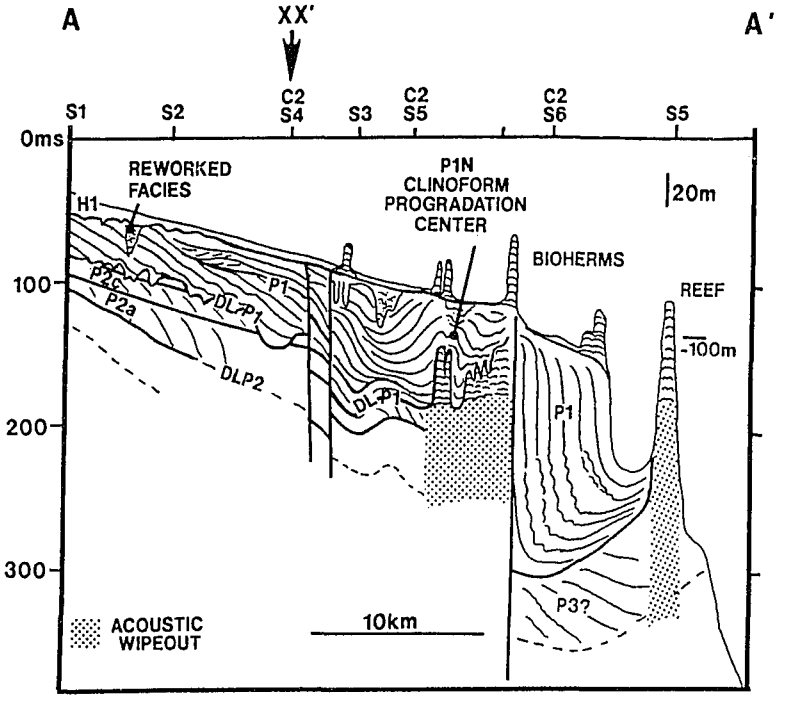
A
XX'
A'
S1
S2
C2 S4
S3
C2 S5
C2 S6
S5
0ms
REWORKED FACIES
H1
P1N CLINOFORM PROGRADATION CENTER
20m
BIOHERMS
REEF
100
P2c
P2a
DLP1
P1
DLP2
100m
200
DLP1
P1
300
P3?
ACOUSTIC WIPEOUT
10km

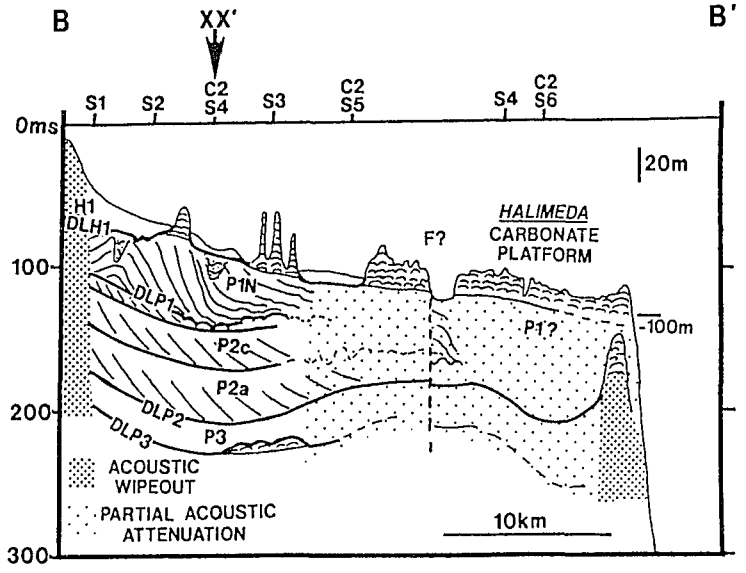
B
XX'
B'
S1
S2
C2 S4
S3
C2 S5
S4
C2 S6
0ms
20m
H1
DLH1
F?
HALIMEDA CARBONATE PLATFORM
100
P1N
DLP1
P1?
100m
P2c
P2a
200
DLP2
DLP3
P3
ACOUSTIC WIPEOUT
PARTIAL ACOUSTIC ATTENUATION
10km
300

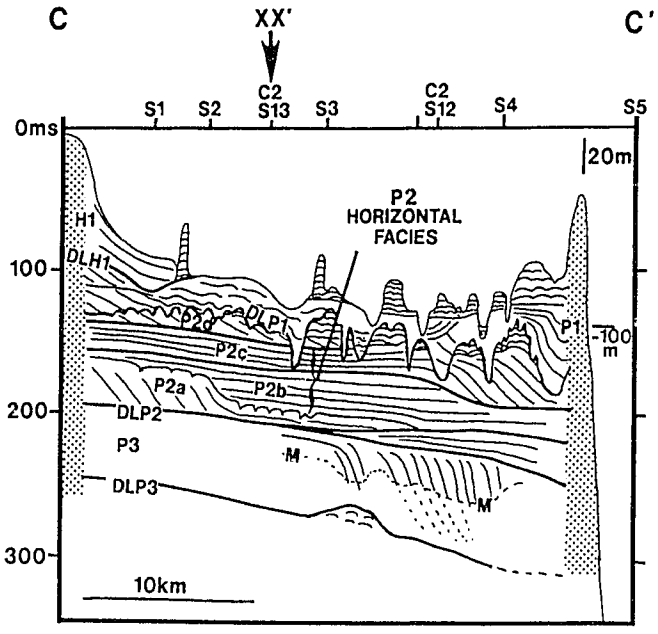
C
XX'
C'
S1
S2
C2
S13
S3
C2
S12
S4
S5
0ms
20m
P2
HORIZONTAL
FACIES
H1
DLH1
100
P2d
DLP1
P1
100
m
P2c
P2a
P2b
200
DLP2
P3
M
M
DLP3
300
10km

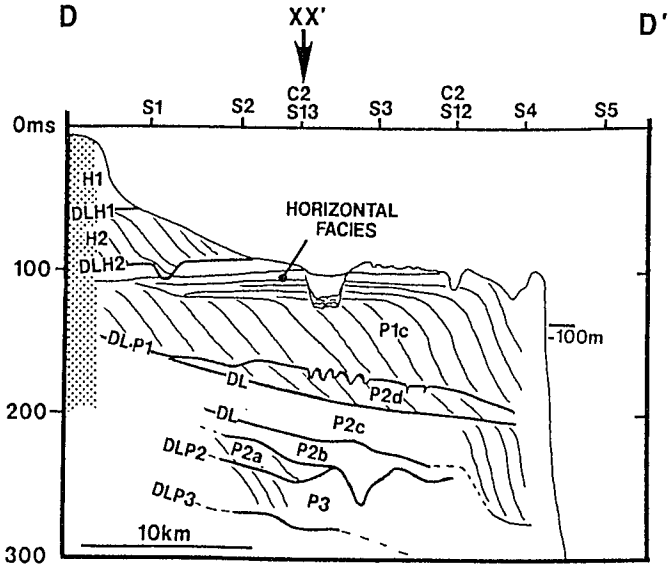
D
XX'
D'
S1
S2
C2
S13
S3
C2
S12
S4
S5
0ms
H1
DLH1
H2
DLH2
HORIZONTAL
FACIES
100
P1c
100m
DLP1
DL
P2d
DL
P2c
DLP2
P2a
P2b
DLP3
P3
200
10km
300

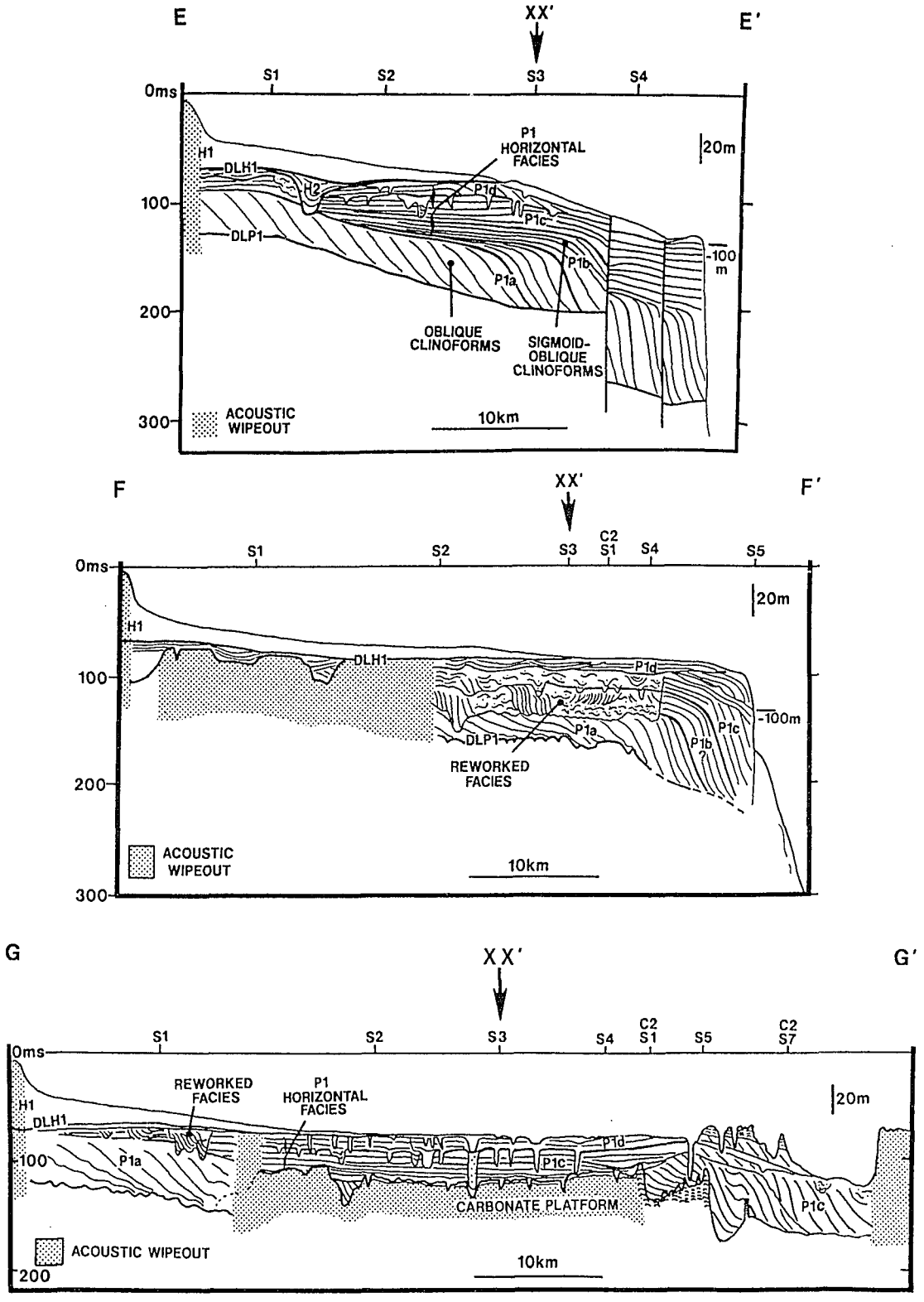
E
XX'
E'
S1
S2
S3
S4
0ms
H1
DLH1
H2
P1
HORIZONTAL
FACIES
20m
P1d
P1c
100
DLP1
P1b
-100
m
P1a
200
OBLIQUE
CLINOFORMS
SIGMOID-
OBLIQUE
CLINOFORMS
300
ACOUSTIC
WIPEOUT
10km
F
XX'
F'
S1
S2
S3
C2
S1
S4
S5
0ms
20m
H1
DLH1
P1d
100
-100m
P1a
P1c
DLP1
P1b
REWORKED
FACIES
200
ACOUSTIC
WIPEOUT
10km
300
G
XX'
G'
S1
S2
S3
S4
C2
S1
S5
C2
S7
0ms
REWORKED
FACIES
P1
HORIZONTAL
FACIES
20m
H1
DLH1
P1d
100
P1a
P1c
CARBONATE PLATFORM
P1c
ACOUSTIC WIPEOUT
10km
200

from sigmoid clinoform to horizontal strata is analogous to the delta front to delta platform transition, which occurs between 5 and 10 m depositional water depth. The Horizontal Unit is therefore interpreted to encompass delta plain and subtidal delta platform deposits. The landward regions where channels are developed within the Horizontal Unit probably represent delta plain deposition. Dimensions of the steep, narrow channel cuts are very similar to distributary and tidal channels of the modern delta plain. Further seaward, where channels are scarce, is interpreted as subtidal delta platform accretion.

The Reworked Unit, associated with erosional trends nested within the Horizontal and Clinoform Units is interpreted as sand prone fluvially dominated channel deposits. The high amplitude basal contact with underlying clinoforms (Figure 4.9) suggests a density contrast across this surface, probably from muddy delta clinoforms to sandy fluvial material. Seismic units with very similar internal reflection configuration and stratigraphic position (incising the top of clinoforms) have been cored in the Gulf of Mexico, and are fluvial in origin (Roberts and Coleman, 1988; Sydow and Roberts, 1994)

Distributions and stratigraphic relationships of the various units and surfaces covered in this chapter, and the model for sequential development of the stratigraphic elements in Chapter 5, will further reinforce the interpretations of depositional environments stated above.

4.2.2 **Pleistocene Cycle P1**

4.2.2.1 Basal Flooding Surface, DLP1

Cycle P1 contains the most recent Clinoform Package beneath the outer shelf. The clinoforms downlap onto Surface DLP1. The structure map on Downlap Surface P1 (Figure 4.32) shows a subtle northeast trending structural high on the middle and outer shelf of the central region (Figures 3.4, and 4.31 sections XX' and BB'), dissected by shore-normal incised shelf-scour channels up to 50 ms deep (Figure

Figure 4.32 Isochron structure map of Surface DLP1, the basal boundary of the P1 Depositional Cycle. Similar to the modern seafloor, the surface represents highstand sea-level flooding of the shelf.

4.22). Fold axes of the subtle structural deformation of Surface DLP1 are mapped in Figure 4.33. Similar to the modern sea-floor, the erosional relief on surface DLP1 in the central region is amplified by buried bioherm platforms perched on the intervening topographic highs (Figures 4.22, 4.23).

Shelf-scour channels terminate on the inner to middle shelf and are filled by downlapping delta clinoforms, not Reworked facies. Channel erosion is thus related to transgressive and highstand flooding of the shelf, not incision by preceding lowstand fluvial processes. Similar erosional features on the modern shelf (Surface DLH1, one sea-level cycle later) suggest that locally, shelf scour processes are focused by abandoned and flooded, shore-normal delta distributaries (Figure 4.13)

4.2.2.2 Two P1 Depocenters

Figure 4.34 is an isochron map which represents the total thickness of all units between Downlap Surfaces DLP1 and DLH1, but excludes the thickness of the overlying Bioherm Unit (ie. thickness of silicilastics during the P1 depositional cycle). The isochrons reveal a northern and a southern depocenter, termed P1N and P1S respectively. Clinoforms of cycle P1 reached the shelf break in the northern and southern regions (Figures 4.3, 4.31 sections AA', FF'), possibly also in the central region (Figure 4.23). The structural high and bioherm buildups beneath Surface DLP1 on the middle shelf of the central region resulted in lack of accommodation space for P1 clinoforms during subsequent lowstand regression. Clinoforms of the P1 delta, if present on the middle shelf of the central region, occur as thin erosional remnants, and as fills in the erosional troughs of Surface DLP1 (Figures 4.23, 4.31 section XX'). In places bioherms beneath Surface DLP1 have amalgamated with Holocene bioherms, the two bioherm cycles are separated by the Upper Truncation Surface.

Clinoforms of the P1N and P1S depocenters overlap slightly on the inner shelf of the central region. The southern lobe is stratigraphically above the northern lobe separated by a downlap surface. The time significance of this downlap surface is

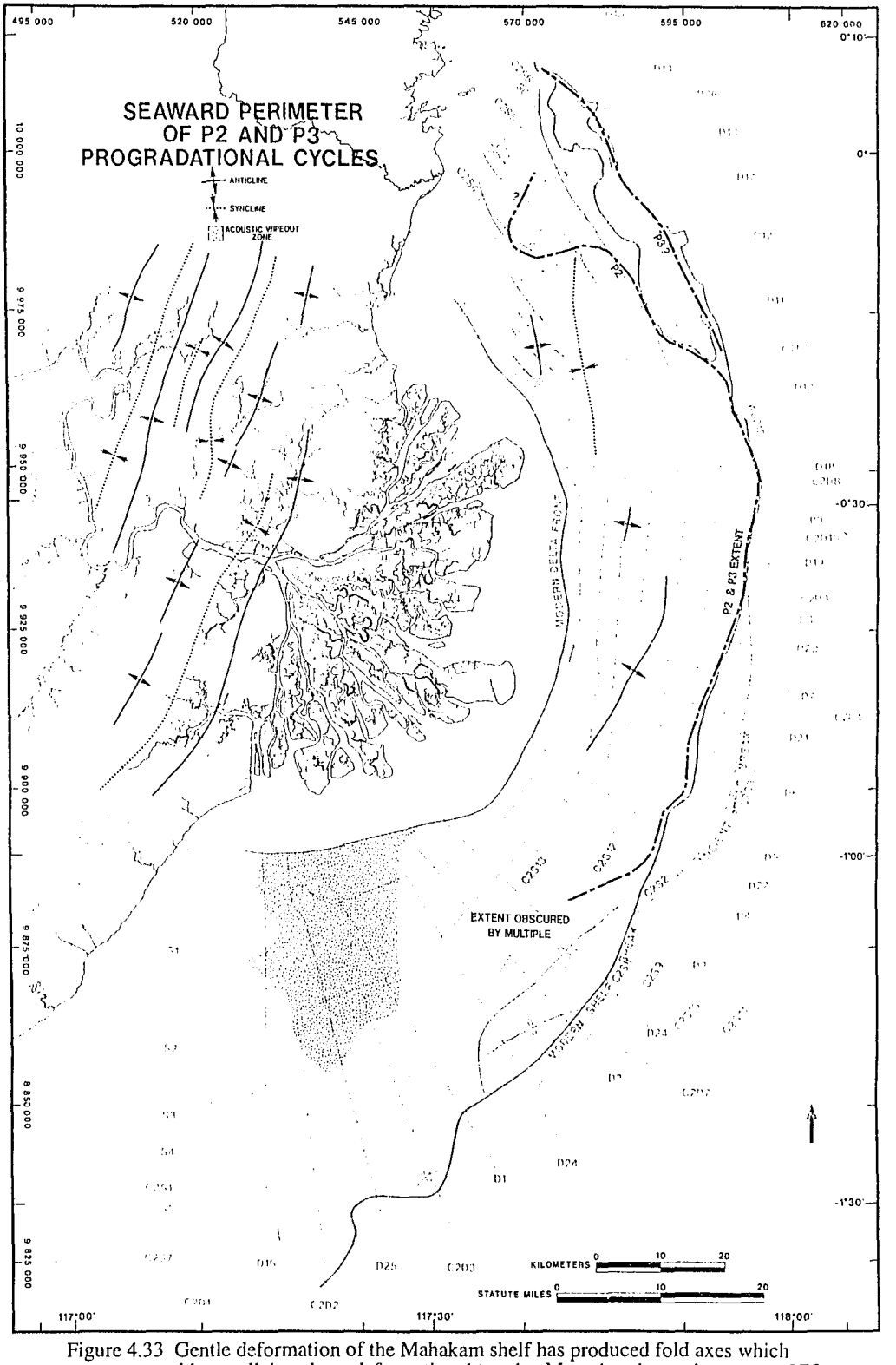

Figure 4.33 Gentle deformation of the Mahakam shelf has produced fold axes which roughly parallel onshore deformational trends. Map also shows the extent of P2 and P3 shelf depocenters.

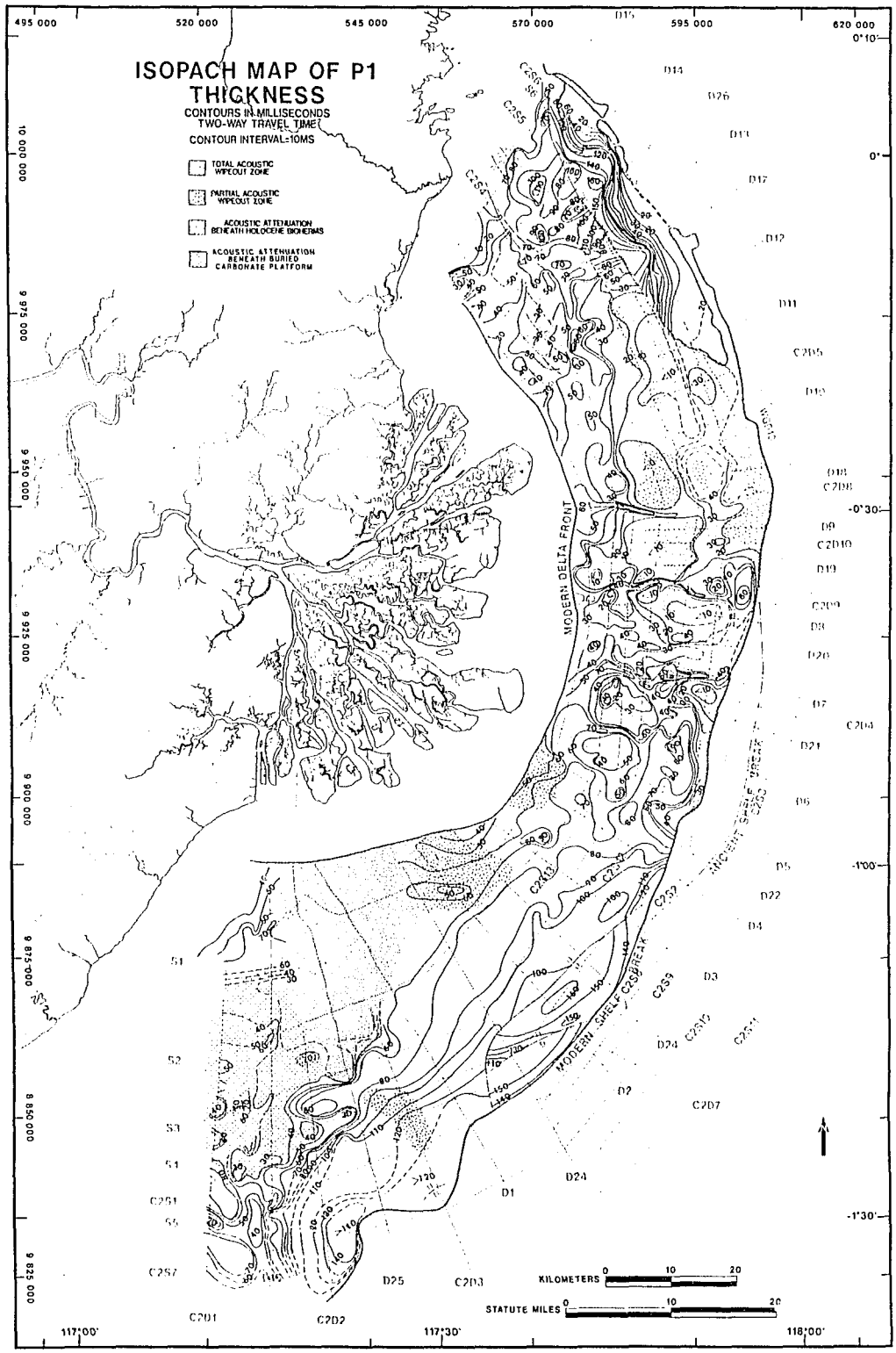

Figure 4.34 Isopach map of Cycle P1 thickness, not including the thickness of P1 cycle carbonates on the modern shelf. Thickness in two-way-travel time (TWT), 10 ms translates to roughly 7.5 m.

unknown, and the temporal relationship between the P1N and P1S shelf-edge depocenters is uncertain.

4.2.2.3 The Southern Depocenter

4.2.2.3.1 Broad, Non-Lobate Delta Front

The southern depocenter (P1S) clinoforms prograded onto a gently seaward dipping (~1:1000) basal surface. Where growth faults occur near the shelf edge the depocenter expands to over 115 m in thickness >115 m (Figures 4.3, 4.31 section EE', 4.34).

The southern depocenter covers a much larger area than the P1N depocenter (Figure 4.34), and contains at least a 5 times greater sediment volume. The successive positions and shape of the delta front are described by lines 1, 2, and 3 in Figure 4.35. Line 1 separates the region of toplapping, oblique clinoforms landward from sigmoid clinoform reflections seaward (Figures 4.4, 4.31 section EE'). There are no progradation-center clinoform geometries evident in the sigmoid clinoform unit of the southern depocenter. The lack of progradation centers together with the plan-view shape of the delta front (Figure 4.35, lines 2 and 3), and the low variability in sigmoid-clinoform dip orientations (Figure 4.35) indicate that the delta advanced along one broad, gently arcuate front, similar to the modern Mahakam delta. The oblique clinoforms landward of line 1 describe a slightly more pronounced lobate delta front (Figure 4.31, section XX').

4.2.2.3.2 Aggrading Delta-Plain/Delta Front

Distribution of the P1 Horizontal Unit is shown in Figure 4.36. The onlapping Horizontal Unit, interpreted as delta plain and subtidal delta platform deposits, constitutes a considerable portion (up to 50%) of the stratigraphic section in the southern P1S depocenter (Figures 4.4, 4.31 section EE'). These strata are syndepositional with sigmoid clinoforms downdip, and clearly represent aggradation due to accommodation created behind the prograding delta front. During the present

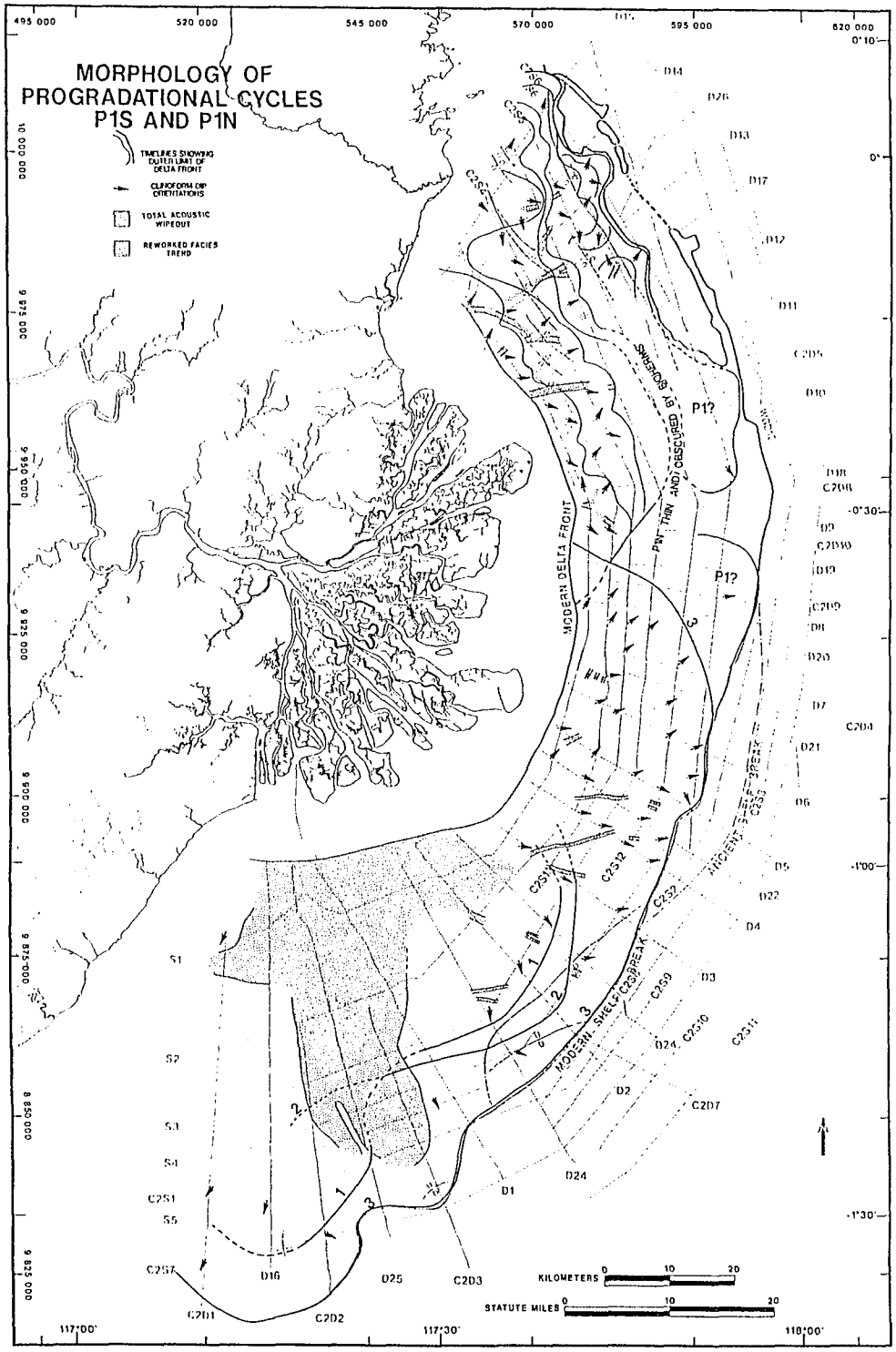

Figure 4.35 Map of P1 delta morphology. Arrows represent direction of clinoform progradation (at seismic profile intersections), solid lines represent the shape and position of the delta front at successive time intervals. The broad, shore-normal Reworked Unit trend and associated wipeout zone obscure underlying deltaic strata in the southern shelf sector. Oblique clinoforms are restricted to landward of line 1 in P1S. Most of P1N consists of oblique clinoforms.

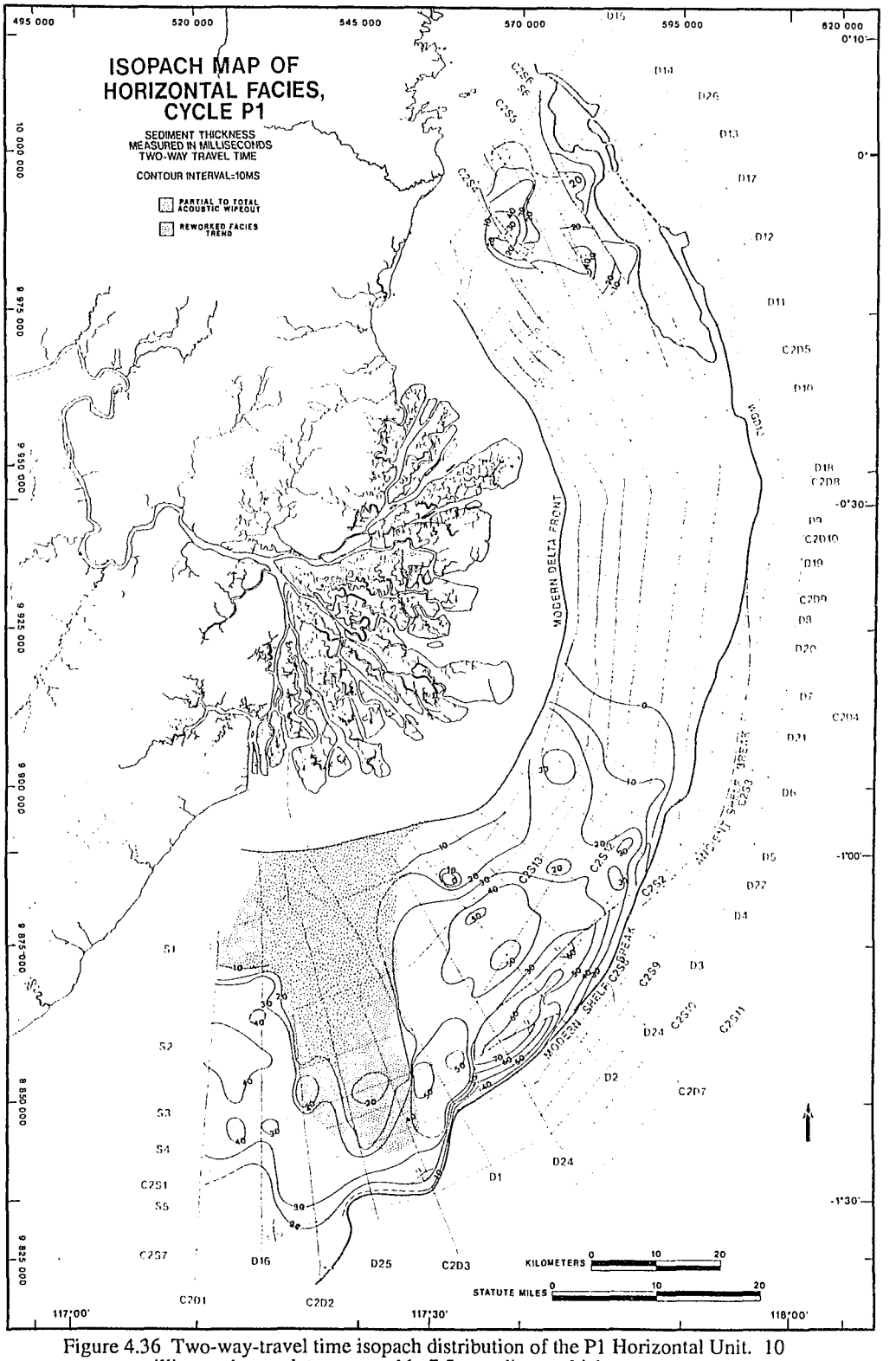

Figure 4.36 Two-way-travel time isopach distribution of the P1 Horizontal Unit. 10 milliseconds translates to roughly 7.5 m sediment thickness.

highstand scenario the modern Mahakam delta plain has accumulated up to 15 m of horizontally stratified delta platform deposits: 3-4 m delta plain, and ~10m subtidal delta platform (Figure 3.12). The 15 m of accommodation generated in less than 5 ky reflects a combination of depositional water depth (5-10 m), and relative sea level rise due to basement subsidence (0.2-0.5 m/ky) and sediment compaction. In contrast with the modern eustatic stillstand, more than 30 m of Horizontal Unit strata accumulated during P1S delta progradation (Figure 4.36). Landward onlap, multiple levels of channels, the stacking pattern of associated downdip sigmoid clinoforms, and more than 30 m of Horizontal Unit aggradation are interpreted to represent delta progradation during an overall rise in relative sea level (Vail et al., 1977) influenced largely by ecstasy.

4.2.2.3.3 Four Growth Increments of P1S

Prominent subdividing reflection events and subtle changes in stratal stacking patterns were used to subdivide the P1S delta package into four growth increments, P1a to P1d (Figure 4.37a-d). Isopachs of increments comprise both clinoforms and, if present, associated horizontal strata. The time represented by each increment is arbitrary and probably not constant.

Increment P1a (Figure 4.37a) represents the distribution of oblique clinoforms landward of line 1 in Figure 4.35. There is no well developed Horizontal facies (delta platform) associated with the oblique clinoforms. The lack of delta-plain facies suggest a lack of accommodation space landward of the proximal prodelta, and probably represents progradation during relative fall in sea level.

Increment 1b (Figure 4.37b - Clinoforms and associated Horizontal facies between lines 1 and 2 of Figure 4.35) represents a small unit with a high aggradation to progradation ratio. Local landward shift in downlap indicates that portions of the delta were abandoned and flooded before P1b progradation. This initial phase of delta-plain aggradation is interpreted as a response to initial relative sea-level rise.

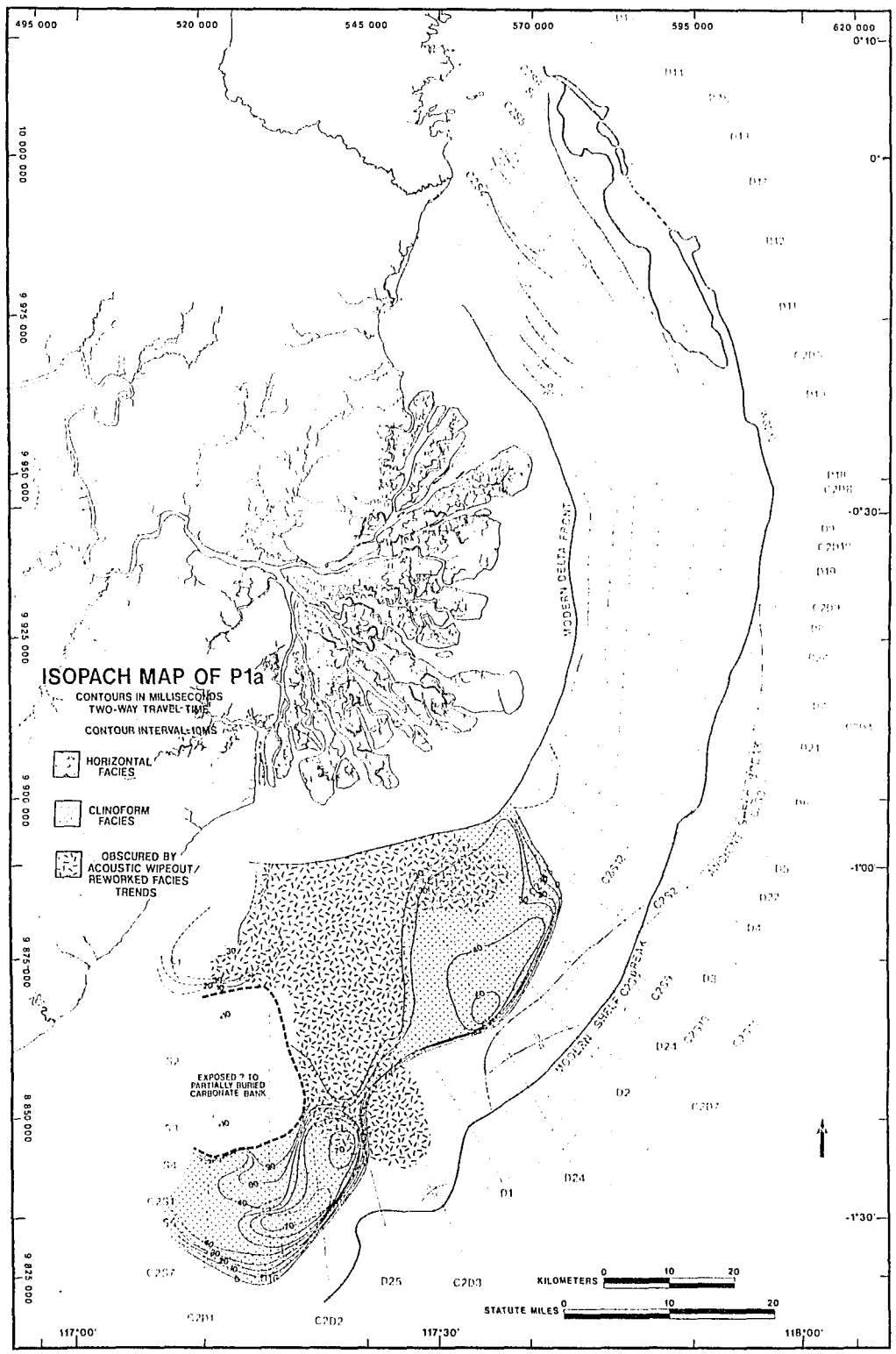

Figure 4.37 a to d Two-way-travel time isopach distributions of four growth increments of P1S delta deposition: P1a to P1d (continued on following three pages).

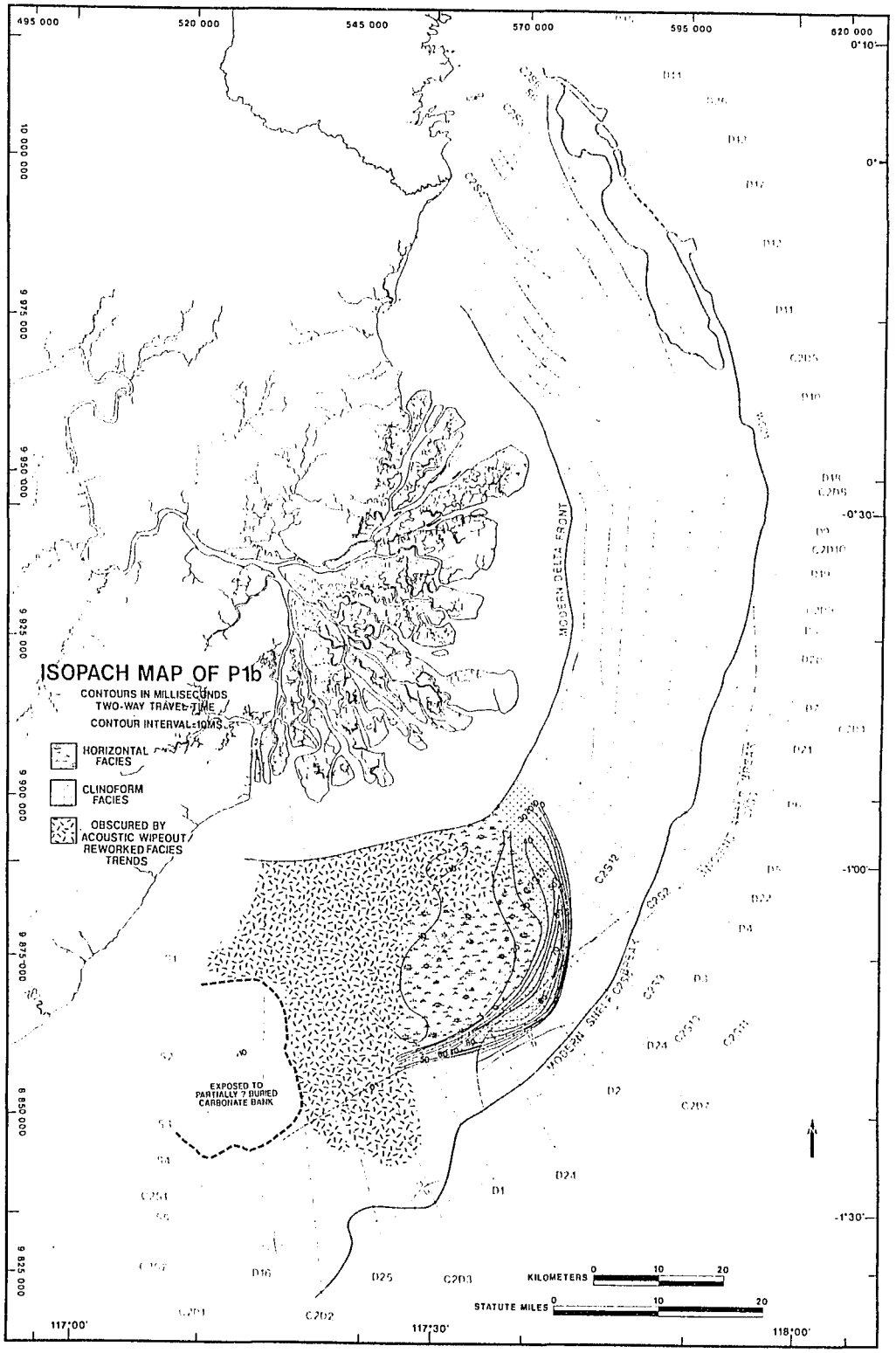
ISOPACH MAP OF P1b
CONTOURS IN MILLISECONDS TWO-WAY TRAVEL TIME
CONTOUR INTERVAL: 10MS
HORIZONTAL FACIES
CLINOFORM FACIES
OBSCURED BY ACOUSTIC WIPEOUT REWORKED FACIES TRENDS
EXPOSED TO PARTIALLY ? BURIED CARBONATE BANK
MODERN DELTA FRONT
MODERN SHELF - OFFSHORE
KILOMETERS 0 10 20
STATUTE MILES 0 10 20
495 000
520 000
545 000
570 000
595 000
620 000
0°10'
0°
-0°30'
-1°00'
-1°30'
117°00'
117°30'
118°00'

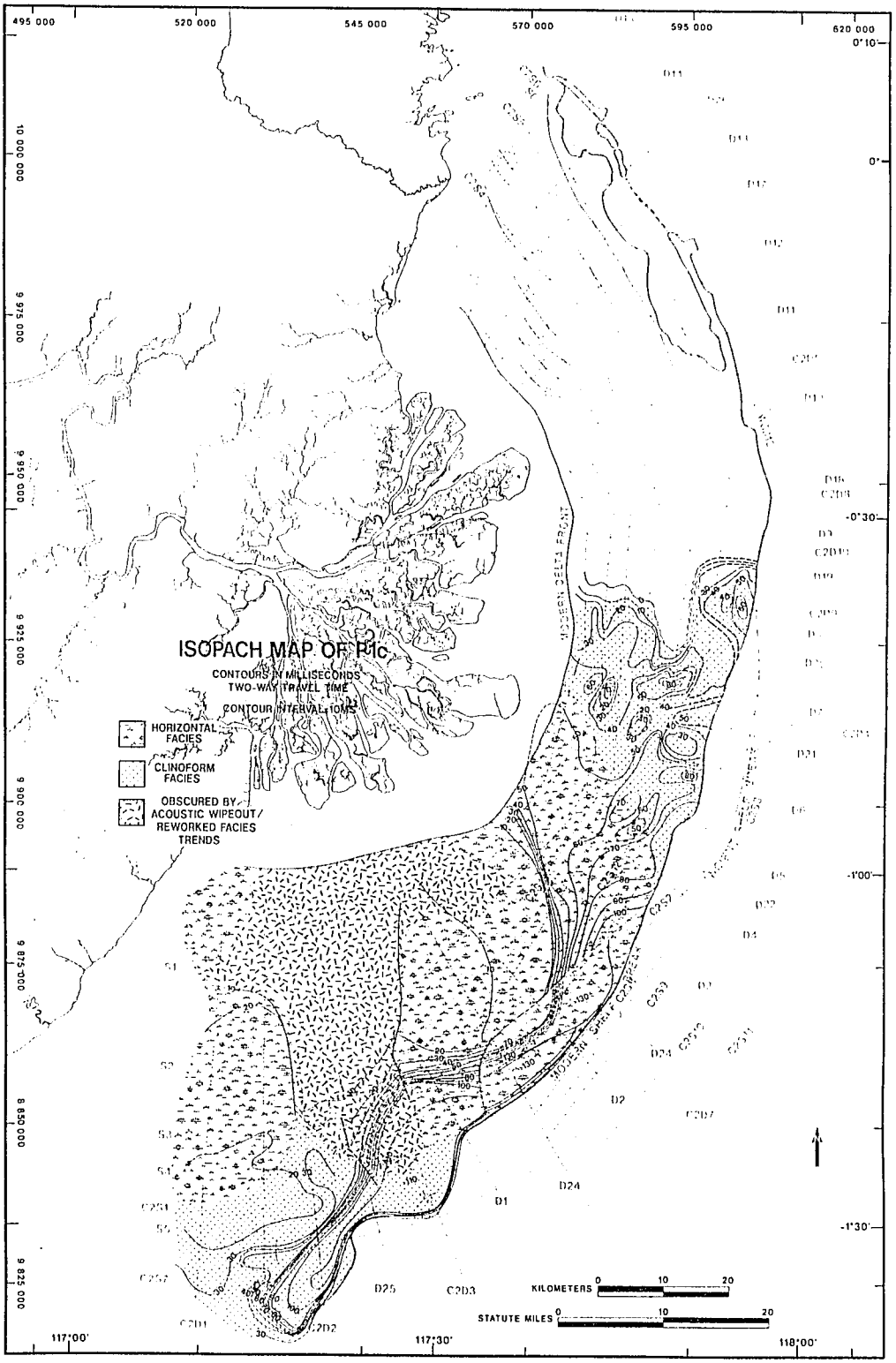
ISOPACH MAP OF P1c
CONTOURS IN MILLISECONDS TWO-WAY TRAVEL TIME
CONTOUR INTERVAL 10MS
HORIZONTAL FACIES
CLINOFORM FACIES
OBSCURED BY ACOUSTIC WIPEOUT/ REWORKED FACIES TRENDS
HOSSEGOR DELTA FRONT
KILOMETERS
STATUTE MILES
495 000
520 000
545 000
570 000
595 000
620 000
0°10'
0°
-0°30'
-1°00'
-1°30'
117°00'
117°30'
118°00'

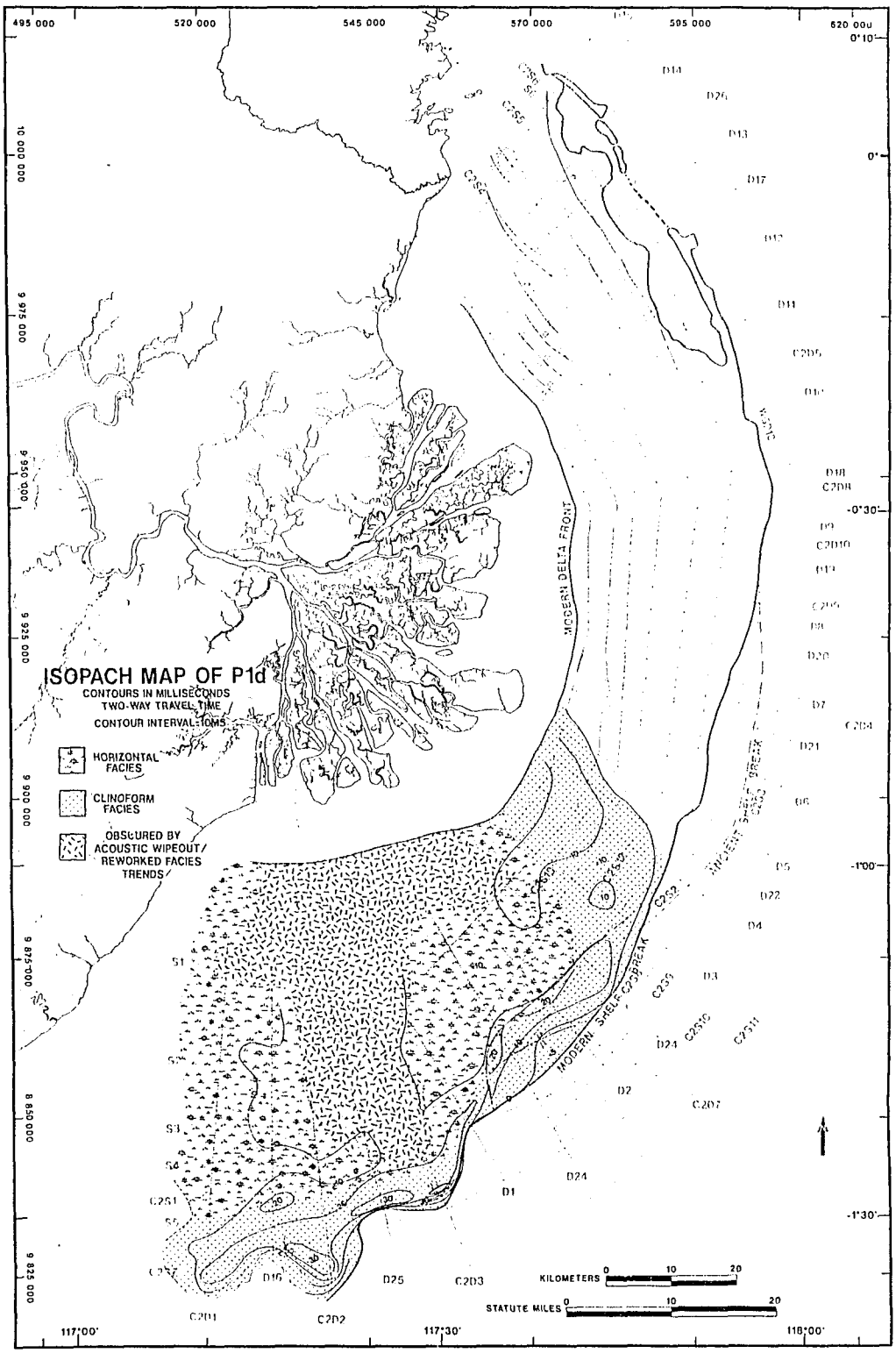
ISOPACH MAP OF P1d
CONTOURS IN MILLISECONDS
TWO-WAY TRAVEL TIME
CONTOUR INTERVAL-10MS
HORIZONTAL FACIES
CLINOFORM FACIES
OBSCURED BY ACOUSTIC WIPEOUT/ REWORKED FACIES TRENDS
MODERN DELTA FRONT
MODERN SHELF-EDGE BREAK
ANCIENT SHELF-EDGE BREAK
KILOMETERS
STATUTE MILES
495 000
520 000
545 000
570 000
595 000
620 000
0°10'
0°
-0°30'
-1°00'
-1°30'
117°00'
117°30'
118°00'

Increment 1c (Figure 4.37c - Clinoforms and associated Horizontal facies deposited between lines 2 and 3 of Figure 4.35) represents a period with a low aggradation to progradation ratio. During this period of extensive progradation the P1S delta front reached the shelf edge. Many mall channels are associated with the upper surface of this growth increment (Narrow, linear feeder trends in P1S of Figure 4.35). The delta did not prograde past the abrupt shelf break. A large slump scar with rotated slump blocks and chaotic strata is situated immediately downdip of the P1S depocenter (Figure 4.35). Clinoforms and horizontal strata are truncated by the shelf edge (Figure 4.3). Pistoncores P9 and P8 within this slump scar retrieved organic rich, unfossiliferous sediments of terrigenous origin. Deep sea mass wasting deposits are thus sourced at the delta front situated along the unstable, steep shelf edge.

Increment 1d is a thin unit that represents a final spurt of delta progradation before the lowstand delta was totally abandoned. Landward shift in downlap indicates that extensive portions of the P1 lobe were abandoned between P1c and P1d deposition (Figure 4.31 section EE'). The small progradational increment P1d represents a temporary offset of the final abandonment and flooding of the lowstand delta

4.2.2.3.4 Feeder System

The broad, shore-normal trend of Reworked Unit deposits, up to 40 ms thick (30m), is interpreted as the main alluvial feeder of the P1S depocenter (Figures 4.8, 4.31 section XX' and FF'). Unfortunately an acoustic wipeout zone is associated with the landward portion of this facies, which obscures the total extent of Reworked Facies (Figure 4.35). The basal erosional surface of this trend has incised into the top of the clinoforms, and total thickness of overlying Reworked Unit fill is a little more than that of the adjacent onlapping Horizontal Unit (Figure 4.31 section FF'). Steep clinoforms within the fill (Figures 4.9, 4.10) suggest lateral accretion deposits, either

from point bar migration in a meandering system, or similar to the lateral accretion bars of the modern Mahakam described by Allen et al. (1979).

Nested within the adjacent Horizontal Unit are narrow (<1 km wide), 20 - 25 ms (15-20 m) deep, linear channel trends. These are probably fluvial distributary trends of increment P1c (Figure 4.35). The exact orientation of these trends is difficult establish with the present seismic grid spacing. The dimensions of the channels are similar to the Modern delta fluvial feeders, and contain an upper and lower channel fill (Figures 4.11 - transverse section, and 4.12, axial-oblique section). The lower channel fill consists of about 10 to 15 ms (7-12 m) thick Reworked Facies, the upper fill consists of low-amplitude horizontal onlapping strata (Figure 4.12). The channels show no evidence for lateral migration which indicates a straight or anastomosing channel system. Multiple channels commonly occur close to one-another, which suggests an anastomosing channel-pattern interpretation (Figures 4.13).

4.2.2.4 The Northern Depocenter

The most striking differences when compared to depocenter P1S is the prevalence of progradation-center clinoform geometries, lack of sigmoid and abundance of oblique clinoforms, a poorly developed Horizontal Unit, and greater control on isopach trends and facies distribution by growth faults and gentle folding. Analysis of clinoform-dip orientations indicates that the small Santan River drainage, which discharges onto the northern edge of the Mahakam Shelf, supplied at least half of the deltaic sediment volume of the northern P1 depocenter (Figure 4.35).

The south to north axial trend of the P1N depocenter (Figure 4.34) coincides with a gentle trough in the underlying downlap surface (Figure 4.31 section BB'). Some of the gentle warping of the shelf is taken up by normal faulting (Figures 3.4, 4.15). Along the western edge of the depocenter the isopach trend is influenced by a series of down-to-the-basin en-echelon growth faults (Figures 3.11, 4.31 section AA'). Dramatic thickening (>50 m) occurs across the large, buried shelf-break fault scarp

(Figure 4.34). Slightly further south the outer shelf region is covered by extensive Holocene Bioherm Facies and Pleistocene data are poor and difficult to interpret. The aforementioned structural high on the outer shelf reduced accommodation and resulted in very thin, if any, P1N deltaic deposition.

4.2.2.4.1 Multi-Lobate Delta Front

Progradation-center geometries (axes of diverging clinoform dips) have previously been mapped in the Gulf of Mexico (Sydow et al., 1992, Sydow and Roberts, 1994), and are interpreted as the product of prograding, lobate delta depocenters associated with advancing delta distributaries. Numerous progradation centers have been identified in strike-oriented profiles across the P1N depocenter (Figures 4.17, 4.18). Mapping of progradation centers and clinoform dip orientations reveal not only that the delta front was multi-lobate, but also that two delta systems were responsible for P1N deposition (Figure 4.35). Mahakam River clinoforms were active in the southern portion of P1N, and the smaller Santan River deposited the northern half of the P1N depocenter. Seismic profiles clearly show clinoforms prograding from the north as a result of influx by this local drainage (Figure 4.16). Clinoform dips along P1N progradation axes related to the ancestral Mahakam River have steep dips of up to 5° (Figure 4.20). Vibracore V5 recovered oxidized fine-grained sand from the top of such steep clinoforms (Figure 4.29).

Two P1N lobes prograded across the large fault scarp on the outer shelf and are presently drowned in over 120 m water depth. The lobate nature of these two progradation centers is clearly evident in seismic and present shelf bathymetry (as illustrated by the modern shelfbreak line in all the maps)(Figures 3.11, 4.17). The lobate shape is actually very similar to the present shape of the Santan River delta platform (Figure 4.35). The larger, northern lobe was produced by the small ancestral Santan River, and the southern lobe possibly by the Mahakam River system.

4.2.2.4.2 Fault Controled Development of Horizontal (Delta Platform) Facies

The onlapping Horizontal Unit is only well developed on the downthrown side of growth faults (Figure 4.36). Elsewhere, oblique clinoforms toplap against the Upper Truncation Surface. Sigmoid clinoforms aggrade some 35 ms over a two kilometer distance of progradation in a localized area on the downthrown side of a growth fault. The Horizontal Unit strata are restricted to this localized area. Syndepositional growthfaulting appears to have caused the downthrown block to experience a local relative sea level rise, and thus aggradation of delta platform deposits.

4.2.2.4.3 Oblique Clinoforms - Relative Sea level Fall

The northern depocenter consists almost exclusively of oblique clinoforms. In accordance with the original seismic stratigraphic concepts of Mitchum et al. (1977), oblique clinoforms are interpreted to represent sediment bypass due to lack of accommodation landward of the prograding delta front during relative sea-level fall. Clinoform topset elevations progressively decrease seaward from -45 to -120 meters (Figure 4.31 section AA'). The 75 m elevation difference is in part due to structural deformation and differential subsidence, but a large portion probably reflects progradation during a falling sea level.

4.2.2.4.4 P1N Fluvial Feeders

P1N fluvial feeder trends, represented by Reworked Unit deposits, are difficult to map with the present data grid (Figure 4.35). Reworked facies and partially filled erosional cuts are evident along the axes of most progradational centers, especially those related to ancestral Mahakam River P1N deposits on the inner and middle shelf (Figures 4.19, 4.20). The channels are up to 1 - 1.5 km wide, with up to 25-30 ms (15-25 m) erosional relief, and do not show evidence for lateral migration. Channel fill commonly consists of a lower Reworked Unit and an overlying subparallel fill. The channels may not be completely filled.

4.2.2.5 Pleistocene/Holocene Transition

Cores V5, V17, V18, V20-23 penetrate the transgressive sequence on top of the P1 lowstand deltas. All the cores have a non-marine/marine contact, the marine section consisting of a thin (0-1.5 m), upward fining fossiliferous sand, or muddy sand/silt layer. A complete transgressive succession is preserved in core V17 (Fig. 4.30), starting with an amalgamated subaerial exposure/bayline flooding surface, paralic mangrove swamp deposits, ravinement surface, and finally shelf/prodelta fossiliferous muds. The coarse texture of the transgressive shelf deposits in many of these cores is a result of reworking by tidal and Throughflow currents.

4.2.3 **Pleistocene Cycles P2 and P3**

Cycles P2 and P3 depocenters have a more central distribution than P1 (Figure 4.33). Unfortunately, because most of the material underlies zones of acoustic attenuation beneath Holocene carbonates, it is difficult to map the details of these Depositional Cycles, and interpretations are therefore highly speculative. The cross sections of Figure 4.31 illustrate P2 and P3 characteristics observed in the seismic data.

Internal characteristics of P3 are usually obscured by multiple interference, but occasionally clinoforms can be identified (Figure 4.23). Clinoforms of the P3 cycle appear to have prograded to the shelf break in the central, and possibly northern regions.

Cycle P2 has been subdivided into 4 units: Units P2a to P2d (Figures 4.15, 4.22). All units are relatively thin <25-30 ms. Unit P2a consists of clinoforms restricted to the inner and middle shelf. Unit P2b consists solely of onlapping Horizontal Facies. Unit P2c is represented by onlapping Horizontal strata on the inner shelf of the central region, and clinoforms on the outer shelf, central region, and across the entire shelf in the northern region. Unit P2d is a thin (<15ms) laterally persistent tabular clinoform unit (Figure 4.31). There are no well developed bioherm facies

separating P2 sub-units. Potential Bioherm Facies are associated with the base of P3, possibly also the top of P3. These young strata have already experienced gentle folding and faulting (Figures 3.4, 4.31).

4.2.4 **Earlier Cycles and Stacking of Successive Cycles**

The Cycle P1 and the combined Cycles P3/P2 suggest that consecutive cycles stack in a laterally-offset, shingled fashion. That is, successive cycles fill-in the topographic lows that exist between the depocenters of earlier cycles. Any one dip profile may not contain clinoforms from every depositional cycle.

Pre-P3 depositional cycles containing clinoforms have been identified in the data set. Stacking of Depositional Cycles beneath the shelf break indicate that the shelf is aggrading vertically, or even in a backstepping pattern (Figure 4.25).

4.2.5 **Chronology and Sea Level Constraints**

At this point in the study the chronologic control in the Pleistocene section is poor due to lack of ground truth boring data. Three semi-continuous platform borings in the northern shelf sector penetrate through both the P1 and P2 cycles. Initial inspection of these cores indicates that materials suitable for radiometric dating (C^{14} and Th^{230}/U^{234}), such as foraminifera and bivalve shells, plant-particulate drapes and roots, are present throughout the sampled sections. Vibracore V18, and pistoncore P11, penetrated the distal-most clinoforms of the P1S depocenter at the shelf edge, and plant material has been sampled for radiocarbon dating. Nevertheless, correlation with radiocarbon dated strata of the MISEDOR boring (Carbonel and Moyes, 1987), and knowledge of the Late Pleistocene sea level curve (Figure 1.11) allow some speculative constraints on the chronology.

Based on foraminifera and ostracode assemblages Carbonel and Moyes (1987) were able to subdivide the MISEDOR boring into regressive-transgressive cycles. The boring is situated some 20 km landward of the modern delta front. By assuming a constant speed of sound in the sediment column of 1600 m/s it is possible to

convincingly correlate Downlap Surfaces DLH1 and DLP1 to distinct flooding events in the MISEDOR boring at 35 to 50 m and 122 to 123 m depth (Figure 4.38). Delta front to prodelta environments occur at these two flooding horizons, and have been radiocarbon dated at 5 to 7 ka and 30 ka, respectively (Allen et al., 1979, Gayet and Legigan, 1987).

A single date of 30 ka may not be convincing, however, this age is supported by an overall isotope stage 3 interstadial highstand between 60 and 30 Ka documented from raised coral reefs (Aharon and Chappel, 1986, Figure 1.10). Four raised, isotope Stage 3 interstadial highstand reefs have been documented by Aharon and Chappel (1986) on the Huon Peninsula, Papua New Guinea. The four raised reefs have $^{230}Th/^{234}U$ dates of 60 ka, 45 ka, 40 ka, and 31-28 ky, with respective calculated sea levels at -28-24 m, -32-45 m, -38 m, and -42-35 m (Aharon and Chappell, 1986; Bloom and Yonekura, 1990). The amplitudes of intervening sea level falls is not known. Biostratigraphic and seismic data from the Gulf of Mexico suggests that two major shelf-edge lowstand depocenters, separated by a shelfwide transgression (highstand), were deposited within the last 100 ky. These lowstands correspond to glacial stadials Stage 2 and probably Stage 4 of the oxygen isotope curve, separated by interstadial highstand Stage 3 (Sydow and Roberts, 1994).

Given the present data, the chronologic interpretation for the Late Pleistocene of the Mahakam shelf is that cycle P1 deposits (both P1N and P1S) prograded from the inner to outer shelf as sea level dropped, starting sometime during isotope Stage 3 (60-30 ka) and into the glacial maximum during Stage 2 (18 to 15 ka). The isotope Stage-3 interstadial highstand that preceded sea level fall was between 30 and 40 m lower than present sea levels (Aharon and Chappell, 1986). Maximum water depths of the oblique clinoform topsets is 100 to 105 m (Figure 1.66), which constrains the maximum estimate of eustatic amplitude during the last glacial maximum. Previous regional estimates of the Stage 2 lowstand minimum are -130 m off the Huon

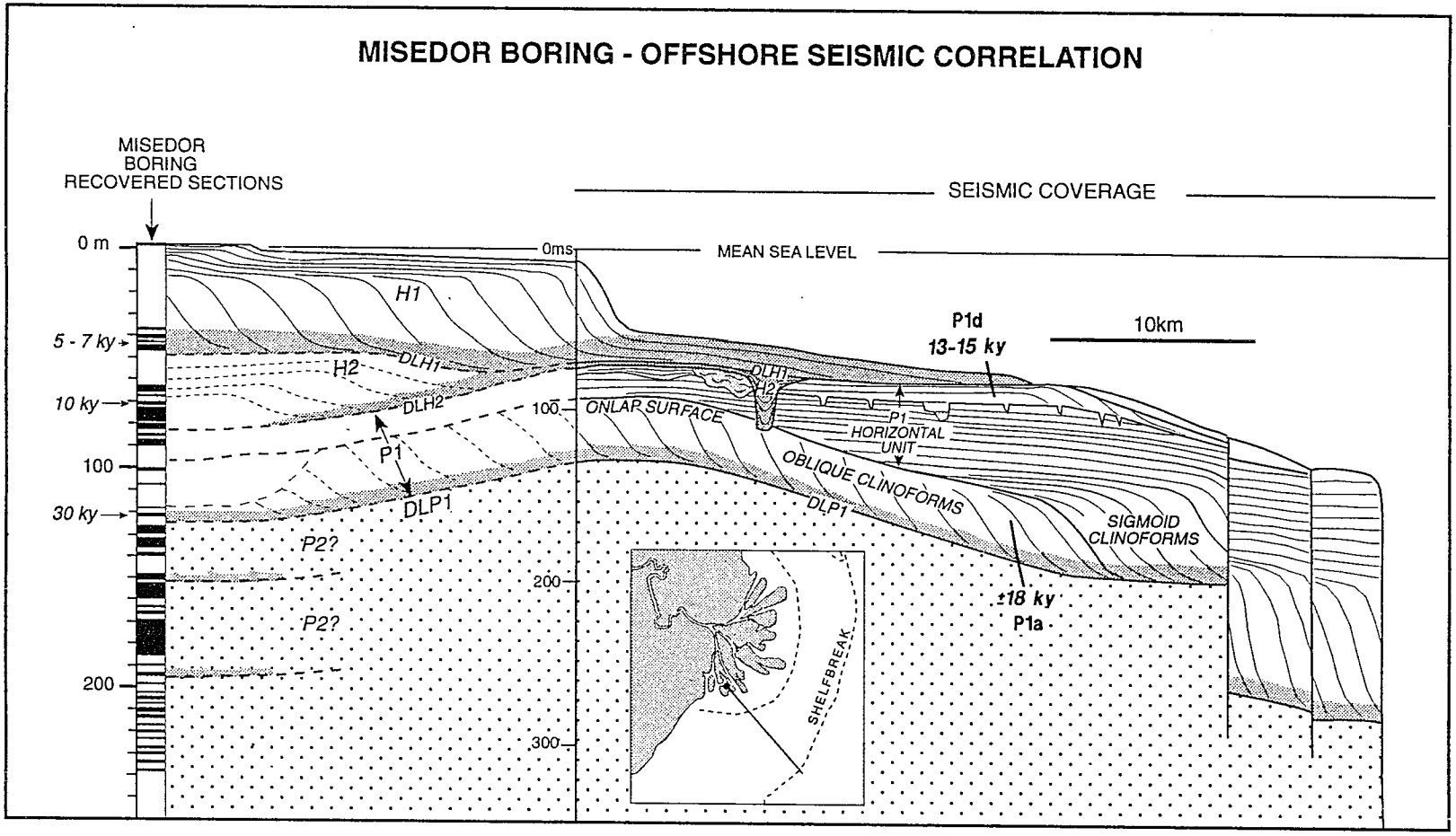

Figure 4.38 Interpreted correlation of the MISEDOR boring and the shelf stratigraphy mapped from seismic. MISEDOR data after Gayet and Legigan (1987), and Carbonnelle and Moyes (1987). Dates in the offshore region are estimates based on interpreted relationship with the Pleistocene sea-level curve.

Peninsula, New Guinea , and -150 m on the northern Australian shelf (Chappell and Schackleton, 1986). Some differences should be expected due to the effects of geoidal and shelf deformation caused by glacio- and hydro-istostasy (Peltier, 1990; Kidson, 1982).

Horizontal strata (deposited in the intertidal to shallow subtidal zone) of increment P1d are situated 70 m below present sea level. The P1S depocenter thus maintained its location at the shelf edge during 30 meters of relative sea level rise, which must represent a considerable time period. A brackish water paired pelecypod shell, at -57 m on the Texas shelf, has been dated at 12.9 ± 0.4 ka, and brackish water peats of similar age from the New England shelf occured at a similar depth (Matthews, 1990). These sea-level indicators suggest that during the Pleistocene-Holocene transgression sea level reached -70 m sometime between 15 and 13 ka. However, Fairbanks' (1989) sea level curve calculated from raised coral terraces offshore Barbados estimate that sea level reached -70 m at 11 ka. Because of the suspect underlying assumption of continuous, steady uplift rates used in calculating the Barbados sea level curve, the older age for P1d is the preferred interpretation (Figure 4.38)

The elevations of stratigraphic features used as sea level proxies on the Mahakam shelf are not only affected by eustatic sea level, but are further influenced by basement subsidence, structural warping, substrate compaction, and isostatic loading by the highstand water column, all of which increase the apparent amplitude of sea level fall on the outer Mahakam shelf (Matthews, 1990). The above elevations therefore overestimate eustatic amplitudes, possibly by 10's of meters.

Depositional Cycles P3 and P2 may be the response to sea level fall during isotope Stage 4 (Cycle P3), and subsequent minor oscillations during isotope Stages 4 and 3 (Cycles P2a to P2d). This interpretation is highly speculative, the strata may very well be older , possibly isotope Stages 6 and 5.

CHAPTER 5. STRATIGRAPHIC MODEL

In this chapter a stratigraphic model is proposed to explain the sequential development of stratigraphic units and surfaces described in the preceding chapters. This model includes suggestions of processes that control the distribution and characteristics of the depositional elements. Ground truth continuous boring data are still to be incorporated, and as such the model has not been calibrated with lithologic, chronostratigraphic and biostratigraphic information. Nevertheless, the model analysis gives insight into the most plausible depositional scenarios, and can be used to guide future data collection and hypothesis testing.

Finally, an initial attempt is made at comparing the same depositional cycle from two very different depositional settings: the Mahakam shelf in Indonesia and the Mississippi-Alabama shelf in the NE Gulf of Mexico. Both of these regions have extensive data sets which have been analyzed at the Coastal Studies Institute. Only the major similarities and differences are explored here, which reflect the relative rates and influence of the various variables controlling the stratigraphic architecture: eustasy, subsidence (at various time scales), structure, climate, sediment supply, sediment distribution processes, and oceanographic factors (water-collumn stratification, currents, tides, nutrient supply).

Once the boring data have been analyzed and a chronostratigraphy established, the data sets from the two regions could be used to callibrate three-dimensional forward stratigraphic models. Such callibrated models could help constrain the relative influences of the aforementioned variables, and thus improve our predictive understanding of possible stratigraphic architectures within each depositional system.

5.1 HIGHSTAND - POOR PRESERVATION POTENTIAL

Highstand deposits which preceeded outer shelf progradation of cycle P1 are buried beneath the modern delta plain on the inner shelf (Figure 4.38). These

prograding highstand deposits downlapped surface DLP1 and were subsequently subaerially exposed and eroded during the last glacial maximum. The highstand period probably corresponds to interstadial isotope Stage 3, when sea level reached a maximum 30 to 40 m below present sea level (Aharon and Chapell, 1987; Bloom and Yonekura, 1990). Accommodation space on the inner shelf was thus more restricted than at present, but a depositional environment very similar to the modern is envisaged, with a broad, tidally influenced delta plain. In the MISEDOR boring the DLP1 downlap/maximum flooding surface is correlated to 30 ka prodelta muds at 123-122 m (Figure 4.38). The subaerial exposure surface, or Onlap Surface, occurs somewhere below the 10 ka (H2) delta plain succession encountered between 60 and 88 m in the boring.

Recovery between 90 and 120 m is poor, traces of coarse grained sands suggests that most of this poor recovery section may be represented by fluvial sands. The P1S Reworked Unit trend further offshore, interpreted as alluvial valley fill, is situated downdip of the MISEDOR site. The P1 highstand deposits are therefore interpreted to be a maximum of 25 m thick, probably much less due to scour by fluvial incision. Delta platform deposits (delta plain and subtidal platform) originally deposited at the top of the highstand succession were most likely completely stripped off by subsequent subaerial exposure during lower sea level. It would be difficult to distinguish true highstand deposits from subsequent falling-stage deposits due to the poor preservation potential.

5.2 FALLING SEA LEVEL - LIMITED DELTA PLAIN EXTENT

Oblique clinoforms probably reflect deposition during a falling relative sea level. Elevations of the truncated clinoform topsets decreases steadily in a seaward direction, in large part due to successively lower depositional base levels, further modified by structural deformation, differential subsidence, and erosion. Most of the P1N deltaic deposits (Mahakam and Santan River) and increment P1a of the southern

depocenter are oblique clinoforms which represent falling stage in sea level (Figures 4.31 sections AA' and EE', 4.35).

The most important difference between falling sea level and highstand is the lack of accommodation space landward of the advancing delta front as sea level is lowered. As a result there is little room for a flat intertidal to subtidal delta platform to develop. What little delta platform deposition that does takes place between the seaward migrating bayline and delta front is subsequently exposed and eroded as sea level keeps falling. The truncated tops of the oblique clinoforms represents subaerial exposure and sediment bypass, and is supported by oxidized non-marine sediments retreived in cores (Figure 4.29). Relatively steep gradients of the newly exposed shelf/deltaic platform (1:1000 - 1:300) results in shallow (20-30 m) fluvial incision of these exposed deposits. The distal limit of incision, landward of the bayline, migrates seaward as sea level falls.

Limited delta plain development has important implications for sediment dispersal processes, and consequently, deltaic architecture. The number of distributary bifurcations accross a narrow delta plain should be less than the that of the modern (three to four) scenario, and with steeper gradients. The falling stage distributary network is consequently hydrologically more efficient. Also, tidal-prism volumes are reduced as a consequence of reduced delta-platform area. Tidal influence on delta platform hydrology is therefore weakened and fluvial influence strengthened. Channel sediment transport to the distributary mouth and delta front is more efficient, with less lateral dispersion of sediments across the delta platform via tidal flooding. More focused sediment deposition at the distributary mouths produces a multi-lobate delta front. Numerous progradation centers observed in strike sections of the Mahakam and Santan P1N depocenter reflect multi-lobate, more fluvially dominated delta systems. Zones of Reworked Unit deposits and partially filled channels are often associated with axes of progradation (Figure 4.20). Oblique-clinoform geometries of increment

P1a, in the southern depocenter, are poorly imaged, but suggest that a single lobe was active in the area (Figure 4.31, section XX').

The increased potential for more efficient bedload transport to the distributary mouth could mean more sand-prone delta front deposits along the axes of distributary progradation. Steep clinoforms along axes of the Mahakam P1N progradation centers may represent such sand-prone distributary mouth bar deposits (Figure 4.20). In the tidally influenced modern Mahakam delta the bedload is trapped within the distributary channels and sandy distributary-mouth bars are poorly developed (Allen et al. 1979).

Another important implication of a smaller delta plain is decreased production of intertidal Nipa palm and Mangrove swamp plant detritus, and consequently, less organic matter incorporated into delta front sediments. Highest microbial activity, and therefore consumption of oxygen, is associated with degradation of autochtonous organic matter from the delta platform (Carbonelle and Hoibian, 1987). Upstream allochtonous organic matter is already highly degraded, and not a good energy source for microscopic biota. Regions of high organic input have acidic and anoxic interstitial pore waters, which influences faunal distribution and shell preservation (Carbonelle and Hoibian, 1987; Sen Gupta, 1995). Falling stage delta front deposits could potentially have less organic content than the modern delta, and a significantly different faunal community preserved in the substrate. The relative volumetric importance of delta plain versus upstream sourced organics on the modern delta front should be quantified in order to assess the potential of the above variable-organic-content process.

The topography of the downlap surface buried by the advancing delta may be very intricate, with deep shelf scour channels, thick carbonate buildups, fault scarps and growth faults. Isopach trends of the overlying deltaic deposits are very complex in such regions (Figures 4.32, 4.34)

Oblique clinoforms of the falling sea level period prograded to the shelf edge in the northern sector, but in the southern sector only reached the middle shelf before lowstand turnaround in sea level (explained in Section 5.3). The delta prograded into a deep lagoonal environment in the north, created by the tall reef ridges further seaward, on the outer edge of the rotated fault block (Figure 3.11). Reef rubble buried beneath P1N clinoform toesets indicate that the reefs preceded the deltas (Figure 3.10). Multi-channel seismic lines from the north show similar reef ridge/fault block geometries buried in the stratigraphy (Van de Weerd and Armin, 1992).

5.3 LOWSTAND TURNAROUND AND INITIAL RISE - P1S DELTA PLATFORM AGGRADATION

5.3.1 Progradational Continuum

Seismic profiles across the southern depocenter clearly show a progradational continuum from falling stage, thru lowstand turnaround, to initial rise in sea level, represented by the transition from truncated oblique clinoforms to sigmoid clinoforms (Figure 4.4). More than half the deltaic material of the P1 Cycle was deposited during lowstand rise (Figure 4.31 sections XX' and EE'). Onlap of aggrading horizontal strata onto the subaerial exposure surface migrated landward at the same time that sigmoid clinoforms prograded seaward. This landward migration of the bayline in the southern depocenter reflects concomitant delta progradation and aggradation, and was not related to the beginning of transgression. Under aggradational conditions the delta reverted again to a more tide-influenced system somewhat similar to the modern highstand setting .

Tidal flooding and currents distributed fines across the aggrading delta plain, and the delta platform prograded along the entire length of the broad, gently arcuate delta front (i.e. not a multi-lobate front)(Figure 4.35). Abundant production of Nipa palm and mangrove organic matter resumed on the intertidal delta plain, much of it incorporated into the accreting delta plain, the remainder exported seaward. The

maximum aerial extent of the lowstand delta plain was at least that of the present highstand delta (Figure 4.36).

The smaller P1N depocenter has a poorly developed Horizontal Unit, restricted to the downthrown sides of growth faults (Figure 4.36). The Mahakam River contribution to the north was apparently abandoned in favor of the south sometime before the lowstand turnaround. The Santan River system, at least an order of magnitude smaller than the Mahakam River, does not supply enough sediments to keep aggrading and prograding during the lowstand rise. The system was probably abandoned soon after sea level turnaround.

5.3.2 **Fluvial Feeders**

The number of distributary bifurcations and tidal channels across the narrow falling-stage delta plain would be less than the present highstand scenario. Reworked facies trends are associated with most of the progradation centers of the P1N depocenter. The number of ancestral Mahakam River progradation centers decreases from about five on the inner shelf, to one on the outer shelf. A single, shallow-incised fluvial feeder is associated with the P1a growth increment of the southern depocenter.

The single, incised fluvial feeder of P1S aggraded together with the delta plain after lowstand turnaround, to produce a broad (10-20 km), thick (30-40 m), shore normal alluvial-valley fill trend (Figures 4.31 section FF', 4.36). Thickness of fill is comparable to adjacent Horizontal Unit thickness. Similar to the modern delta, a network of narrow, straight fluvial distributaries and tidal channels developed across the widening delta plain (Figures 4.11, 4.12, 4.35). Fluvial discharge through the aggrading alluvial valley probably diminished, and was finally abandoned at the end of increment P1c.

Reworked Unit trends of the P1N depocenter are thickened on the downthrown side of growth faults (Figure 4.19), and very thin if present at all on the inner shelf (4.20). The less extensive development of Reworked facies in the north possibly

reflects abandonment of ancestral Mahakam River supply before commencement of aggradation associated with the lowstand turnaround.

The modern Mahakam River is actively incising landward of the delta, and consequently there is no alluvial valley-fill (river floodplain) element associated with the present highstand scenario.

5.3.3 **Overall Sea-Level Rise - Potential Impact of Higher Order Fluctuations**

Relative sea level rise was a response to the combined effects of eustatic rise, sediment compaction, basement subsidence, structural warping, and local growth faulting, with eustasy as the dominant factor. Accumulation thickness of horizontal strata indicates the delta prograded under the influence of 35 m total relative sea level rise (Figure 4.38). Locally, more than 60 m of horizontal facies accumulated on the downthrown side of growth faults (Figures 4.3, 4.36).

Prominent subdividing surfaces within the Horizontal Unit, landward shifts in downlap, mutiple levels of channels, complex alluvial-valley fill, and the subtle changes in stacking patterns of growth increments P1a to P1d, suggest that the detailed picture is a little more complicated than an overall, simple relative sea level rise. A broad, level aggrading delta plain would have been very sensitive to superimposed, minor sea level fluctuations. Even a small sea level drop of 2 m would have exposed the entire delta plain, and have significant consequences for delta hydrology, sediment dispersal, preservation of organic material, and basic sedimentological characteristics of delta plain deposits. Numerous exposure and flooding levels may have been preserved within the overall accreting Horizontal Unit.

5.3.4 **Potential for Peat Development**

Abundant low-ash coal horizons are associated with aggraded delta plain deposits of the Tertiary beneath the shelf (Duval et al., 1992), however, significant accumulations of low sulphur, low "ash" (clay content) peat are not present in the Modern delta. Domed peat deposits are extensively developed within fresh-water

coastal alluvial floodplains on the west and south coast of Borneo (Anderson, 1983; Staub and Esterle, 1994). There is no aggradational alluvial floodplain associated with the modern Mahakam delta setting, instead, the Mahakam river is actively incising the uplifted onshore region. Without an extensive fresh-water floodplain environment there is no room for development of thick, low ash peat deposits. Most of the delta plain is covered by brackish water Nipa swamps, which are not suitable for thick, fresh water peat development. The nearest modern peat forming areas are situated 150 km up-river, within the extensive alluvial floodplain of the subsiding Semayang Lakes area (Flores, 1993).

Extensive floodplain and peat environments may not be associated with the present highstand scenario, but would most probably have developed during the lowstand turnaround period within the aggrading alluvial valley.of the delta plain. It is possible that the shallow acoustic wipeout region that obscures the proximal portions of the P1 Reworked zone (Figure 4.35) is related to biogenic gas generated within peat horizons of the fluvial channel fill. Alternatively, the wipeout zone may be organic rich muds deposited in a tidally dominated estuary that developed within the flooded alluvial valley during transgression.

5.4 LOWSTAND SHELF EDGE DELTA

Lowstand delta clinoforms of P1 and older cycles are situated at the shelf edge (Figure 4.25), but substrate instability due to steep slope gradients inhibit delta progradation past the abrupt shelf break. The P1S delta depocenter prograded to the shelf edge during the initial sea level rise period (Figure 4.35). The thick, aggraded horizontal unit at the shelf edge (Figure 4.3) suggests the delta occupied the shelf edge location for a considerable period. Large volumes of delta material undoubtedly calved off the perched delta front to form mass wasting and turbid flows destined for deep water deposition. Shelf-edge reentrants observed in older Clinoform Packages are interpreted as canyon/slump scar incision features. However, due to the steep

nature of the upper slope there is no need for canyon formation and associated shelf bypass of terrigenous sediments in order to generate large volumes of deep water siliciclastics. The outer shelf and steep slope are inherently unstable. Growth faults and fault scarps on the outer shelf, slump scars, chaotic units and infilled canyons on the slope, are evidence of this instability. A major slump feature is situated immediately downdip of the P1S depocenter (Figure 4.27, 3.11). Melecek et al. (1993) have identified thick wedges of sediment in intraslope and basinal settings which they have linked to sand prone deposits on the upper shelf.

5.5 TRANSGRESSION AND MAXIMUM FLOODING - DELTA ABANDONMENT AND CARBONATE ACCRETION

5.5.1 Delta Abandonment

Accelerating rates of sea level rise eventually outstripped the ability of sediment supply to fill new shelf accommodation, the delta front was abandoned, and transgression of the coastline began. Due to the smaller sediment supply the P1N depocenter was probably abandoned much earlier than P1S, sometime soon after sea level turnaround. The main bayline flooding periods were synchronous between the northern and southern depocenters, as they were a response to initial sea level rise following lowstand turnaround. However, in the north bayline flooding was associated with transgression, and in the south with progradation and aggradation and progradation of the delta platform.

The transgression was apparently not continuous, but occurred in at least three backstepping pulses. Increment P1d (-70 m), marks the end of the first transgressive pulse of the southern depocenter (Figures 4.31 sections XX', EE' to GG', and 4.37d). Prograding clinoforms of P1d represent a momentary reversal at the beginning of the overall transgression, possibly even subaerial exposure due to a minor sea level fall. Holocene cycle H2 (-40 m) marks the end of the second transgressive increment (Figures 3.13, 4.38). The modern H1 delta lobe marks the end of the final

transgressive increment. There are possibly other backstepping transgressive increments between H2 and H1 that are obscured beneath the modern delta

Vibracore V17, into the top of increment P1d (southern P1 depocenter), reveals oxidized delta plain deposits (subaerially exposed?), followed by an exposure/ flooding surface, mangrove peat of a paralic swamp deposit, transgressive ravinement surface, and finally, fossiliferous shelf muds and prodelta deposits (Figure 4.30). The main exposure/bayline flooding surface in P1S occurs lower in the section, at the Onlap Surface, and is not related to transgression. (Figure 4.38). Superimposed minor sea level oscillations tapparently complicated the detailed stratigraphy of the Horizontal Unit, and produced more than one exposure or flooding event.

Similar to P1S, a reversal of the overall transgression is suggested by a small progradational increment perched on top of the P1N depocenter, at -75 m on the outer shelf (Figure 4.16). Similarities in elevation of the P1d and the P1N transgressive reversals indicates that they are probably synchronous and driven by eustacy.

Vibracore V5 penetrates the P1N ravinement surface at 5.1 m sediment depth, represented by a non-marine/marine contact (Figure 4.29) . Seismic profiles show that the contact is an amalgamation of the subaerial exposure, bayline flooding, transgressive ravinement, and maximum flooding surfaces . Locally, the exposure and ravinement surfaces of P1N may be separated (Figure 4.18), probably by a transgressive paralic unit.

5.5.2 **Ravinement Processes**

Physical processes that created the ravinement surface were dominated by shore normal tidal, and shore parallel Indonesian Throughflow currents, and were not restricted to the nearshore marine (above fair-weather wavebase), as is the case for most wave dominated settings. Due to the influence of the Throughflow current, and possibly internal-tide currents, erosional ravinement appears to be active today, even at depths of 100 m or more. Scour is amplified by topographic effects between

carbonate buildups. During the initial, shallow water flooding of the delta, tidal currents were apparently focussed by abandoned distributary channels (Figure 4.13), which enlarged these channels to form the deep shore-perpendicular cuts associated with marine flooding surfaces DLP1 and DLP2 (Figures 4.22, 4.32). These deep, linear scour trends could easily be confused with incised alluvial valleys, but they are filled with deltaic clinoforms, not fluvial facies (Figures 4.32, 4.34).

5.5.3 **Carbonates and the Condensed Section**

During the transgression the influx of terrigenous sediments shifted to the inner shelf. Throughflow current transport on the flooded shelf deflected the turbid river plume and associated planktonic blooms to the south, and also diluted suspended sediment concentrations in the plume. At some point during the transgression sufficiently clear water conditions developed on the outer shelf of the northern and central sectors for proliferation of photosynthetic, carbonate precipitating green-algal *Halimeda* communities. Nutrient enriched waters favor the proliferation of calcareous green algal communities dominated by *Halimeda* over the more common framework building coral reef communities (Hallock and Schlager, 1986).

The highly stratified nature of the Makassar water column may be an important controlling factor on carbonate accretion. Progressive nutrient enrichment of the upper thermocline occurs along the Indonesian Throughflow transport path, probably due to vertical mixing by internal tides and possibly upwelling (Gordon, 1986, Ffield and Gordon, 1992). The tops of tall *Halimeda* bioherms commonly coincide closely with the highly stratified top of the thermocline, between 40 and 50 m water depth. Pinnacles and reefs may penetrate the top of the thermocline, but tend to have higher reflection "hard" returns on side scan sonograms more typical of calcareous algal communities. The coincidence of the top of thermocline and upper limit of *Halimeda* bioherm accretion suggests that the upper mixed layer above the thermocline is unsuitable for proliferation of *Halimeda* algal communities. Vertical mixing of

nutrients is probably restricted across the large density contrast associated with the top of the thermocline. Nutrient enrichment of the mixed surface layer is unlikely as this would promote planktonic blooms, which would limit light penetration and thus inhibit photosynthetic communities on the sea floor.

Onset of *Halimeda* bioherm accretion during sea level rise may thus be dependent on when thermocline waters encroach onto the shelf. Oxygen isotope values of planktonic foraminifera from deep sea cores suggest that regional water stratification characteristics may change from glacial to interglacial periods (Barmawidjaja et al., 1993; Ahmad et al., 1995), which further complicates interpretations on factors controlling carbonate accretion.

Halimeda bioherms have very rapid accretion rates, 20 to 30 m is common for the Holocene, locally up to 50 m. The 100 m high reef trends represent more than one cycle of growth. Similar *Halimeda* bioherms at the southern end of the Makassar Strait have measured accretion rates ranging between 2.8 and 5.9 m/ky (Roberts et al., 1987; Phipps and Roberts, 1988). Given these rates, bioherms would have to be established on the shelf at an early stage of the transgression in order to attain a thickness of 50 m.

The southerly Throughflow current, inner shelf location of the terrigenous sediment source, and water depth appear to have a first-order control on carbonate distribution, favoring the middle to outer shelf of the northern and central sectors. These shelf regions have abundant carbonates in the underlying Tertiary sequences (Van de Weerd and Armin, 1992). At a more local scale, individual bioherms are established on the topographic highs of drowned delta lobes (Figure 4.17), and favor the edges of scour channels and fault scarps (Figure 3.7). Once bioherms are established they probably focus the current scour in intervening lows.

Sometime after initial highstand progradation of the modern delta the more seaward extent of the river sediment plume decreased the depth of the photic zone on

the shelf and severely impacted the carbonate community. Carbonate accretion was largely terminated. Local, massive carbonate buildups along the outer shelf, presently within 20 m of the sea surface, may still be within the photic zone and actively accreting.

Siliciclastic dominated shelves are typically sediment starved during transgression and maximum flooding (Vail et al., 1977; Posamentier et al., 1988). Sediment starved condensed sections are represented on the modern sea floor of the Mahakam shelf by regions of low deposition (southern sector) of shelly shelf muds, and regions of scour. Regions of thick carbonate accretion are time equivalent to these condensed zones

5.6 CYCLES P2 AND P3 - MODIFIED SEA LEVEL HISTORY ?

Depositional Cycles P2 and P3 are not well imaged, but are clearly somewhat different to cycle P1. Much of this stratigraphic variation could be explained by varied development of shelf accommodation during successive cycles in response to the complex eustatic history of the Late Pleistocene (Figure 1.11).

Cycle P3 appears to be a major regressive phase represented by prograding clinoforms. The widespread onlapping horizontal strata of P2 reflect an overall aggradational phase. Landward shifts in downlap of prograding clinoforms within P2 indicate that abandonment and transgressions occured at the end of Cycles P3, P2b, P2c, and P2d (Figure 4.31). Cycle P2b experienced a partial transgression, as aggradation of horizontal strata during P2b and P2c was apparently uninterrupted in the central sector (Figure 4.31, section CC', Figure 4.22). The lack of significant carbonate buildups during transgressions indicates that clear water conditions were not established. The uniform, relatively thin distribution of the P2 subcycles suggests restricted accommodation space, and therefore, relatively small amplitude sea level fluctuations. The volume of material represented by the combined Cycles P3 and P2 is similar to that of Cycle P1, which suggests a similar total duration of sediment

supply. Given the present data, the simplest explanation is that the combined P3 and P2 strata represent an overall depositional cycle similar in duration and amplitude of sea level change to Cycle P1 (<40 ky, 70-100 m), but modified by superimposed moderate amplitude (10-30 m), higher frequency (<10 ky) sea level fluctuations. The falling stage of Cycle P1 is therefore similar to P3, and the lowstand rise period is represented by P2. Radiometric dates from the platform boring samples of these cycles will help establish the link to the sea level curve. Sediment supply could be another important variable, but is more difficult to assess.

5.7 STACKING OF SUCCESSIVE LOWSTAND DEPOCENTERS

Cycles P3 and P1 suggest that consecutive cycles stack in a laterally-offset, shingled fashion. That is, successive cycles fill-in the topographic lows that exist between the depocenters of earlier cycles. Any one dip profile may not contain clinoforms from every depositional cycle. Subtle structural deformation and faulting, especially in the northern region, and extensive carbonate accretion, further influences local lowstand accommodation, and therefore, depocenter distribution on the outer shelf. Location of the shelf-edge depocenters has important implications for deep water sediment supply and distribution.

5.8 SEQUENCE STRATIGRAPHY

In this section the stratigraphic elements of the model are linked to sequence stratigraphic terminology. The approach used to subdivide the stratigraphy in the above model is really the same as that of sequence stratigraphic methodology (Mitchum et al., 1977; Posamentier and Vail, 1988; Van Wagoner et al., 1990; Vail et al., 1991; Posamentier et al., 1992; Hunt and Tucker, 1992; Nummedal and Molenaar, 1995). The concepts and methodology of sequence stratigraphy have altered somewhat in recent years, introducing new terms and definitions, and adding some confusion about what is meant when the original, strictly defined terms of Van Wagoner et al.(1988) are applied. In order to avoid introduction of inappropriate

concepts that may be associated with the sequence stratigraphic terminology, this terminology was not used in the above model.

The major mappable surfaces that subdivide the Depositional Cycles into subunits on the Mahakam Shelf are the: Downlap Surface, Onlap Surface, erosional base of the alluvial valley, and Upper Truncation Surface. These surfaces define the: oblique Clinoform Unit; sigmoid Clinoform Unit, Horizontal Unit, Reworked Unit fill of the alluvial valley; and Carbonate Unit (Figure 5.1).

5.8.1 **Surfaces**

The least controversial, most easily defined, and mappable surface is the Downlap Surface. In the study area the Downlap Surface defines the base of the progradational wedge, and passes on top of the Carbonate Bioherm Unit. The truncational surface at the base of the bioherms, the Upper Truncation Surface, is the transgressive ravinement surface. Where carbonates are not present the Downlap and Upper Truncation Surfaces are separated by a thin Upper Unit (reworked transgressive shelf material), and in shelf-scour regions the surfaces are amalgamated. The Downlap Surface corresponds to maximum flooding and condensed sections, except where carbonates are present. Carbonates are correlative to the condensed sections, but are obviously not "condensed" as they commonly exceed 20 m in thickness. Maximum flooding of the shelf corresponds to a zone within the top of the bioherms.

The P1S Onlap Surface is interpreted as a subaerially exposed sediment bypass surface related to lowering of sea level, and is therefore identified as the Sequence Boundary. The P1N subaerial exposure surface is amalgamated with the overlying transgressive ravinement. The erosional base of the Reworked Unit fill of the alluvial valley in P1S, although physically not the same surface as the Onlap Surface, is also part of the Sequence Boundary.

5.8.2 **Systems Tracts**

Progradational deposits below the Sequence Boundary belong to the Lowstand Systems Tract of the forced regression model (Posamentier et al., 1992), or the Forced Regressive Wedge Systems Tract (FRWST) of Hunt and Tucker (1992), or the Falling Stage Systems Tract (FSST) of Nummedal and Hardenbol (1995). These deposits prograded during relative sea level fall to sea level minimum. Early sequence stratigraphic models failed to recognize these falling sea level deposits (Posamentier and Vail, 1988; Van Wagoner et al., 1990), and assigned them to the Highstand Systems Tract (HST). True HST deposits on the inner shelf have poor preservation potential, and probably can not be easily differentiated from the falling stage deposits.

The Horizontal Unit, associated sigmoid Clinoform Unit, and alluvial valley fill, related to initial lowstand rise in sea level belong to the Lowstand Systems Tract (LST). The base of the Transgressive Systems Tract (TST) may be difficult to pinpoint in P1S, as it probably occurs somewhere near the top of the aggrading Horizontal Unit. In P1N the base of the TST is amalgamated with the Sequence Boundary, transgressive ravinement, downlap, and maximum flooding surfaces. The thin Upper Unit and Carbonate Unit belong to the TST. The top of the TST is the maximum flooding surface, which passes through somewhere near the top of the bioherms, as bioherms were probably active into the early part of modern Mahakam Delta progradation (HST).

Growth faulting would cause local relative sea level histories quite different from the rest of the shelf, and associated surfaces may thus not be correlative to similar surfaces elsewhere on the shelf.

5.9 THE P1 CYCLE OF THE MAHAKAM AND MOBILE RIVER DELTAS: SIMILARITIES AND DIFFERENCES

A comparison of depositional cycles from the Mahakam and Mississippi-Alabama shelves provides an opportunity to assess the impact of different geological settings on the stratigraphic framework. As explained in the introduction, stratigraphic studies based on single-channel seismic imaging of Late Pleistocene shelf stratigraphy, calibrated against borings, have numerous advantages over the more traditional approach of studies based on the ancient rock record. Therefore, process-response concepts developed to explain the detailed stratigraphic frameworks observed in these high-resolution data sets are relatively well constrained. The P1 Depositional Cycle from the Mahakam and Mississippi-Alabama shelves have been mapped using two of the most complete stratigraphic data sets available from the Late Pleistocene shelf setting. These two P1 depocenters formed in response to the same eustatic cycle but in very different depositional settings. The influence of eustasy on the two depositional systems should be similar. Differences between the stratigraphic frameworks of the ancestral Mahakam and Mobile River systems on these two shelves should therefore reflect differences in the relative influence of the other important variables, for example: climate, subsidence, sediment supply, sediment dispersal processes, oceanographic factors, etc. Due to the overriding influence of eustasy on shelf accommodation in high frequency depositional cycles it is usually very difficult to distinguish the relative influence of the other variables on the stratigraphic framework.

For the sake of brevity, the reader is referred to detailed stratigraphic descriptions of the ancestral Mobile River shelf edge delta of the Mississippi-Alabama shelf in Sydow (1992), Sydow et al. (1992), and Sydow and Roberts (1994). The distributions of the P1 Cycle, and schematic representation of the stratigraphic framework of the Mahakam and Mobile River P1 deltas, are summarized in Figures

5.1 and 5.2. Table 5.1 summarizes the important differences in depositional settings of the ancestral Mobile and Mahakam River Deltas. The Mahakam shelf is notably different in that it is structurally very active, experiences an order of magnitude greater basement subsidence, receives a larger sediment supply (rough estimate based on relative volumes of Cycle P1 deposits), experiences almost no wave impact, is mesotidal, receives a higher river discharge, has a strong longshore current, is near the equator, and represents a mixed siliciclastic/carbonate system.

5.9.1 **Similarities**

1) The two depocenters were formed during the same large amplitude (60-100m), rapid (< 40 ky) glacio-eustatic cycle. Eustasy is one of the variables common to both systems, is the primary control on shelf accommodation, and is responsible for the most significant feature in common to both shelves. In both regions shelf stratigraphy is dominated by a progradational continuum that represents deposition from highstand, through sea level fall, and finally initial rise in relative sea level. Highstand deposition is poorly preserved on the inner shelf, and progradational deposits on the outer shelf formed during sea level lowstand.

2) Successive lowstand depocenters on the outer shelf stack in a laterally offset, shingled fashion. The areal extent of a lowstand depocenter is restricted by sediment supply, shelf morphology, and duration and amplitude of the sea-level cycle. A lowstand depocenter does not occupy the entire length of the shelf edge during every lowstand, but instead tend to stack vertically only every two or three cycles. This shingled stacking is an important point for two reasons. First, lateral switching controls the location of the deep water sediment source. Second, such laterally offset depocenters would be difficult to differentiate in subsurface multi-channel seismic, and can not be resolved biostratigraphically (at best 1 my resolution). Laterally offset stacking of successive cycles may explain why sequences of higher than 3rd order cyclicity are difficult to recognize, and are overlooked, in the rock record.

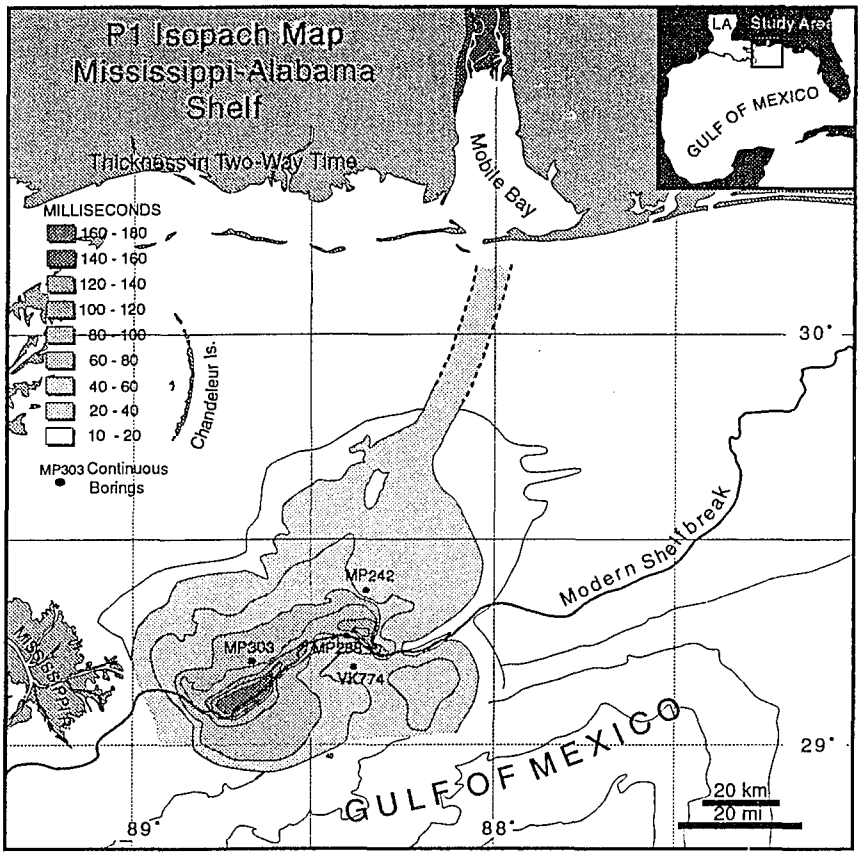

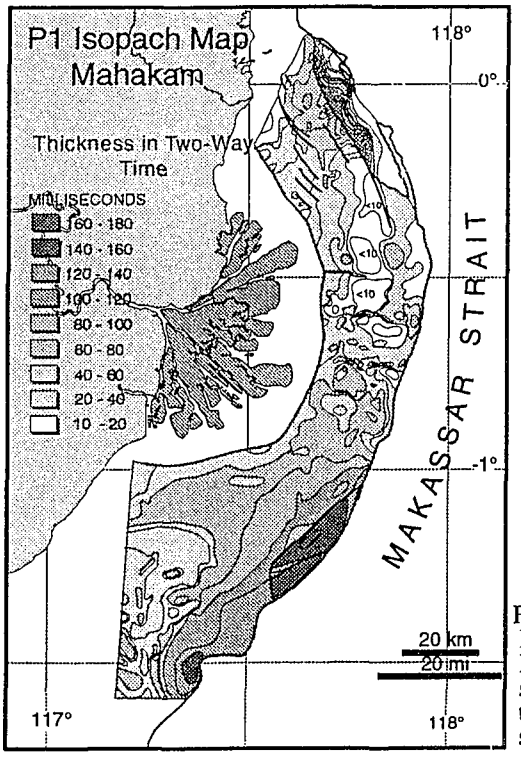

Figure 5.1 Isopach maps of the P1 Depositional Cycle on the Mississippi-Alabama and Mahakam shelves. Thicknesses in two-way travel time. Both maps have the same scale.

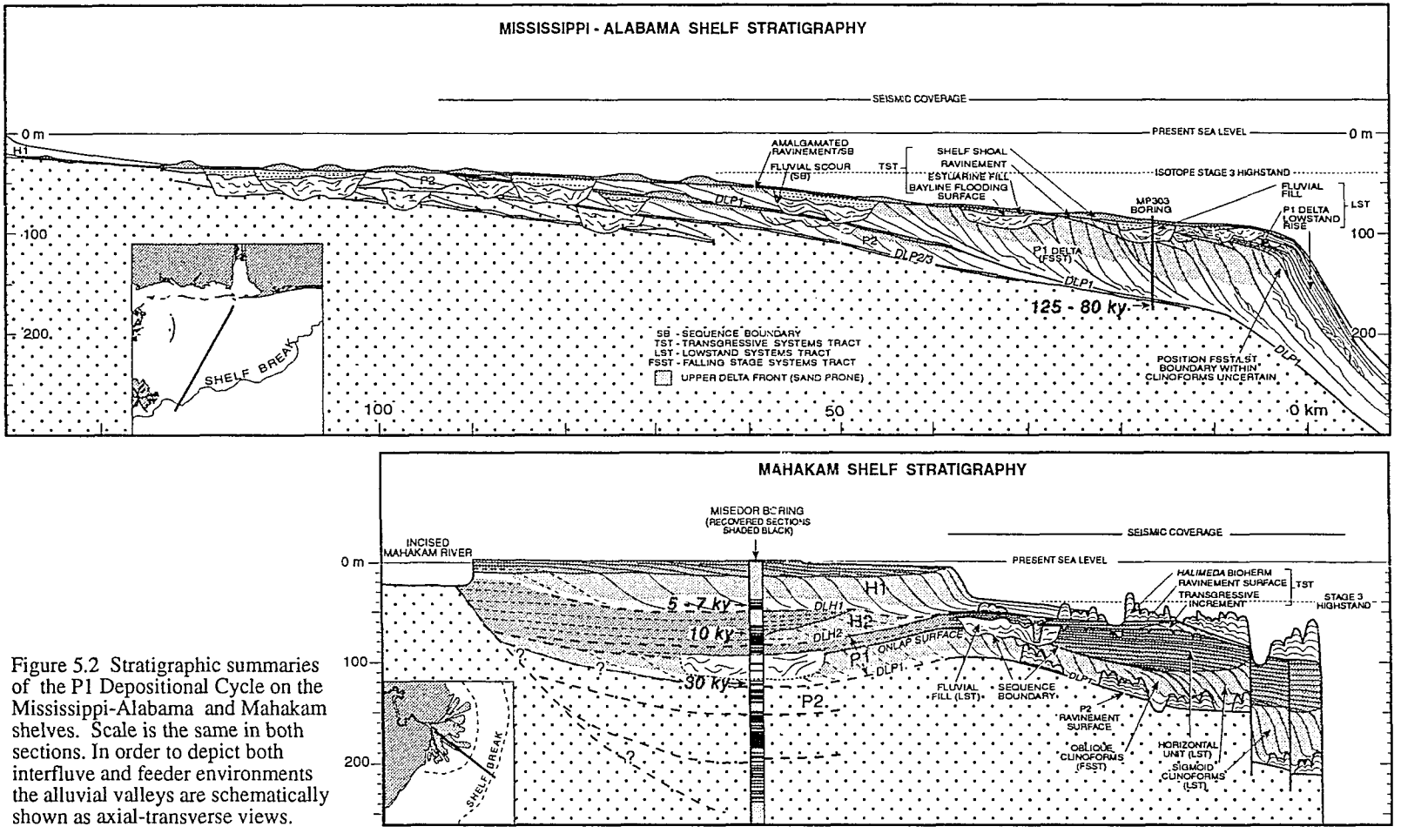

Figure 5.2 Stratigraphic summaries of the P1 Depositional Cycle on the Mississippi-Alabama and Mahakam shelves. Scale is the same in both sections. In order to depict both interfluve and feeder environments the alluvial valleys are schematically shown as axial-transverse views.

Table 5.1 Depositional Settings: Mississippi-Alabama and Mahakam Shelves

	Mississippi.-Alabama shelf (Mobile R.)	Mahakam Shelf (Mahakam R.)
Climate	Temperate	Equatorial monsoonal
Drainage Basin	~75 000 km^2	~75 000 km^2
Discharge	less than Mahakam	~3 000 m^3/s
Sediment Supply	less than Mahakam (75% ?)	~10×10^6 tons/yr
Cycle P1 sediments preserved on shelf	~180 km^3	~250 km^3
Tectonics	Stable Slow basement subsidence (30 m/my last 15 my)*	Active: folding and faulting Fast basement subsidence (200-350 m/my last 15 my)
Shelf Morphology	70 - 100 km wide Shelf gradient 1:300-1000 Slope gradient < 5°	100 - 150 km wide Shelf Gradient 1:1000 Slope gradient < 25°
Physical Processes of Receiving Basin	Microtidal Low wave energy Storms No dominant Shelf Current Water temperature 15-28°C	Mesotidal Very low wave energy No Storms Strong longshore current Water temperature >28°C Nutrient loading of thermocline Internal Tides
Intertidal Vegetation	Marsh grasses	Nipa Palm and Mangrove

* Greenlee and Moore (1988)

5.9.2 **Differences**

1) The Mahakam shelf has accreted vertically for more than 5000 m during the Neogene. In comparison, substantial progradation of the Mississippi-Alabama shelf has occurred since the Middle Miocene (Greenlee and Moore, 1988), despite the Mobile River system supplying less sediments than the Mahakam drainage. This stacking pattern reflects the order of magnitude higher basement subsidence rate, and therefore accommodation space, of the Mahakam shelf. The Mahakam River supplies barely enough sediments to fill the large shelf accommodation generated by subsidence during each depositional cycle, and relatively little sediments are bypassed into deep water. The large disparity in accretion rates between the shelf and deep water over a number of cycles has resulted in a very steep slope gradient, up to 25°, reinforced by carbonate accretion on the outer shelf. The important point is that once the steep slope is established the lowstand delta is not able to prograde past the abrupt shelf break. The steep slope is also inherently unstable, with normal to listric faulting along the shelf edge, and abundant slumping of the slope. Slope gradients in the NE Gulf of Mexico are less than 3°. Lowstand systems are able to prograde past the shelf break, abundant deposition occurs on the slope, and the shelf margin is more stable.

2) Initial sea level rise deposits of the lowstand turnaround are very well represented on the Mahakam shelf, more than half the P1 deltaic deposits belong to this Lowstand Systems Tract. The equivalent deposits of the ancestral Mobile River are restricted to a small volume of sediments at the shelf edge, minimal onlapping delta plain strata, and aggraded alluvial valley fill sediments. Similar to the Santan River depocenter on the northern Mahakam shelf, the main reason for poor representation in the Mobile River lowstand delta is probably a smaller sediment supply.. Perhaps much of the coastal and delta plain strata in the rock record actually represent aggradation during the lowstand turnaround, and not during the relatively poorly preserved highstand period. During periods of low amplitude, low frequency

sea level oscillations such aggradational LST deposits may have been significant, even for relatively small depositional systems.

3) Tidal influence of the Mahakam delta results in a very different deltaic architecture. The falling stage deltaic deposits of the Mahakam were multi-lobate, and probably had relatively strong fluvial influence, but nothing like the Mobile River delta which shows evidence for delta switching processes and vertical stacking of lobes typical of river dominated systems (Coleman and Gagliano, 1964). During the lowstand rise the Mahakam system transformed into a more tidally dominated delta, similar to the modern scenario. The delta front is a gently arcuate feature, with no multi-lobate structure.

4) The Transgressive Systems Tract of the two systems is quite different. Firstly, transgressive ravinement on the Mahakam shelf is produced by tidal currents and the longshore Throughflow current, not wave reworking. On a world-wide scale wave energy in the gulf of Mexico is relatively low, yet considerably higher than in the Makassar Strait, and tidal fluctuations are very weak. Wave reworking on the landward migrating shoreface controls ravinement on the NE Gulf of Mexico shelf, and drowned shelf shoals are prevalent features on the modern shelf (Figure 5.2). Tidal reworking is restricted to migrating barrier inlets. There is no abundant evidence for wave reworked shelf shoals on the Mahakam shelf. Secondly, the tropical setting and the southerly Throughflow current result in abundant carbonate accretion on the middle to outer Mahakam shelf, and consequently, a mixed carbonate - siliciclastic depositional system. Nutrient loading of the shallow water column by internal tides apparently favor *Halimeda* algal communities over more common coral reef organisms. The transgressed Mississippi-Alabama shelf is starved of sediments and represented by a condensed section

5) Structural warping and faulting of the shelf, shelf-scour topography, and the complex distribution of thick carbonate buildups significantly impact lowstand

accommodation and thus, distribution, of Mahakam delta deposits. Distribution of Mobile River lowstand deltaic deposits is relatively uncomplicated.

CHAPTER 6. CONCLUSIONS

1) The cyclic framework of the Late Pleistocene stratigraphy on the Tropical Mahakam shelf is a response to the interaction of numerous important variables:

- A relatively large sediment influx from the Mahakam River, with an additional, one order smaller contribution by the Santan River on the northern shelf.
- Shelf accommodation space is primarily controlled by eustasy, with significant contributions from rapid basement subsidence, structural warping and faulting, distribution of earlier depocenters and thick carbonate accretion.
- Sedimentary facies distributions are influenced by the relative balance of an intermediate tidal range, very low wave energy, high fluvial discharge, and a strong longshore shelf current. In addition, water column stratification and nutrient loading of the upper thermocline are potentially important for carbonate accretion.

2) Within a depositional cycle deltaic deposits are volumetrically the most important, and represent a progradational continuum, from highstand on the inner shelf, through sea level fall, to early lowstand rise.

3) Falling stage deposits are represented by oblique clinoforms truncated by an interpreted exposure surface. Lowstand rise progradational deposits are represented by sigmoid clinoforms and their updip horizontal extensions which onlap the exposure surface. The present highstand delta represents the beginning of the progradational continuum of a new Depositional Cycle, but has poor preservation potential due to eventual subaerial exposure and erosion during the subsequent sea level fall.

4) Delta architecture of the falling and lowstand rise stages are significantly different. The falling stage delta is multi-lobate, has restricted delta platform extent, and is probably more fluvially dominated. The lowstand rise delta is similar to the modern, with a single, broad, arcuate lobe, extensive delta platform aggradation, and strong tidal influence. A broad, thick aggraded alluvial valley is associated with the

lowstand delta, in addition to narrow, linear distributary feeders which dissect the broad delta plain.

5) Due to steep slope gradients the lowstand delta can not prograde past the shelf break. Deep sea mass wasting and turbid flows are sourced at the perched shelf edge delta.

6) Volumetric constraints of sediment supply, and lateral variation in shelf accommodation result in shingled, laterally offset stacking of successive lowstand depocenters, which has important consequences for location of the deep sea sediment source.

7) The warm tropical setting, southerly Indonesian Throughflow current, and probably nutrient loading of the upper thermocline, result in extensive, thick calcareous green-algal *Halimeda* bioherm accretion during significant shelf flooding periods and into early highstand. Increased terrigenous sediment influx during highstand delta progradation terminates the carbonate accretion.

8) Significant differences exist between the P1 Depositional Cycles of the Mahakam and Mississippi-Alabama shelves, which reflect differences in the depositional settings. Eustasy, the main influence on shelf accommodation, and a variable common to both settings, is responsible for the stratigraphic feature in common to both regions - the progradational continuum from highstand to lowstand rise. The most obvious differences are the poorly developed lowstand rise deposits and lack of thick carbonates on the Mississippi-Alabama shelf.

REFERENCES

Aharon, P., and J. Chappel, 1986. Oxygen isotopes, sea level changes and temperature history of a coral reef environment in New Guinea over the last 10^5 years. Paleogeography, Paleoclimatology, Paleoecology, 56: 337-379.

Ahmad, S.M., F. Guichard, K. Hardjawidjaksana, M.K. Adisaputra, and L.D. Labeyrie, 1995. Late Quaternary paleoceanography of the Banda Sea. Marine Geology, 122: 385-397.

Allen, G.P., D. Laurier, and J. Thouvenin, 1979. Etude Sedimentologique du Delta de la Mahakam. Notes et Memoires No. 15, Compagnie Francaise des Petroles (TOTAL), Paris, 156 pp.

Anderson, J.A.R., 1983. The tropical peat swamps of western Malesia. In: A.J.P. Gore (ed.), Ecosystems of the World 4B, Mires: Bog, Fen, and Moor, Regional Studies, Elsevier Scientific Publishing Co., New York, p. 181-199.

Anderson, J., K. Abdulah, and S. Sarzalejo, in press. Late Quaternary Sedimentation and high-resolution sequence stratigraphy of the east Texas shelf. In: M.de Baptist et al. (editors), Geology of Siliciclastic Seas, Special Publication, the Geological Society of London.

Apel, J.R., J.R. Holbrook, A.K. Liu, and J.J. Tsai, 1985. The Sulu Sea internal soliton experiment. Journal of Physical Oceanography, 15: 1625-1651.

Barmawidjaja, B.M., E.J. Rohling, W.A. van der Kaars, C. Vergnaud Grazzini, and W.J. Zachariasse, 1993. Glacial conditions in the northern Molucca Sea region (Indonesia). Palaeogeography, Palaeoclimatology, Palaeoecology, 101: 147-167.

Bellotti, P., F.L. Chiocci, S. Milli, P. Tortora, and P. Valeri, 1994. Sequence stratigraphy and depositional setting of the Tiber delta: integration of high-resolution seismics, well-logs, and archeological data. Journal of Sedimentary Research, B64(3): 416-432.

Bloom, A.L., 1983. Sea level and coastal morphology of the United States through the Late Wisconsin glacial maximum. In: H.E. Wright, and S. Porter (eds.), Late Quaternary Environments of the United States, v. 1, University of Minnesota Press, p. 215-229

Bloom, A.L., and N. Yonekura, 1990. Graphic analysis of dislocated Quaternary shorelines. *In*:: Sea Level Change. Geophysics Study Committee. Commission on Physical Sciences and Resources, National Research Council, National Academy Press, Washington, p. 104-115.

Boyle, E.A., and L.D. Keigwin, 1985. Comparison of Atlantic and Pacific paleochemical records for the last 215,000 years: changes in deep ocean circulation and chemical inventories. Earth and Planetary Science Letters, 76: 135-150.

Brickman, D., and J.W. Loder, 1993. Energetics of the internal tide on the northern Georges Bank. Journal of Physical Oceanography, 23: 409-424.

Butman, B., M. Noble, and D.W. Folger, 1979. Long-term observations of bottom current and bottom sediment movement on the mid-Atlantic continental shelf. Journal of Geophysical Research, 84(C3): 1187-1205.

Carbonel, P., and J. Moyes, 1987. Late Quaternary paleoenvironments of the Mahakam delta (Kalimantan, Indonesia). Palaeogeography, Palaeoclimatology, Palaeoecology, 61: 265-284.

Carbonel, P., and T. Hoibian, 1987. The impact of organic matter on Ostracods from an equatorial deltaic area, the Mahakam Delta - southeastern Kalimantan. *In*:: T. Hanai (ed.), Proceedings of the 9th International Symposium on Ostracoda, Shizuoka, Japan, p. 353-366.

Carbonel, P., T. Hoibian, and J. Moyes, 1987. Ecosystems et paleoenvironnements de la zone deltaique de la Mahakam depuis la fin de Neogene. Le Sondage Misedor. Editions Technip, Paris, p. 85-135.

Coleman, J.M., 1976. Deltas: processes of deposition and models for exploration. Champaign, Illinois, Continuing Education Publication Company, pp. 102.

Coleman, J.M., and S.M. Gagliano, 1964. Cyclic sedimentation in the Mississippi River deltaic plain. Gulf Coast Association for Geological Societies Transactions, 14: 67-80.

Coleman, J.M., and H.H. Roberts, 1988. Sedimentary development of the Louisiana continental shelf related to sea level cycles, part 1: sedimentary sequences. Geo-Marine Letters, 8: 63-108.

Combaz, A. (editor), 1987. Le Sondage Misedor. Editions Technip, Paris, p. 384.

Curray, J.R., 1960. Sediments and history of Holocene transgression, continental shelf, northwest Gulf of Mexico. In: F.P. Shepard, F.B. Phleger, and T.H. van Andel (eds.), Recent sediments, northwest Gulf of Mexico, Tulsah, Oklahoma, American Association for Petroleum Geologists, p. 221--266.

Duplessy, J.C., N.J. Schackleton, R.G. Fairbanks, L. Labeyrie, D. Oppo, and N. Kallel, 1988. Deepwater source variations during the last climatic cycle and their impacts on the global deepwater circulation. Paleoceanography, 3(3): 343-360.

Duval, B.C., G.C. de Janvry, and B. Loiret, 1992. Detailed geoscience reinterpretation of Indonesia's Mahakam Delta scores. Oil and Gas Journal, August 10: 67-72.

Eisma, D., J. Kalf, M. Karmini, W.G. Mook, A. Van Put, P. Bernard, and R. Van Grieken, 1989. Dispersal of suspended matter in Makasar Strait and the Flores Basin. Netherlands Journal of Sea Research, 24(4): 383-398.

Fairbanks, R.G., 1989. A 17,000-year glacio-eustatic sea-level record: influence of glacial melting rates on the Younger Dryas event and deep-ocean circulation. Nature, 342(Dec): 637-642.

Ffield, A., and A.L. Gordon, 1992. Vertical mixing in the Indonesian thermocline. Journal of Physical Oceanography, 22: 184195.

Fieux, M., C. Andrie, P. Delecuse, A. Ilahude, A. Kartavtseff, F. Mantisi, R. Molcard, and J. Swallow, 1994. Measurements within the Pacific-Indian oceans throughflow region. Deep-Sea Research, 41(7): 1091-1130.

Flohn, H., 1986. Indonesian droughts and their teleconnections. Berliner Geographische Studien, 20: 251-265.

Flores, R.M., 1993. Geologic and geomorphic controls of coal development in some Tertiary Rocky Mountain basins, USA. International Journal of Coal Geology, 23: 43-73.

Gayet, J., and P. Legigan, 1987. Etude sedimentologique du sondage Misedor (delat de la Mahakam Kalimantan, Indonesie). Le Sondage Misedor. Editions Technip, Paris, p. 23-71.

Gordon, A.L., 1995. When is appearance reality? A comment on why does the Indonesian throughflow appear to originate from the North Pacific. Journal of Physical Oceanography, 25: 1560-1567.

Gordon, A.L., 1986. Interocean exchange of thermocline water. Journal of Geophysical Research, 91(C4): 5037-5046.

Greenlee, S.M., and T.C. Moore, 1988. Recognition and interpretation of depositional sequences and calculations of sea-level changes from stratigraphic data, offshore New Jersey and Alabama Tertiary. *In* : C.K.Wilgus, B.S. Hastings, and C.G. St. C. Kendall, H.W. Posamentier, C.A. Ross, and J.C. Van Wagoner (eds.), Sea-level Changes: an Integrated Approach, SEPM Special Publication 42, p. 329-356.

Guidish, T.M., I. Lerche, C.G. St. C. Kendall, and J.J. O'Brien, 1984. Relationship between eustatic sea level changes and basement subsidence. Ameican Association of Petroleum Geologists Bulletin, 68: 164-177.

Gupta, A., A. Rahman, W.P. Poh, and J. Pitts, 1987. The old alluvium of Singapore and the extinct drainage system to the South China Sea. Earth Surface Processes and Landforms, 12: 259-275.

Hallock, P. and W. Schlager, 1986. Nutrient excess and the demise of coral reefs and carbonate platforms. Palaios, 1:389-398.

Heathershaw, A.D., A.L. New, and P.D. Edwards, 1987. Internal Tides and sediment transport at the shelf break in the Celtic Sea. Continental Shelf Research, 7(5): 485-517.

Holloway, P.E., 1985. A comparison of semidiurnal internal tides from different bathymetric locations on the Australian North West Shelf. Journal of Physical Oceanography, 15: 240-251.

Holloway, P.E., 1984. On the semidiurnal internal tide at a shelf-break region of the Australian North West Shelf. Journal of Physical Oceanography, 14: 1787-1799.

Hunt, D., and M.E. Tucker, 1992. Stranded parasequences and the forced regressive wedge systems tract: deposition during base-level fall. Sedimentary Geology, 81: 1-9.

Hutchison, C.S., 1989. Displaced terranes of the southwest Pacific. *In:* Z. Ben-Avraham (ed.), The Evolution of the Pacific Ocean Margins, Oxford University Press, New York, p. 161-175.

Huthnance, J.M., 1981. Waves and currents near the continental shelf edge. Progress in Oceanography, 10:193-226.

Ilahude, A.G., 1978. On the factors affecting the productivity of the southern Makassar Strait. Marine Research Indonesia, 21: 81-107.

Katili, J.A., 1973. On fitting certain geological and geophysical features of the indonesian island arc to the new global tectonics. In: The Western Pacific: Island Arcs, Marginal Seas, Geochemistry. University of Western Australia Press, Nedlands, W.A., p. 287-305.

Kindinger, J.L., 1988. Seismic stratigraphy of the Mississippi-Alabama shelf and upper continental slope. Marine Geology, 83: 79-94.

Kindinger, J.L., 1989. Depositional history of the Lagniappe delta, northern Gulf of Mexico. Geo-Marine Letters, 9: 59-66.

Lek, L., 1938. Die ergebnisse der Strom und Serienmessungen. The Snellius Expedition 1929-1930, Royal Netherlands Meteorological Institute, Vol.II, Oceanographic Results, part 3, Brill, London, 169 pp.

Magnier, P.H., T. Oki, L.Witoelar Karataadiputra, 1975. The Mahakam Delta, Kalimantan, Indonesia. Proceedings: Ninth World Petroleum Congress, v. 2, p. 239-250.

Matthews, R.K., 1990. Quaternary sea-level change. *In*:: Sea Level Change. Geophysics Study Committee. Commission on Physical Sciences and Resources, National Research Council, National Academy Press, Washington, p. 88-103.

McCabe R., and J. Cole, 1989. Speculations on the Late Mesozoic and Cenozoic evolution of the southeast Asian margin. *In:* Z. Ben-Avraham (ed.), The Evolution of the Pacific Ocean Margins, Oxford University Press, New York, p. 143-160.

Melecek, S.J., C.M. Reaves, W.S. Atmadja, and K.O. Widiantara, 1993. Seismic stratigraphy of Miocene and Pliocene age outer shelf and slope sedimentation in the Makassar PSC, offshore Kutei Basin. Proceedings IPA, 22nd Annual Convention p. 345-371

Miall, A.D., 1992. Exxon global cycle chart: an event for every occasion. Geology, 20: 787-790.

Milliman, J.D., and R.H. Meade, 1983. World-wide delivery of river sediment to the oceans. The Journal of Geology, 91(1): 1-21.

Mitchum, R.M., P.R. Vail, and J.B. Sangree, 1977. Seismic stratigraphy and global changes of sea level, part 6: stratigraphic interpretation of seismic reflection patterns in depositional sequences. In: C.E. Payton (ed.), Seismic Stratigraphy: Applications to Hydrocarbon Exploration, AAPG Memoir 26, p. 117-134.

Moore, T.C. Jr., W.H. Hutson, N. Kipp, J.D. Hayes, W. Prell, P. Thompson, and G. Boden, 1981. The biological record of the ice-age ocean. Palaeogeography, Palaeoclimatology, Palaeoecology, 35: 357-370.

Munk, W., 1981. Internal waves and small-scale processes. *in*: B. Warren and C. Wunsch (eds.), Evolution of Physical Oceanography, The MIT Press, 623 pp.

Nummedal, D., and C.M. Molenaar, 1995. Sequence stratigraphy of ramp-setting strand plain successions: the Gallup Sandstone, New Mexico. *In:* J.C. Van Wagoner, and G.T. Bertram (eds.), Sequence Stratigraphy of Foreland Basin Deposits - Outcrop and Subsurface Examples from the Cretaceous of North America, AAPG Memoir 64, p. 277-310.

Osborne, A.R., and T.L. Burch, 1980. Internal solitons in the Andaman Sea. Science, 208: 451-460.

Peltier, W.R., 1990. Glacial isostatic adjustment and relative sea-level change. *In*:: Sea Level Change. Geophysics Study Committee. Commission on Physical Sciences and Resources, National Research Council, National Academy Press, Washington, p. 73-87.

Philander, S.G., 1992. El Nino. Oceanus, 35(2): 56-61.

Phipps, C.V.G., and H.H. Roberts, 1988. Seismic characteristics and accretion history of Halimeda bioherms on Kalukalukuang Bank, eastern Java Sea (Indonesia). Coral Reefs 6: 149-159.

Pingree, R.D., and G.T. Mardell, 1981. Slope turbulence, internal waves and phytoplankton growth at the Celtic Sea shelf-break. Philosophical Transactions Royal Society London, A302: 663-682.

Piper, D.J.W., and C. Perissoratis, 1991. Late Quaternary sedimentation on the north Aegean continental margin, Greece. American Association of Petroleum Geologists Bulletin, 75: 46-61.

Posamentier, H.W., and P.R. Vail, 1988. Eustatic controls on clastic deposition II: sequence and systems tract models. *In* : C.K.Wilgus, B.S. Hastings, and C.G. St. C. Kendall, H.W. Posamentier, C.A. Ross, and J.C. Van Wagoner (eds.), Sea-level Changes: an Integrated Approach, SEPM Special Publication 42, p. 125-154.

Posamentier, H.W., G.P. Allen, D.P. James, and M. Tesson, 1992. Forced regressions in a sequence stratigraphic framework: concepts, examples, and exploration significance. American Association of Petroleum Geologists Bulletin, 76: 1687-1709.

Prior, D.B., Z.S. Yang, B.D. Bornhold, G.H. Keller, N.Z. Lu, W.J. Wiseman, Jr., L.D. Wright, and J. Zhang, 1986. Active slope failure, sediment collapse, and silt flows on the modern subaqeous Huanghe (Yellow River) Delta. Geo-Marine Letters, 6: 85-95.

Prokasih Mahakam Component, anonymous, 1993. Mahakam River preliminary study. Technical Report, Kantor Gubernur Lantai III, Samarinda Kalimantan Timur, Indonesia, pp. 52.

Ritsema, A.R., R.P. Sudarmo, and I. Putu Pudja, 1989. The generation of the Banda arc on the basis of its seismicity. Netherlands Journal of Sea Research, 24(3): 165-172.

Roberts, H.H., 1980. Sediment characteristics of Mississippi River delta front mudflow deposits. Gulf Coast Association of Geological Societies Transactions, 30: 485-496.

Roberts, H.H., C.V.G. Phipps, and L. Effendi, 1987. Halimeda bioherms of the eastern Java Sea, Indonesia. Geology, 15: 371-374.

Roberts, H.H., and J. Sydow, 1995. Stratigraphic framework and sedimentology of the modern and Late Pleistocene offshore Mahakam delta. Modern Mahakam Delta Phase 1 and Phase 2 Final Report, VICO in-house report, Section 1, pp. 32.

Roberts, H.H., J. Sydow, and A.H. Bouma, 1993. Seismic stratigraphy, sedimentology, and reservoir potential of a Late Pleistocene shelf-edge delta. Gulf Coast Association of Geological Societies Transactions, 43: 345-347.

Ropelewski, C.F., and M.S. Halpert, 1987. Global and regional scale precipitation patterns associated with the El Nino/Southern Oscillation. Monthly Weather Review, 115: 1606-1626.

Rosenfeld, L.K., 1990. Baroclinic semidiurnal tidal currents over the continental shelf off northern California. Journal of Geophysical Research, 95(C12): 22153-22172.

Satchell, L.S., and J.H. Wrenn, 1995. Offshore organic facies - quantitative palynology of surface sediment samples. Modern Mahakam Delta Phase 1 and Phase 2 Final Report, VICO in-house report, Section 3, pp. 15.

Sen Gupta, B.K., and W.T. Maul, 1995. Micropaleontology - benthic foraminifera. Modern Mahakam Delta Phase 1 and Phase 2 Final Report, VICO in-house report, Section 2, pp. 24.

Staub, J.R., and J.S. Esterle, 1994. Peat-accumulating depositional systems of Sarawak, East Malaysia. Sedimentary Geology, 89: 91-106.

Suter, J.R., and H.L. Berryhill, 1985. Late Quaternary shelf margin deltas, northwest Gulf of Mexico. American Association of Petroleum Geologists Bulletin, 69: 77-91.

Sydow, J, 1992. The stratigraphic framework of a shelf edge delta, northeast Gulf of Mexico. M.S. thesis, Louisiana State University, Baton Rouge, pp. 135.

Sydow, J., and H.H. Roberts, 1994. Stratigraphic framework of a Late Pleistocene shelf-edge delta, northeast Gulf of Mexico. American Association of Petroleum Geologists, 78: 1276-1312.

Sydow, J., H.H. Roberts, A.H. Bouma, and R. Winn, Jr., 1992. Constructional subcomponents of a shelf-edge delta, northeast Gulf of Mexico. Gulf Coast Association of Geological Societies Transactions, 42: 717-726.

TAD-Transmigration Area Development Project Report, 1982. Rainfall records, East Kalimantan, report: analysis summaries and histograms. Samarinda, Kalimantan Timur, Indonesia, pp. 21.

Tesson, M., G.P. Allen, and C. Ravenne, 1993. Late Pleistocene shelf-perched lowstand wedges on the Rhone continental shelf. Special Publications International Association of Sedimentologists, 18: 183-196.

Thorpe, M.B., M.F. Thomas, T. Martin, and W.B. Whalley, 1990. Late Pleistocene sedimentation and landform development in western Kalimantan (Indonesian Borneo). Geologie en Mijnbouw, 69: 133-150.

TOTAL, 1986. Meteorological and Oceanographical Campaign Balikpapan Final Report. TOTAL internal Report, pp. 67.

Trincardi, F., A. Correggiari, and M. Roveri, 1994. Late Quaternary transgressive erosion and deposition in a modern epicontinental shelf: the Adriatic semienclosed basin. Geo-Marine Letters, 14: 41-51.

Vail, P.R., R.M. Mitchum, and S. Thompson, III, 1977. Changes of sea level from coastal onlap. *In*: C.E. Payton (ed.), Seismic Stratigraphy: Applications to Hydrocarbon Exploration, AAPG Memoir 26, p.63-81.

Vail, P.R., F. Audemard, S.A. Bowman, P.N. Eisner, and C. Perez-Cruz, 1991. The stratigraphic signatures of tectonics, eustacy and sedimentology: an overview. *In*: G, Einsele, W. Ricken, and A. Seilacher (eds.), Cycles and Events in Stratigraphy, New York, Springer Verlag, p. 617-659.

Van de Weerd, A.A., and R.A. Armin, 1992. Origin and evolution of the Tertiary hydrocarbon bearing basins in Kalimantan (Borneo), Indonesia. American Association of Petroleum geologista Bulletin, 76:1778-1803.

Van der Kaars, W.A., 1991. Palynology of eastern Indonesian marine piston cores: A late Quaternary vegetational and climatic record for Australasia. Palaeogeography, Palaeoclimatology, Palaeoecology, 85: 239-302.

Van Hinte, J.E., 1978. Geohistory analysis - application of micropaleontology in exploration geology. Ameican Association of Petroleum Geologists Bulletin, 62: 201-222.

Van Wagoner, J.C., H.W. Posamentier, R.M. Mitchum, P.R. Vail, J.F. Sarg, T.S. Loutit, and J. Hardenbol, 1988. An overview of the fundamentals of sequence stratigraphy and key definitions. *In* : C.K.Wilgus, B.S. Hastings, and C.G. St. C. Kendall, H.W. Posamentier, C.A. Ross, and J.C. Van Wagoner (eds.), Sea-level Changes: an Integrated Approach, SEPM Special Publication 42, p.39-45.

Van Wagoner, J.C., R.M. Mitchum, K.M. Campion, and V.D. Rahmanian, 1990. Siliciclastic sequence stratigraphy in well-logs, cores, and outcrops. AAPG Methods in Exploration Series 7, pp. 55.

Verstappen, H.Th., 1980. Quaternary climatic changes and natural environment in SE Asia. Geojournal, 4(1): 45-54.

Winker, C.D., and M.B. Edwards, 1983. Unstable progradational clastic shelf margins. In: D.J. Stanley, and G.T. Moore (eds.), The Shelf Break: Critical Interface on Continental Margins, SEPM Special Publication 33, p. 139-157

Wiseman, W.J., Jr., 1986. Estuarine-shelf interactions. Baroclinic Processes on Continental Shelves, Coastal and Estuarine Sciences 3, American Geophysical Union, p. 109-115.

Wright, L.D., 1989. Dispersal and deposition of river sediments in coastal seas: models from Asia and the tropics. Netherlands Journal of Sea Research, 23(4): 493-500.

Wunsch, C, 1975. Internal Tides in the ocean. Reviews of Geophysics or Space Physics, 13: 167-182.

Wyrtki, K, 1961. Physical oceanography of the Southeast Asian waters. Naga Report II, Scripps Institute of Oceanography, 195 pp.

Xiao, J, S.C. Porter, Z. An, H. Kumai, and S. Yoshikawa, 1995. Grain size of quartz as an indicator of winter monsoon strength on the Loess plateau of central China during the last 130,000 yr. Quaternary Research, 43: 22-29.

APPENDIX

LITHOLOGY KEY FOR CORE LOGS

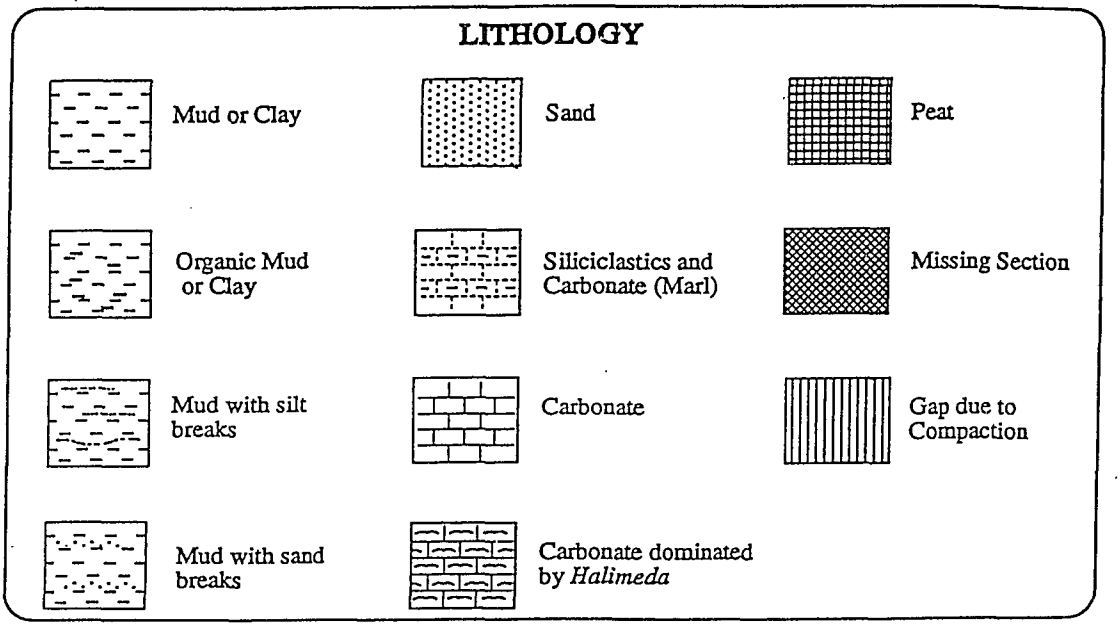

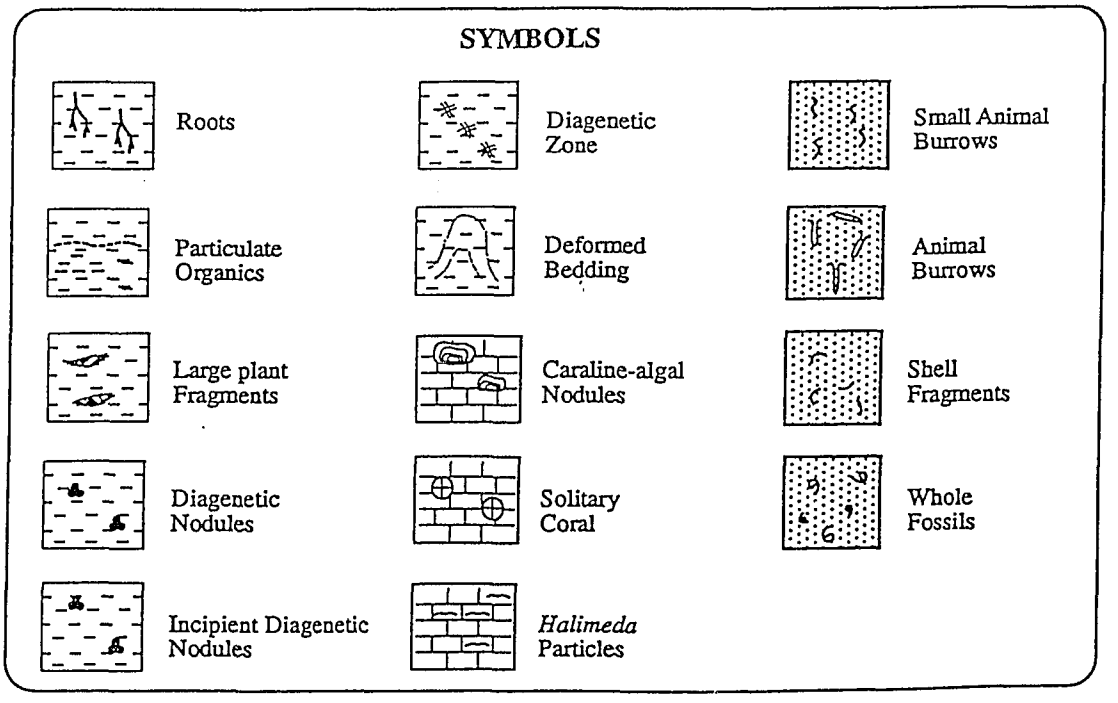

VITA

Johan Sydow was born in Sweden in 1966, and moved with his family to South Africa in 1974. He graduated at the University of Cape Town, South Africa, in 1988 with a BSc Honours degree in geology, with special emphasis on marine geology. In 1992 Johan completed his M.S. degree in geology at Louisiana State University. The thesis title was "The Stratigraphic Framework of a Shelf Edge Delta, Northeast Gulf of Mexico". Johan will start working with British Petroleum Exploration in Houston, Texas, in 1996.

DOCTORAL EXAMINATION AND DISSERTATION REPORT

Candidate: Johan C. Sydow

Major Field: Oceanography and Coastal Sciences

Title of Dissertation: Holocene to Late Pleistocene Stratigraphy of the Mahakam Delta, Kalimantan, Indonesia

Approved:

Major Professor and Chairman

Dean of the Graduate School

EXAMINING COMMITTEE:

Date of Examination:

12/18/95